Title	THERMODYNAMIC PROPERTIES OF SOME FERROELECTRICS
Author(s)	Higashigaki, Yoshiyuki
Citation	大阪大学, 1977, 博士論文
Version Type	VoR
URL	https://hdl.handle.net/11094/31590
rights	
Note	

THERMODYNAMIC PROPERTIES

OF

SOME FERROELECTRICS

by

Yoshiyuki Higashigaki

M.S., Osaka University, 1972

THESIS

Submitted to the Faculty of Science of the

Osaka University in Partial Fulfilment of the

Requirements for the Degree of Doctor of Science

Osaka University

1977

Doctoral Comitee:

Professor Hideaki Chihara, Chairman

Professor Ryôiti Kiriyama

Professor Shigerô Ikeda

Associate Professor Hiroshi Suga

ACKNOWLEDGMENTS

CONTENTS

Chapter 1   Introduction

1.1   Introductory remarks

Heat capacity at constant pressure is a fundamental quantity
characterizing various substances and is related to other important
thermodynamic quantities. First, the heat capacity means the tempera-
ture derivative of enthalpy H; $Cp = \left(\frac{\partial H}{\partial T}\right)_p$. Secondly, this can also be
related to entropy S by the equation $Cp = T\left(\frac{\partial S}{\partial T}\right)_p$. Moreover, this gives
the second derivative of Gibbs energy with respect to the thermodynamic.
temperature, $Cp = -T\left(\frac{\partial^2 G}{\partial T^2}\right)_p$. Gibbs energy is the thermodynamic potential
at an arbitrary temperature and pressure and determines the stability
of the system. Thus, heat capacity measurements prove to be highly
sensible and powerful means to investigate the properties of the system
which we are interested in.

The above thermodynamic functions give us macroscopic description
on the properties of substances. On the other hand, microscopic aspects
are obtained by other experiments such as spectroscopy with electromagnetic
waves, neutrons and so on. Statistical mechanics informs us of not only
microscopic and macroscopic but also static and dynamic properties of
the substances to be investigated. Here we intend to study five ferro-
electric substances, NH_4HSO_4, ND_4DSO_4, $RbHSO_4$, $RbDSO_4$, and $(ND_4)_2SO_4$,
concentrating upon their ferroelectric phase transitions, cation effects,
and isotope effects in terms of statistical thermodynamics.

1.2   Review of previous works on the five ferroelectrics to be

        investigated

        Besides amorphous state and glassy state, crystalline state may be

distinguished from liquid state and gaseous state by its periodicity and

anisotropy.   Therefore a crystal is characterized as one of 230 space

groups, which are subdivided into 32 crystal classes.   Among them only

10 classes show pyroelectricity.   Ferroelectric crystals have the

spontaneous polarization P_s, i.e., they display pyroelectric properties;

this describes only a necessary condition.   Reversibility of P_s under

an applied electric field would be sufficient criterion.[1]   Recently,

however, the sufficient condition has been modified from reversibility

to mere reorientability of P_s at a fixed angle differing from 180°.[2]

For example Schmid was the first to detect such ferroelectric behavior

in boracites.[3]

        The first ferroelectric was Rochelle salt discovered by Valasek[4]

in 1920.   In 1940 Müller[5] developed his phenomenological theory on

Rochelle salt to explain its macroscopic properties observed since its

discovery. KH_2PO_4 and its isomorphous group, known as hydrogen bonded

ferroelectrics, were shown to be ferroelectric in 1935.[6]   Statistical

theory on KH_2PO_4 was first published by Slater[7] in 1941, arousing

experimentalist's and theoretist's interest for ferroelectric transition

phenomena.   Ferroelectricity of $BaTiO_3$ and its isomorphous with a

perovskite structure, known as an oxide ferroelectrics, were found in

1945[8] and antiferroelectric behavior of $PbZrO_3$ was observed in 1951.[9]

In general form Devonshire[1] proposed in 1954 a purely thermodynamical,

phenomenological theory of various ferroelectrics and antiferroelectrics

observed heretofor.   In 1956 Matthias and Remeika[10] first found that

$(NH_4)_2SO_4$ becomes ferroelectric below its transition point at -49.5°C.
In those days the N-H···O bonds, which did not appear in any ferroelectric
except alum, was anticipated to be important for the occurrence of
ferroelectricity. In 1958 Pepinsky, et al.[11] reported that NH_4HSO_4
became ferroelectric only in the limited temperature between -3 and -119°C
and it showed comparatively low coercive field. In 1959 Pepinsky and
Vedam,[12] moreover, observed ferroelectric behavior of $RbHSO_4$ below -15°C.

Various kinds of experiments have been done after discovery of
ferroelectricity in $(NH_4)_2SO_4$, NH_4HSO_4, and $RbHSO_4$ to elucidate the
nature of their ferroelectric behavior. Now a brief review of their
results will be given in the following sections.

Dielectric Study

Pepinsky and his coworkers[11] found that NH_4HSO_4 exhibits a large
dielectric anomaly (ε_c) on passing from a paraelectric to a ferroelectric
phase and another small but sharp decrease from a value of 16 to 9 on
passing to the lowest phase (piezoelectric), while dielectric constants
ε_a and ε_b remain practically constant. Dielectric constant of $RbHSO_4$
measured by Pepinsky and Vedam[12] shows a fairly sharp maximum along
the c axis similar to NH_4HSO_4 but no second transition could be detected
in the temperature range -15°C to -196°C, unlike in NH_4HSO_4. The most
remarkable difference between NH_4HSO_4 and $RbHSO_4$ appeared in their
magnitude of coercive field, amounting to only 1.1 kV/cm at -118°C for
NH_4HSO_4 and 23 kV/cm at -170°C for $RbHSO_4$. The saturated spontaneous
polarization along the c axis was 0.8 $\mu C/cm^2$ for NH_4HSO_4 and 0.65 for
$RbHSO_4$, small when compared with KH_2PO_4 (4.8)[13] or $BaTiO_3$[14] (15.5).

Kasahara and Tatsuzaki[15] reported the temperature dependence of
the dielectric constant ε_c for ND_4DSO_4 (92 % D), which was quite similar

to that of NH_4HSO_4 except for two unusual transition temperature shifts.

The dielectric constant ε_c of $(NH_4)_2SO_4$[16] shows quite a strange behavior that it suddenly jumps to a maximum value at $-49.5°C$ and then drops to nearly the value at room temperature. This unusual behavior, showing large deviation from the Curie-Weiss law, could not be explained by conventional phenomenological theory and seemed to be responsible for a domain wall movement.[17] Another unusual behavior appeared in the temperature dependence of spontaneous polarization along its orthorhombic c axis; Pepinsky and his coworkers gave a constant value of ca. $0.45\mu C/cm^2$ below T_c but Unruh[18] reported a gradual decrease of spontaneous polarization and a reproducible change of its sign at $-188.5°C$. Unruh was the first to detect ferrielectricity in $(NH_4)_2SO_4$.

Sturctural Study

Crystal structure of NH_4HSO_4 was determined by Pepinsky and his coworkers,[11] Ogawa and his coworkers,[19] and Nelmes.[20] Crystal data are given in Table 1.2.1. From this table it is seen that all the three phases may be characterized as having the pseudo-orthorhombic symmetry. Crystal structures of each phase are summerized as follows;

Phase I   The unit cell in this non-ferroelectric phase contains two inequivalent sulfate units, which are related by a pseudo-symmetry. The two inequivalent sulfate tetrahedra are distorted and linked by short hydrogen bonds into chains to the very short b axis. Neutron diffraction data[20] revealed that the hydrogen atoms are ordered onto acentric sites in hydrogen bonds. The detailed analysis of unusually large thermal parameters for oxygen atoms in one of HSO_4^- ions (named as S_1 by Nelmes) led to the conclusion that S_1 is statistically disordered between two sites. An ammonium ion named N_1 is coordinated by ten oxygens

with N-O separations less than 3.5 $\overset{\circ}{A}$ and N_2 by nine, respectively.
Figure 1.2.1 shows the room temperature structure projected on planes
(a, b, c), using the results of Nelmes.

Phase II   The asymmetric unit of the pseudo-orthorhombic unit
cell (Space group Ba) contains four formula units which are related in
pairs by a center of inversion in the non-ferroelectric phase above the
upper transition. X-ray analysis by Nelmes shows that the ferroelectric
structure corresponds to an ordering of sulfate groups which are
disordered in the room-temperature structure, an ordering which is
antisymmetric with respect to the room-temperature center of inversion.
The temperature dependence of intensity ratio of $I(204) / I(20\bar{4})$[19]
resembles that of spontaneous polarization given by Pepinsky, et al.,[11]
and leads to an interesting conclusion that the lower the temperature
in this phase goes, the more marked pseudo-orthorhombic cymmetry the
crystal shows.

Phase III   No detailed crystal structures are reported with
respect to the phase III. This phase exhibits no ferroelectricity but
pizoelectricity and marked twining, the plane of which is (001).

Crystal structures of $RbHSO_4$ determined by X-ray diffraction[12,21]
are given in Table 1.2.2. $RbHSO_4$ is found to be isomorphous with NH_4HSO_4,
and both high and low temperature phases show pseudo-orthorhombic
symmetry as in the case of NH_4HSO_4, $Rb^+(1)$ named by Mumme is surrounded
by nine oxygens with the Rb-O distances of 2.97 to 3.27 $\overset{\circ}{A}$ and $Rb^+(2)$ by
ten oxygens with distances of 2.91 to 3.15 $\overset{\circ}{A}$.

Detailed crystal structural analysis of $(NH_4)_2SO_4$, using three
dimensional neutron diffraction, was made by Schlemper and Hamilton,[22]
who sumarized their crystal data for both phases as given in Table 1.2.3.

At room temperature the sulfur atom, two oxygen atoms, the nitrogen
atoms, and four hydrogen atoms lie on the mirror planes as shown in
Fig. 1.2.2 which was depicted by using their results. The rest of the
atoms are in general positions. At low temperature all atoms occupy
general positions. The environment of $NH_4(I)$ is determined by the
configurations of five sulfate ions taking part in the N-H$\cdots$O bonding,
while that of $NH_4(II)$ by six. Using the thermal parameters of both
phases, the anisotropic torsional frequencies for two ammonium ions in
both phases are determined, and they concluded that within experimental
error the root-mean-square frequencies of the ammonium ions remain
virtually unchanged in passing through the transition. The concluding
remark reached by Schlemper and Hamilton was that the transition is
not of the order-disorder type but rather involves a change in the
hydrogen bonding of the ammonium ions to the sulfate ions which results
in stronger hydrogen bonds in the ferroelectric phase; these are made
possible by the loss of the mirror plane perpendicular to the c axis,
which is the ferroelectric axis.

Anisotropic thermal expansions of $(NH_4)_2SO_4$[16) were observed by
precise X-ray measurement of lattice constants with temperature, showing
that the orthorbombic b and c axes exhibit sudden small shrinkage and
on the other hand the a axis sudden large expansion on passing through
the transition and results in increase of cell volume in the ferroelectric
phase.

Though $KHSO_4$ is not ferroelectric, the crystal structure of $KHSO_4$,
which shows complete orthorhombic symmetry, is given in Table 1.2.4 to
be compared with that of $RbHSO_4$.

NMR Study

The line width and second moments of proton magnetic resonance[23]
in the powdered NH_4HSO_4, which is the same as the calorimetric sample,
shows no distinct change on passing through two inherent transitions
and their low values are assigned as that of the isotropic reorientation
of NH_4^+. The temperature dependence of proton spin-lattice relaxation
time revealed the relatively low activation energy E_a for reorientation
of NH_4^+ as 8.4 kJ mol^{-1} for Phase II and Phase I below 320 K and
11.1 kJ mol^{-1} for Phase III above 96 K, showing agreement with the results
by Miller and his coworkers.[24] While the temperature dependence of
deuteron spin-lattice relaxation time in ND_4DSO_4[25] gave E_a = 9.1 kJ mol^{-1}
for Phase I, E_a = 12.0 kJ mol^{-1} for Phase II, and E_a = 7.41 kJ mol^{-1}
for Phase III, respectively. Judging from the low value of the activation
energy Miller, et al.,[24] suggested that the upper transition was not
connected with NH_4^+ ordering, but was more likely due to a change in
the equilibrium distribution of protons along the O-H-O bonds. Above
statement of equilibrium distribution of protons was modified by Nelmes[20]
and Kasahara and Tatsuzake.[26] From the rotation patterns at 20°C of
first order quadrupole shifts of deuteron magnetic resonance in $RbDSO_4$[26]
it is concluded that the deuterium is not in a disordered state but in
fact stays on acentric position in each hydrogen bond even in the
paraelectric phase. The rotational displacement of SO_4^{--} ions was
confirmed by the shift in the principal Z axis of EFG in the ferroelectric
phase. The temperature dependence of quadrupole splitting is shown to
be proportional to the spontaneous polarization obtained by the
pyroelectric method.[26] An interesting result in this connection is
the separation of resonance lines and spontaneous polarization depend

on temperature as $(T_c - T)^\beta$, with β of 0.33 or 0.28 in the limited temperature range, from -30 to -100°C. Proton magnetic resonance study of RbHSO$_4$[27] reported an anomalous temperature behavior of the proton spin-lattice relaxation time, which showed a large hysteresis and marked change in magnitude like a first order transition, and concluded that the transition is caused by a combination of slow proton tunneling and SO$_4^{--}$ deformation.

Blinc and Levstek[28] explained their NMR and ir data in terms of half "frozen-in" and half "rapidly reorienting" ammonium ions, disagreeing with the interpretation of neutron diffraction data by Schlemper and Hamilton. The deuteron nuclear magnetic resonance of single crystals of (ND$_4$)$_2$SO$_4$[29] showed that the principal coordinate system of the EFG tensor rotates by about 30° in the transition to the ferroelectric phase. From the measurements of proton spin-lattice relaxation time and proton relaxation time along the rf field[29] it was found that activation energies for reorientation of NH$_4^+$ was determined as E_a = 9.6 kJ mol^{-1} above T_c and 16.3 kJ mol^{-1} for NH$_4^+$(I) and 11.3 kJ mol^{-1} for NH$_4^+$(II) below T_c and that the NH$_4^+$(II) is undergoing quantum-mechanical tunneling at 20 K. From above results O'Reilly and Tsang proposed an order-disorder mechanism for the phase transition in which NH$_4^+$ tetrahedra are disordered with respect to the crystal ab plane. This statement is also in contrast with results given by Schlemper and Hamilton.

Spectroscopic Study

From splitting of infrared spectra of NH$_4$HSO$_4$ and RbHSO$_4$ into a doublets on transition through the upper Curie point, Myasnikova and

Yatsenko[30] deduced the conclusion that ferroelectricity of $RbHSO_4$ and NH_4HSO_4 was due to hydrogen bonds O-H-O.

The temperature dependence of the infrared spectra of $(NH_4)_2SO_4$ and $(ND_4)_2SO_4$ between 17 and 298 K was analyzed by Schutte and Heyns[31] and they supported the evidence of the neutron diffraction data of Schlemper and Hamilton that there is an increase in hydrogen bonding strength below T_c. An interesting correlation was established between the temperature variation of the peak heights (bands at 612, 1047, and 3305 cm^{-1}) at about 160 K and the NMR line width transition at 163 K. The variation of the bands in the N-D stretching with temperature was explained by the possible existence of three phases in $(ND_4)_2SO_4$ (T_c = 225 and 223 K).[16]

The recent Raman and ir spectra of $(NH_4)_2SO_4$ and $(ND_4)_2SO_4$[32] showed no anomalous changes in either frequencies or peak widths, and the normal mode frequencies of the NH_4^+ ions were those expected for a tetrahedral rather than a disordered configuration. Either of the simple models of the phase transition, which have been reported by Schlemper and Hamilton and O'Reilly and Tang, was not supported.

1.3 Theoretical considerations

When we examine the properties of the macroscopic system which has s degrees of freedom and is described by the time-independent hamiltonian H, then we are able to write down the following expressions for the thermodynamic functions, which are to be obtained from the heat capacity, assuming the canonical distribution.

According to the standard text,[33] the canonical distribution ρ is given by Eq.1-1

$$\rho = e^{-\beta H}/Z \qquad 1-1$$

where $kT\beta = 1$ and Z is the partition function defined as

$$Z = \text{Tr } e^{-\beta H}. \qquad 1-2$$

Helmholtz energy A is related to Z by Eq.1-3

$$-\beta A = \ln Z . \qquad 1-3$$

Generally, the entropy of the system is defined as the mean value of the logarithm of the distribution function.

$$S/k = -<\ln \rho > \qquad 1-4$$

Eqs.1-3 and 4 lead to the expression for the internal energy U which is merely the thermal average of mechanical hamiltonian.

$$U = A + TS$$
$$\qquad 1-5$$
$$= < H >$$

The thermal average of certain mechanical quantity B(p,q) can be written explicitly as:

$$< B > = \text{Tr } \rho B \qquad \text{(in quantal)}$$
$$= \int \rho_{cl} B \ d\Gamma \qquad \text{(in classical)} \qquad 1-6$$

$$\rho_{cl} = h^s e^{-\beta H} / Z_{cl}$$

$$Z_{cl} = \int' e^{-\beta H} h^s \, d\Gamma \qquad\qquad 1\text{-}7$$

$$d\Gamma = dp_1 \dots dp_s \cdot dq_1 \dots dq_s / h^s$$

$$= dpdq / h^s$$

The prime on the integral sign shows that we must integrate only over

the region of phase spase which corresponds to physically distinct

microscopic state of the system. Heat capacity at constant volume is

defined as the first temperature derivative of internal energy.

$$C_v = (\partial U/\partial T)_v$$

$$= k\beta^2 \langle (H-\langle H\rangle)^2\rangle \qquad\qquad 1\text{-}8$$

which is also obtained by $C_v = T(\partial S/\partial T)_v$. Eq.1-8 shows that the heat

capacity is directly related to the fluctuation of the energy.

Assuming that our many-body system is regarded as the particular

aggregation composed of the completely independent particles, then

we can describe the normal thermodynamic behaviors in the following

cases;

A Free rotator in three dimensions

Eigen value $\quad E_J = J(J+1)\, \hbar^2/2I, \qquad J = 0,1,2,\dots$

Degeneracy $\quad g_J = (2J+1)^2$

$$T_{red} = \hbar^2/2kI$$

$T_{red} = 0.26$ K for the tetrahedral SO_4^{2-} with the

S-O bond length of 1.49 Å and $T_{red} = 8.6$ K for the

tetrahedral NH_4^+ with the N-H bond length of 1.02 Å.

B Free rotator in two dimensions

Eigen value $\quad E_n = n(n+1)\, \hbar^2/2I, \qquad n = 0,1,2,\dots$

Degeneracy $g_n = 2n + 1$

$$T_{red} = \hbar^2/2kI$$

$T_{red} = 0.30$ K for the planar $CO_3{}^{2-}$ with the C-O bond

length of 1.29 Å and $T_{red} = 7.7$ K for the methyl group

CH_3 with the C-H distance of 1.09 Å.

C One dimensional harmonic oscillator and librator

Eigen value $E_n = \hbar\omega(n +1/2)$, $n = 0,1,2,\ldots$

$$T_{red} = \hbar\omega/k$$

$\omega = \sqrt{K/M}$ for the translational vibration

$\omega = \sqrt{K/I}$ for the librational vibration

where K is an effective force constant.

This model leads to the Einstein heat capacity which is often

applied for the internal vibrations of molecules and also for

the librational vibrations of molecules as a whole.

D Particle in one dimensional box

Eigen value $E_n = (\pi^2\hbar^2/2ma^2)n^2$, $n = 1,2;3,\ldots$

$$T_{red} = \pi^2\hbar^2/2mka^2$$

$T_{red} = 240$ K for the hydrogen in the O-H...O bond,

in which it moves freely in the range of 1.0 Å.

The temperature dependence of thermodynamic functions for above

simple models is calculated and illustrated in the reduced form in

Fig. 1.3.1 (left). The heat capacity due to three dimensional free

rotator has a peak of 2.11 R at T = 0.60 T_{red} before it attains the

classical value of 1.5 R about T = 2 T_{red}. On the other hand, that of

two dimensional free rotator has a relatively broad peak of 1.098 R

at T = 0.80 T_{red}. Harmonic oscillator model has no hump in the heat

capacity curve and shows merely a monotonously increasing behavior.

Free particle in one dimensional box has a larger value than 0.5 R above

T = 1.30 T_{red}, which is obtained in the limit of infinitely large width

in classical mechanics, and shows a very gradual hump amounting to 0.562

R at T = 2.8 T_{red} and has a value of 0.555 R even at T = 5.2 T_{red}.

Model A has been applied for explaining the heat capacity of

symmetric top molecules in gaseous phase in semiclassical statistics.

But model A as well as model B was employed by Pauling[34] for the model

of rotational phase which appears above the rotational transition in

condensed phase such as N_2, CH_4 and so on. Using the two dimensional

free rotational entropy (model B) and the librational entropy (model C),

Frenkel, Todes and Ismailow[35] calculated the transition entropy of solid

HCl at 98 K, which showed a good agreement with the experimental results

given by Giauque and Wiebe[36] and Chihara and Inaba.[37] It is

interesting to be able to estimate the transition entropy in terms of

superposition of two aspects of thermodynamic entropies in which the

cooperative effect is not taken into account.

Now we consider the thermodynamic properties of systems of many

strongly interacting particles. As a representative system we may take

a crstal in which a constituent atom interacts with its neighbour atoms.

In the harmonic approximation the thermodynamic functions are additive

functions of the normal mode frequencies. Among them, the heat

capacity at constant volume can be expressed as

$$C_v/k = \sum_{\underline{k}j} X_{\underline{k}j}^2 / \sinh^2 X_{\underline{k}j} \qquad\qquad 1-9$$

$$X_{\underline{k}j} = \hbar\omega_j(\underline{k}) / 2kT,$$

where the notation have usual meanings.[38,39] Since the number of atoms

in a crystal is very large and the eigen values are very dense and

bounded, it is more convevient to deal with the frequency distrbution

function, or frequency specrum $g(\omega)$, than the individual frequencies. The useful analytic spectrum is the Debye spectrum which is derived from an elastic continuum model;

$$g(\omega) = 3\omega^2/\omega_D^3, \qquad 0 \leq \omega \leq \omega_D$$

$$= 0, \qquad \omega > \omega_D$$

where ω_D is an artificial limiting frequency which leads to the correct normalization of the crystal. Using the Debye spectrum, one obtains

$$C_v = \frac{3rNk}{x^3} \int_0^x \frac{x^4 e^x}{(e^x - 1)^2} \, dx \qquad \qquad 1\text{-}10$$

$$x = \Theta_D/T$$

$$\Theta_D = \hbar\omega_D/k$$

where Θ_D is called the Debye characteristic temperature. In the high temperature limit, the Debye heat capacity gives the Dulong-Petit's law and in the limit of low temperature the "Debye T^3 law".

The harmonic crystal shows no anomalous behavior of which is depicted in Fig. 1.3.1(c). These properties of themodynamic functions can be explained by the facts that for the atomic vibrations in a crystal the principal axis transformation which diagonalizes the corresponding hamiltonian in zero order re-expresses it as the sum of the hamiltonians of individual, independent, harmonic oscillators (phonons). As the temperature goes up, however, most of real crystals exhibit anharmonic behaviors of not only thermal expansion and thermal conductivity[40] but also the shift and damping[41] of the vibrational frequency due to a phonon-phonon interaction.

In calculating the thermodynamic functions of anharmonic crystals

the phonon-phonon interactions are treated by the operator renormalization method (renormalized phonon)[42] or by the self-consistent method (self-consistent phonon)[43]. The basic idea of the former is to obtain improved phonon creation and annihilation operators representing "dressed" phonons which do not interact with one another in first-order perturbation and then calculate the energies of these phonons in the second-order perturbations. On the other hand, the basic idea of the later is to introduce an effective harmonic potential Φ_h and write

$$H = H_o + (\Phi - \Phi_h) \qquad \qquad 1-11$$

where H_o is an effective harmonic hamiltonian and Φ is the potential in the real crystal and Φ_h is to be determined so that the perturbation "$\Phi - \Phi_h$" is small in the statistical sense. The temperature-dependent shift of the self-consistent phonon frequency is naturally introduced and hence this theory has been applied for the displacive and other deformation-related transitions.[44]

It should be stated here that unfortunately the results of above two methods are expressed in so complicated fashion that the direct comparison with experimental result such as excess heat capacity cannot be made with ease.

In terms of thermodynamic perturbation theory we would descrbe the excess thermodynamic functions in somewhat general form, which allow us to compare the theoretical results with the experimental.

In the calculation of the thermodynamic quantities of the system of many body particles, there occur cases when the hamiltonian H can be written as $H = H_o + H_1$ where H_1 represents the small terms which

can be neglected in an initial approximation. For instance, we may
regard H_1 as the anharmonic hamiltonian for the vibrations in the
crystal or as the potential energy of the system in an external field
or as the hamiltonian with the symmery which belongs to the subgroup
of the symmetry group which keeps the hamiltonian H_o invariant.

The partition function is

$$Z = \text{Tr } e^{-\beta H} = Z_o <V> \qquad \text{1-12}$$

$$Z_o = \text{Tr } e^{-\beta H_o} \qquad \text{1-13}$$

where $V = e^{\beta H_o} e^{-\beta H}$ and $<V>$ is the average of V with $\rho_o = e^{-\beta H_o}/Z_o$.
The density matrix is

$$\rho = e^{-\beta H}/Z = \rho_o V/<V>. \qquad \text{1-14}$$

The excess Helmholtz energy $A - A_o$ is given by

$$-\beta(A - A_o) = \ln Z - \ln Z_o \qquad \text{1-15}$$

$$= \ln <V>$$

The excess energy $U - U_o$ is

$$U - U_o = \text{Tr } \rho H - \text{Tr } \rho_o H_o \qquad \text{1-16}$$

$$= (<VH_1> + <\Delta V \Delta H_o>)/<V>$$

where the notation $\Delta X = X - <X>$.
The excess entropy $S - S_o$ is given by

$$(S - S_o)/k = -\text{Tr } \rho \ln \rho + \text{Tr } \rho_o \ln \rho_o \qquad \text{1-17}$$

$$= \frac{<V>\ln <V> - <V\ln V>}{<V>} + \beta\frac{<\Delta V \Delta H_o>}{<V>}$$

The excess heat capacity $C_v - C_{v_o}$ is given by

$$(C_v - C_{v_o})/k\beta^2 = \text{Tr}\, \rho(H - \text{Tr}\,\rho H)^2 - \text{Tr}\, \rho_o(H_o - \text{Tr}\,\rho_o H_o)^2 \qquad \text{1-18}$$

$$= <H_o>^2 + \frac{1}{<V>}(<\Delta V \Delta H_o^2> + <VH_o H_1> + <VH_1 H_o> + <VH_1^2>) -$$

$$(\frac{<VH_1> + <VH_o>}{<V>})^2$$

Using the next theorems (Eq. 1-19 and 20), we obtain final formula for the excess thermodynamic functions when $\beta^2 <(\Delta H_1)^2> << 1$.

$$G(\beta) = e^{\beta\Delta H_o}\, e^{-\beta\Delta H}$$

$$G(\beta) = 1 - \int_0^\beta dx\, e^{x\Delta H_o}\, \Delta H_1\, e^{-x\Delta H_o} \qquad \text{1-19}$$

$$B(\beta) = e^{\beta\Delta H_o}\, \Delta H_1\, e^{-\beta\Delta H_o}$$

$$B(\beta) = \Delta H_1 + \int_o^\beta dx\, [\Delta H_o,\, B(x)] \qquad \text{1-20}$$

$$\Delta A = <H_1> - \frac{\beta}{2}<(\Delta H_1)^2> + ..., \qquad \text{1-21}$$

$$\Delta U = <H_1> - \frac{\beta}{2}(<(\Delta H_1)^2 \Delta H_o> + <\Delta(\Delta H_1)^2 \Delta H_1>) + ..., \qquad \text{1-22}$$

$$\Delta S/k = \beta<H_1> + \frac{\beta^2}{2}<(\Delta H_1)^2> - \frac{\beta^3}{2}<\Delta(\Delta H_1)^2\Delta H_o> + ..., \qquad \text{1-23}$$

$$C_v/k\beta^2 = 2<\Delta H_o \Delta H_1> - \frac{\beta^2}{2}<\Delta(\Delta H_1)^2\Delta(H_o + H_1)^2> +$$

$$\beta^2<\Delta(\Delta H_1)^2\Delta(H_o + H_1)><(H_o + H_1)> +.... \qquad \text{1-24}$$

Thus, the first-order correction to the free energy is simply equal to the mean value of the perturing H_1. The second order correction is always negative and is determined by the mean

square deviation of H_1 from its mean value. In particular, if the mean value $\langle H_1 \rangle$ becomes zero then the Helmholtz energy decreases as a result of the perturbation.

When H_1 is the anharmonic term for the vibrations in solids, then $\langle H_1 \rangle$ is evaluated by various authors[45] and is expressed as

$$\langle H_1 \rangle = A_2 T^2 + A_0 + A_{-2} T^{-2}. \qquad\qquad 1\text{-}25$$

The first term is the leading term due to anharmonicity. The anharmonic coefficient A_2 can be determined by the calorimetric results. For example among the alkali halides with the NaCl type structure, lattice vibrations in $RbCl$[46] was found to be most anharmonic.

The vibration of crystal lattices up to this point has been restricted to perpect lattices. Next we pay attention to the thermodynamical properties of the crystals containing impurities and lattice imperfections.

It is well known now that even a small concentration of defects (impuritues) in a crystal can radically alter the frequencies of the normal modes of vibration of the atoms in the crystal and the pattern of the atomic displacements in these modes. For example, the lacalized modes[38] appear in the gaps of forbidden frequencies and in addition to localized modes, so called resonance, or quasi-localized modes[38] can also occur, whose frequencies lie in the bands of allowed frequencies, and which are characterized by a large amplitude of vibration of the impurity atom or of those atoms with which they interact directly. Thus, the resonance modes rather than the localized modes may be reflected in the temperature dependence of the low temperature heat capacity. Especially, metals containing impurities have been primarily examined calorimetrically by several authors.[47]

Thermally activated point defects[48] are present in the equilibrium structure of crystals at non-zero temperature. Atomic motion associated with thermal energy causes atomic coordinates to fluctuate about their time average values, and arbitrary large excursions are, in principle, possible.

Vacancies (Schottky defect) and interstitials (Frenkel defect) may be regarded repectively as solutions of the vacuum and of solvent atoms in the host crystal. When thermal equilibrium is established, the chemical potential μ of these defects must be zero; for the Gibbs energy is

$$G = n_o \mu_o + n\mu \qquad \qquad 1\text{-}26$$

and when $\partial G/\partial n = 0$ we find

$$\mu = g + RT \ln c = 0, \qquad \qquad 1\text{-}27$$

where there are n moles of solute and n_o moles of solvent and g is called the g-function to distinguish it from the chemical potential, c is given by

$$c = n/(n + n_o) = e^{-g/RT} \qquad \text{for Schottky defect,}$$

and

$$c = n/\nu(n_o - n) = e^{-g/RT} \qquad \text{for Frenkel defect,}$$

where ν is the number of interstitial sites per lattice point.

Although $\mu = 0$, G must be less than $G_o = n_o \mu_o^o$ or disorder would not be generated in the perfect crystal; thus $\mu_o < \mu_o^o$, with μ_o^o the chemical potential of atoms in the absence of disorder. This inequality is derived from the equation

$$\mu_o = \mu_o^o + RT \ln (1 - c). \qquad \qquad 1\text{-}28$$

The number of defects changes with temperature during any process

that preserves equilibrium in the real crystal. The heat capacity is given quite generally by

$$C_p = n_o \bar{C}_{po} + (\partial (nh)/\partial T)_p \qquad 1\text{-}29$$

Since n_o is the total amount of atoms present, the excess molar heat capacity is obtained as

$$\Delta C_p = (1/n_o)(\partial (nh)/\partial T)_p$$

$$= (n/n_o)\{(\partial h/\partial T)_p + ((n_o \pm n)/n_o)(h/RT)^2 R\} \qquad 1\text{-}30$$

where the + sign applies to Schottky defect and the − to Frenkel defect. When $n \ll n_o$, then for the both defects

$$\Delta C_p = (n/n_o)\{(\partial h/\partial T)_p + (h/RT)^2 R\} \qquad 1\text{-}31$$

The enthalpy of defect formation h is usually rather temperature independent and h/RT has for a typical order of magnitude the ratio of the cohesive to the thermal energy; the second term in braces therefore dominates the defect heat capacity and

$$\Delta C_p = e^{s/R} R(h/RT) e^{-h/RT} \qquad 1\text{-}32$$

The practical application of this equation will be shown in section 4.3.

Up to this point we have focussed attention chiefly on the noncooperative behavior of the heat capacity. The following section will be concerned with the cooperative effects, which usually give rise to so called λ-type heat capacity anomalies.

Such cooperative anomalies appear in the phase transitions accompanied by the onset of ferromagnetism in the magnetic dipole (spin) system, ferroelectricity in the insulators, superconductivity

in the electronic system, superfluidity in liquid helium, molecular rotation in crystals and order-disorder in binary alloys and so on. Although cooperative phenomena are now known to occur in numerous substances, there exist many cases where the detailed explanation of the cooperative process or transition mechanism is unknown or known only to a limited extent.

Especially, as to the ferroelectric transition phenomena, there are two main theoretical approaches. The first one is the thermodynamical and phenomenological theory which was advanced by Mueller[5] and Devonshire[1] to explain the ferroelectric behaviors in the first and second order transitions and was further developed by Landau[49] and Ginzberg[50] to shed light on the thermal behaviors in more general form. Their approachs are based on the idea that the thermodynamic potential employed is able to be expanded by the order parameters (polarization and strain in the case of ferroelectrics). The validity of analytic expansion was later examined by Pippard, Fisher and others[51] The second one is the lattice dynamical theory suggested by Anderson, Cochran and others[52] to produce ferroelectric polarization in ionic crystals such as $BaTiO_3$. As Aizu[53] and Takagi et al.[54] developed the phenomenological theory combined with the group theory of the ferroelectric transitions of NH_4HSO_4 and $(NH_4)_2SO_4$, their results will be compared with the experiments in Chapter 4.

References to Chapter 1

1) A. F. Devonshire, Phil. Mag. Sappl., $\underline{3}$, 85 (1954).

2) L. A. Shuvalov, J. Phys. Soc. Japan, Suppl., $\underline{28}$, 38 (1969).

3) J. Kobayashi, I. Mizutani, H. Hara, N. Yamada, O. Nakada, A. Kumada, and H. Schmid, J. Phys. Soc. Japan, Suppl., $\underline{28}$, 69 (1969).

4) J. Valasek, Phys. Rev., $\underline{15}$, 537 (1920) and $\underline{17}$, 475 (1921).

5) H. Mueller, Phys. Rev., $\underline{57}$, 829, $\underline{58}$, 565, and $\underline{58}$, 805 (1940).

6) G. Bush and P. Scherrer, Naturewiss., $\underline{23}$, 737 (1935).

7) J. C. Slater, J. Chem. Phys, $\underline{9}$, 16 (1941).

8) A. von Hippel, R. G. Breckenridge, F. G. Chesley, and L. Tisza, Ind. Eng. Chem., $\underline{38}$, 1097 (1946).

   B. Wul and I. M. Goldman, Compt. rend. Acad. Sci. U.R.S.S., $\underline{46}$, 139 (1945).

9) G. Shirane, E. Sawaguchi, and Y. Takagi, Phys. Rev., $\underline{84}$, 476 (1951).

10) B. T. Matthias and J. P. Remeika, Phys. Rev., $\underline{103}$, 262 (1956).

11) R. Pepinsky, K. Vedam, S. Hoshino, and Y. Okaya, Phys. Rev., $\underline{111}$, 1508 (1958).

12) R. Pepinsky, K. Vedam, Phys. Rev., $\underline{117}$, 1502 (1960).

13) A. von Arx and W. Bantle, Helv. Phys. Acta, $\underline{16}$, 211 (1943).

14) W. J. Merz, Phys. Rev., $\underline{76}$, 1221 (1949).

15) M. Kasahara and I. Tatsuzaki, J. Phys. Soc. Japan, $\underline{29}$, 1392 (1970).

16) S. Hoshino, K. Vedam, Y. Okaya, and R. Pepinsky, Phys. Rev., $\underline{112}$, 405 (1958).

17) H. Ohshima and E. Nakamura, J. Phys. Chem. Solids, $\underline{27}$, 481 (1966).

18) H. G. Unruh, Solid State Communications, $\underline{8}$, 1951 (1970).

   H. G. Unruh and U. Rüdiger, J. Phys. (Paris) $\underline{33}$, C2-77 (1972).

19) K. Ogawa, Y. Yamada, I. Taguchi, K. Osaki, T. Watanabe, and I. Nitta, Sci. Rep., Col. Gen. Educ. Osaka Univ.,

20) R. J. Nelmes, Acta Cryst., B27, 272 (1971).

        Presented at the 2nd European Meeting on Ferroelectricity, Dijan (France), Sept. (1971)

        Ferroelectrics, 4, 133 (1972).

        Acta Cryst., A28, 445 (1972).

21) W. G. Mumme, Acta Cryst., B29, 1076 (1973).

22) E. O. Schlemper and W. C. Hamilton, J. Chem. Phys., 44, 4498 (1966).

23) T. Mozume, G. Soda, and H. Chihara, private communication.

24) S. R. Millor, R. Blinc. M. Brenman, and J. S. Waugh, Phys. Rev., 126, 528 (1962).

25) Z. Trontelj and M. Rebic, Solid State Communications, 11, 1337 (1972).

26) M. Kasahara and I. Tastuzaki, J. Phys. Soc. Japan, 37, 167 (1974) and 38, 1389 (1975).

27) A. A. Silvidi, A. J. Falzone and J. L. Roupe, Solid State Communications, 7, 359 (1969).

28) R. Blinc and I. Levstek, J. Phys. Chem. Solids, 12, 295 (1960).

29) D. E. O'Reilly and Tung Tsang, J. Chem. Phys., 46, 1291 (1967).

30) T. P. Myasnikova and A. F. Yatsenko, Soviet Phys. Solid State, 4, 475 (1962).

31) C. J. Schutte and A. M. Heyns, J. Chem. Phys. 52, 864 (1970).

32) B. H. Torrie, C. C. Lin, O. S. Binbrek and A. Anderson, J. Phys. Chem. Solids, 33, 697 (1972).

33) L. D. Landau and E. M. Lifshitz, "Statistical Physics" Chapter 3 Pergamon Press, New York 1958

34) L. Pauling, Phys. Rev., 36, 430 (1930)

35) J. Frenkel, O. Todes, and S. Ismailow, Acta Physicochim. U.R S.S., 1, 97 (1934)

36) W. F. Giauque and R. Wiebe, J. Amer. Chem. Soc., 50, 101 (1928)

37) H. Chihara and A. Inaba, J. Chem. Thermodynamics, 8, 915 (1976)

38) A. A. Maradudin, E. W. Montroll. G. H. Weiss and I. P. Ipatova,

" Solid State Physics" Vol. 4 Academic Press, New York and London

1971

39) M. Born and K. Huang, "Dynamical Theory of Crystal Lattices"

Oxford Univ. Press, London and New York 1954

40) R. E. Peierls, "Quantum Theory of Solids" Chapter 2

Clarendon Press 1955

E. A. Stern, Phys. Rev., 111, 786 (1958)

J, Ranninger, Phys. Rev., 140, A2031 (1965)

41) R. A. Cowly, Rep. Prog. Phys. 31, 123 (1968)

K. N. Pathar, Phys. Rev., 139, A1569 (1965)

W. Cochran and R. A. Cowley, in "Handbuch der Physik" (S. Flugge, ed.),

Vol. XXV, 59 (1967) (Springer, Berlin)

42) D. J. Hooton, Phil. Mag., 46, 422 and 433 (1955)

D. C. Wallace, Phys. Rev., 152, 247 (1966)

P. Choquard, " The Anharmonic Crystal" W. A. Benjamin, Inc., 1967

43) D. J. Hooton, Phil. Mag., 3, 49 (1958)

N. S. Gillis, N. R, Werthamer and T. R. Koehler,

Phys. Rev., 165, 951 (1968)

N. R. Wertharmer, Phys. Rev., B1, 572 (1970)

44) R. E. Nettleton, Z. Physik, 220, 401 (1969)

P. B. Miller and P. C. Kwok, Phys. Rev., 175, 1062 (1968)

45) D. C. Wallece, "Thermodynamics of Crystals" Chapter 4

John Wiley & Sons, Inc. 1972

A. A. Maradudin, P. A. Flinn and R. A. Coldwell-Horsfall,

Ann. Phys.(N.Y.), 15, 337 and 360 (1961)

46) Y. Higashigaki and H. Chihara, Bull. Chem. Soc. Japan, 49, 2089 (1976)

47) J. A. Cape, G. W. Lehman, W. V. Johnston and R. E. DeWames,

Phys. Rev. Lett., 16, 892 (1966)

R. J. Elliott, J. A. Krumhansl and P. L. Peath,

Rev. Mod. Phys., 46, 465 (1974)

48) C. P. Flynn, "Point Defects and Diffusion" Chapter 2

Clarendon Press Oxford 1972

49) L. D. Landau, "Collected Papers of L. D. Landau" edited by D. ter

Haar, No 17 and 29, Pergamon Press 1965

50) V. L. Ginzberg, Soviet Physics– Solid State, 2, 1824 (1960)

51) A. B. Pippard, "Elements of Classical Thermodynamics" Chapter 7

Cambridge Univ. Press, Cambridge 1957

M. E. Fisher, Rep. Prog. Phys., 30, 615 (1967)

C. Domb, Adv. Phys., 9, 149 (1968)

H. E. Stanley, "Introduction to Phase Transitions and Critical

Phenomena" Part V, Clarendon Press Oxford 1971

D. J. Amit, J. Phys. Chem. Solids, 31, 1099 (1970)

52) W. Cochran, Adv. in Phys., 9, 387 (1960) and 10, 401 (1961)

K. K. Kobayashi, J. Phys. Soc. Japan, 24, 497 (1968)

53) K. Aizu, J. Phys. Soc. Japan, 36, 937 (1974)

54) A. Sawada, Y. Takagi and Y. Ishibashi,

J. Phys. Soc. Japan, 34, 748 (1973)

T. Kondo, Y. Ishibashi and Y. Takagi,

J. Phys. Soc. Japan, 39, 1326 (1975)

Table 1.2.1   Crystal Data of NH_4HSO_4

| Phase | Space Group | Z | Cell dimension | | | |
			a (A)	b (A)	c (A)	β (degree)
Phase I[a] (R.T.)	B2₁/a	16	24.904	4.540	14.902	90°18'
	P2₁/c	8	14.511	4.540	14.902	120°18'
Phase II[b] (at -30°C)	Ba	16	24.37	4.62	14.80	~90°
	Pc	8	14.26	4.62	14.80	121°18'
Phase III[a]	B1	16	24.43	4.56	15.15	$\left(\begin{array}{l}\beta = 91°12', \\ \alpha \approx 90°, \ \gamma \approx 90°\end{array}\right.$
	P1	8	14.24	4.56	15.15	$\left(\begin{array}{l}\beta = 123°24' \\ \alpha \approx 90°, \ \gamma \approx 90°\end{array}\right.$
Phase I[b] (R.T.)	B2₁/a	16	24.66	4.60	14.82	89.87°
Phase II[c] (at -70°C)	Ba	16	24.48	4.56	14.75	90.0°

a) Pepinsky and his coworkers, Phys. Rev. 111, 1508 (1958).

b) R. J. Nelmes, Acta Cryst. B27, 272 (1971).

c) R. J. Nelmes, Ferroelectrics, 4, 133 (1972).

Table 1.2.2   Crystal Data of $RbHSO_4$ and $RbDSO_4$

| Phase | Space Group | Z | Cell dimension | | | |
| | | | a | b | c | β |
			A	A	A	degree
Phase I[a)]	$B2_1/a$	16	24.612	4.622	14.807	90°3'
	$P2_1/c$	8	14.356	4.622	14.807	120°59'
Phase II[a)]	Pc	8	----	----	----	----
Phase I[b)]	$P2_1/c$	8	14.354	4.618	14.808	----
Phase I[c)]	$P2_1/c$	8	14.29	4.61	14.76	120.4
Phase I[d)]	$P2_1/c$	8	14.329	4.623	14.808	

a) R. Pepinsky and K. Vedam, Phys. Rev., 117, 1502 (1960).

b) H. Ashmore, unpublished Data.

c) W. G. Mumme, Acta Cryst., B29, 1076 (1973).

d) M. Yamada, Presented at the 28th annual meeting of Physical Society of Japan, 5a-F-5 (1973).

Table 1.2.3   Crystal Data of $(NH_4)_2SO_4$ [a]

Phase	Space Group	Z	Cell dimension			
			a	b	c	V
			$\overset{\circ}{A}$	$\overset{\circ}{A}$	$\overset{\circ}{A}$	$\overset{\circ}{A}{}^3$
Phase I (at 298 K)	Pnam	4	7.782	10.636	5.993	496.0
Phase II (at 180 K)	Pna2$_1$	4	7.837	10.61	5.967	496.2

a) E. O. Shlemper and W. C. Hamilton, J. Chem. Phys., <u>44</u>, 4498 (1966)

Table 1.2.4   Crystal Data of $KHSO_4$ [a]

Space Group	Z	Cell dimension			
		a	b	c	V
		$\overset{\circ}{A}$	$\overset{\circ}{A}$	$\overset{\circ}{A}$	$\overset{\circ}{A}{}^3$
Pbca	16	8.40	9.79	18.93	1557

a) L. H. Loopstra and C. H. MacGillavry, Acta Cryst., <u>11</u>, 349 (1958)
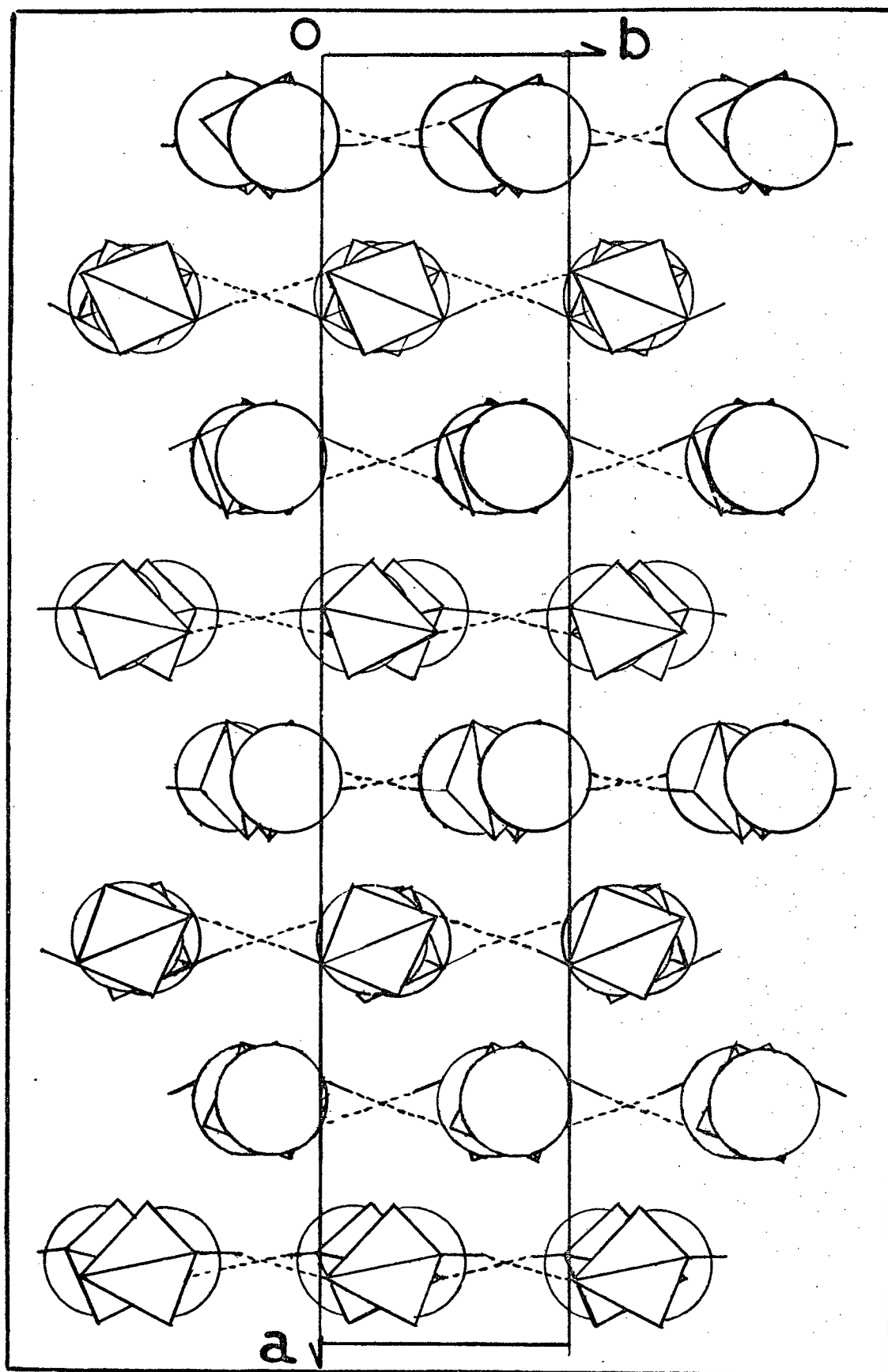
Fig. 1.2.1 An (0 0 1) projection of the structure of NH_4HSO_4 in phase I.
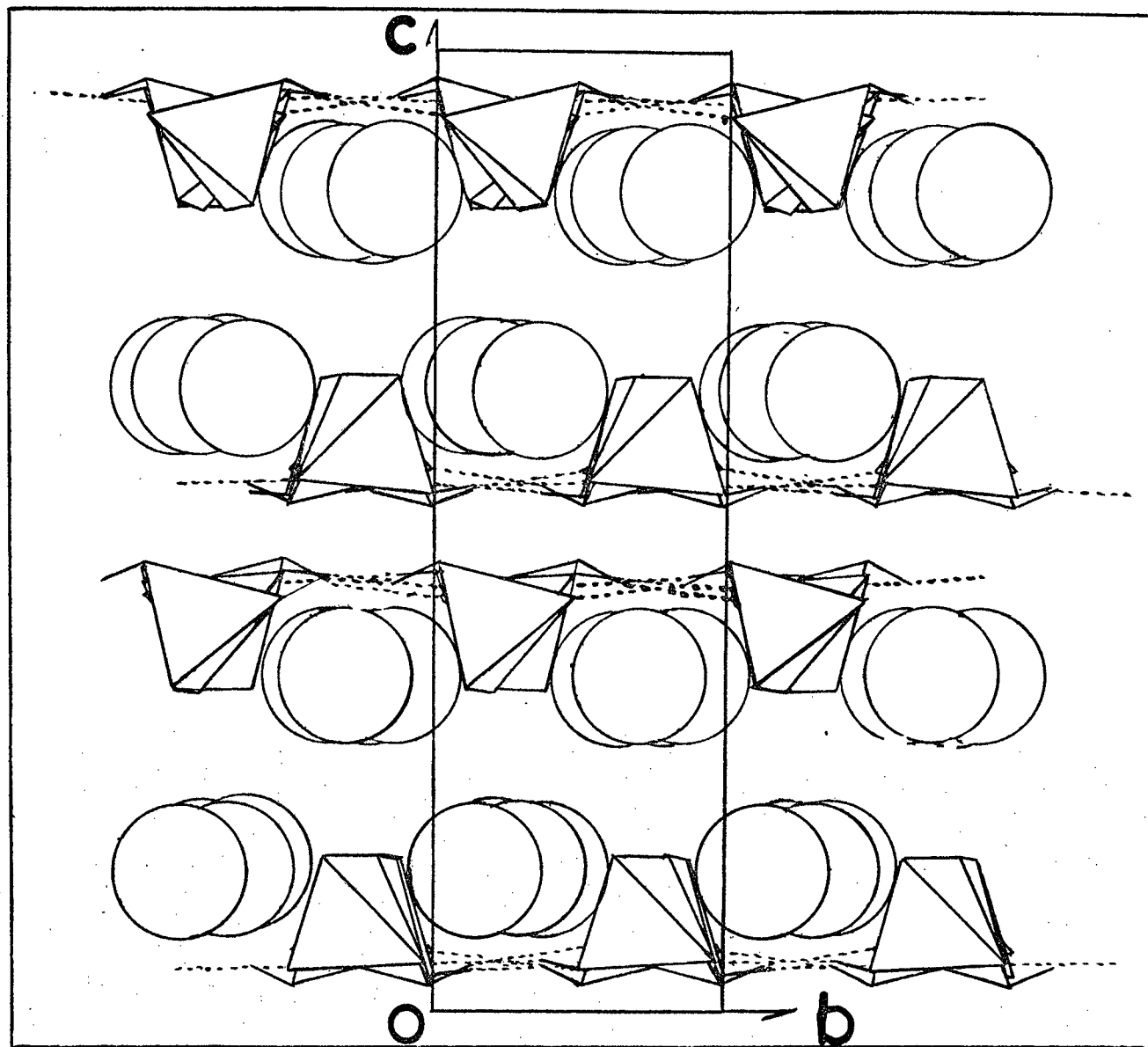
Fig. 1.2.1 A (1 0 0) projection of the structure of NH_4HSO_4 in phase I.
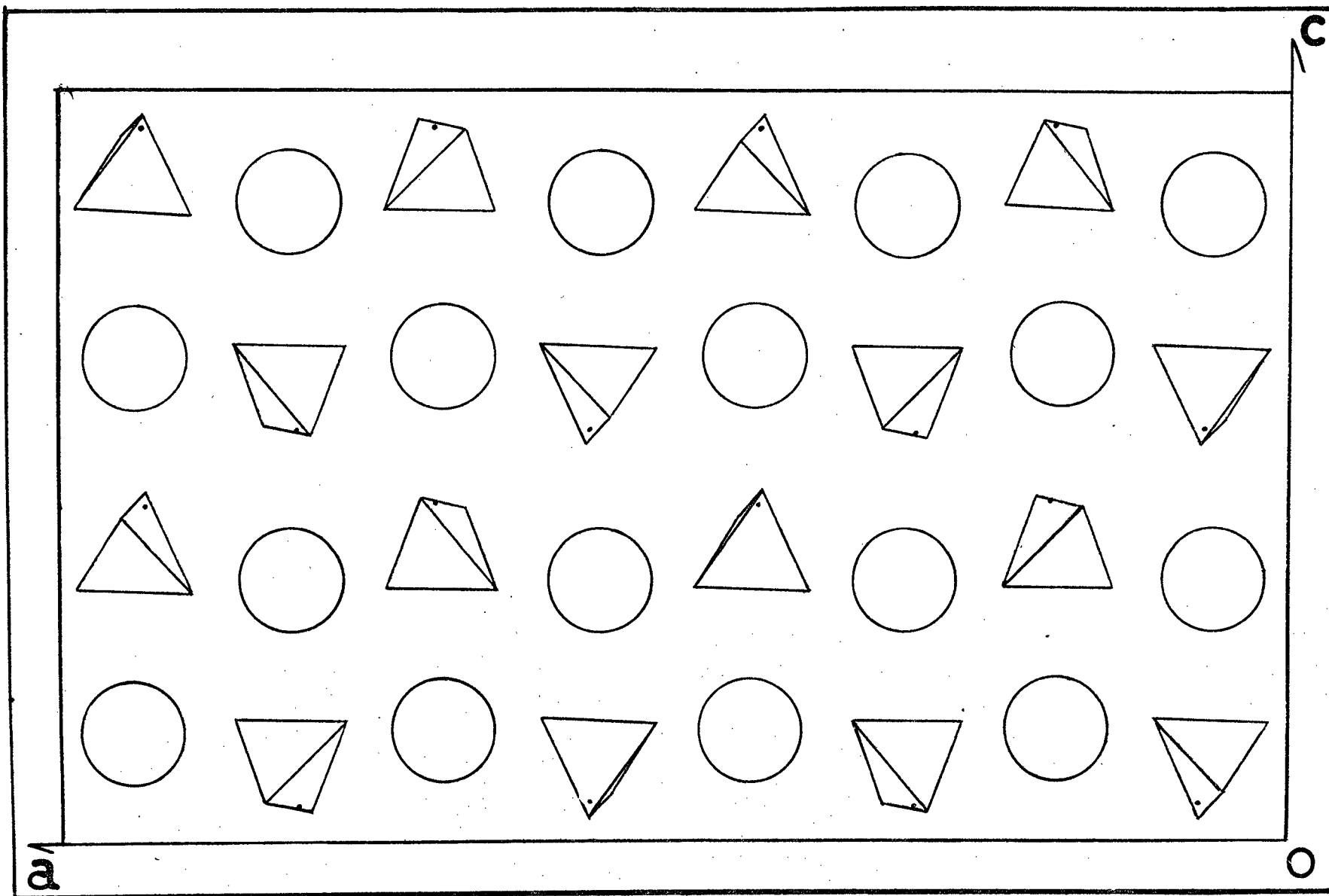
Fig. 1.2.1   An (0 1 0) projection of the structure of NH_4HSO_4 in phase I.

Para. phase

Pnam

Ferro. phase

Pna2₁
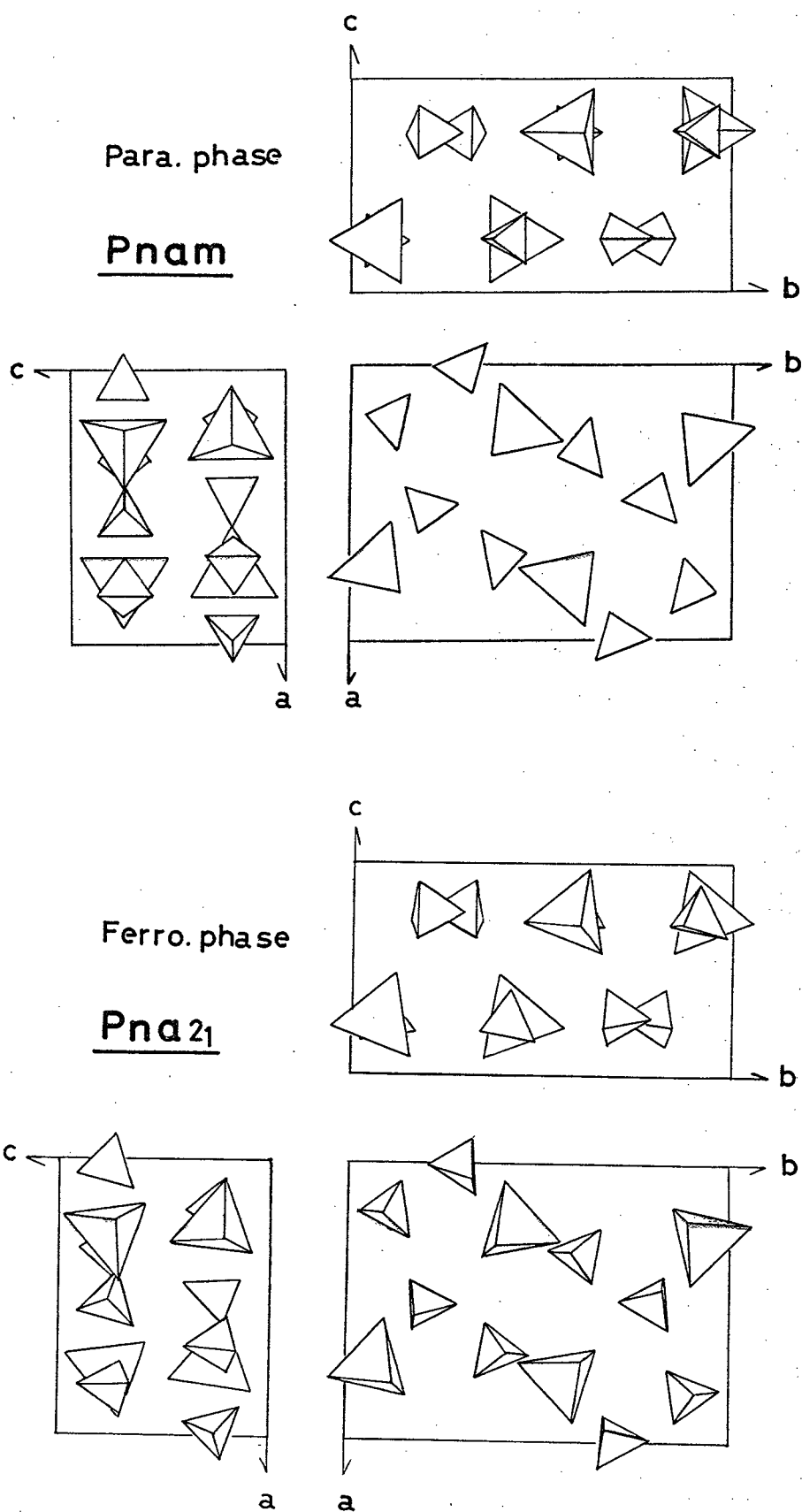
Fig. 1.2.2   Crystal sturcture of $(NH_4)_2SO_4$.
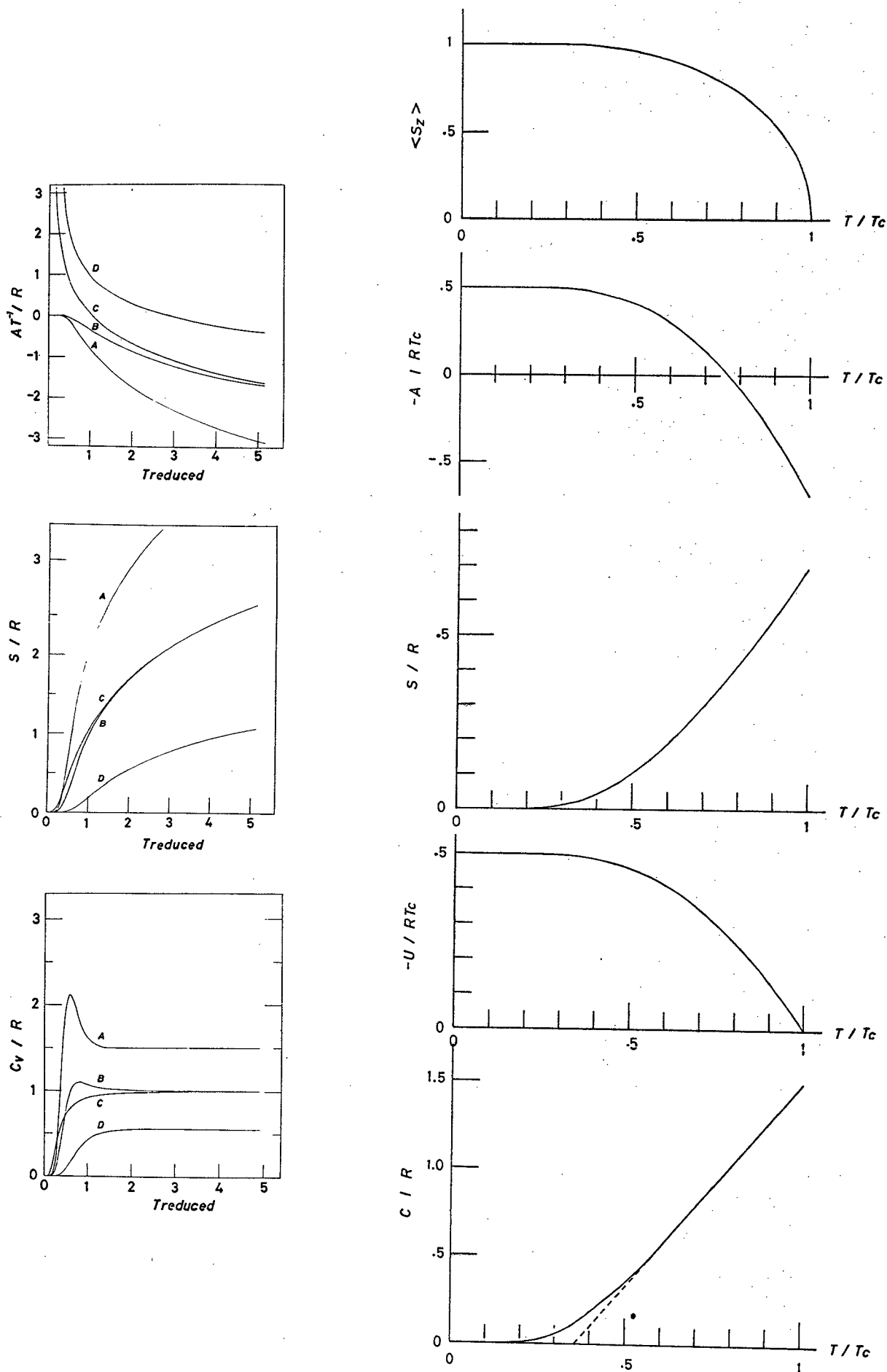
Fig. 1.3.1   Comparison of normal and anomalous thermodynamic behavior.

Chapter 2   Construction of the calorimeter apparatus

2.1   Introduction

Present construction of calorimeter and cryostat is intended to get accurate heat capacity of solids including ferroelectric substances and to be able to measure it up to 60 K, using liquid helium as coolant when liquid hydrogen is not available.

In order to measure the heat capacity at constant pressure it is necessary to measure the heat added on the calorimeter vessel insulated thermally from its surroundings and the temperature change ΔT due to heat input, and to maintain the calorimeter at any desired temperature in the cryostat to observe the temperature dependence of heat capacity. The calorimeter vessel provides not only a container for the sample itself, but also a well-defined part of the apparatus where heat input and the corresponding temperature changes are accurately measured. The general requirements for the vessel are mechanical and chemical stability and good thermal diffusivity, together with high electric insulation and so on. Similarly, constructing the cryostat, similtaneous fulfilment of all the requirements usually required a certain amount of compromise in the design and fabrication.

The newly constructed calorimeter and cryostat proved to satisfy these necessary conditions and its detailed descriptions are given in following sections.

2.2 Calorimeter apparatus

2.2.1 Cryostat

The cryostat made of essentially metallic materials is of adiabatic type and is depicted in Fig. 2.1. The primary function of this cryostat assembly is to maintain the calorimeter vessel at any desired temperature between 2 and 320 K in a state of thermal insulation, so that no heat is virtually exchanged between the calorimeter and its surroundings even when an electrical heater is turned on during measurement.

The entire cryostat assembly suspended in the metal Dewar L on the jack M is fixed at the top plate of the iron frame B with the large cover plate (Brass) A equipped with six pipes (a, b, c, d, e, f) for transfering and pumping on coolants such as liquid nitrogen, hydrogen, and helium and for evacuating two vacuum spaces. Two chromium-plated, brass (1 mm in wall thickness), refrigerant tanks (D and F) for holding liquid nitrogen or hydrogen and helium provide low temperature sinks. (D; internal volume of 609 cm^3, F; internal volume of 1394 cm^3) In order to establish adiabatic conditions heat exchange between the calorimeter and its environment due to gas convection can be eliminated by maintaining a high vacuum (less than 10^{-5} Torr at room temperature) within two vacuum tanks. These tanks consist of outer brass vacuum jacket H (chromium-plated inside and outside, 1.2 mm in wall thickness), and inner vacuum jacket G (chromium-plated inside and outside, 1.0 mm in wall thickness) made of copper to realize thermal homogeneity around the adiabatic shield J, and they are connected with Wood's metal to the top plate C and the tank D called nitrogen can, respectively, and are joined through the stainless steel pipes to the separate evacuation systems equipped with a liquid nitrogen trap, an oil-diffusion pump, a rotary pump and so on.

All the pipes in the cryostat are made of SUS-27 stainless steel (non-plated, non-polished, outer diameter of 9-15 mm, 0.2 mm in wall thickness) with low thermal conductivity and mechanical stability so as to minimize the heat conduction through them between the top of cryostat and the nitrogen can and between the nitrogen can and helium can by means of structurally extendent thermal conduction path.

In this calorimetric design various special precautions are taken to minimize the heat conduction along the electric lead wires. They enter the cryostat through the inlet of leads, which is made of pyrex glass attached on a branch of vacuum line and covered with picein cement. Passing through the evacuation tube, these leads are thermally anchored to the thermal station E, which is attached at the bottom of the nitrogen can and absorb most of the heat conducted down the leads, thus conserving liquid helium. The leads are then anchored to the smaller cylindrical part of the liquid helium can, from which they pass to a floating ring I which equips a non-inductively wound, double silk-insulated mangain wire heater (B.S. # 36) so as to regulate heat conduction between the lower tank and the adiabatic shield. Between each of the stages enumerated, the bundle of leads makes loops supported by nylon and silk threads in a vacuum space to lengthen the heat conduction path. The final tempering of the leads before they reach the calorimeter vessel K is accomplished by placing them on the cylindrical portion of the adiabatic shield wound by the non-inductive heater in a helical grove. The total number of the electric leads including spare wires amounts to 62, and each runs about 12 m from the adiabatic shield to the terminal box outside the cryostat.

All the leads are double silk-insulated copper wires (B.S. # 36) and the bundle of them below the upper tank are protected electrically by the tapes of aluminium foil, which prevent spilled flux (H_3PO_4) from

damaging electric insulation between leads. And all the lead wires are varnished tightly where they are thermally anchored with glyptal lacquer (G.E. adhesive No.7031), taking care to avoid extraneous e.m.f.

Furthermore, the temperature of the upper and lower tanks, the floating ring and the temperature difference between the ring and the top adiabatic shield are monitored and measured with four constantan versus chromel-P thermocouples of which the temperature scale has been calibrated in our laboratory.

2.2.2   Calorimeter vessel and its surroundings

The calorimeter vessel constructed is shown in Fig. 2.2. This vessel is made of copper (0.3 mm in wall thickness) and provided with twelve vertical vanes of thin copper C (0.2 mm in thickness) to aid in the rapid distribution of heat from the heater and in the subsequent reestablishment of thermal equilibrium within the vessel. All the interior and exterior surfaces of this vessel are electroplated with gold to reduce the extent of chemical corrosion and tarnishing. The cap A is connected with Wood's alloy to the inlet for loading a sample, through which the copper pipe (1 mm in diameter) is guided into the branch of vacuum line and sealed off after the helium gas (less than 5 Torr) is added to provide thermal conductivity between the sample and the calorimeter vessel. The platinum resistance thermometer D (Minco Products, Inc., type S 1055-1; calibrated on the IPTS-68, laboratory designation alpha) is connected with solder to the copper holder E, on which the calorimeter heater G (double nylon insulated KARMA wire with a low temperature coefficient of resistance, Driver-Harris Company, B.S. # 36) is wound tightly in a non-inductive fashion and fixed by the G.E. 7031 adhesive. This thermometer-heater assembly is cast in the re-entrant well at the center of the vessel with Wood's alloy to minimize temperature gradients and covered with the

gold-plated radiation plate I at the bottom. The germanium resistence thermometer J (Cryo Cal, Inc., type CR 1000; laboratory designation epsilon) is placed in the copper sheath with high vacuum silicone grease for good thermal contact, the sheath being soldered on to the bottom face. All the leads (double silk insulated copper, B.S. # 36) from the platinum and germanium thermometers and the calorimeter heater are wound and fixed with the G.E. 7031 adhesive on the cylindrical surface to bring them to the temperature of the calorimeter surface prior to their departure in the bundle F. At a third of vessel height each of them is connected to thinner copper wire (Formvar coated, B.S. # 38) to minimize the heat leakage along them. Especially at this place the number of the heater leads increases to three and the heater circuit becomes a four terminal circuit at the side of the adiabatic shield. The purpose of this circuit connection is that the joule energy that occur in the copper wire for the heater is partitioned evenly and also experimentally to the vessel and to the shield. All the lead wires from the calorimeter vessel are bundled and suspended by silk and nylon threads, and make a loop round the vessel (See Fig. 2.4) and amount to 150 cm in length to the terminal point near the side adiabatic shield. One end of thermocouples (gold + 2.1 mole per cent cobalt versus copper) to detect the temperature difference between the vessel and the side adiabatic shield is fixed with glyptal lacquer and covered with thin copper sleeve K, which is soldered to secure good thermal contact with the vessel even at liquid helium temperatures. The other end connected by Wood's alloy to the side shield is also the end of thermocouples of the top and bottom adiabatic shields, which are controlled independently to supply the thermal homogeneity around the vessel. The calorimeter vessel is suspended with four thin nylon threads from the top adiabatic shield.

In order to get a high accuracy in the determination of the sample

heat capacity it is necessary that the tare heat capacity is relatively

small compared with that of the sample over the temperatures measured.

This calorimeter vessel weighs 91 g, including necessary attachments and

its internal volume is 76 cm^3. Two tare heat capacities of present

copper vessel and gold vessel[1] (110 g in weight, internal volume 50 cm^3)

are compared in Fig. 2.3. The copper calorimeter vessel is more suitable

for construction of the vessel with the small tare heat capacity than

the gold one at the lowest temperatures because the Debye characteristic

temperature of copper is twice as high as that of gold. However, as the

atomic weight of copper is about a third of that of gold, the tare capacity

of the copper vessel becomes larger than that of the gold at high temper-

atures according to the Dulong and Petit's law.

2.3   Measurement system

After adiabatic conditions are realized with the electronic control

systems supplying the adiabatic shield heaters with the regulated electric

currents according to the amplified signals from the three differential

thermocouples, the equilibrium temperature of the calorimeter vessel is

measured with the platinum or germanium resistance thermometer in con-

junction with a six-dial double thermofree microvolt potentiometer

(Minneapolis Honeywell Regulator Co., Rubicon Instruments Division,

model 2773). Electrical energy is then supplied with a bank of batteries

to the calorimeter heater installed, in the similar adiabatic conditions

mentioned above. During heating period the voltage and current are

measured with the double potentiometer or with the automatic data

acquisition system. The heating time is determined with an electronic

counter (Takeda Riken Industry Co., Ltd., type TR-124B). Further details

of these circuit systems were described elsewhere.[2,3,4]

2.4   Temperature Scales

2.4.1   Introduction

Thermodynamic temperature scale can be established from experimental measurements of quantities that appear in any Second Law equation. At present the gas thermometer, using the principle of an ideal or perfect gas, is regarded as the primary instrument for realizing the thermodynamic scale in the range from above the gold point at 1337.6 K down to the liquid helium region, to about 1.3 K. At higher temperatures the Planck radiation formula can be used to determine the values of temperature on the thermodynamic scale. At lower temperatures, measurements of the magnetic susceptibility of an ideal paramagnetic salt which obeys the Curie's law or the Curie-Weiss law enable us to determine temperatures.

Accurate measurements of values of temperature on the thermodynamic scale are fraught with experimental difficulties; yet all values of temperature should be traceable to the Kelvin thermodynamic scale. Therefore, "Practical" temperature scales are intended to give values of temperature that are comparatively easily reproduced but are based on functions that are not related to the first and second law of thermodynamics. Among them the International Practical Temperature Scales of 1968 (abbreviated as IPTS-68) was adopted by the Comité International des Poids et Measures at its meeting in October 1968,[5] which is represented by the Standard Platinum Resistance Thermometer (SPRT) exhibiting the prerequisite stability and reproducibility from 10 to 904 K.

At low temperatures, however, the sensitivity, $(1/R)\, dR/dT$, for the platinum is not so high and decreases so rapidly with decrease in temperature. Therefore, other thermometers such as semiconductor devices which show higher sensitivity than platinum thermometers are used to obtain more accurate temperature.

Comparison of temperature scales heretofore proposed is summarized in Table 2.1.

2.4.2 Calibration of platinum resistance thermometers

Four working platinum resistance thermometers (Leeds & Northrup Co., laboratory designation alpha (type 8164) gamma (type 8164) and Minco Products, Inc., laboratory designation alpha (type S 1055-1) and beta (type S 1059-1)) were calibrated against the Leeds & Northrup platinum thermometer (laboratory designation delta (type 8164)) certified at the National Bureau of Standards (U. S. A.), basing on the IPTS-68. Four thermometers were calibrated with a continuous current of 1.0 mA above 50 K and 2.0 mA below 50 K. In order to obtain the IPTS-68 below 0°C, it is necessary to measure the resistance values at eight defining fixed points from 13.81 to 373.15 K. At the neighbourhood of fixed points we measured the resistances of the four thermometers to be calibrated, which were in good thermal contact with copper block (Fig.2.4) in the same location as the calorimeter vessel in the newly-built cryostat, using the electric circuit shown in Fig. 2.5. It took about an hour to measure the resistances of the four thermometers at one temperature near a fixed point. While measuring, the temperature drift of copper block was, on the average, 0.48 mK/min at TP $e-H_2$, 0.034 at BP $e-H_2$, 0.020 at NBP $e-H_2$, 0.008 at NBP Ne, 0.001 at TP O_2, 0.001 at NBP O_2, 0.15 at TP H_2O, 0.17 at NBP H_2O, respectively. The results are given in the Table 2.2. The very resistance value at each fixed point was calculated by the method of least squares, fitting five or more calibration points near the fixed points to a linear function between resistance and temperature, T_{68}, given by the thermometer calibrated at N.B.S. All of the thermometers to be calibrated are found to satisfy the condition for the SPRT: $R(100°C)/R(0°C) \geq 1.3925$. The necessary coefficients for the IPTS-68 below 0°C

were calculated, based on the references,[5,6] and given in Table 2.3, and used to generate the table with which we can calculate the temperature at any resistance by the interpolation method. The error introduced by using linear interpolation will be less than 0.1 mK.

In order to obtain the IPTS-68 above 0°C it is necessary to observe the resistance value at the freezing point of Sn or Zn. These temperature are so high that we cannot realize them in our apparatus. Therefore we are obliged to adopt the trial formula instead of quadratic interpolation formula plus correction function defined in the reference.[5] As we seldom encounter the experiment above the temperature 100°C, the resistance values of thermometers were measured from 255 to 380 K with the temperature interval of 5 K. Observed values both temperatures based on the IPTS-68 and resistances are fitted to the following trial formula:

$$R(t) = R(0) \ [1 + A_5 t + B_5 t^2 + C_5 (t - 100) t^3].$$

Coefficients A_5, B_5, C_5 with which we make the table from 0°C to 100°C are listed in Table 2.3.

Necessary calculations mentioned above were carried out with the FORTRAN programmed by the author and with the high speed electronic computer at Osaka University.

The Leeds & Northrup platinum resistance thermometer (alpha) was calibrated in 1966, based on the IPTS-48 and the provisional NBS-55 temperature scale, and it was recalibrated in 1975, based on the IPTS-68. The IPTS-48 and the NBS-55 can be converted to the IPTS-68 by the reference.[6] The temperature change ($\Delta T = T_{75} - T_{66}$), where T_{75} and T_{66} are based on the IPTS-68, is -90 mK at 14 K, -35 mK at 20 K, -3.8 mK at 50 K, 2.0 mK at 100 K, 7.2 mK at 200 K, 15 mK at 300 K, respectively. The heat capacity values determined by the alpha thermometer calibrated in

1966 is larger by 0.8% at 14 K than that determined with the IPTS-68. And the deviation thus introduced is negligible above 20 K.

The root mean square of fluctuation of temperature is given by[7]

$$\{\overline{(\Delta T)^2}\}^{1/2} = T\{k/C_v\}^{1/2}$$

where k is the Boltzmann constant, C_v the heat capacity at constant temperature of the system whose temperature is measured. As the calibration block used weighs 300 g, the r.m.s. of fluctuation of temperature is 6.2×10^{-9} K at 1 K, 4.9×10^{-11} K at 20 K, and 1.0×10^{-10} K at 300 K. This temperature fluctuation is inherent in the equilibrium state. However, this fluctuation is too small to be detected by the present instruments.

2.4.3   Calibration of germanium thermometers

Four working germanium resistance thermometers (Cryo Cal, Inc., laboratory designation beta, delta, epsilon, zeta (CR 1000)) were calibrated against the germanium thermometer (Cryo Cal, Inc., laboratory designation gamma (CR 1000)) which had been calibrated in this laboratory. Electric circuit for calibration measurement is a circuit similar to the one used for the calibration of platinum thermometers. Resistance value of these germanium thermometers is ca. 1000 Ω at 4.2 K and calibration current of ca. 5 μA was chosen to avoid excessive Joule heating. Measured values of resistance at calibrated temperature are listed in Table 2.4.

In the case of germanium thermometers there does not exist the established functional relationship between temperature and resistance.[8]

$$\log R = \sum_{i=1}^{N} A_i (\log T)^{K+i} \quad ,$$

was used to fit the calibration data. The variance of data, V,

$$(M - 1) \; V^2 = \sum_{i=1}^{M} \left(R_i(\text{observed}) - R_i(\text{smoothed}) \right)^2 \; ,$$

where M is the number of calibration points, and the temperature dependence of the first and second derivatives of log R with respect to log T was used as a measure of fitting. Table 2.5 gives the variance of data of beta and epsilon thermometers. From this table it is found that the larger the initial inverse power becomes and the more the expansion terms are taken, the smaller the variance of data leads to.

However, the temperature dependence of the second derivative appeared wavy when the initial inverse power was larger. Considering the number of data, we may take the initial power as -2 and the number of expansion terms as 10. Table 2.6 gives the coefficients of the trial function thus determined. Fig. 2.6 shows that the deviation of the temperature determined by these four thermometers from the absolute temperature is within 5 mK from 1.8 to 15 K.

2.5   Operation and performance

To begin a series of heat capacity measurement, the calorimeter is first cooled to the desired starting temperature; if necessary, using the upper and/or lower tank filled with liquid and/or solidified refrigerant such as nitrogen, hydrogen, and helium. The calorimeter vessel is cooled rapidly by breaking the vacuum with small amount of helium exchange gas, which is pumped out when the desired temperature is reached. Especially in case of measurement from 2 to 60 K, exchange gas is pumped out at 20 K to maintain a high vacuum and prevent the gas from adsorbing on the vessel. Below 20 K, the vessel is cooled only with the heat conduction along the leads. In present calorimeter design, it took about 3 hr and consumed liquid helium of about 4ℓ to cool the

vessel from 50 K to the lowest temperature of 2 K.

In measuring heat capacity at temperature between 2 and 60 K, liquid helium is used as coolant. When the upper tank is cooled to 50 K by pumping on liquid nitrogen within it, the consumption rate of liquid helium is estimated as follows;[9,10]

heat transfer by radiation
$$\dot{Q} = 17 \text{ mW} \sim 0.020 \text{ } \ell/h$$

heat transfer through the 60 copper leads
$$\dot{Q} = 25 \text{ mW} \sim 0.029 \text{ } \ell/h$$

heat transfer through the three stainless steel pipes
$$\dot{Q} = 42 \text{ mW} \sim 0.049 \text{ } \ell/h$$

Total consumption rate of liquid helium amounts to 0.10 ℓ/hr and the lower tank filled with liquid helium is expected to become empty in 14 hr. In the measurement of heat capacity from 2 to 15 K, however, it took about 6 hr or 10 hr for liquid helium by a single charging to become exhausted depending on whether the upper tank contained solid nitrogen or solid hydrogen. Considering that heat transfer through the leads from the calorimeter vessel is neglected, these holding times are in agreement with the calculated values.

Total consumption rate would be determined primarily by the heat exchange with the top plate through radiation if the present cryostat were not equipped with the upper tank, because the consumption rate due to radiation would then increases to 0.13 ℓ/hr. Thus this vertical cascade type with two refrigerant containers proved to be not only useful in long-run experiment at liquid helium temperature, but also economical of liquid helium.

Using the automatic temperature controllers, the adiabatic shields (and the ring if necessary) are then heated to the temperature of calorimeter to establish adiabatic conditions and prevent further cooling by radiation and conduction along leads. After steady adiabatic conditions have been established, the temperature of the calorimeter is observed at chosen time intervals. Following the determination of the initial temperature, electrical energy is supplied to the calorimeter. After a heating period, the temperature of the calorimeter again is followed as a function of time. These observations establish the final temperature for the heat capacity measurement and the initial temperature for the next measurement of the series.

Equilibration rates of the vessel containing $(ND_4)_2SO_4$ varied greatly. At temperatures below about 20 K, the sample reached equilibrium within a few minutes or within some seconds. At higher temperatures it reached equilibrium within about 15 min., except near the ferroelectric transition temperature. And it took about half an hour for the sample to reach thermodynamic equilibrium at room temperatures.

The curvature correction for the non-linearity of C_p versus T is given approximately by

$$C_p(Tav) \doteq (\Delta H/\Delta T)_p - (1/24)(\Delta T)^2 (d^2 C_p/dT^2)_{T=Tav}$$

where the first term is the observed heat capacity at Tav, ΔT the temperature increment. Thus the energy input was selected in advance to produce a temperature increment small enough to minimize curvature corrections. The temperature rise due to the heating rate of 0.5 K/min at the lowest temperatures and 2.5 K/20 min at room temperatures needed practically no curvature correction except near the transition region.

The accuracy and precision of the heat capacity measurement are

governed by a number of factors such as the validity of the temperature

scale, the accuracy of temperature and energy measurement, the exactness

of adiabaticity, the (physical and chemical) purity of the sample, the

smallness of the ratio of the tare heat capacity to the sample heat

capacity and so on.

The temperature scale used has been described in section 2.3.

The resistance of the platinum and germanium thermometers is measured

potentiometrically by comparison with the reference resistance with good

stability. In measuring, the overall constancy of the working current

and measuring current is realized and supplied with a bank of batteries

and the stable decade resistors. The measurement procedures include

steps to cancel non-IR voltages due to stray e.m.f.. The measurement

error of the resistance of the thermometer can be estimated by

$$|\Delta R/R| \leqq |\Delta EMF1/EMF1| + |\Delta EMF2/EMF2| + |\Delta Rr/Rr|$$

where Rr is the resistance value of the reference resistance, and EMF

the e.m.f. observed. If the reference resistance remains constant, the

0.2 mm error resulted in reading the scale amplified with the galvanometer

corresponds to the uncertainty of the temperature; 0.24 mK at 300 K,

0.16 at 200 K, 0.08 at 100 K, 0.03 at 50 K, 0.05 at 30 K, and 0.38 at

14 K for the platinum thermometer and 0.21 mK at 10 K, and 0.10 at 5 K

for the germanium thermometer. This resolution of temperature results

in the uncertainty of the heat capacity of about 0.05%.

The uncertainty of the energy measurement is about 0.01% and is

not the main factor of inaccuracy and imprecision of heat capacity.

It is not possible to construct a calorimetric system that can be

treated as truly adiabatic at all times and under all conditions. So

detectable heat exchange between calorimeter and shield results from

non-uniform temperature of the shield and calorimeter surfaces, and erroneous thermocouple signals caused by stray e.m.f.'s from inhomogeneities or strains in the thermocouple wires. If heat exchange is significant, the thermocouple signals are suppressed to minimize heat exchange as small as possible. The rate of exchange can be detected by observing the temperature drift of the calorimeter and an appropriate correction is applied, if necessary.

Contribution of the heat capacity of $(ND_4)_2SO_4$ (48.9g) to the total heat capacity was 23% at 2 K, 54% at 10 K, 64% at 30 K, 59% at 100 K, more than 60% above 140 K.

References to chapter 2

1) H. Chihara and M. Nakamura, Bull. Chem. Soc. Jpn., 45, 133 (1972).

2) T. Shinoda, Ph. D. Thesis, Osaka University.

3) T. Atake and H. Chihara, J. Chem. Thermodynamics, 3, 51 (1971).

4) T. Atake and H. Chihara, Bull. Chem. Soc. Jpn., 49, 2126 (1974).

5) Metrologia, 5, 35 (1969).

6) J. L. Riddle, G. T. Furukawa, and H. H. Plumb, Platinum Resistance Thermometry (NBS MONOGRAPH 126) 1973.

7) L. D. Landau and E. M. Lifshitz; Statistical Physics, Chapter 18, Pergamon Press, New York, 1958.

8) T. J. Quinn and J. P. Compton, Rep. Prog. Phys. 38, 151 (1975).

9) G. K. White, Experimental Techniques in Low-Temperature Physics, Clarendon, Oxford (1959).

10) D. C. Ginnings and E. D. West; Principles of Calorimetric Design. In Experimental Thermodynamics, Vol. 1, J. P. McCullough D. W. Scott; editor. Butterworth: London, 1968.

TABLE 2.1   Comparison of temperature scales

	ITS-27	ITS-48	IPTS-48	IPTS-68
$R(100\ ^{\circ}C)/R(0^{\circ}C)$ of Pt.	$\geqq 1.390$	>1.3910	$\geqq 1.3920$	$\geqq 1.3925$
Temperature Range	-190 to $0\ ^{\circ}C$	-182.970 to $0\ ^{\circ}C$	-182.97 to $0\ ^{\circ}C$	13.81 to $273.15\ K$
Interpolating Formula	quartic[a]	quartic[a]	quartic[a]	reference function[c] plus deviation polynomials[d]
Calibration Temperatures	NBP O_2, ice point, NBP H_2O,& NBP S	NBP O_2, ice point, NBP H_2O,& NBP S	NBP O_2, TP H_2O, NBP H_2O,& NBP S or FP Zn	TP e-H_2, BP e-H_2 (25/76atm), NBP e-H_2, NBP Ne, TP O_2, NBP O_2, TP H_2O, NBP H_2O or FP Sn,& FP Zn
Temperature Range	0 to $660\ ^{\circ}C$	0 to $630.5\ ^{\circ}C$	0 to $630.5\ ^{\circ}C$	0 to $630.74\ ^{\circ}C$
Interpolating Formula	quadratic[b]	quadratic[b]	quadratic[b]	quadratic[b] plus correction function[e]
Calibration Temperatures	ice point, NBP H_2O,& NBP S	ice point, NBP H_2O,& NBP S	TP H_2O, NBP H_2O, & NBP S	TP H_2O, NBP H_2O or FP Sn,& FP Zn.

NBP ; normal boiling point

TP ; triple point

FP ; freezing point

a   Quartic interpolation formula : $R(t) = R(0)[1 + At + Bt^2 + C(t-100)t^3]$

b   Qudratic interpolation formula : $R(t) = R(0)(1 + At + Bt^2)$

c   Reference function : $T = \sum_{i=0}^{20} A_i [\ln W*(T)]^i$

    (Values of coefficients A_i are given in the reference[5])

d   Deviation polynomials : $\Delta W(T) = W(T) - W*(T)$

       13.81 to 20.28 K : $\Delta W(T) = A_1 + B_1 T + C_1 T^2 + D_1 T^3$

       20.28 to 54.361 K : $\Delta W(T) = A_2 + B_2 T + C_2 T^2 + D_2 T^3$

       54.361 to 90.188 K : $\Delta W(T) = A_3 + B_3 T + C_3 T^2$

       -182.962 to 0°C : $\Delta W(t) = A_4 t + C_4 t^3 (t - 100°C)$

where $T = t_{68} + 273.15$, $t = t_{68}$, $W* = W_{CCT-68}$, $W(T) = R(T)/R(0°C)$.

e   Quadratic interpolation formula plus correction function :

       $R(t')/R(0) = 1 + At' + Bt'^2$ plus

$$t_{68} = t' + 0.045 \left(\frac{t'}{100°C}\right)\left(\frac{t'}{100°C} - 1\right)$$

$$\left(\frac{t'}{419.58°C} - 1\right)\left(\frac{t'}{630.74°C} - 1\right)$$

TABLE 2.2
The calibration of platinum resistance thermometers
January 1975

	LEEDS & NORTHRUP COMPANY		MINCO PRODUCTS, INC.	
	ALPHA	GAMMA	ALPHA	BETA
TEMPERATURE	RESISTANCE	RESISTANCE	RESISTANCE	RESISTANCE
KELVIN	ABS. OHMS	ABS. OHMS	ABS. OHMS	ABS. OHMS
13.7055	0.031550	0.029694	0.035114	0.134742
13.7443	0.031778	0.029918	0.035352	0.135575
13.8066	0.032166	0.030293	0.035749	0.137075
13.8394	0.032385	0.030488	0.035962	0.137908
13.9003	0.032748	0.030867	0.036334	0.139344
16.9491	0.0595192	0.0575479	0.0635389	0.243930
17.0171	0.0603020	0.0583350	0.0643757	0.247001
17.0272	0.0604130	0.0584489	0.0644664	0.247406
17.1149	0.0614453	0.0594810	0.0655261	0.251348
17.1587	0.0618933	0.0600207	0.0660590	0.253539
20.2305	0.109309	0.107296	0.114500	0.439523
20.2518	0.109724	0.107712	0.114879	0.441119
20.2735	0.110123	0.108124	0.115295	0.442771
20.3096	0.110816	0.108808	0.115999	0.445452
20.3506	0.111627	0.109628	0.116835	0.448674
27.0267	0.304537	0.302444	0.315215	1.213047
27.0709	0.306251	0.304159	0.316893	1.219453
27.1034	0.307531	0.305434	0.318153	1.224547
27.1372	0.308850	0.305675	0.319432	1.229723
27.1797	0.310513	0.308426	0.321108	1.236346
54.30370	2.339746	2.335870	2.392123	9.147390
54.32383	2.341710	2.337832	2.394117	9.155308
54.32801	2.342136	2.338279	2.394553	9.157307
54.36003	2.345332	2.341508	2.397818	9.170018
54.38737	2.348056	2.344226	2.400555	9.180576
54.42182	2.351496	2.347634	2.404019	9.193983
90.10544	6.216150	6.208028	6.332847	24.278315
90.15079	6.221378	6.213251	6.338207	24.298785
90.19217	6.225961	6.217823	6.342864	24.316574

TEMPERATURE	ALPHA RESISTANCE	GAMMA RESISTANCE	ALPHA RESISTANCE	BETA RESISTANCE
KELVIN	ABS. OHMS	ABS. OHMS	ABS. OHMS	ABS. OHMS
90.23882	6.231163	6.222986	6.348163	24.337273
90.27277	6.234904	6.226753	6.351978	24.351467
273.0674	25.539273	25.508113	26.002240	99.684856
273.0883	25.541419	25.510263	26.004285	
273.1004	25.542666	25.511524	26.005962	99.698985
273.1069	25.543300	25.512129	26.006379	99.700536
273.1326			26.009104	99.711639
273.1379	25.546489	25.515363	26.009483	
273.1423	25.546870	25.515738		99.715083
273.1438	25.547091	25.515887	26.010187	99.715323
273.1647	25.549123	25.518031	26.012385	99.724397
273.1682	25.549519	25.518366		99.725217
273.1750			26.013466	99.728418
273.1784	25.550596	25.519451	26.013770	99.728867
273.1803	25.550768	25.519608	26.013798	
273.1929	25.552054	25.520918		99.735234
273.2238	25.555167	25.524041	26.018175	
273.2261	25.555409	25.524294	26.018754	99.748834
273.2289	25.555742	25.524568	26.019025	99.748770
273.2415	25.556965	25.525807		
373.0548	35.570339	35.526967	36.212553	
373.0580				138.82782
373.0877				138.83928
373.1193	35.576772	35.533376	36.219111	
373.1207	35.576767	35.533386	36.218893	
373.1371				138.85828
373.1513	35.579744	35.536323	36.222006	
373.2033	35.584789	35.541501	36.227113	
373.2102				138.88608
373.2458				138.90014
373.2632	35.590848	35.547459	36.233224	

| TEMPERATURE | ALPHA RESISTANCE | GAMMA RESISTANCE | ALPHA RESISTANCE | BETA RESISTANCE |
KELVIN	ABS. OHMS	ABS. OHMS	ABS. OHMS	ABS. OHMS
254.9979	23.693491	23.664555	24.124242	92.480439
260.6227	24.269210	24.239591	24.710052	94.727297
265.0219	24.718767	24.688556	25.167358	96.483102
262.2714	24.744215	24.714004	25.193281	96.580500
270.1475	25.241907	25.211178	25.699906	98.525098
274.9755	25.733893	25.702556	26.200455	100.44490
280.0713	26.252086	26.220069	26.727872	102.466884
285.1085	26.763609	26.731060	27.248393	104.462673
290.0499	27.264775	27.231541	27.758496	106.418327
295.1150	27.777617	27.743773	28.280515	108.42171
300.0217	28.273710	28.239294	28.785874	110.357965
305.0139				112.320125
305.0317	28.744404	28.779425	29.300237	
309.9823	29.278397	29.242743	29.808183	
310.3454				114.418168
314.9984	29.783236	29.74028	30.322515	
315.1271				116.296516
319.9681				118.194365
319.9758	30.283413	30.246616	30.831094	
324.9937	30.787796	30.750372	31.344543	120.162523
329.9870				122.114481
330.0515	31.291600	31.253729	31.857912	
334.9810				124.063943
334.9869	31.987331	31.748847	32.362377	
340.0003	32.288009	32.248909	32.872090	
340.0375				126.034572
345.1017				128.006071
345.0275	32.789380	32.749682	33.382357	
350.0103				130.111776
350.0427	33.288642	33.248370	33.890686	
355.0045	33.782074	33.741186	34.392894	
355.0053				131.851830
360.0109				133.790794
360.0323	34.281329	34.239593	34.900816	
364.9760	34.771308	34.729002	35.399422	
365.0036				135.721714

TEMPERATURE	ALPHA RESISTANCE	GAMMA RESISTANCE	ALPHA RESISTANCE	BETA RESISTANCE
KELVIN	ABS. OHMS	ABS. OHMS	ABS. OHMS	ABS. OHMS
369.9900				137.647321
370.0115	35.269556	35.226578	35.906585	
374.9734	35.759614	35.716048	36.405080	
375.0036				139.580998
380.0387	36.259394	36.215164	36.913756	

TABLE 2.3

	LEEDS & NORTHRUP COMPANY	
	ALPHA	GAMMA
TEMPERATURE	RESISTANCE	RESISTANCE
KELVIN	ABS. OHMS	ABS. OHMS
13.81	0.032192 ± 0.000008	0.030317 ± 0.000006
17.042	0.060585 ± 0.000019	0.058632 ± 0.000011
20.28	0.110259 ± 0.000010	0.108252 ± 0.000010
27.102	0.307475 ± 0.000005	0.305381 ± 0.000007
54.361	2.345307 ± 0.000014	2.341578 ± 0.000023
90.188	6.225464 ± 0.000061	6.217322 ± 0.000062
273.15	25.547685 ± 0.000028	25.516537 ± 0.000025
373.15	35.579672 ± 0.000084	35.553630 ± 0.000070

	ALPHA	GAMMA
$\dfrac{R(100^{\circ}C)}{R(0^{\circ}C)}$	1.392677 ± 0.000004	1.393356 ± 0.000003
A_4	8.0301167×10^{-7}	8.0471366×10^{-7}
C_4	$1.6148580 \times 10^{-14}$	$3.8502564 \times 10^{-15}$
A_3	$-3.8693829 \times 10^{-4}$	$-4.5984204 \times 10^{-4}$
B_3	5.6980083×10^{-6}	6.4086597×10^{-6}
C_3	$-3.0230120 \times 10^{-8}$	$-3.1805442 \times 10^{-8}$
A_2	$-1.4470049 \times 10^{-4}$	$-2.1250598 \times 10^{-4}$
B_2	$-8.0184807 \times 10^{-7}$	$-2.3151180 \times 10^{-6}$
C_2	$-3.7010225 \times 10^{-8}$	3.8059239×10^{-8}
D_2	$8.1632410 \times 10^{-10}$	$1.2723121 \times 10^{-10}$
A_1	$-3.9505916 \times 10^{-5}$	$-1.5404991 \times 10^{-4}$
B_1	$-1.2601418 \times 10^{-5}$	$-3.0987596 \times 10^{-6}$
C_1	3.5933160×10^{-7}	$-3.1105636 \times 10^{-7}$
D_1	$-2.6493368 \times 10^{-9}$	1.2238873×10^{-8}
A_5	3.9867861×10^{-3}	3.9871538×10^{-3}
B_5	$-6.0031146 \times 10^{-7}$	$-6.0370126 \times 10^{-7}$
C_5	$-3.1257391 \times 10^{-13}$	$1.3411406 \times 10^{-13}$

TABLE 2.4

The calibration of germanium resistance thermometers (Cryo Cal, Inc.)

October 1974

	DELTA	EPSILON	ZETA	BETA
TEMPERATURE	RESISTANCE	RESISTANCE	RESISTANCE	RESISTANCE
KELVIN	ABS. OHMS	ABS. OHMS	ABS. OHMS	ABS. OHMS
1.7754	4863.4	7976.9	8548.6	6599.3
1.9912	3763.5	5907.6	6311.0	4941.2
2.3060	2756.2	4106.9	4378.7	3475.1
2.5118	2305.0	3326.7	3543.5	2833.0
2.6483	2078.6	2944.8	3137.5	2516.2
2.8469	1815.4	2505.5	2669.9	2148.6
3.0158	1626.7	2202.0	2350.5	1895.6
3.2390	1428.8	1887.4	2018.6	1628.5
3.4308	1289.7	1669.7	1789.6	1443.0
3.6236	1171.6	1488.5	1600.3	1287.9
4.1554	921.15	1116.8	1211.2	965.50
4.3208	863.04	1031.8	1122.5	891.26
4.5138	799.10	940.95	1027.8	811.31
4.7156	740.52	858.05	941.75	738.95
4.9024	692.20	791.12	872.02	682.06
5.0941	647.85	729.37	807.43	625.40
6.3554	437.31	450.84	514.73	381.70
6.8298	383.67	383.55	442.66	323.61
7.2285	345.80	337.17	392.48	283.89
7.5010	322.57	308.64	361.72	260.18
7.7807	301.133	283.905	333.911	238.851
8.1520	275.817	254.556	301.090	213.635
8.4629	257.008	232.924	277.021	196.205
8.7993	238.468	212.332	253.371	178.966
9.1369	222.330	194.433	232.932	164.17

TABLE 2.3

(Continued)

	MINCO PRODUCTS, INC.	
	ALPHA	BETA
TEMPERATURE	RESISTANCE	RESISTANCE
KELVIN	ABS.OHMS	ABS.OHMS
13.81	0.035770 ± 0.000005	0.137185 ± 0.000037
17.042	0.064656 ± 0.000011	0.248127 ± 0.000076
20.28	0.115440 ± 0.000021	0.443266 ± 0.000036
27.102	0.318103 ± 0.000022	1.224382 ± 0.000135
54.361	2.397891 ± 0.000017	9.170142 ± 0.000187
90.188	6.342356 ± 0.000072	24.314734 ± 0.000322
273.15	26.010799 ± 0.000108	99.718193 ± 0.000423
373.15	36.221944 ± 0.000134	138.863239 ± 0.000026

	ALPHA	BETA
$\dfrac{R(100^{\circ}C)}{R(0^{\circ}C)}$	1.392573 ± 0.000008	1.392557 ± 0.000004
A_4	$-2.3361857 \times 10^{-7}$	$-3.9967867 \times 10^{-7}$
C_4	$-3.6647444 \times 10^{-15}$	$-2.1771610 \times 10^{-14}$
A_3	1.1584273×10^{-3}	$-2.1640101 \times 10^{-4}$
B_3	$-2.4775105 \times 10^{-5}$	5.2314583×10^{-6}
C_3	1.3675917×10^{-7}	$-2.7049714 \times 10^{-8}$
A_2	2.2888385×10^{-4}	$-1.2869972 \times 10^{-3}$
B_2	$-3.9992850 \times 10^{-5}$	1.0762855×10^{-4}
C_2	1.6402976×10^{-6}	$-2.7074933 \times 10^{-6}$
D_2	$-1.6722395 \times 10^{-8}$	2.1321887×10^{-8}
A_1	$-5.8803328 \times 10^{-4}$	$-4.3104896 \times 10^{-3}$
B_1	1.1236588×10^{-4}	7.8447150×10^{-4}
C_1	$-7.4263556 \times 10^{-6}$	$-4.7402943 \times 10^{-5}$
D_1	1.5784284×10^{-7}	9.4203194×10^{-7}
A_5	3.9865149×10^{-3}	3.9860347×10^{-3}
B_5	$-6.0707621 \times 10^{-7}$	$-6.0363763 \times 10^{-7}$
C_5	$1.4363509 \times 10^{-12}$	$-2.5355292 \times 10^{-13}$

TEMPERATURE	DELTA RESISTANCE	EPSILON RESISTANCE	ZETA RESISTANCE	BETA RESISTANCE
KELVIN	ABS. OHMS	ABS. OHMS	ABS. OHMS	ABS. OHMS
9.5417	204.812	175.495	211.011	148.65
9.9406	189.607	159.37	192.105	135.44
10.3201	176.745	146.09	176.344	124.57
10.7085	165.04	134.19	162.08	114.84
11.0886	154.79	123.97	149.74	106.49
11.515	144.57	113.96	137.56	98.329
12.0144	134.04	103.78	125.17	90.090
12.5360	124.43	94.815	113.98	82.722
12.9658	117.43	88.359	105.93	77.442
13.4749	110.02	81.655	97.539	71.968
13.9949	103.32	75.696	90.062	67.062
14.4898	97.6214	70.7186	83.7443	62.9574
14.9391	92.9353	66.6905	78.6319	59.6270

Table 2.5

Variance of Beta Germanium thermometer

NN \ KK	-6	-5	-4	-3	-2	-1	0	1
5	18.38		54.94	30.75	37.99	31.81	13.75	304.75
6	32.99		23.72	20.26	11.45	33.75	8.21	106.86
7	8.76		5.52	1.82	4.10	4.00	2.50	42.06
8	6.40		1.82	1.82	2.10	2.34	2.41	14.60
9	1.22		2.47	2.54	2.55	2.61	2.58	6.12
10	0.59		1.04	1.40	1.80	2.20	2.48	3.60
11	0.76		0.94	1.14	1.38	1.67	2.00	2.63
12	0.48		0.73	0.89	1.09	1.33	1.61	2.00

Variance of Epsilon Germanium thermometer

NN \ KK	-6	-5	-4	-3	-2	-1	0	1
5		154.59	89.44	16.31	35.55	37.04	21.93	367.72
6		8.82	21.20	23.52	18.33	5.85	5.69	133.08
7		11.75	9.30	4.41	3.02	4.11	3.38	53.28
8		5.92	3.33	2.57	2.71	2.93	3.05	17.90
9		2.21	3.10	3.42	3.41	3.38	3.28	7.66
10		1.01	1.33	1.73	2.21	2.71	3.06	4.44
11		1.25	1.38	1.58	1.84	2.16	2.52	3.24
12		0.83	1.02	1.24	1.50	1.80	2.14	2.59

NN: Number of expansion term

KK: Initial power

TABLE 2.6

	BETA	DELTA
A_1	0.4395758484 E + 00	0.3943662741 E + 00
A_2	-0.7641864511 E + 01	-0.7003820100 E + 01
A_3	0.6112943066 E + 01	0.5738853641 E + 02
A_4	-0.2376963065 E + 03	-0.2279950520 E + 03
A_5	0.6021605065 E + 03	0.5918718310 E + 03
A_6	-0.9921608912 E + 03	-0.9972354294 E + 03
A_7	0.1061936876 E + 04	0.1087419481 E + 04
A_8	-0.7154627207 E + 03	-0.7414999821 E + 03
A_9	0.2755354806 E + 03	0.2868440158 E + 03
A_{10}	-0.4611421441 E + 02	-0.4791102747 E + 02

	EPSILON	ZETA
A_1	0.5436522647 E + 00	0.6502644490 E + 00
A_2	-0.9516395821 E + 01	-0.1138149153 E + 02
A_3	0.7581490836 E + 02	0.8979756330 E + 02
A_4	-0.3020390373 E + 03	-0.3604893259 E + 03
A_5	0.7787268084 E + 03	0.9296541209 E + 03
A_6	-0.1305342291 E + 04	-0.1554390146 E + 04
A_7	0.1419303100 E + 04	0.1681325047 E + 04
A_8	-0.9670222693 E + 03	-0.1135699280 E + 04
A_9	0.3743490270 E + 03	0.4344979158 E + 03
A_{10}	-0.6262106112 E + 02	-0.7168708018 E + 02

	BETA	DELTA	EPSILON	ZETA
V/OHM	1.796	1.395	2.214	2.392

$$\log R = \sum_{i=1}^{10} A_i \ (\log T)^{i-3}$$

$$(N - 1) \ V^2 = \sum_{i=1}^{N} (R_i(\text{observed}) - R_i(\text{smoothed}))^2$$

N ; Number of data

a

(d, e, f)

b

c

A

B

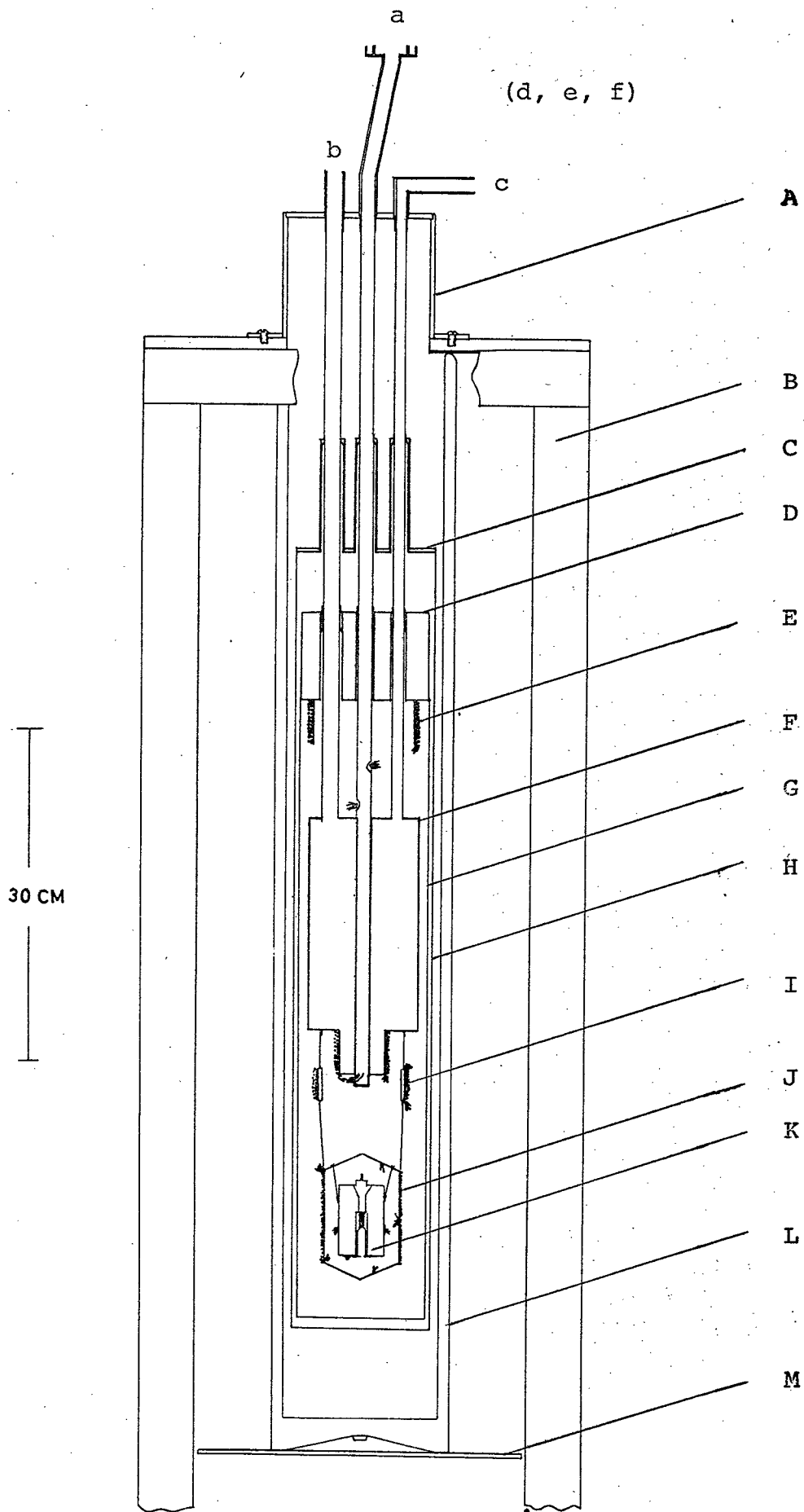C

D

E

F

G

H

I

J

K

L

M

30 CM

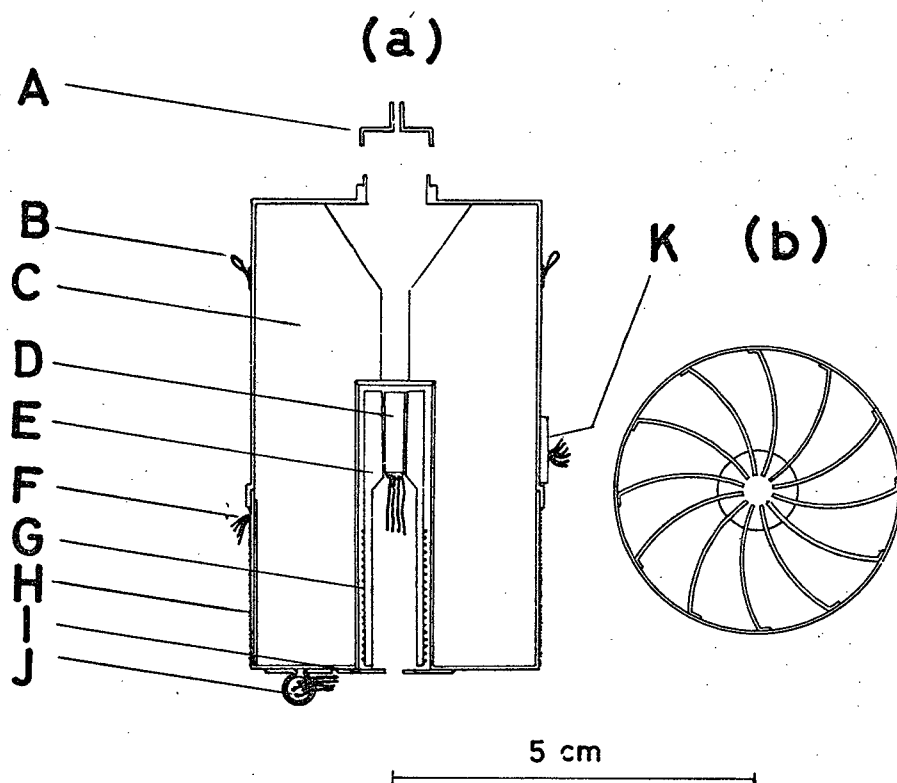Fig. 2.1   SECTIONAL DRAWING OF THE CALORIMETER ASSEMBLY

Fig. 2.2　SECTIONAL DRAWING OF CALORIMETER VESSEL

(a) : vertical　　　(b) : horizontal
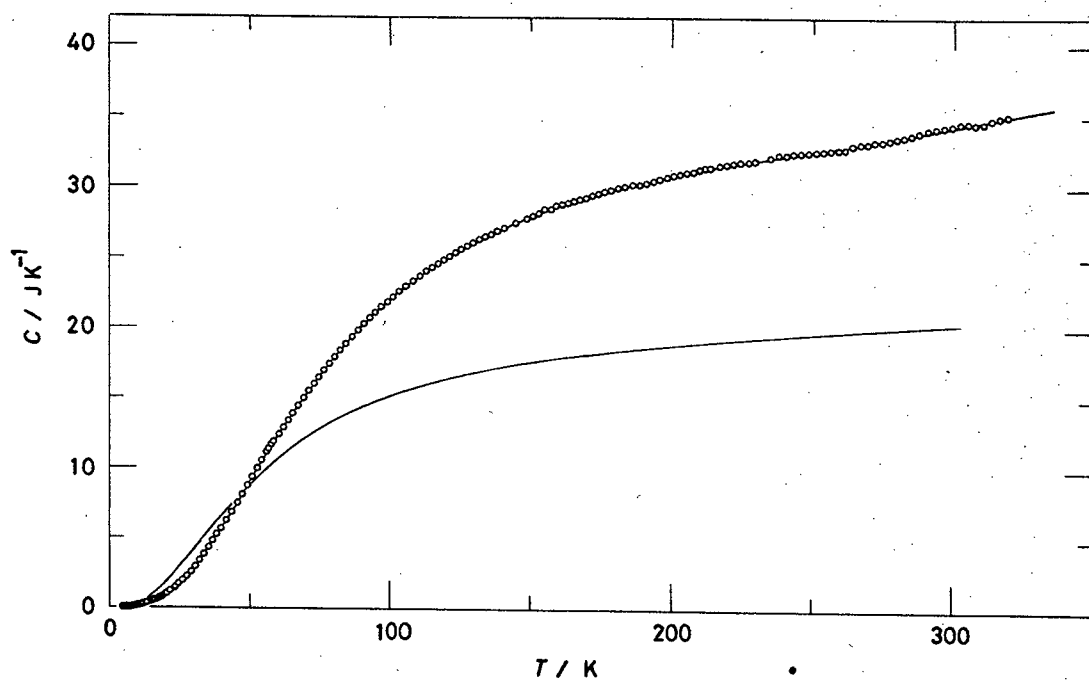

Fig. 2.3　COMPARISON OF TARE HEAT CAPACITY

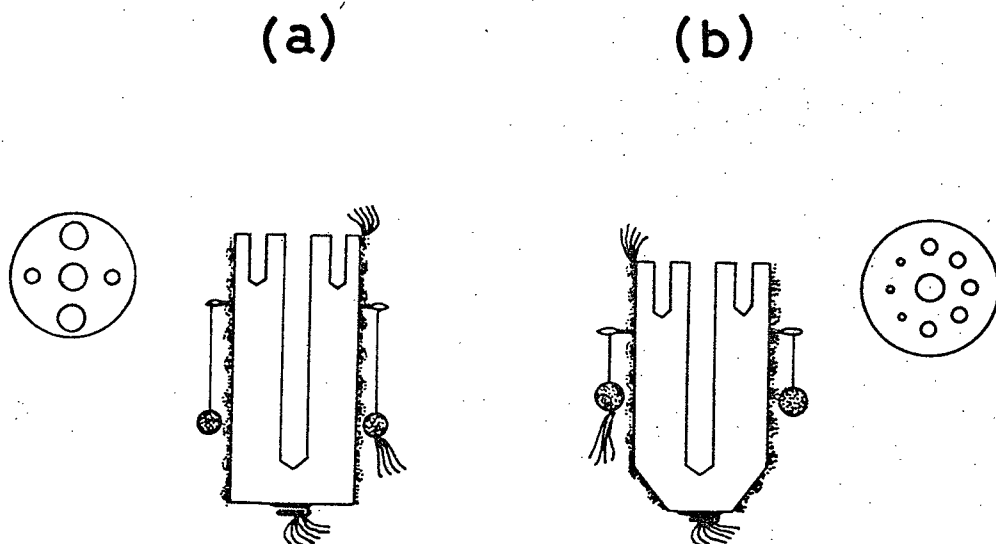(—o—o— ; Present vessel, ——— ; Gold vessel)

Fig. 2.4   COPPER BLOCK FOR CALIBRATION

(a) platinum thermometer   (b) germanium thermometer
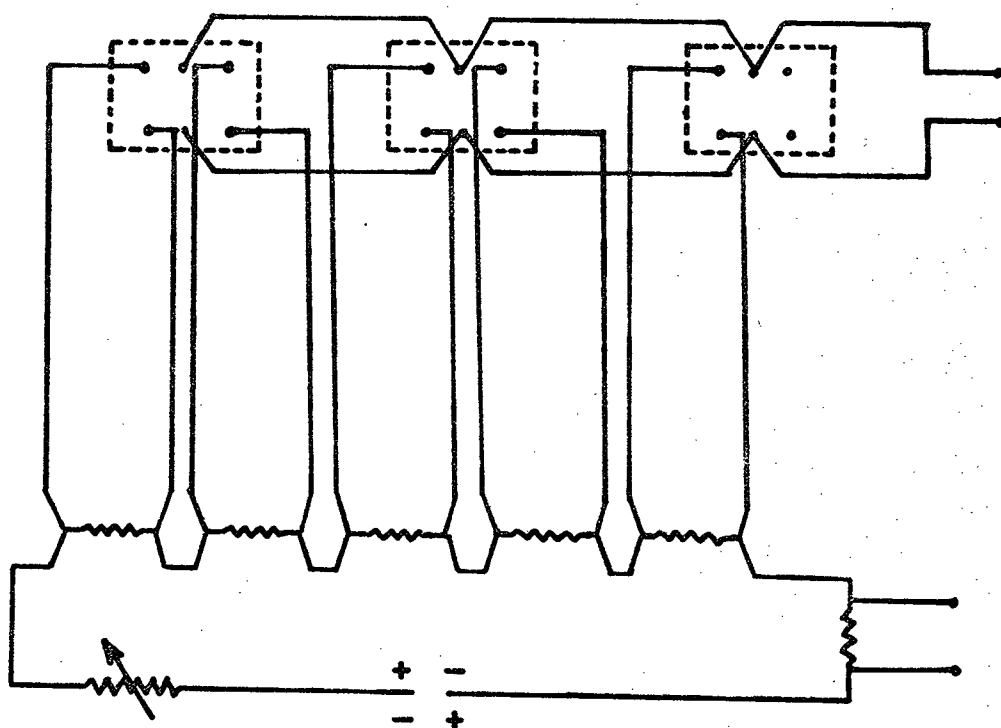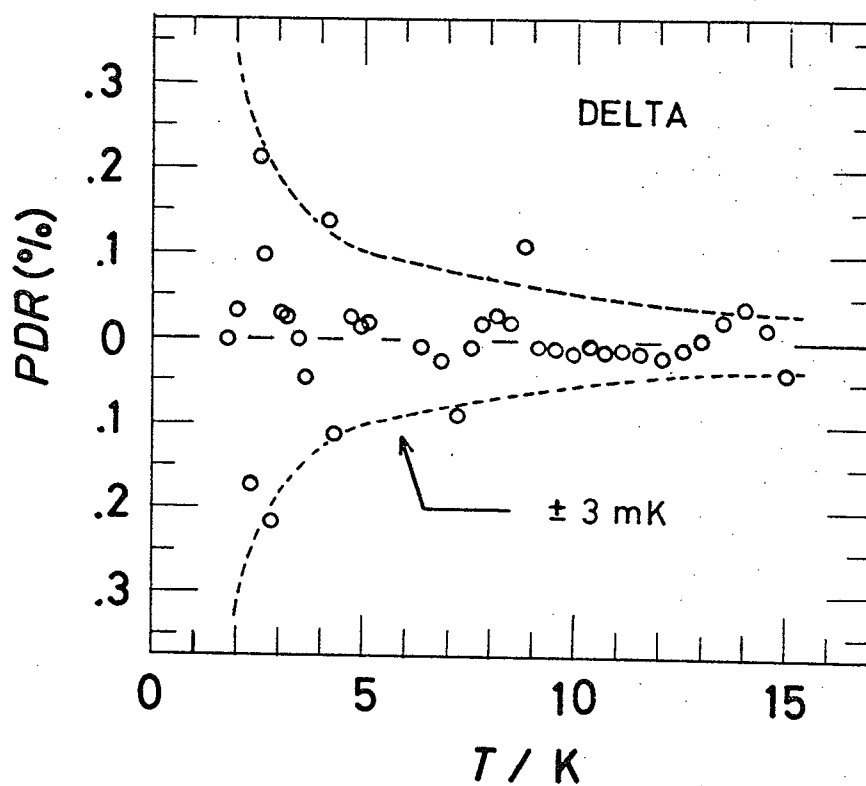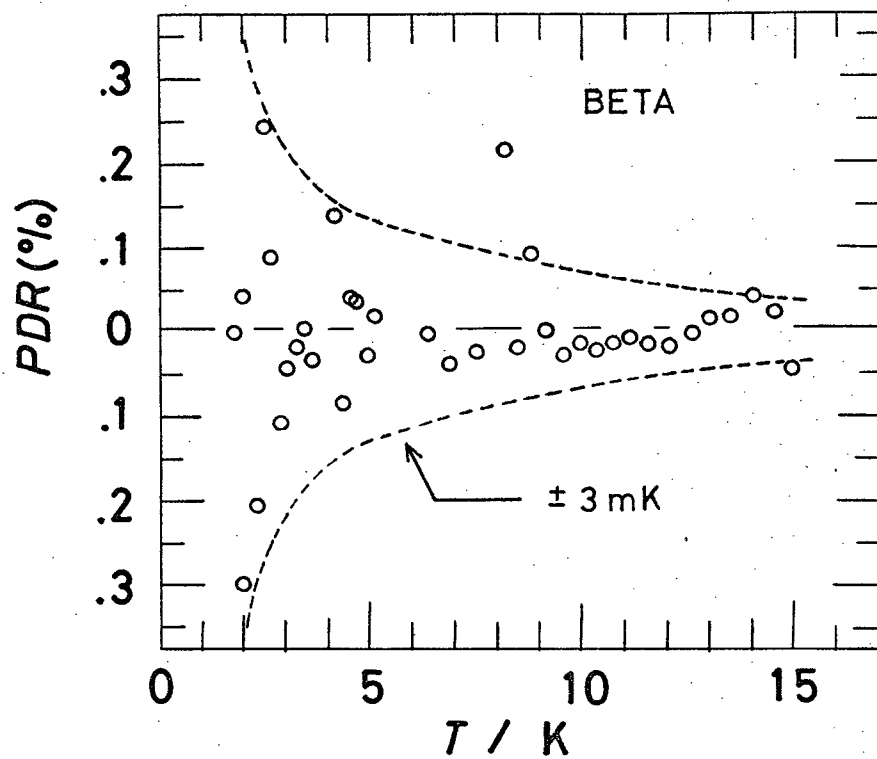

Fig. 2.5   ELECTRIC CIRCUIT FOR CALIBRATION

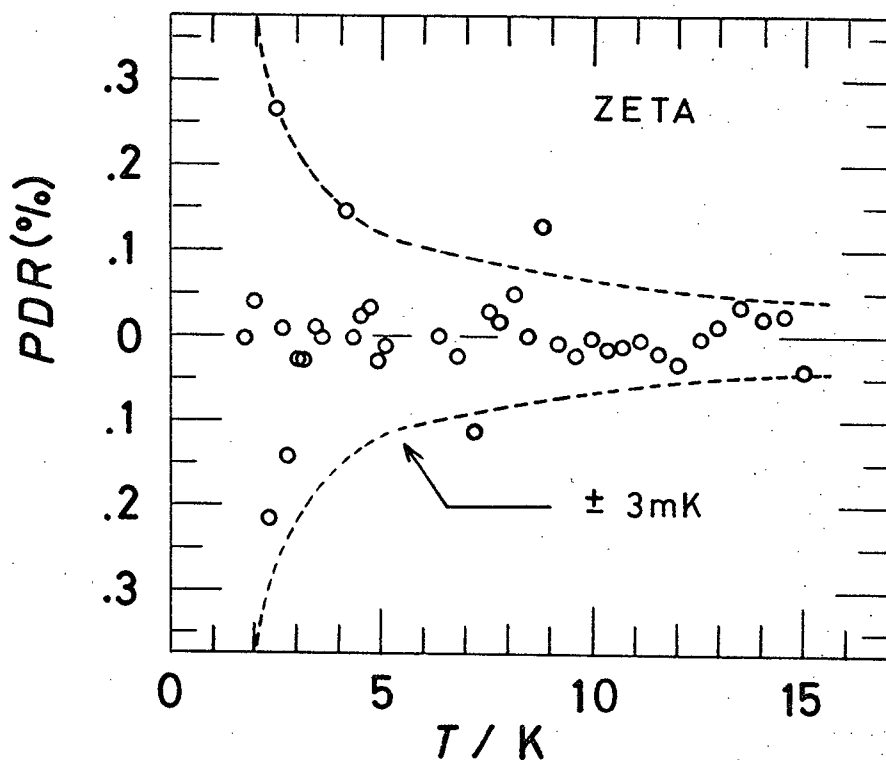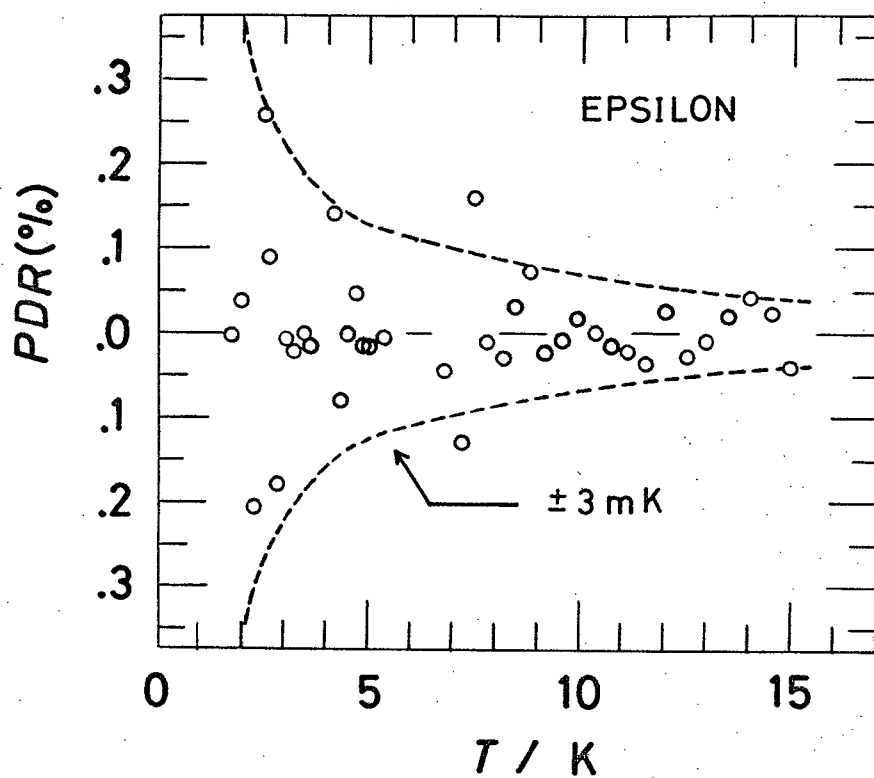Fig. 2.6   PERCENT DEVIATION OF RESISTANCE FROM THE

SMOOTHED CURVE

Fig. 2.6   PERCENT DEVIATION OF RESISTANCE FROM
THE SMOOTHED CURVE

Chapter 3   Experimental and Results

3.1   Preparations of calorimetric specimens

3.1.1   Preparation of NH_4HSO_4

To prepare NH_4HSO_4 as the calorimetric sample two different procedures were taken. The first one was the method[1] proposed by Pepinsky, et al., who used the following chemical reaction;

$$CH_2ClCONH_2 + H_2SO_4 \xrightarrow[\text{Hydrolysis}]{+H_2O} NH_4HSO_4 + CH_2ClCOOH$$
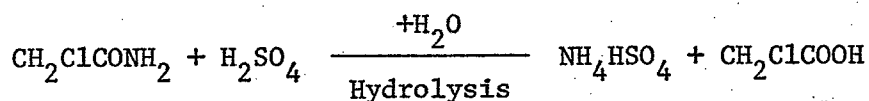
Recrystalized $CH_2ClCONH_2$ (52 g) was dissolved in distilled water (150 ml) and hydrolyzed slowly in an ice bath with dilute H_2SO_4 (350 ml), the equivalent amount of $CH_2ClCONH_2$ used. Extra water and by-product, $CH_2ClCOOH$, were removed from solution by vacuum distillation, and then the sample thus obtained was washed over a glass filter with a large amount of EtOH to remove the by-product completely, and then dried over silica gel in the evacuated desiccator for two days. The DTA thermogram of this sample is shown in Fig. 3.1.2, where a small endothermic peak due to $(NH_4)_2SO_4$ appeared and the lower melting point ($Tm = 407$ K) than the reported value (417 K)[2] was found. This low melting point may be ascribed to presence of small amount of $CH_2ClCOOH$ ($Tm = 335$ K). Subsequent washing with EtOH led to an increase of $(NH_4)_2SO_4$ content in NH_4HSO_4, shown in Fig. 3.1.2. Instead of EtOH,[3] $(Me)_2CO$ and MeCOOEt were then used to separate $CH_2ClCOOH$ impurity from solid sample but high hydroscopicity of NH_4HSO_4 did not allow repeated washings with such solvents.

It seemed difficult to prepare the sample of high purity from the above chemical reaction. So another procedure was taken. The sample used for calorimetry was prepared according to the ternary system of $(NH_4)_2SO_4$, H_2SO_4, and H_2O.[4] Thus, 119 g of $(NH_4)_2SO_4$ (recrystalized

once, Nakarai Chemicals, Ltd.), 151 ml of concentrated H_2SO_4, and 74 ml of distilled water were mixed in a flask and warmed in an oil bath, equipped with a conventional temperature controller, to 70°C, where this mixture became transparent, and then cooled down to 30°C along the solubility curve of NH_4HSO_4 in the phase diagram of these three components.

Precipitated crystals were washed with freshly dried Et_2O to remove extra free acid and water attached on their surfaces. (See Fig. 3.1.1). Sample thus handled was dried in vacuo and then its purity was checked by the DTA and elemental analysis. When any extraneous heat anomaly due to impurity such as $H_2SO_4 \cdot 2H_2O$ ($Tm = 234$ K) appeared on the DTA thermogram from 100 K to above melting point, further purification procedures mentioned above were repeated. The final results of elemental analysis for the calorimetric sample were $S = 27.8 \pm 0.2$ % (27.85), $N = 12.1 \pm 0.2$ % (12.17), $H = 4.6 \pm 0.3$ % (4.4), respectively, where calculated values are given in parentheses. Taking into account of hydroscopic nature, the powder samples were put in the calorimeter vessel in a dry box filled with dried nitrogen gas. Weight of specimen used was 47.2837 g (in vacuo), amounting to 0.41079 mol.

3.1.2   Preparation of $RbHSO_4$

Calorimetric sample of $RbHSO_4$ was first prepared by slow evaporation of equimolar aqueous solution Rb_2SO_4 and H_2SO_4.[5] Crystals so obtained, however, showed a small heat anomaly just below its melting point ($Tm = 482.5$ K), approximately 2.0 % in area of the melting peak on the DTA thermogram (Fig. 3.1.3). This small peak was not reduced by washing crystals with Et_2O. Elemental analysis gave $S = 17.21$ %, somewhat lower than the calculated value $S = 17.56$ %. This sample was not used for calorimetry because presence of such a peak was open to questioning.

Though no phase diagram has been reported of the ternary system: Rb_2SO_4 – H_2SO_4 – H_2O, we prepared $RbHSO_4$ from the above system, assuming that it would be similar to the ternary system: K_2SO_4 – H_2SO_4 – H_2O.[4] The transparent aqueous solution with Rb_2SO_4 (83 g, Nakarai, Chemicals, Ltd.) and concentrated H_2SO_4 (46 ml) and distilled water (66 ml) is cooled down to room temperature in a pyrex flask. Precipitated crystals were purified by the apparatus shown in Fig. 3.1.1, using following reactions:

$$2H_2O + CaH_2 = Ca(OH)_2 + H_2$$

$$H_2SO_4 + CaH_2 = CaSO_4 + 2H_2$$
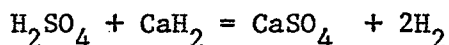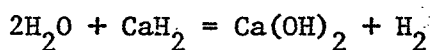
$RbHSO_4$ used for the calorimetry showed no anomalous behavior near the melting point (Tm = 486.8 K) on the DTA thermogram and was characterized by elemental analysis as S = 17.50 = 0.04 %. Weight of specimen used for heat capacity measurements was 72.2473 g (in vacuo), amounting to 0.39580 mol.

3.1.3   Preparation of $RbDSO_4$

$RbDSO_4$ was prepared by using the $KHSO_4$ solubility curve in the ternary system: K_2SO_4 – H_2SO_4 – H_2O,[4] in a way analogous to the preparation of $RbHSO_4$. Recrystallized Rb_2SO_4 (67 g, Nakarai Chemicals, Ltd.) was dissolved in D_2SO_4 (Merk, 99.7 % D(claimed)) in a pyrex flask, into which degassed D_2O (74 ml, Merk, 99.75 % D (claimed)) was introduced by vacuum distillation. Precipitated crystals were washed quickly with freshly dried Et_2O on a glass filter and washed in the reflux assembly (Fig. 3.1.1) for 8 h. The DTA thermogram of the sample dried under vacuum is given in Fig. 3.1.3, which shows that two small peaks appear at 258.7 K and at 249.7 K both on cooling and on heating and coalesce at 252.9 K after passing its melting point (Tm = 482.3 K). Elemental

analysis of this sample gave S = 17.40 % (Calculated value 17.47 %) and the integral intensity of high resolution NMR (AD-60, Varian Associats) showed 99.4 % D. The peak at 258.7 K may be correlated to the anomalous diffuse scattering of neutrons at 258 K.[6] Being subject to several drying procedures under vacuum, the upper peak shifted upwards but the lower remained practically constant. In this connection the peak area of a broad endothermic anomaly from 373 to 397 K, which appeared only on a high sensitive DTA thermogram, diminished but did not disappear completely. To examine whether the two peaks were doubtful or not, sample thus obtained was dissolved in previous mother liquor once more, in which small amounts of D_2SO_4 and D_2O were added to compensate. $RbDSO_4$ so recrystallized was used as calorimetric specimen, which was characterized as 17.48 % sulfur and 99.1 % deuterium isotope, and showed T_m = 484 K, higher than previous one. The powder samples were transfered into the calorimeter vessel in a drybox to exclude atmospheric moisture. Weight of specimen used was 54.6592 g (in vacuo), corresponding to 0.29781 mol.

3.1.4   Preparation of $(ND_4)_2SO_4$

$(NH_4)_2SO_4$ (Nakarai Chemicals, Ltd.) was first recrystallized in distilled water and dried under vacuum. The hydrogens of recrystallized $(NH_4)_2SO_4$ (75 g) were replaced by deuteriums of heavy water. The degassed heavy water with various deuterium concentrations (48.1 % 99.83 %) was transfered in vacuum line to prevent pick-up of atmospheric water and then aqueous solution was evaporated to dryness in the Dewar filled with hot water. The deuterium concentration of water distilled was monitored with the high resolution NMR at each substitution step. Water distilled

at the final step was estimated to be 99.6 % deuterium substitution.
$(ND_4)_2SO_4$ thus obtained showed small heat anomaly above the large
ferroelectric transition at -50°C on the DTA thermogram, which is likely
to be due to D_2O occluded in $(ND_4)_2SO_4$. These crystals were pulverized
and warmed to 80°C under vacuum but this small peak did not disappear
completely. So $(ND_4)_2SO_4$ crystals were dissolved in D_2O again and
recrystallized on slow cooling and separated from the solution by
filtration, and dried under vacuum. $(ND_4)_2SO_4$ thus purified also gave
a smaller heat anomaly at the same temperature as before, which dis-
appeared on the several thermal cycles between room temperature and
liquid nitrogen temperature. Deuterium content of this sample was
determined to be 99.3 % from the D content in the distilled water of
mother liquor. Elemental analysis gave N = 19.90 % (19.98), S = 22.95 %
(22.87). The powder samples were put into the gold-plated cupper vessel
in a conventional dry box. Weight of specimen used for calorimetry was
48.6682 g (in vacuo), amounting to 0.34717 mol.

3.1.5   Preparation of ND_4DSO_4

The deuterium analog of NH_4HSO_4 was prepared from the transparent
solution with three components, $(ND_4)_2SO_4$ (99.1 % deuterium substitution
of $(NH_4)_2SO_4$, 118 g), D_2SO_4 (Merk, 99.1 % D (claimed), 120 ml) and D_2O
(CEA, 99.83 % D (claimed), 83 ml). The vacuum-distilled D_2O from mother
liquor was 99.4 % D, the value of which was determined from the integral
intensity of high resolution NMR. The precipitated crystals were at
first separated by filtration in an evacuated desiccator in three days
and washed quickly in glass filter with distilled Et_2O (200 ml) freshly
dried with CaH_2. Crystals dried under vacuum gave the results of

elemental analysis of N = 14.4 %, and S = 22.6 % and the DTA thermogram shown in Fig. 3.1.2, where a small peak at 232 K was likely to be due to the melting of $D_2SO_4 \cdot 2D_2O$. Subsequent purification procedure similar to the case of NH_4HSO_4 was taken. Final analysis, found: N = 11.6 %, and S = 26.8 %, calculated: N = 11.7 % and S = 26.7 %. The DTA thermogram of the calorimetric sample was shown in Fig. 3.1.2, where no extraneous peak appeared from 110 K to the temperatures above Tm = 416.4K. The powder samples thus obtained were put in the calorimeter vessel in a conventional dry box. The sample used for heat capacity measurements weighed 48.7977 g (in vacuo), corresponding to 0.40619 mol.

3.2 Heat capacity measurements and results

3.2.1 Heat capacity measurements of NH_4HSO_4

Calorimeter and Cryostat   The calorimeter and cryostat used for the heat capacity measurement of NH_4HSO_4 was of adiabatic type, which has been reported elsewhere.[7,8] Helium exchange gas was put into the calorimeter vessel to aid in thermal equilibration within it.   In the series from I to XVIII the vessel contained 3.5×10^{-4} mol of helium gas and 1.1×10^{-5} mol in the series from XIX to XXI.   Correction for the difference in the amount of the exchange gas was made in calculating heat capacity values.

Temperature Scales   The working thermometer above 14 K was the Leeds & Northrup platinum resistance thermometer (model 8164, laboratry designation α), the temperature scale of which was based on the IPTS-68.   Below 15 K the working thermometer was the germanium

resistance thermometer (CR-1000, CryoCal, Inc., laboratry designation β). The detailed procedures of calibration of both platinum and germanium resistance thermometers were described in Chapter 2.

Calorimetric Results   Molar heat capacity values of NH_4HSO_4 had been first determined on the IPTS-48 and the provisional NBS-55 scales and were later converted to the IPTS-68 and are listed in Table 3.2.1 in chronological sequence so that temperature increments usually can be approximately deduced from the adjacent mean temperatures.   The temperature dependence of the heat capacity is shown in Fig. 3.2.1.   The temperature rise in each measurement was small and therefore no curvature correction was necessary except in the transition region.   For example, curvature correction amounted to -0.2 % at 10 K, corresponding to about a tenth of the experimental error (precision) and decreasing to less than 0.08 % above 100 K.   The heat capacity of the sample itself was 50 % of the total at 4 K and exceeded 60 % above 20 K.   Scatter of the measurements was within 5 % below 15 K, decreasing to 0.6 % above 20 K except in the transition region (Fig. 3.2.2).   Thermodynamic functions of NH_4HSO_4 based on the smoothed heat capacity curve are given at selected temperatures in Table 3.2.2.   The entropies, enthalpies, and Gibbs functions have not been adjusted for nuclear spin and isotope mixing contributions, and hence are practical values for use in chemical thermodynamic calculations.   Our results are compared with the results reported by two different groups of authors in Fig. 3.2.3.   The results of Pepinsky, et al. are higher than our smoothed values by about 15 % at almost all temperatures measured and, furthermore, their results suggest that the lower transition appeared as if there were two consecutive heat anomalies.   Strukov and Danilysheva measured the heat capacity at only limited temperatures between 205 and 240 K and between

260 and 285 K, which deviated from ours by -10 % at room temperature.

These disagreements may be attributed the difference of not only purity

of the sample but also accuracy of measurements.

3.2.2   Heat capacity measurement of RbHSO$_4$

Calorimeter and Cryostat   The calorimeter was of adiabatic type,

the description of which has been reported elesewhere.[7,8] Helium

exchange gas less than 9.4 × 10^{-6} mol was used to enhance thermal contact

between the sample and calorimeter. No correction was made for the

presence of the exchange gas in calculating the heat capacity values.

Temperature Scales   The working thermometer above 14 K was the

platinum resistance thermometer (Model 8164, Leeds & Northrup Co.,

laboratory designation α), the temperature scale of which was fixed by

comparison with another thermometer (Model 8164, laboratory designation δ)

calibrated at the U. S. National Bureau of Standards, based on the IPTS-

68. Below 15 K the thermometer was the germanium resistance thermometer

CCR-1000, CryoCal, Inc., laboratory designation β), which had been

calibrated in our laboratory. (See chapter 2)

Calorimetric results   The experimental heat capacities for

RbHSO$_4$ are presented in chronological sequence at the mean temperatures

of determination in Table 3.2.3 and are illustrated in Fig. 3.2.4.

Temperature increments employed in the measurements were small and

therefore curvature corrections were not applied, but may be computed

from Table 3.2.3 since each series is a result of continuous measurements.

The heat capacity of the sample itself was more than 63 % of the total

in the whole region of temperature measured. Scatter of the measurements,

as shown in Fig. 3.2.5, was within 8 % below 15 K, decreasing to 0.6 %

between 15 and 30 K, almost within 0.2 % above 30 K. The smoothed heat

capacities and associated thermodynamic functions presented in Table
3.2.4 were obtained by the method of least squares, fitting measured
heat capacity values to an appropriate polynomial of T at selected
temperature region.

3.2.3   Heat capacity measurement of RbDSO$_4$

Calorimeter and Cryostat   Measurements were made in the adiabatic
cryostat previously described elsewhere.[7,8]   Helium exchange gas
amounting to 8.9×10^{-6} mol was used to facilitate achievement of rapid
equilibrium in the calorimeter vessel. No correction was applied for
the presence of the exchange gas in computing the heat capacity values.

Temperature Scales   The working thermometer above 14 K was a
Leeds & Northrup platinum thermometer (Model 8164, laboratory designation α).
This was based on 1968 International Practical Temperature Scales. The
germanium resistance thermometer (CR-1000, CryoCal, Inc., laboratory
designation β) was used for the region below 15 K. The calibration
procedures of above two thermometers was described in detail in Chapter 2.

Calorimetric Results   The measured heat capacity values are
listed in chronological sequence in Table 3.2.3. Curvature corrections
were not applied since the temperature increments employed were small
as inferred from each series of continuous measurements in Table 3.2.3.
The results are plotted in Fig. 3.2.6, which shows a gradual transition
at about 250 K which resembles the heat capacity anomaly of RbHSO$_4$ except
for the transition point. The heat capacity of the sample itself exceeded
55 % of the total for the temperature region measured. Scatter of the
measurements was within 7 % below 15 K and almost within 0.3 % above
15 K except the two temperature regions. (Fig. 3.2.7) The positive

systematic deviation between 50 and 70 K was estimated to be due to 4.4×10^{-4} moles of air which happened to enter the calorimeter vessel in pinching off the copper tube, through which the exchange gas was introduced. At 100 K this gaseous contaminant is estimated to contribute 0.03 % of the heat capacity of the sample. Large scatterings at about 250 K were due to small temperature increments employed near the transition. The thermodynamic functions were calculated from the smoothed heat capacity values which were determined by plotting the experimental values on the large graph for the transition region and fitting them to an appropriate polynomial of T for suitable temperature region. The results thus obtained are presented in Table 3.2.4.

3.2.4   Heat capacity measurement of $(ND_4)_2SO_4$

Calorimeter and Cryostat   The newly-built calorimeter and cryostat of adiabatic type was used to measure the heat capacity of $(ND_4)_2SO_4$, the detailed description of which was given in Chapter 2. The heat capacity of the empty calorimeter was determined in a separate set of measurements over the entire temperature range, 2.5 to 320 K. Helium gas less than 3.6×10^{-5} mol to accelerate thermal equilibration within the sample space was used for series from I to XII, and 1.5×10^{-5} mol for series from XIII to XV, respectively.

Temperature Scales   The working thermometer above 14 K was a platinum thermometer (S 1055-1, Minco Products, Inc., laboratory designation α), the temperature scale of which was based on the IPTS-68. Below 15 K a working thermometer was a germanium thermometer (CR-1000, CryoCal, Inc., laboratory designation ε), which was calibrated in our laboratory (See Chapter 2).

Calorimetric Results   The experimental molar heat capacity obtained for the $(ND_4)_2SO_4$ sample is tabulated in chronological sequence at the mean temperatures of determination in Table 3.2.7 and illustrated in Fig. 3.2.8. The temperature rise in each measurement was small as inferred from the differences in the adjacent mean temperature and hence no curvature corrections were not applied. The heat capacity of the sample was 23 % of the total at 3 K, increasing to 54 % at 10 K and exceeding 60 % above 100 K. Scatter of the measurements was within 15 % below 8 K, decreasing to 2 % from 8 to 15 K, within 1 % from 15 K to 50 K, and 0.5 % above 50 K, as shown in Fig. 3.2.9. The thermodynamic functions of $(ND_4)_2SO_4$ are evaluated from the smoothed heat capacity. The contributions from the heat capacities below 3 K are estimated by a smooth extrapolation. The results are presented at rounded temperatures in Table 3.2.8.

3.2.5   Heat capacity measurement of ND_4DSO_4

Calorimeter and Cryostat   Heat capacity measurements on ND_4DSO_4 were made in the newly-machined cryostat described in Chapter 2. The calorimeter used was a gold-plated thin-walled copper vessel with eight vertical vanes to enhance thermal equilibration of the sample and vessel. To facilitate repid thermal equilibration within the vessel, small amounts of helium gas (8.1×10^{-6} mol) were introduced. No correction was applied for the presence of the exchange gas in calculating the heat capacity values.

Temperature Scale   The working thermometer above 14 K was a platinum thermometer (S1055-1, Minco Products, Inc., laboratory designation α), the temperature scale of which was based on the IPTS-68. Below 15 K a working thermometer was a germanium·thermometer (CR-1000,

CryoCal, Inc., laboratory designation ε), which was calibrated in our laboratory (See Chapter 2).

Calorimetric Results   ,   The molar heat capacity values measured from 2.5 to 305 K are presented in Table 3.2.9 and illustrated in Fig. 3.2.10. The results are presented in chronological sequence so that the magnitude of the temperature increments employed may be inferred from the differences between adjacent mean temperatures of the deter- minations. No curvature corrections were applied because of small temperature rise. The heat capacity of the sample was 40 % of the total at 3 K, 70 % at 10 K and about 60 % above 50 K. Scatter of the measurements, as shown in Fig. 3.2.11, was almost within 15 % below 5 K and 1 % below 40 K and decreasing to 0.3 % except in the transition region. Poor precision below 5 K was primarily due to poor adiabatic conditions. Large scatterings at about 35 K was attributed to sudden break of insulating vacuum when liquid helium was exhausted. Based on the smoothed heat capacity, the thermodynamic functions are calculated and given in Table 3.2.10, where the contributions below 3 K have been estimated by extrapolating the measured heat capacities below 15 K.

3.3   Spectroscopic measurements and results

The Stokes Raman spectra of five ferroelectric crystals of NH_4HSO_4, ND_4DSO_4, $RbHSO_4$, $RbDSO_4$ and $(ND_4)_2SO_4$, the heat capacity measurements of which have been described in preceding sections, were obtained with a laser Raman spectrophotometer (Model R750, Japan spectroscopic, Co., Ltd), where the exciting laser was 5145 $\overset{o}{A}$ and supplied with the NEC Ar gas laser. The temperature of specimen was measured with a cromel-p

versus constantan thermocouple, and controlled within 1 K.

The infrared absorption spectra of these ferroelectrics were recorded at various temperatures by the KBr pellat technique with a infrared spectrophotometer (Model DS-402G, Japan spectroscopic Co., Ltd) and the far infrared spectra with a far infrared spectrometer (Model FIS-3, Hitachi). The temperature of samples in a conventional cryostat was measured with a copper versus constantan thermocouple, and controlled to within 1 K by dropping liquid nitrogen.

The results of Raman and IR measurements are summerized in Figs. from 3.3.1 to 3.3.16.

References to Chapter 3

1) R. Pepinsky, K. Vedam, S. Hoshino, and Y. Okaya, Phys. Rev., 111, 1508 (1958).

2) C. H. Shomate and B. F. Naylor, J. Amer. Chem. Soc., 67, 72 (1945).

3) H. B. Dunnicliff, J. Chem. Soc., 123, 476, 731 (1923).

4) A. Seidel, "Solubility of Inorganic and Metal Organic Compounds", D. van Nostrand Co. (1940). "Gmelins Handbuch der Aorganishen Chemie" system number 23, Berlin Verlag Chemie.

5) R. Pepinsky and K. Vedam, Phys. Rev., 117, 1502 (1960).

6) M. Yamada, presented at the 28th annual meeting of Physical Society of Japan, 5a-F-6 (1973).

7) T. Atake and H. Chihara, J. Chem. Thermodynamics, 3, 51 (1971).

8) H. Chihara and M. Nakamura, Bull. Chem. Soc. Jpn., 45, 133 (1972).

9) B. A. Strukov and M. N. Danilycheva, Sov. Phys. Solid State, 5, 1253 (1963).

Table 3.2.1   Molar heat capacities of NH_4HSO_4

Weight of specimen 47.2837g.   Molecular weight 115.103.   IPTS-68

T	Cp	T	Cp	T	Cp
K	$J\ K^{-1}mol^{-1}$	K	$J\ K^{-1}mol^{-1}$	K	$J\ K^{-1}mol^{-1}$
Series I		278.229	139.04	45.383	27.84
(Upper transition		Series III		46.789	28.92
region, run 1)		13.177	2.302	48.217	30.06
260.155	142.67	13.806	2.665	49.664	31.18
261.576	143.09	14.510	3.033	51.140	32.32
262.672	143.82	15.336	3.532	52.655	33.47
263.605	143.96	16.341	4.160	54.245	34.66
264.525	144.24	17.977	4.901	55.886	35.88
265.426	145.30	18.508	5.675	Series VI	
266.312	145.85	19.569	6.466	171.201	110.00
267.196	146.28	20.713	7.353	172.784	110.49
268.076	146.98	21.903	8.298	174.413	111.09
268.952	147.35	Series IV		176.093	111.89
269.826	147.66	21.352	7.861	177.826	112.53
270.705	145.07	22.472	8.767	179.612	113.16
271.606	138.09	23.563	9.670	181.434	113.92
272.523	137.52	24.639	10.57	183.276	114.73
Series II		25.715	11.46	185.121	115.33
(Upper transition		26.799	12.38	186.962	116.02
region, run 2)		27.901	13.29	188.791	116.72
261.419	143.953	29.059	14.28	190.610	117.45
262.612	144.07	30.318	15.35	192.423	118.07
263.796	144.63	31.773	16.59	194.239	118.68
264.984	145.29	33.404	17.98	196.057	119.37
266.168	145.94	35.172	19.49	197.866	120.02
267.337	146.56	36.975	20.99	199.666	120.80
268.578	147.38	38.661	22.39	201.357	121.30
269.814	148.23	Series V		203.039	121.91
270.983	143.40	37.476	21.45	204.813	122.54
272.182	138.34	39.169	22.85	206.300	123.20
273.550	138.18	40.772	24.16	208.052	123.72
275.076	138.45	42.394	25.45	209.807	124.50
276.628	138.51	43.955	26.69	211.569	125.02

T	Cp	T	Cp	T	Cp
K	J K^{-1}mol^{-1}	K	J K^{-1}mol^{-1}	K	J K^{-1}mol^{-1}
213.328	125.64	278.189	139.19	78.382	51.70
215.094	126.12	279.956	139.69	79.950	52.69
216.861	126.84	281.763	140.03	81.506	53.67
218.648	126.60	283.613	140.98	83.043	54.76
220.451	128.08	285.509	140.92	84.515	55.67
222.253	128.71	287.442	141.38	Series IX	
224.045	129.32	289.396	141.77	81.343	53.59
225.834	129.62	291.373	142.17	82.878	54.58
227.628	130.25	293.371	142.69	84.395	55.56
229.436	131.24	295.406	143.10	85.903	56.50
231.246	131.13	297.494	143.87	87.403	57.48
233.050	132.20	299.799	144.19	88.914	58.53
234.860	132.66	302.324	144.72	90.455	59.42
236.702	133.40	304.632	145.37	92.012	60.43
238.515	133.68	Series VIII		93.594	61.37
240.344	134.58	51.358	32.48	95.209	62.43
242.173	135.08	52.918	33.65	96.843	63.49
244.007	135.73	54.439	34.79	98.487	64.47
245.860	136.63	55.936	35.91	100.142	65.51
247.730	137.35	57.413	37.00	101.809	66.51
249.622	137.43	58.873	38.08	103.472	67.56
251.522	139.13	60.318	39.15	105.123	68.58
253.426	139.58	61.750	40.17	106.775	69.55
255.349	140.51	63.171	41.17	108.408	70.51
257.252	141.08	64.595	41.74	Series X	
259.144	141.98	66.019	43.62	109.112	71.02
261.038	142.89	67.451	44.18	110.824	72.06
262.922	143.61	68.908	45.20	112.612	73.16
Series VII		70.388	46.24	114.382	74.29
271.689	139.64	71.955	47.29	116.134	75.35
273.226	138.68	73.588	48.42	117.875	76.41
274.787	138.73	75.202	49.50	119.604	77.51
276.466	139.16	76.800	50.56	121.322	78.60

T	Cp	T	Cp	T	Cp
K	J K⁻¹mol⁻¹	K	J K⁻¹mol⁻¹	K	J K⁻¹mol⁻¹

T (K)	Cp ($\mathrm{J\,K^{-1}mol^{-1}}$)	T (K)	Cp ($\mathrm{J\,K^{-1}mol^{-1}}$)	T (K)	Cp ($\mathrm{J\,K^{-1}mol^{-1}}$)
123.033	79.68	163.481	107.59	152.179	98.56
124.737	80.50	165.195	107.55	Series XIV	
126.432	81.86	Series XII		(Lower transition	
128.116	82.92	(Upper transition		region, run 2)	
129.792	84.00	region, run 3)		142.265	91.88
131.461	85.10	253.379	139.50	144.081	93.01
133.122	86.17	254.764	139.83	145.865	94.24
134.778	87.20	255.999	140.03	147.629	95.32
Series XI		257.087	141.00	149.375	96.70
(Lower transition		258.143	141.79	151.113	97.69
region, run 1)		259.108	141.50	152.843	99.18
133.127	86.54	260.001	142.83	154.553	100.40
134.797	87.51	260.878	142.89	156.241	102.47
136.630	88.76	261.746	142.60	157.862	112.09
138.462	89.94	262.607	144.24	158.873	615.30
140.043	90.96	263.484	143.12	159.144	3357.1
141.626	92.12	264.363	143.93	159.232	3606.8
143.283	93.12	265.268	144.65	159.382	1432.3
144.938	94.21	266.169	145.23	160.339	143.20
146.591	95.24	267.017	145.19	161.882	106.35
148.246	96.45	267.863	145.95	163.339	107.43
149.904	97.50	268.707	146.51	164.869	107.88
151.565	98.73	269.551	146.19	166.476	108.31
153.228	100.01	270.396	144.57	Series XV	
154.893	101.28	271.250	141.00	(Lower transition	
156.551	103.97	272.120	137.36	region, continuous	
158.095	127.95	273.000	136.88	heating, run 1 and 2)	
158.982	698.51	Series XIII		Series XVI	
159.191	3595.2	143.862	92.74	(Upper transition	
159.268	4205.7	145.512	93.71	region, run 4)	
159.394	1662.8	147.186	94.80	264.762	144.95
160.211	167.08	148.865	96.06	265.255	145.16
161.784	107.49	150.541	97.33	265.743	145.12

T	Cp	T	Cp	T	Cp
K	J K^{-1}mol^{-1}	K	J K^{-1}mol^{-1}	K	J K^{-1}mol^{-1}
266.225	145.34	region, continuous		9.474	0.8554
266.707	145.15	heating, run 3)		10.009	0.9521
267.184	146.31	Series XVIII		10.596	1.220
267.648	146.41	162.263	106.55	11.271	1.476
268.081	146.19	163.659	107.14	11.908	1.736
268.484	146.82	165.047	107.67	12.465	1.979
268.887	146.50	166.505	108.34	13.064	2.192
269.289	146.77	168.039	109.14	13.839	2.673
269.690	146.68	169.584	109.64	Series XX	
270.087	147.22	171.130	110.25	7.485	0.4022
270.475	146.41	172.676	111.06	8.636	0.5059
270.858	144.02	Series XIX		8.559	0.6190
271.247	138.94	5.252	0.1230	9.028	0.7360
271.637	137.38	5.822	0.1848	9.447	0.8520
272.027	136.48	6.415	0.2471	9.957	1.010
272.442	136.18	6.940	0.3212	10.584	1.216
272.906	136.79	7.412	0.3901	11.177	1.441
273.395	136.75	7.884	0.4770	Series XXI	
Series XVII		8.377	0.5759	4.134	0.0522
(Lower transition		8.914	0.7022	4.645	0.0812

TABLE 3.2.2 Thermodynamic functions of NH_4HSO_4 to 300 K

T	C_p^o	$S^o(T)$	$(H^o(T) - H^o(o))T^{-1}$	$-(G^o(T) - H^o(o))T^{-1}$
K	J K^{-1}mol^{-1}	J K^{-1}mol^{-1}	J K^{-1}mol^{-1}	J K^{-1}mol^{-1}
5	0.105	0.0312	0.0214	0.0098
10	1.011	0.3157	0.2408	0.0749
15	3.332	1.113	0.8414	0.2711
20	6.813	2.528	1.882	0.6460
25	10.87	4.478	3.268	1.210
30	15.10	6.832	4.886	1.946
35	19.35	9.478	6.649	2.830
40	23.50	12.33	8.497	3.838
45	27.51	15.34	10.389	4.948
50	31.44	18.44	12.30	6.141
60	38.91	24.83	16.11	8.721
70	45.94	31.37	19.88	11.49
80	52.70	37.94	23.56	14.38
90	59.28	44.54	27.17	17.37
100	65.35	51.10	30.68	20.41
110	71.51	57.62	34.12	23.50
120	77.76	64.10	37.49	26.61
130	84.22	70.58	40.84	29.75
140	90.70	77.06	44.17	32.89
150	97.26	83.54	47.49	36.05
155	101.31	86.79	49.15	37.64
165	107.92	100.71	59.64	41.06
170	109.74	103.96	61.09	42.86
180	113.45	110.33	63.90	46.43
190	117.22	116.57	66.60	49.97
200	120.88	122.67	69.23	53.44
210	124.49	128.66	71.77	56.89
220	127.85	134.53	74.25	60.28
230	131.07	140.28	76.65	63.63
240	134.31	145.93	78.98	66.95
250	138 08	151.49	81.27	70.22
260	142.28	156.98	83.53	73.45
270	147.14	162.45	85.80	76.65
280	139.57	167.52	87.72	78.80
290	141.89	172.46	89.55	82.91
300	144.25	177.31	91.33	85.98
273.15	138.15	164.04	86.40	77.33
298.15	143.79 ± 0.17	176.41 ± 0.26	91.00 ± 0.10	85.41 ± 0.36

Table 3.2.3   Molar heat capacities of RbHSO$_4$

Weight of specimen 72.2473g.   Molecular weight 182.533.   IPTS-68

T	Cp	T	Cp	T	Cp
K	J K^{-1}mol^{-1}	K	J K^{-1}mol^{-1}	K	J K^{-1}mol^{-1}
Series I		263.771	115.49	178.692	88.53
(Transition region		265.358	109.58	180.269	89.00
run 1)		266.976	109.53	181.840	89.43
217.816	99.45	268.586	109.76	183.407	89.94
219.589	99.54	270.357	110.07	184.968	90.45
221.353	100.75	272.126	110.67	188.114	91.07
223.107	101.14	273.904	110.76	189.717	91.61
224.847	101.72	275.847	111.19	191.328	92.01
226.574	102.35	277.781	111.71	192.951	92.51
228.293	102.85	279.709	111.95	194.586	92.99
230.005	103.35	281.635	112.24	196.222	93.40
231.709	103.96	283.564	112.39	197.860	93.96
232.982	104.60	285.485	112.99	199.498	94.47
234.249	104.79	287.402	113.54	201.137	94.84
235.934	105.63	289.314	114.19	202.787	95.43
237.611	106.15	291.225	114.64	204.448	95.78
239.281	106.55	293.127	115.44	206.205	96.40
240.947	107.14	295.032	116.06	207.972	96.72
242.609	107.62	296.940	116.76	209.668	97.33
244.266	108.01	298.855	116.79	211.375	97.83
245.913	108.83	300.768	117.53	213.094	98.27
247.554	109.39	302.673	117.69	214.826	98.71
249.192	109.99	304.414	118.28	217.006	99.33
250.825	110.34	Series II		Series III	
252.283	111.16	164.246	84.23	4.660	0.1360
253.570	111.45	165.837	84.61	5.149	0.1863
254.851	112.27	167.415	85.13	5.791	0.2751
256.122	112.70	169.056	85.66	6.601	0.4195
257.385	113.27	170.686	86.19	7.432	0.6078
258.641	113.68	172.305	86.63	8.198	0.8271
259.893	114.24	173.915	87.11	8.936	1.084
261.140	114.76	175.515	87.53	9.644	1.370
262.380	115.83	177.107	88.04	10.342	1.723

T	Cp	T	Cp	T	Cp
K	J K^{-1}mol^{-1}	K	J K^{-1}mol^{-1}	K	J K^{-1}mol^{-1}
Series IV		17.588	7.065	50.568	41.59
5.320	0.2081	18.296	7.768	Series IX	
5.849	0.2869	19.043	8.478	(Transition region	
6.504	0.3978	19.934	9.498	run 2)	
7.230	0.5574	20.980	10.64	258.530	113.37
7.904	0.7398	22.138	11.95	259.267	113.56
8.555	0.9482	23.347	13.35	259.869	113.96
Series V		Series VIII		260.333	114.21
6.845	0.4654	21.145	10.84	260.771	114.63
7.632	0.6649	22.126	12.64	261.206	114.92
8.373	0.8814	23.107	13.08	261.635	114.93
9.187	1.182	24.086	14.24	262.112	115.80
10.062	1.565	25.062	15.39	262.587	116.35
10.998	2.032	26.035	16.54	263.008	116.35
12.014	2.646	27.007	17.69	263.428	117.26
Series VI		27.971	18.82	263.847	116.60
12.978	3.156	28.929	19.96	264.270	114.37
13.836	3.809	29.892	21.09	264.701	110.82
14.573	4.401	30.976	22.36	265.138	109.71
15.240	4.961	32.157	23.75	265.576	109.69
15.964	5.561	33.305	25.08	266.068	109.68
16.748	6.271	34.441	26.37	266.561	109.55
17.477	6.971	35.579	27.63	267.003	109.51
18.186	7.670	36.730	28.87	267.499	109.74
18.937	8.422	37.909	30.12	268.113	109.73
19.772	9.321	39.119	31.38	Series X	
20.736	10.37	40.368	32.61	48.793	40.21
Series VII		41.811	34.02	49.900	41.10
13.321	3.409	43.404	35.51	50.981	42.03
14.171	4.062	44.941	36.91	52.038	42.74
15.012	4.759	46.418	38.18	53.202	43.65
15.867	5.499	47.845	39.39	54.466	44.58
16.768	6.290	49.226	40.53	55.770	45.47

$\dfrac{T}{K}$	$\dfrac{C_p}{J\ K^{-1}\ mol^{-1}}$	$\dfrac{T}{K}$	$\dfrac{C_p}{J\ K^{-1}\ mol^{-1}}$	$\dfrac{T}{K}$	$\dfrac{C_p}{J\ K^{-1}\ mol^{-1}}$
57.054	46.31	90.782	62.38	129.884	74.42
58.266	47.12	92.402	62.94	131.412	74.82
59.473	47.85	93.814	63.43	132.938	75.20
60.677	48.66	95.232	63.93	134.472	75.65
61.881	49.33	96.664	64.43	136.006	76.27
63.107	50.04	98.111	64.90	137.539	76.46
64.377	50.77	99.579	65.36	139.073	76.93
65.685	51.54	101.063	65.79	140.605	77.47
67.004	52.12	102.558	66.30	142.135	77.94
68.330	52.85	104.069	66.76	143.671	78.53
69.673	53.59	105.599	67.32	145.203	78.84
71.036	54.21	107.146	67.73	146.597	79.28
72.417	54.92	108.697	68.22	147.998	79.72
73.827	55.56	110.237	68.70	149.459	80.19
75.249	56.22	111.783	69.21	150.923	80.60
76.667	56.87	113.325	69.66	152.464	81.24
78.085	57.48	114.846	70.16	154.008	81.45
79.505	58.13	116.360	70.59	155.558	82.00
80.922	58.68	117.865	71.05	157.109	82.43
82.976	59.50	119.364	71.48	158.663	82.96
85.022	60.33	120.858	71.97	160.218	83.37
86.427	60.87	122.338	72.18	161.776	83.90
Series XI		123.820	72.29	163.336	84.26
86.310	60.76	125.309	73.05	164.904	84.65
87.750	61.29	126.817	73.49		
89.160	61.81	128.348	73.91		

TABLE 3.2.4 Thermodynamic functions of $RbHSO_4$ to 300 K

T	C_p^o	$S^o(T)$	$(H_T^o - H_O^o)T^{-1}$	$-(G_T^o - H_O^o)T^{-1}$
K	$J\ K^{-1}mol^{-1}$	$J\ K^{-1}mol^{-1}$	$J\ K^{-1}mol^{-1}$	$J\ K^{-1}mol^{-1}$
5	0.168	0.0555	0.0418	0.0137
10	1.535	0.5401	0.3749	0.1652
15	4.741	1.705	1.243	0.4617
20	9.589	3.705	2.699	1.006
25	15.33	6.449	4.641	1.808
30	21.25	9.767	6.915	2.851
35	27.02	13.48	9.379	4.101
40	32.24	17.44	11.92	5.518
45	36.96	21.51	14.44	7.067
50	41.18	25.62	16.91	8.718
60	48.20	33.78	21.56	12.22
70	53.69	41.64	25.78	15.86
80	58.32	49.11	29.56	19.56
90	62.24	56.22	32.98	23.24
100	65.43	62.95	36.07	26.88
110	68.59	69.33	38.88	30.45
120	71.58	75.43	41.49	33.95
130	74.42	81.27	43.91	37.36
140	77.35	86.89	46.19	40.70
150	80.39	92.33	48.37	43.96
160	83.38	92.33	48.37	43.96
170	86.10	102.75	52.48	50.27
180	88.90	107.75	54.43	53.32
190	91.74	112.63	56.32	56.32
200	94.62	117.41	58.16	59.25
210	97.41	122.10	59.96	62.13
220	100.27	126.70	61.73	64.97
230	103.37	131.22	63.47	67.75
240	106.58	135.69	65.20	70.49
250	110.14	140.11	66.93	73.18
260	114.15	144.51	68.67	75.84
270	109.86	148.75	70.28	78.46
280	111.86	152.78	71.73	81.05
290	114.46	156.75	73.16	83.59
300	117.22	160.67	74.58	86.09
273.15	110.46	150.01	70.74	79.28
298.15	116.70	159.95	74.32	85.63

Table 3.2.5   Molar heat capacities of RbDSO$_4$

Weight of specimen 54.6592g.   Molecular weight 183.540.   IPTS-68

T	Cp	T	Cp	T	Cp
K	J K^{-1}mol^{-1}	K	J K^{-1}mol^{-1}	K	J K^{-1}mol^{-1}
Series I		Series IV		35.735	28.26
3.423	0.0502	13.002	3.265	37.034	29.74
4.034	0.0812	13.934	3.971	38.368	31.09
4.553	0.1265	14.923	4.786	39.621	32.34
5.129	0.1929	16.125	5.844	40.869	33.55
5.839	0.2930	17.529	7.168	42.127	34.76
6.609	0.4383	18.941	8.595	43.379	35.94
7.365	0.6116	20.237	10.03	44.617	37.05
8.184	0.8505	21.471	11.41	45.854	38.20
9.072	1.171	22.673	12.81	47.092	39.28
9.948	1.721	Series V		48.337	40.35
10.727	1.941	13.917	4.010	49.689	41.49
11.686	2.473	15.024	4.910	51.130	42.72
12.637	3.053	16.120	5.839	52.548	43.83
Series II		17.297	6.949	53.938	44.96
3.773	0.0722	18.699	8.372	55.313	46.15
4.221	0.1033	20.130	9.898	Series VII	
4.721	0.1482	21.409	11.34	49.999	41.77
5.355	0.2269	22.586	12.70	51.416	42.89
6.136	0.3471	23.698	14.02	52.816	44.18
6.934	0.5108	Series VI		54.222	45.24
7.713	0.7106	20.934	10.81	55.615	46.39
8.575	0.9852	22.225	12.30	56.972	47.43
Series III		23.428	13.69	58.318	48.76
7.563	0.6664	24.579	15.12	59.764	49.29
8.317	0.8945	25.711	16.44	61.303	50.28
9.098	1.181	26.983	17.95	62.740	51.21
9.849	1.510	28.378	19.57	64.136	51.96
10.579	1.868	29.718	21.23	65.571	52.58
13.355	2.288	30.988	22.80	66.994	53.05
12.215	2.794	32.204	24.32	68.411	53.67
13.148	3.405	33.385	25.67	69.829	54.22
14.263	4.291	34.554	26.93	71.157	54.82

T	Cp	T	Cp	T	Cp
K	J K^{-1}mol^{-1}	K	J K^{-1}mol^{-1}	K	J K^{-1}mol^{-1}
193.666	95.06	244.753	112.90	248.302	115.86
195.429	95.66	245.568	113.90	248.728	116.04
197.191	96.16	246.361	114.62	249.152	116.17
198.955	96.87	247.137	115.89	249.576	116.75
200.719	97.31	247.891	115.34	250.426	115.91
202.484	97.93	248.611	115.40	250.985	113.40
204.246	98.59	249.303	116.08	251.678	112.28
206.007	99.15	249.970	115.91	252.374	111.64
Series XII		250.628	114.42	253.102	111.03
(Transition region		251.296	109.35	253.954	110.82
run 1)		251.973	111.76	254.943	110.80
206.078	98.91	252.756	110.73	256.002	110.73
207.694	99.46	253.653	110.45	257.115	110.98
209.503	100.26	254.550	110.05	Series XIV	
211.302	100.75	255.462	110.27	(Transition region	
213.071	101.43	256.391	110.55	run 3)	
214.836	101.73	Series XIII		243.386	112.68
216.591	103.06	(Transition region		244.356	112.87
218.347	102.78	run 2)		245.110	113.29
220.098	103.83	233.093	108.36	245.691	113.79
221.836	104.49	234.736	109.07	246.212	113.55
223.572	105.14	236.351	109.90	246.714	114.24
225.303	105.70	238.002	110.58	247.198	114.45
227.024	106.26	239.614	111.34	247.675	115.37
228.730	106.80	241.108	111.91	248.124	116.19
230.422	107.51	242.486	112.54	248.547	116.22
232.092	108.21	243.654	113.30	248.973	116.07
233.732	109.16	244.486	113.91	249.392	115.04
235.345	109.44	245.071	114.68	249.764	115.22
236.941	110.04	245.607	114.23	250.198	115.43
238.503	110.35	246.105	115.17	250.601	115.01
240.038	111.12	246.570	114.96	251.008	112.68
241.400	111.90	247.013	115.32	251.416	111.90
242.592	112.30	247.447	115.64	251.826	111.56
243.759	112.66	247.875	115.55	252.238	111.33

T	Cp	T	Cp	T	Cp
K	J K^{-1}mol^{-1}	K	J K^{-1}mol^{-1}	K	J K^{-1}mol^{-1}
72.474	55.38	302.732	121.85	137.858	78.20
73.870	56.01	305.346	122.45	139.803	78.77
75.270	56.65	Series IX		141.574	79.39
76.688	57.39	84.241	60.55	143.333	79.57
78.091	57.93	85.717	61.07	145.251	80.39
79.464	58.88	87.188	61.77	147.158	80.97
80.840	58.79	88.653	62.21	149.055	81.56
82.197	59.77	90.118	62.77	150.905	82.16
83.553	60.25	91.592	63.32	152.742	82.82
84.933	60.77	93.080	63.84	154.608	83.43
86.324	61.42	94.586	64.37	156.474	84.01
Series VIII		96.115	64.92	158.336	84.52
255.982	110.48	97.659	65.47	160.187	85.22
257.675	110.93	99.216	65.97	162.031	85.80
259.418	111.17	100.791	66.47	163.875	86.36
261.184	111.77	102.380	66.94	165.713	86.95
262.966	112.20	103.988	67.50	167.542	87.57
264.760	112.71	105.617	68.10	Series X	
266.566	113.04	107.261	68.60	168.132	87.47
268.390	113.57	108.916	69.12	170.019	87.92
270.235	113.99	110.581	69.72	171.900	88.57
272.090	114.57	112.261	70.25	173.744	89.12
273.955	114.96	113.956	70.66	175.576	89.70
275.837	115.21	115.659	71.25	177.398	90.21
277.734	115.92	117.359	71.73	179.209	90.86
279.653	116.29	119.916	72.27	181.011	91.45
281.611	116.74	120.775	72.80	182.811	91.96
283.614	117.13	122.494	73.40	184.608	92.51
285.662	117.59	124.418	73.72	186.315	93.08
287.752	118.25	126.525	74.64	188.017	93.56
290.068	118.75	128.594	75.31	189.799	94.05
292.601	119.43	130.625	75.92	191.572	94.52
295.153	119.99	132.621	76.61	Series XI	
297.719	120.79	134.594	77.16	190.132	94.09
300.213	121.13	136.231	77.73	191.897	94.58

T	Cp	T	Cp	T	Cp
K	$J\ K^{-1}mol^{-1}$	K	$J\ K^{-1}mol^{-1}$	K	$J\ K^{-1}mol^{-1}$
252.640	110.95	253.960	110.28	256.039	110.67
253.061	111.00	254.491	110.57		
253.477	110.15	255.177	110.64		

TABLE 3.2.6   Thermodynamic functions of RbDSO$_4$ to 300 K

T	C_p^o	$S^o(T)$	$(H_T^o - H_0^o)T^{-1}$	$-(G_T^o - H_0^o)T^{-1}$
K	J K^{-1}mol^{-1}	J K^{-1}mol^{-1}	J K^{-1}mol^{-1}	J K^{-1}mol^{-1}
5	0.1794	0.0566	0.0427	0.0138
10	1.579	0.5092	0.3869	0.1223
15	4.871	1.7085	1.2811	0.4274
20	9.799	3.753	2.769	0.9843
25	15.58	6.551	4.745	1.806
30	21.63	9.923	7.053	2.870
35	27.52	13.705	9.561	4.144
40	32.73	17.73	12.14	5.588
45	37.38	21.86	14.69	7.166
50	41.66	26.02	17.18	8.843
60	48.77	34.27	21.87	12.40
70	54.22	42.21	26.12	16.09
80	58.76	49.76	29.92	19.84
90	62.72	56.91	33.35	23.56
100	66.19	63.70	36.46	27.24
110	69.41	70.16	39.31	30.85
120	72.50	76.34	41.95	34.39
130	75.59	82.26	44.42	37.84
140	78.79	87.98	46.76	41.22
150	82.03	93.53	49.00	44.53
160	85.20	98.92	51.17	47.75
170	88.22	104.18	53.26	50.92
180	91.14	109.31	55.28	54.03
190	94.07	114.31	57.25	57.06
200	97.14	119.21	59.16	60.05
210	100.38	124.03	61.05	62.98
220	103.79	128.78	62.91	65.87
230	107.34	133.47	64.77	68.70
240	111.28	138.12	66.62	71.50
250	116.81	142.76	68.50	74.26
260	111.30	147.13	70.15	76.98
270	113.81	151.37	71.72	79.65
280	116.21	155.56	73.27	82.29
290	118.68	159.68	74.78	84.89
300	121.21	163.74	76.29	87.45
273.15	114.58	152.69	72.21	80.48
298.15	120.73	162.99	76.02	86.98

Table 3.2.7 Molar heat capacities of $(ND_4)_2SO_4$
Weight of specimen 48.668g. Molecular weight 140.18.   IPTS-68

T	Cp	T	Cp	T	Cp
K	$J\ K^{-1}mol^{-1}$	K	$J\ K^{-1}mol^{-1}$	K	$J\ K^{-1}mol^{-1}$
Series I		107.848	99.63	165.597	148.74
58.928	47.25	111.738	101.34	167.634	150.88
60.517	49.09	113.643	103.20	169.640	152.89
62.272	51.04	115.560	104.54	171.618	155.24
64.032	53.09	117.493	106.33	173.571	157.23
65.698	54.97	119.437	108.07	175.496	159.48
67.403	56.85	121.401	109.77	177.392	161.81
69.071	58.82	123.386	111.16	179.268	163.90
70.609	60.50	125.397	113.70	181.110	165.88
72.192	62.19	127.429	114.96	182.939	168.13
73.746	63.87	129.478	116.96	184.748	170.72
75.274	65.57	131.546	118.66	186.530	173.30
77.041	67.49	133.610	120.52	188.293	175.73
78.705	69.34	136.073	122.61	190.117	178.43
80.170	70.88	138.614	124.75	191.999	181.54
81.710	72.74	140.823	126.89	193.861	184.63
83.310	74.17	142.997	128.65	195.692	188.33
85.039	76.03	145.136	130.53	197.494	191.16
86.765	77.82	147.530	132.60	199.285	194.80
88.435	79.45	149.855	134.50	201.062	198.68
90.147	81.13	151.916	136.22	202.812	202.79
91.910	82.97	154.054	138.12	204.535	207.06
93.689	84.96	156.257	140.10	206.229	211.27
95.464	86.43	158.533	142.34	207.882	214.99
97.234	88.09	160.864	144.48	209.515	219.23
99.020	89.76	163.162	146.75	211.123	224.11
100.823	91.51	165.438	149.03	212.699	229.43
102.703	93.18	167.696	151.32	214.247	234.81
104.572	95.04	169.437	153.72	215.832	239.68
106.456	96.64	172.152	155.84	217.381	249.53
Series II		Series III		Series IV	
106.111	96.31	161.730	144.67	(Transition region, run 1)	
107.979	97.98	163.626	146.68	204.289	205.81

T	Cp	T	Cp	T	Cp
K	J K^{-1}mol^{-1}	K	J K^{-1}mol^{-1}	K	J K^{-1}mol^{-1}
205.812	209.74	249.345	180.83	223.921	12020
207.387	214.12	251.436	181.59	223.956	14578
208.939	218.56	Series VII		223.998	8796.6
210.466	222.70	251.347	181.54	224.539	356.40
211.959	227.18	253.364	182.32	225.922	175.58
213.422	233.37	255.769	182.99	227.655	175.74
214.928	238.64	258.315	183.76	229.387	175.90
216.397	247.09	260.849	184.54	Series IX	
217.766	254.84	263.129	185.00	(Transition region, run 3	
219.097	262.68	265.391	186.08	and 4. continuous heating)	
220.391	273.24	267.893	187.13	Series X	
221.642	286.11	270.474	187.74	14.104	1.839
222.842	304.90	273.136	188.73	15.134	2.313
223.675	939.0	275.800	189.40	16.220	2.885
223.934	17323	278.443	190.13	17.664	3.784
223.973	11975	281.145	191.71	20.500	5.903
224.291	704.52	283.912	192.02	23.827	8.765
225.365	177.25	286.676	193.05	Series XI	
227.013	175.99	289.426	193.96	14.033	1.806
Series V		292.244	194.77	14.927	2.201
(Transition region, run 2.		295.120	195.62	16.724	3.184
continuous heating)		298.051	196.67	17.722	3.818
Series VI		301.049	197.74	18.911	4.646
226.035	175.34	Series VIII		20.191	5.619
227.674	175.31	(Transition region, run 3)		21.398	6.593
229.314	175.89	210.335	223.03	22.526	7.559
230.872	175.90	211.674	227.11	23.604	8.522
232.503	176.53	213.135	232.13	Series XII	
234.210	176.71	214.564	238.37	24.117	9.017
235.985	176.78	215.965	242.98	25.106	9.949
237.827	177.47	217.347	250.33	26.086	10.90
239.670	177.90	218.696	259.07	27.166	11.94
241.517	178.71	220.010	269.11	28.325	13.05
243.450	179.44	221.282	281.20	29.299	14.02
245.456	179.51	222.502	297.61	30.243	15.02
247.394	180.36	223.499	482.00	31.299	16.11

T	Cp	T	Cp	T	Cp
K	J K^{-1}mol^{-1}	K	J K^{-1}mol^{-1}	K	J K^{-1}mol^{-1}
32.453	17.25	3.546	0.0193	10.203	0.5751
33.698	18.47	3.988	0.0270	11.374	0.8543
34.990	20.20	4.411	0.0401	12.523	1.191
36.283	21.78	4.807	0.0504	13.637	1.605
37.493	23.21	5.183	0.0625	Series XV	
38.694	24.48	5.571	0.0798	3.948	0.0253
40.063	25.89	Series XIV		4.237	0.0346
41.536	27.45	2.814	0.0083	4.521	0.0422
42.917	28.45	3.117	0.0113	4.812	0.0535
44.259	30.44	3.439	0.0167	5.192	0.0699
45.608	31.95	3.756	0.0221	5.675	0.0850
47.005	33.49	4.066	0.0294	6.194	0.1081
48.487	35.20	4.368	0.0348	6.765	0.1405
49.969	36.92	4.692	0.0450	7.392	0.1855
51.380	38.52	5.005	0.0547	8.165	0.2592
52.738	40.08	5.334	0.0725	9.015	0.3683
54.058	41.54	5.669	0.0847	9.910	0.5179
55.344	43.07	6.064	0.1014	10.841	0.7174
56.600	44.50	6.502	0.1260	11.747	0.9549
57.940	46.06	7.003	0.1567	12.605	1.217
59.351	47.68	7.579	0.2014	13.461	1.526
Series XIII		8.307	0.2747	14.362	1.938
3.121	0.0121	9.179	0.3905		

Table 3.2.8　Thermodynamic functions of $(ND_4)_2SO_4$ to 300 K

T	C_p^o	S^o	$(H_T^o - H_0^o)T^{-1}$	$-(G_T^o - H_0^o)T^{-1}$
K	$J\ K^{-1}mol^{-1}$	$J\ K^{-1}mol^{-1}$	$J\ K^{-1}mol^{-1}$	$J\ K^{-1}mol^{-1}$
5	0.0546	0.0180	0.0135	0.0045
10	0.5353	0.1584	0.1208	0.0376
15	2.233	0.6456	0.4999	0.1457
20	5.467	1.695	1.308	0.3871
25	9.833	3.367	2.561	0.8061
30	14.75	5.589	4.178	1.411
35	20.14	8.261	6.068	2.193
40	25.69	11.31	8.174	3.139
45	31.22	14.66	10.43	4.230
50	36.79	18.23	12.78	5.450
60	48.26	25.95	17.73	8.213
70	59.76	34.27	22.94	11.34
80	70.77	42.98	28.23	14.74
90	81.08	51.91	33.54	18.38
100	90.75	60.96	38.78	22.18
110	99.86	70.04	43.92	26.12
120	108.61	79.11	48.95	30.16
130	117.30	88.14	53.87	34.27
140	126.01	97.16	58.72	38.44
150	134.52	106.14	63.49	42.65
160	143.59	115.11	68.20	46.90
170	153.60	124.11	72.93	51.18
180	164.76	133.20	77.72	55.48
190	178.29	142.45	82.64	59.81
200	196.49	152.03	87.85	64.18
210	221.0	162.18	93.58	68.61
220	269.1	173.38	100.27	73.11
230	175.8	190.67	112.76	77.91
240	178.0	198.19	115.43	82.76
250	181.1	205.52	117.99	87.53
260	184.4	212.69	120.49	92.20
270	187.6	219.71	122.91	96.80
280	190.8	226.59	125.28	101.31
290	194.0	233.34	127.59	105.75
300	197.3	239.97	129.86	110.11
273.15	188.5	221.88	123.66	98.22
298.15	196.6	238.74	129.44	109.30

Table 3.2.9   Molar heat capacities of ND_4DSO_4

Weight of specimen 48.7977g.   Molecular weight 120.135.   IPTS-68

T / K	Cp / $J\ K^{-1}mol^{-1}$	T / K	Cp / $J\ K^{-1}mol^{-1}$	T / K	Cp / $J\ K^{-1}mol^{-1}$
Series I		245.429	143.32	288.323	148.06
181.597	120.09	247.507	144.09	290.766	148.40
182.887	120.66	249.567	144.90	293.204	148.71
184.736	121.47	251.6101	145.76	295.654	149.47
186.903	122.25	Series III		298.129	150.28
189.133	122.99	(Upper transition		300.598	151.05
191.432	123.79	region, run 1)		303.030	151.78
193.792	124.71	253.683	146.70	305.465	152.72
196.259	125.56	255.708	148.40	Series IV	
198.641	126.37	257.330	149.27	(Upper transition	
200.890	127.22	258.558	149.91	region, run 2)	
203.128	127.91	259.610	149.96	241.716	141.39
205.356	128.82	260.233	150.11	243.782	142.61
207.625	129.38	260.728	151.28	245.884	143.31
209.897	130.19	261.220	151.92	246.973	144.23
Series II		261.773	152.25	249.996	145.14
208.768	130.00	262.329	149.98	251.759	146.12
210.997	130.51	262.831	144.05	253.010	146.90
213.213	131.45	263.340	143.52	254.002	147.33
215.423	131.23	263.850	141.33	254.989	147.15
217.716	133.14	264.423	141.31	255.871	148.35
219.800	133.65	265.116	141.52	256.555	148.87
222.858	134.76	265.919	141.78	257.042	149.54
223.899	135.27	267.821	142.45	257.431	149.75
226.052	136.09	270.163	143.62	257.821	148.52
228.272	136.80	271.950	143.80	258.208	149.66
230.545	137.75	273.665	144.35	258.595	150.88
232.743	138.78	275.513	144.46	258.980	150.00
234.880	139.38	277.620	145.15	259.365	150.52
237.009	140.26	279.706	145.49	259.742	151.05
239.131	140.61	281.765	145.97	260.176	151.03
241.239	141.99	283.816	146.45	260.609	151.16
243.338	142.59	285.975	146.75	260.995	152.00

T	Cp	T	Cp	T	Cp
K	J K^{-1}mol^{-1}	K	J K^{-1}mol^{-1}	K	J K^{-1}mol^{-1}
261.429	152.06	168.784	115.94	2.494	0.0061
261.859	152.08	170.868	116.59	2.792	0.0101
262.241	152.41	173.196	117.38	3.106	0.0155
262.629	145.29	175.508	117.74	3.426	0.0244
263.024	144.42	177.513	119.12	3.759	0.0306
263.420	143.18	179.627	119.77	4.100	0.0449
263.818	142.14	181.770	120.44	4.448	0.0599
Series V		183.915	121.08	Series IX	
(Lower transition		Series VI		2.192	0.0054
region, run 1)		(Lower transition		2.571	0.0024
128.269	89.04	region, run 1)		2.855	0.0178
129.018	89.97	149.614	102.81	3.132	0.0191
131.316	90.97	151.763	104.19	3.477	0.0245
132.900	91.95	153.886	105.58	3.854	0.0349
134.611	93.02	155.994	107.00	4.238	0.0502
136.378	94.16	158.079	108.60	4.618	0.0704
138.356	95.42	159.664	109.81	5.038	0.1043
140.493	96.84	160.755	111.10	5.446	0.1277
142.558	98.09	161.702	112.37	5.953	0.1869
144.604	99.44	162.504	114.31	6.587	0.2580
146.589	100.94	163.403	299.36	7.280	0.3641
148.671	102.19	163.926	7644.3	8.106	0.5241
150.837	103.70	163.983	5446.4	Series X	
152.977	105.13	164.111	1875.8	7.435	0.3901
155.099	106.49	164.917	186.58	8.201	0.5407
157.199	107.97	166.023	115.12	8.866	0.6973
159.272	109.59	167.075	115.03	9.526	0.8828
161.318	111.55	168.842	115.75	10.221	1.103
163.145	156.43	Series VII		10.973	1.377
164.025	2703.7	(Lower transition		11.866	1.737
164.166	4876.4	region, run 3		13.044	2.275
164.977	260.95	continuous heating)		14.305	2.972
166.694	115.19	Series VIII		Series XI	

T	Cp	T	Cp	T	Cp
K	J K^{-1}mol^{-1}	K	J K^{-1}mol^{-1}	K	J K^{-1}mol^{-1}
5.556	0.1485	27.638	13.41	70.349	50.32
6.276	0.2263	28.726	14.31	72.160	51.71
7.097	0.3296	29.840	15.39	73.894	53.01
7.876	0.4834	30.980	16.38	75.646	54.32
8.568	0.6232	32.240	17.46	77.486	55.78
9.242	0.7963	33.604	18.24	79.383	57.16
9.902	0.9998	34.968	20.20	81.333	58.58
10.582	1.233	36.271	21.60	83.238	59.94
11.866	1.746	37.595	22.77	85.159	61.35
13.218	2.356	39.006	23.95	87.056	62.55
13.997	2.774	40.313	24.99	88.944	63.59
Series XII		41.534	26.02	91.307	65.56
13.841	2.731	42.909	27.17	93.641	67.18
14.733	3.239	44.463	28.53	95.487	68.33
15.549	3.717	46.129	29.98	97.372	69.56
16.384	4.254	47.906	31.55	99.300	70.89
17.364	4.928	49.687	33.12	101.252	72.05
18.286	5.599	51.379	34.58	103.173	73.29
19.091	6.199	52.990	35.95	105.083	74.57
Series XIII		54.572	37.30	106.964	75.70
13.537	2.585	56.176	38.70	108.800	76.87
14.545	3.144	Series XIV		110.704	78.08
15.863	3.927	50.116	33.54	112.666	79.27
17.218	4.842	51.954	35.09	114.636	80.50
18.346	5.668	53.697	36.58	116.512	81.58
19.351	6.417	55.421	38.06	118.435	82.86
20.308	7.234	57.129	39.58	120.398	84.09
21.298	7.936	59.352	41.39	122.399	85.10
22.373	8.871	61.537	43.23	124.393	86.66
23.446	9.791	63.204	44.59	126.359	87.95
24.471	10.69	64.968	46.04	128.292	89.24
25.492	11.58	66.785	47.49	130.251	90.49
26.558	12.52	68.578	49.00		

Table 3.2.10 Thermodynamic functions of ND_4DSO_4 to 300 K

$\dfrac{T}{K}$	$\dfrac{C_p^o}{J\ K^{-1}mol^{-1}}$	$\dfrac{S^o}{J\ K^{-1}mol^{-1}}$	$\dfrac{(H_T^o - H_O^o)T^{-1}}{J\ K^{-1}mol^{-1}}$	$\dfrac{-(G_T^o - H_O^o)T^{-1}}{J\ K^{-1}mol^{-1}}$
5	0.768	0.026	0.020	0.006
10	1.030	0.668	0.480	0.188
15	3.390	1.484	1.018	0.466
20	6.932	2.920	2.033	0.887
25	11.15	4.960	3.262	1.698
30	15.69	7.392	4.954	2.438
35	20.20	10.15	6.810	3.340
40	24.69	13.14	8.765	4.376
45	29.12	16.31	10.78	5.523
50	33.45	19.60	12.83	6.765
60	41.95	26.45	16.98	9.471
70	50.10	33.56	21.15	12.40
80	57.62	40.74	25.25	15.50
90	64.65	47.94	29.24	18.70
100	71.27	55.10	33.11	21.98
110	77.69	62.19	36.87	25.32
120	83.63	69.21	40.53	28.68
130	89.14	76.17	44.11	32.07
140	94.30	83.09	47.62	35.47
150	99.17	89.96	51.10	38.87
160	103.77	96.83	54.56	42.28
170	108.14	111.91	65.93	45.98
180	112.30	118.65	68.82	49.83
190	116.30	125.22	71.59	53.63
200	120.12	131.63	74.26	57.37
210	123.76	137.90	76.85	61.05
220	127.27	144.05	79.37	64.69
230	130.65	150.09	81.82	68.27
240	133.89	156.02	84.22	71.80
250	136.97	161.87	86.58	75.29
260	139.90	167.68	88.94	78.73
270	142.74	173.12	91.00	82.13
280	145.53	178.36	92.90	85.47
290	148.28	183.52	94.76	88.76
300	150.77	188.59	96.59	92.01
273.15	143.64	174.77	91.60	83.18
298.15	150.53	187.65	96.25	91.41

To vacuum line

$CaCl_2$ tube

H_2O

H_2O

Sample

Mantle Heater

Ether
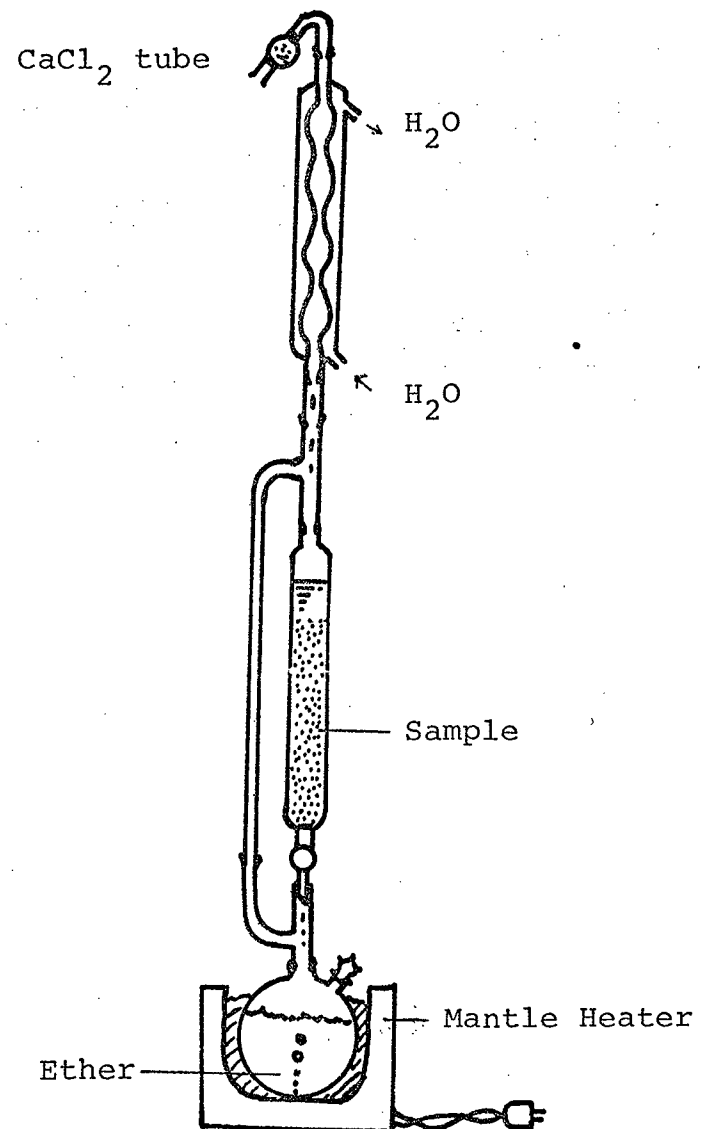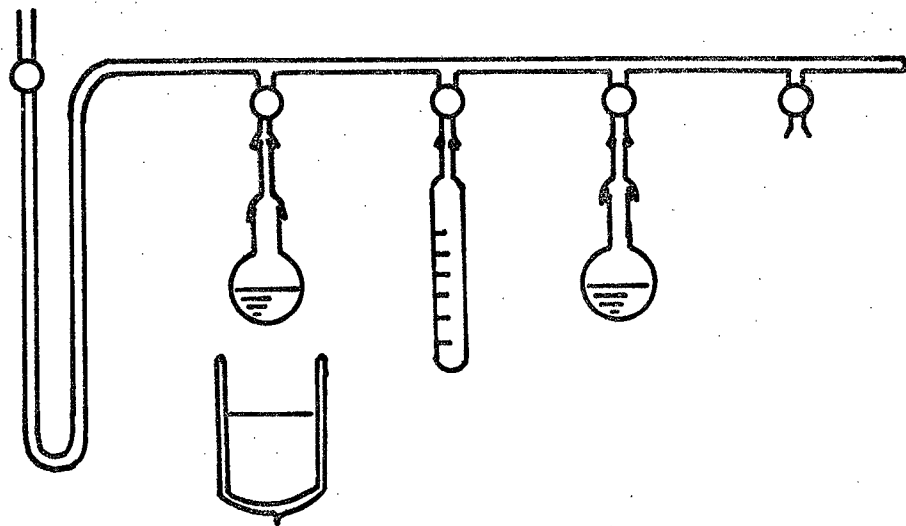
Fig. 3.1.1   Apparatus for preparation (left) and purification (right).
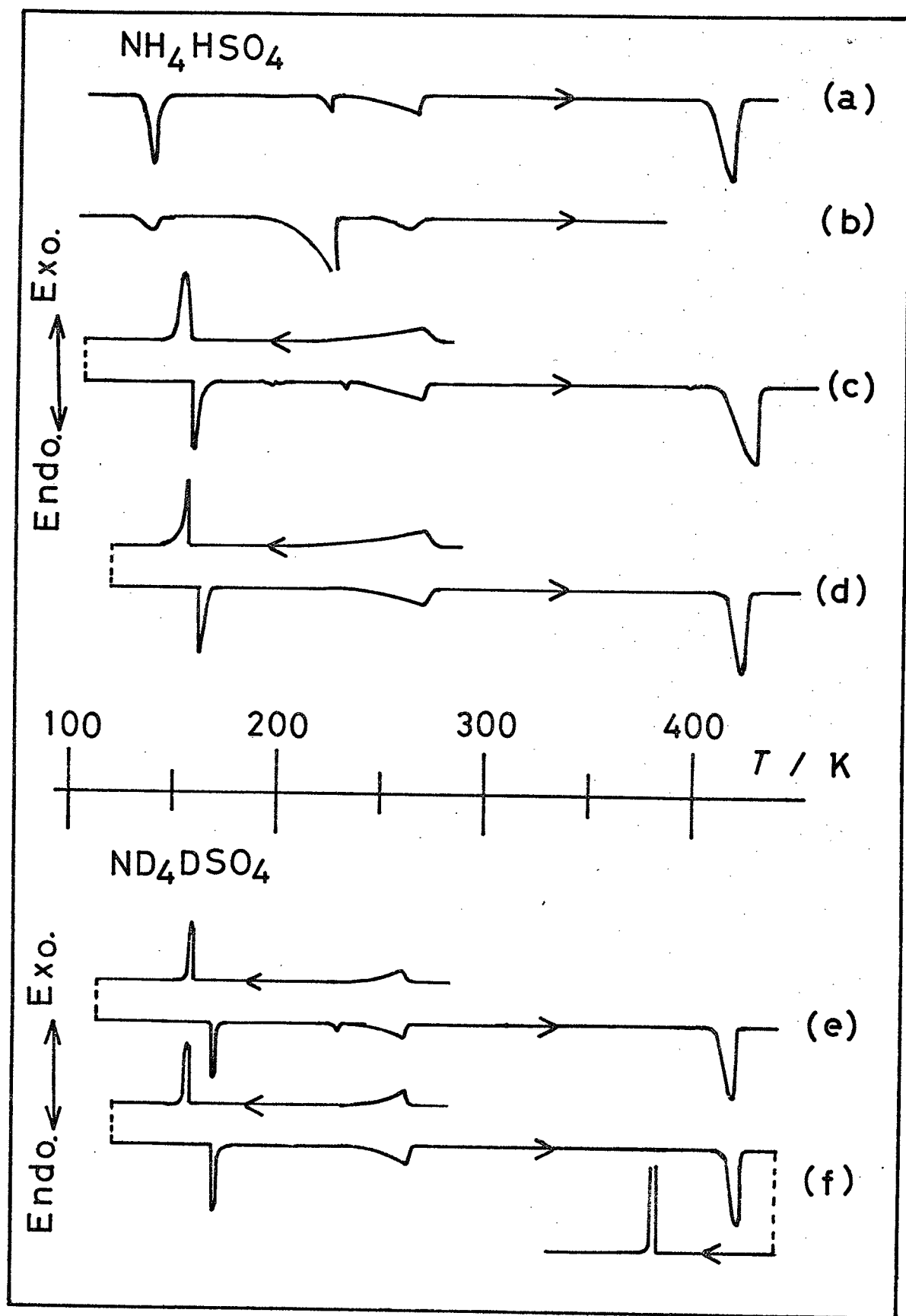
Fig. 3.1.2   Differential thermogram of NH_4HSO_4 and ND_4DSO_4.
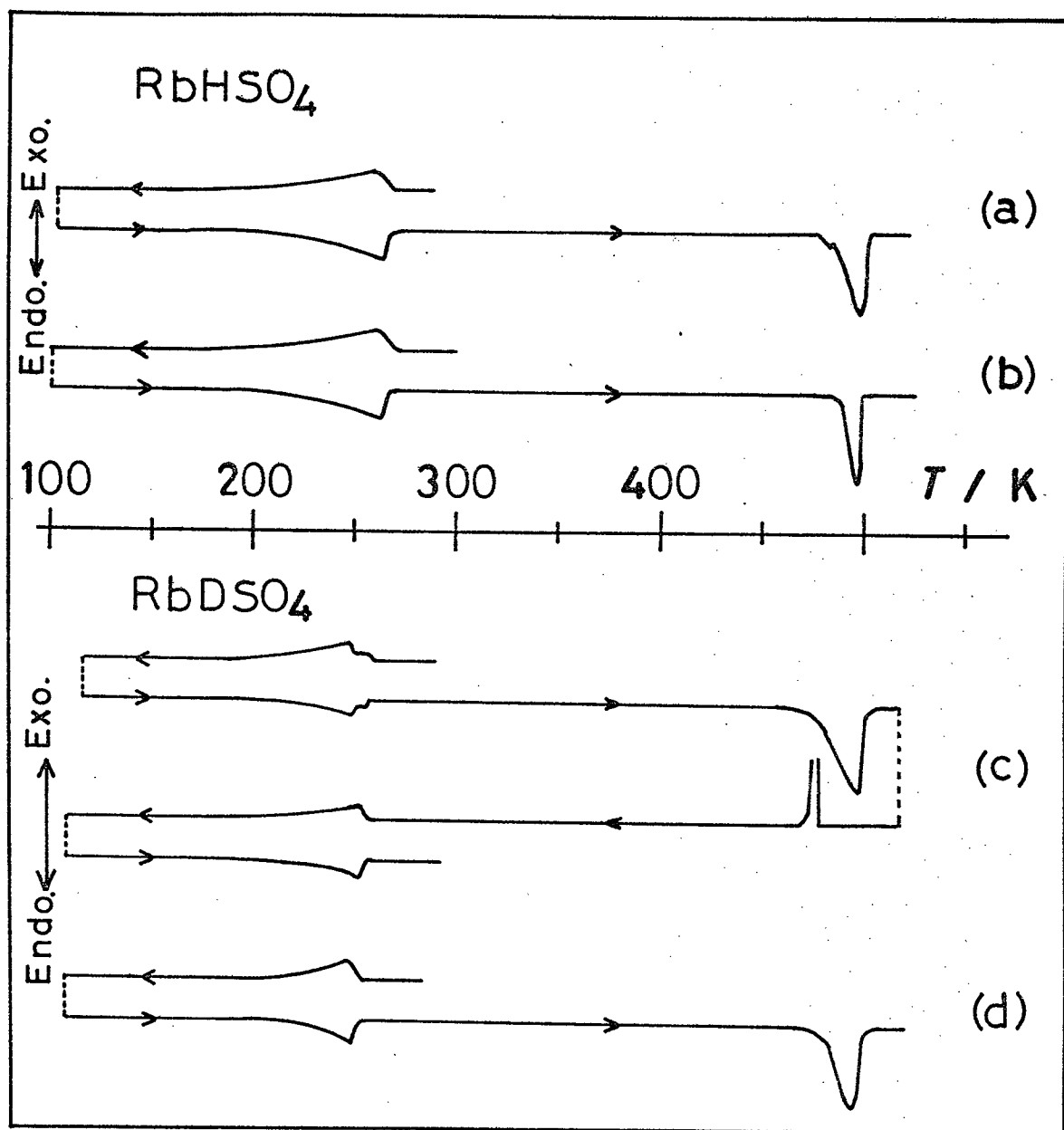
Fig. 3.1.3   Differential thermogram of $RbHSO_4$ and $RbDSO_4$.
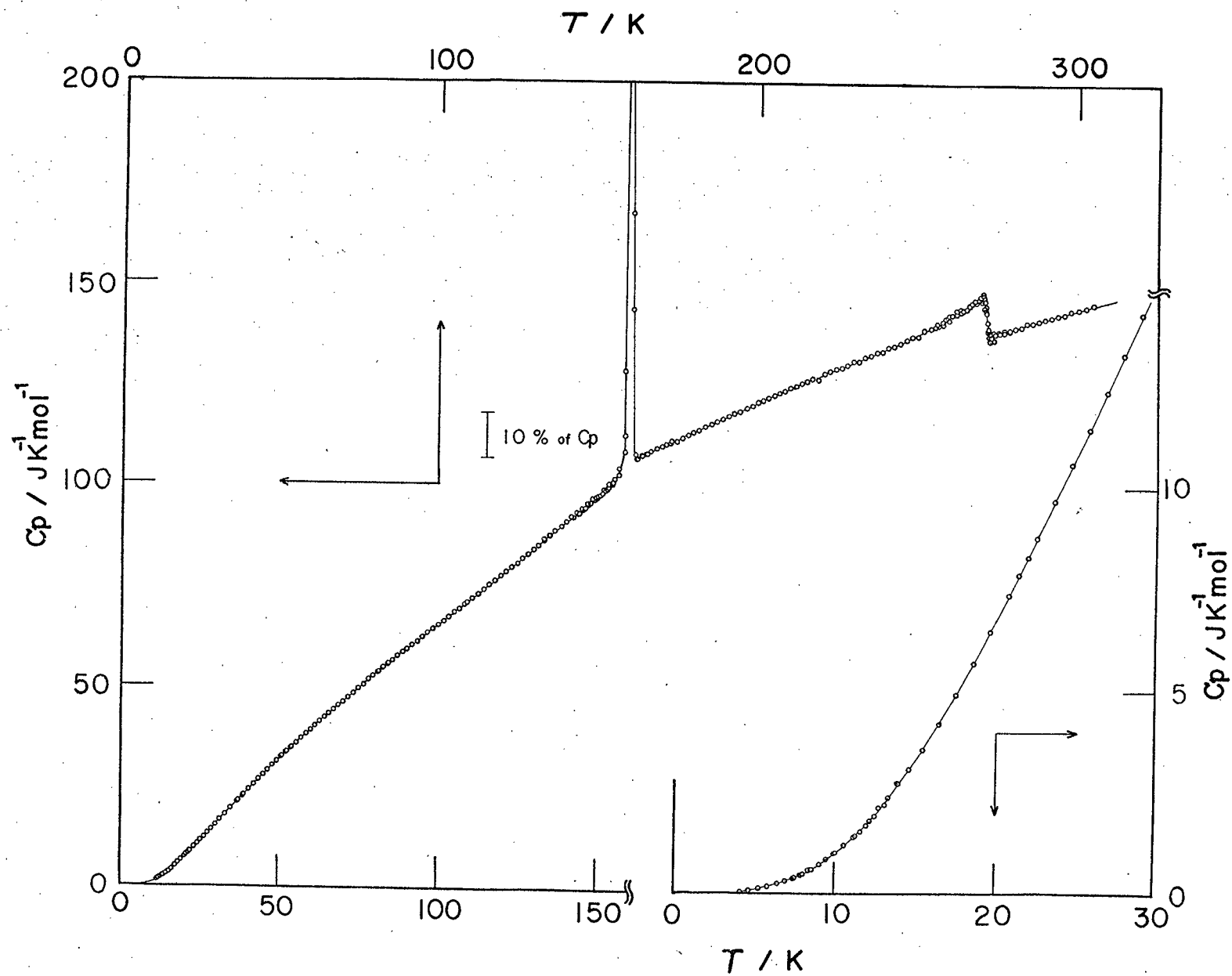
Fig. 3.2.1   Molar heat capacity of NH_4HSO_4.
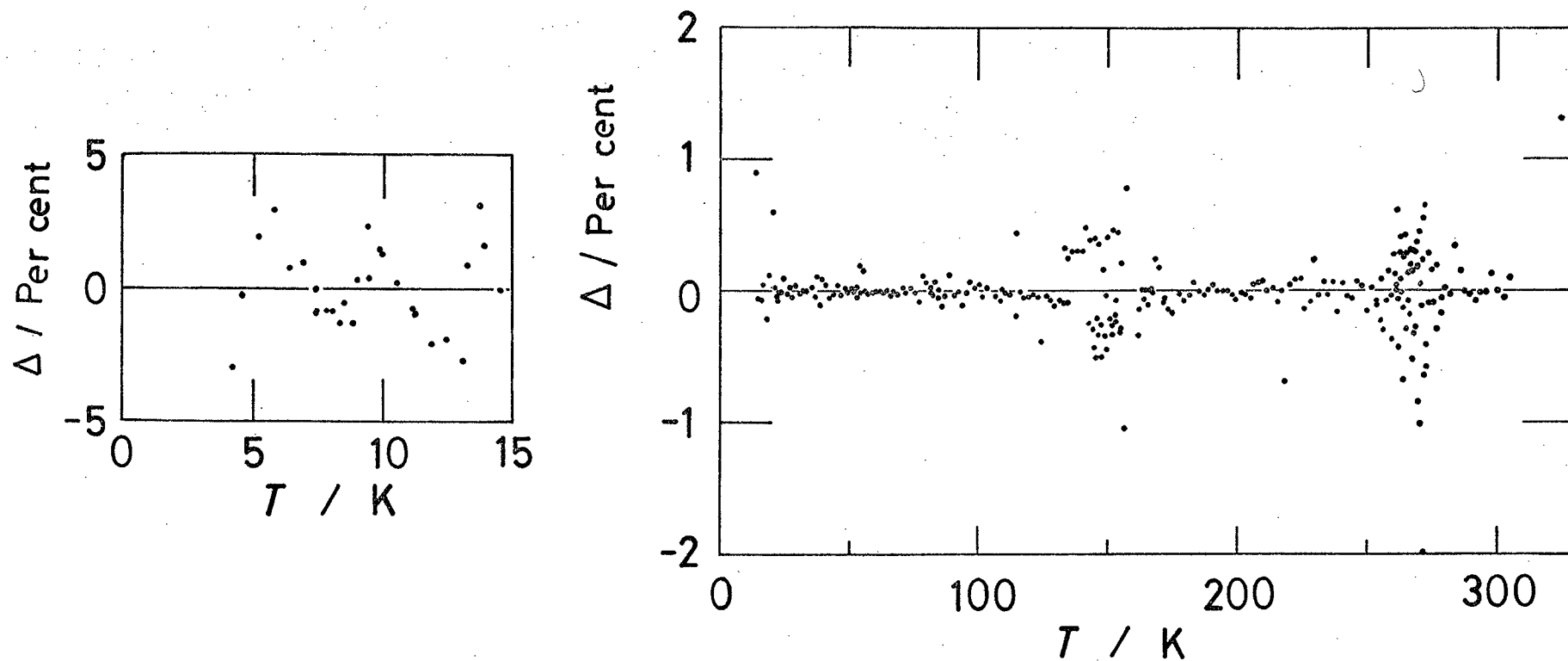
Fig. 3.2.2   Per cent deviations from the smoothed heat capacity of NH_4HSO_4.
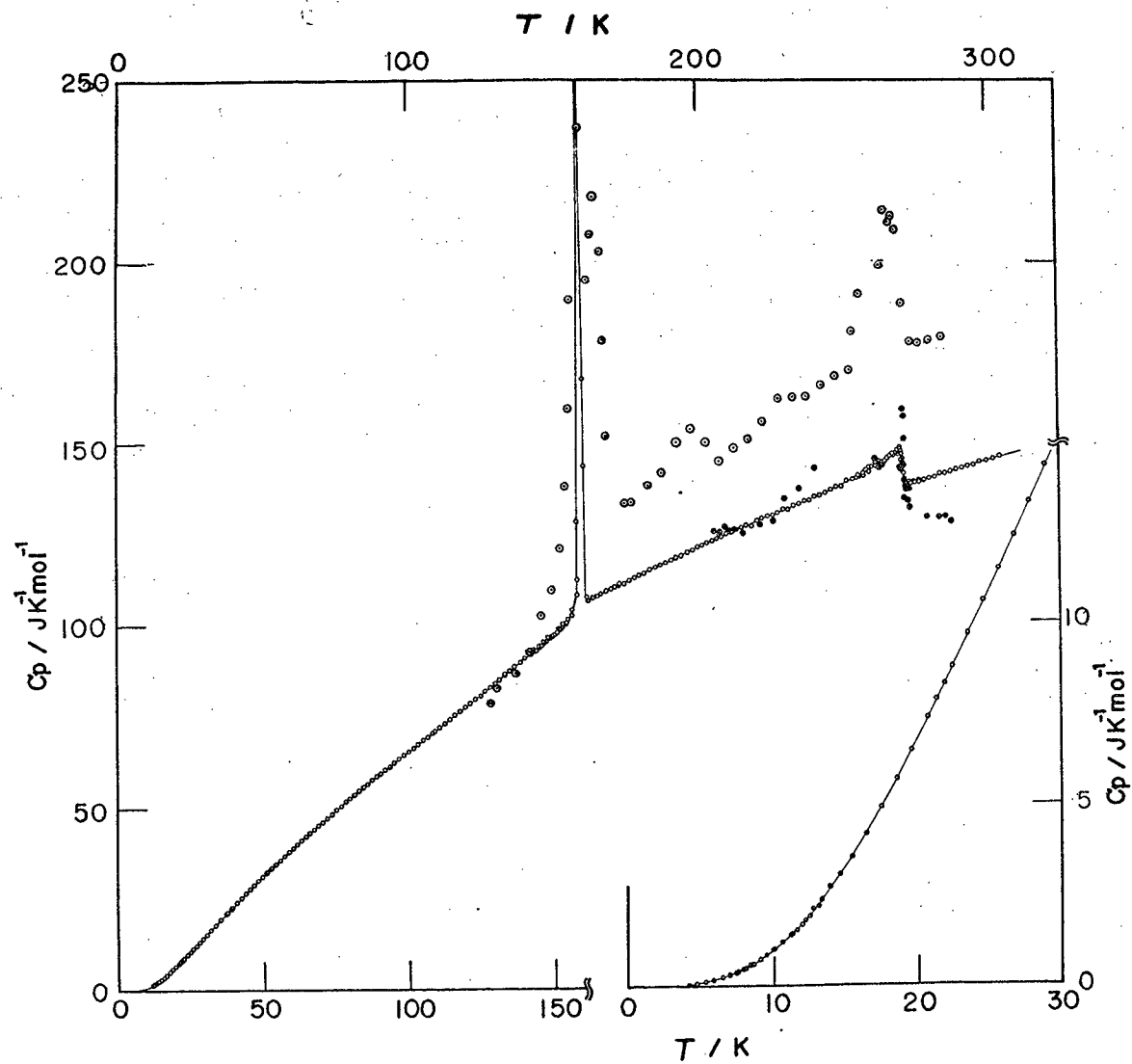
Fig. 3.2.3   Comparison of heat capacity of NH_4HSO_4.

(-O-O-   : present work, ⊙ : Pepinsky, et.al., • : Strukov and Danilycheva)
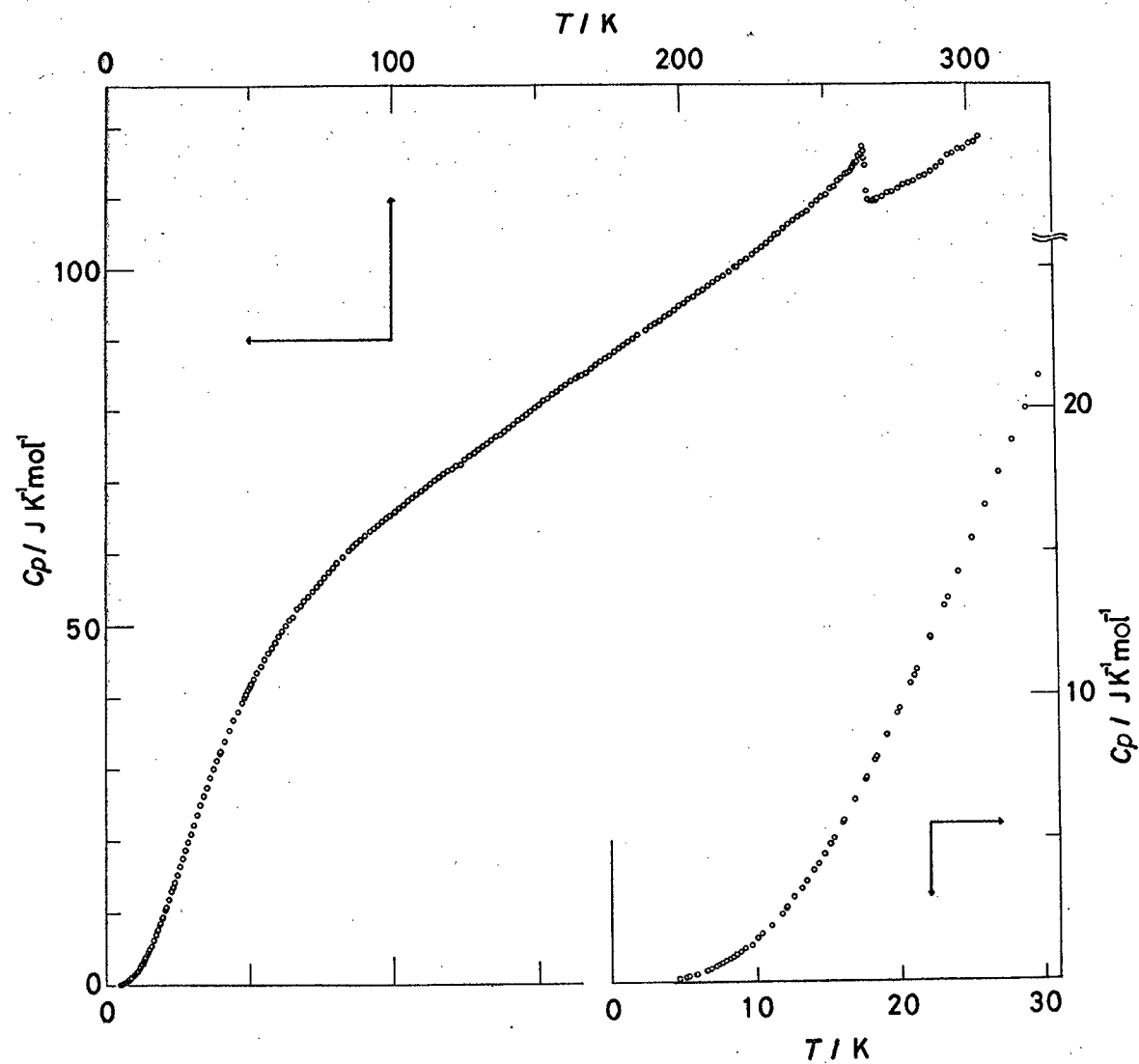
Fig. 3.2.4   Molar heat capacity of RbHSO$_4$.
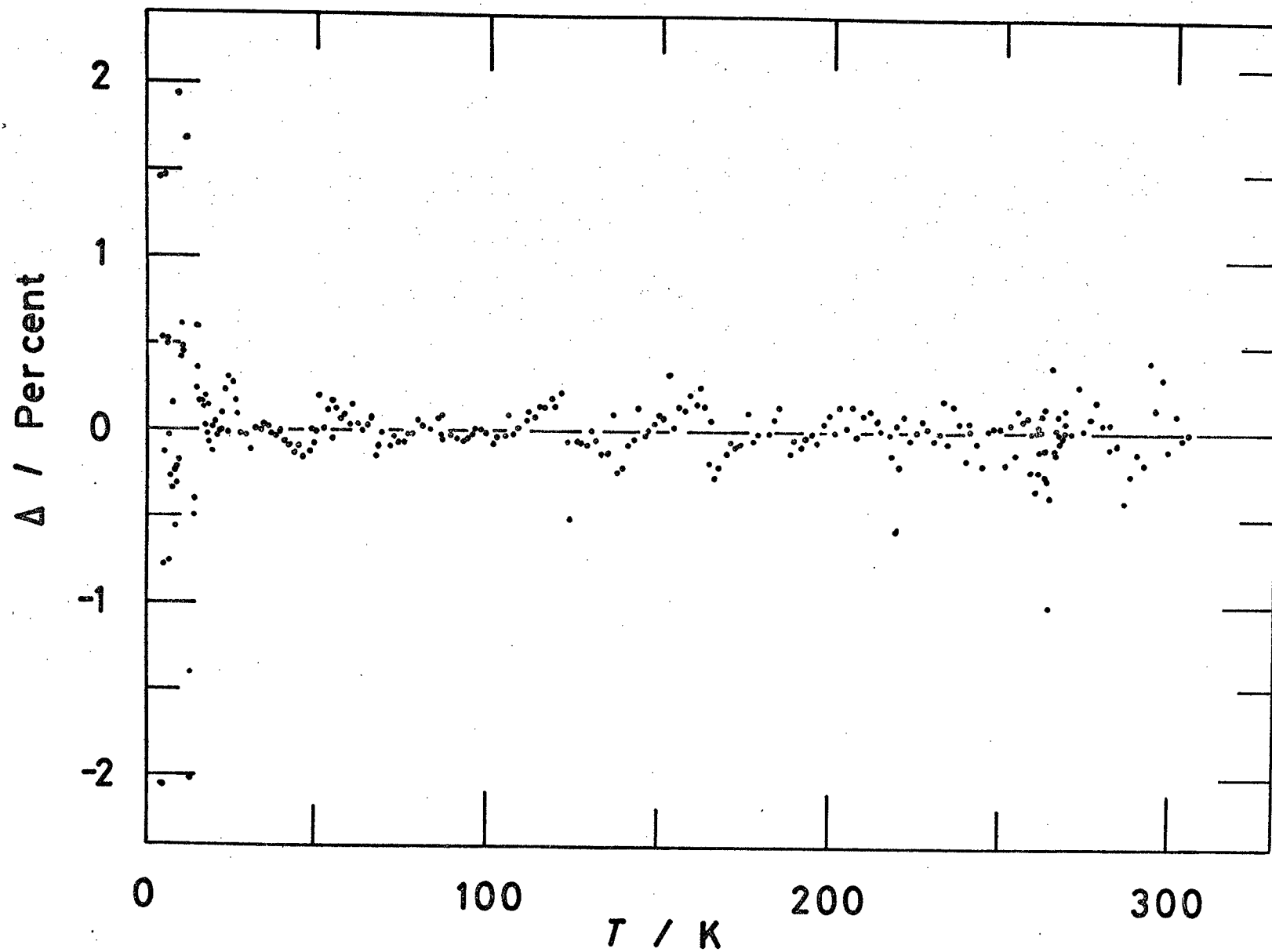
Fig. 3.2.5   Per cent deviations from the smoothed heat capacity of $RbHSO_4$.
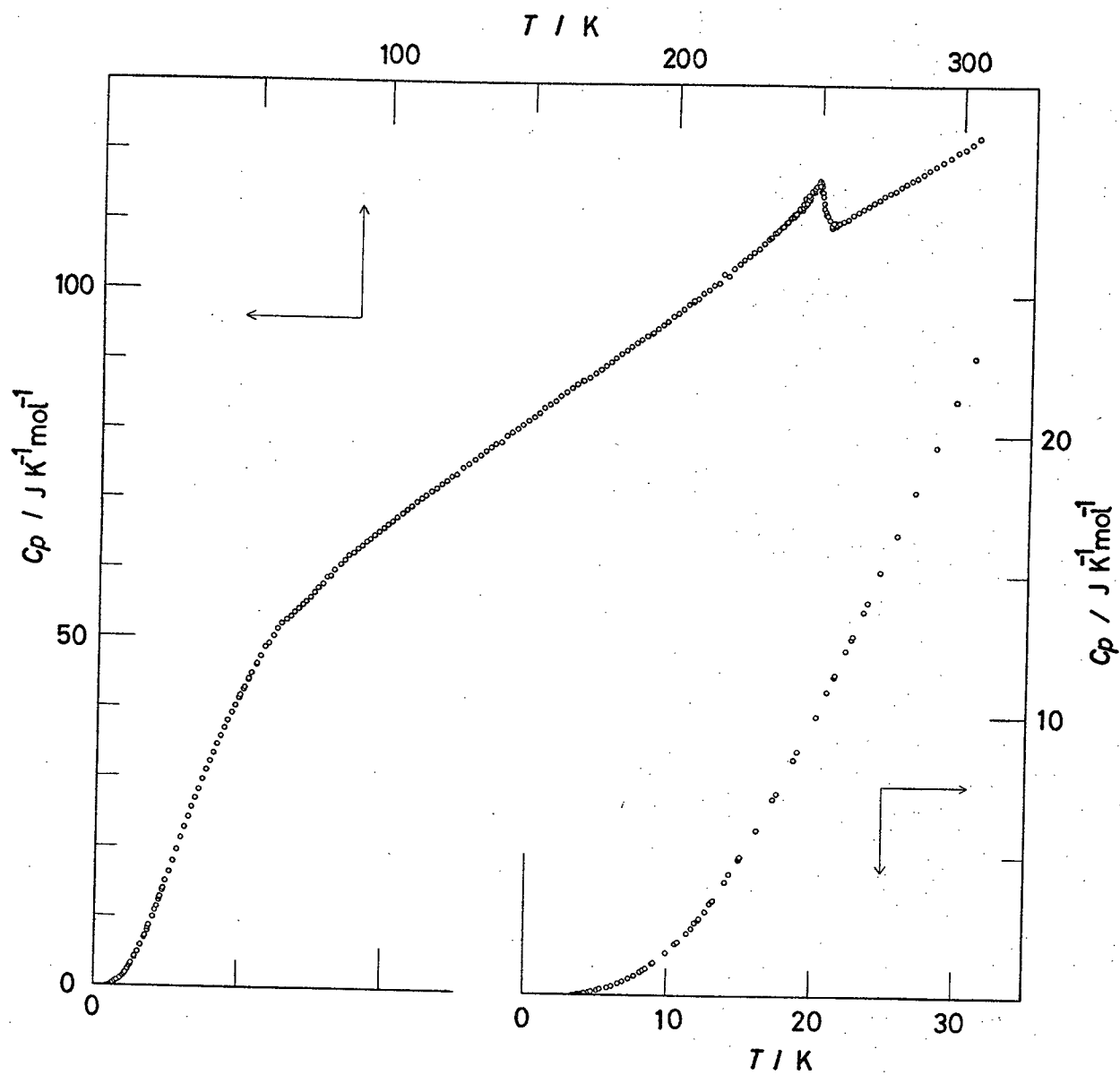
Fig. 3.2.6   Molar heat capacity of RbDSO$_4$.
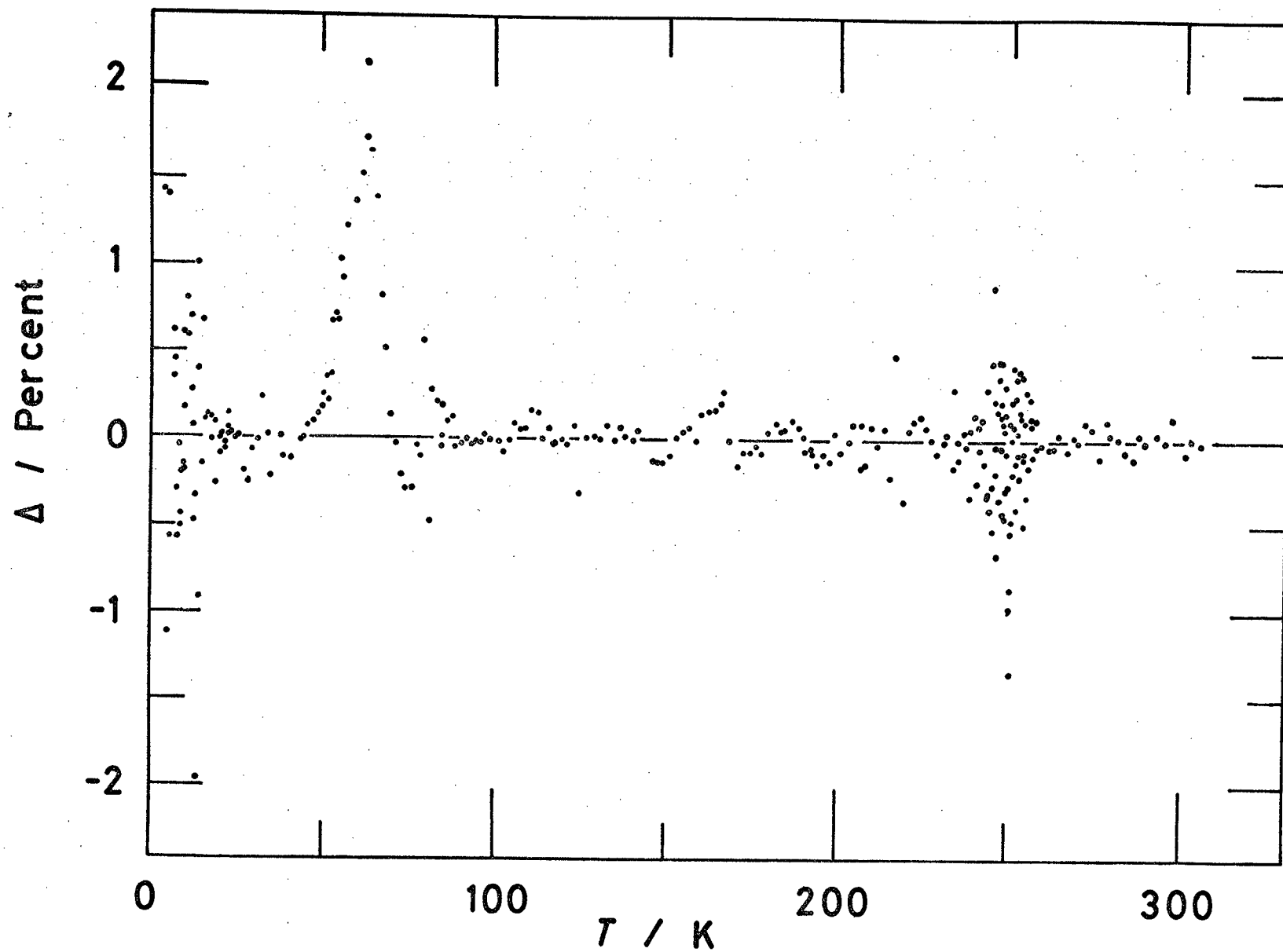
Fig. 3.2.7   Per cent deviations from the smoothed heat capacity of $RbDSO_4$.
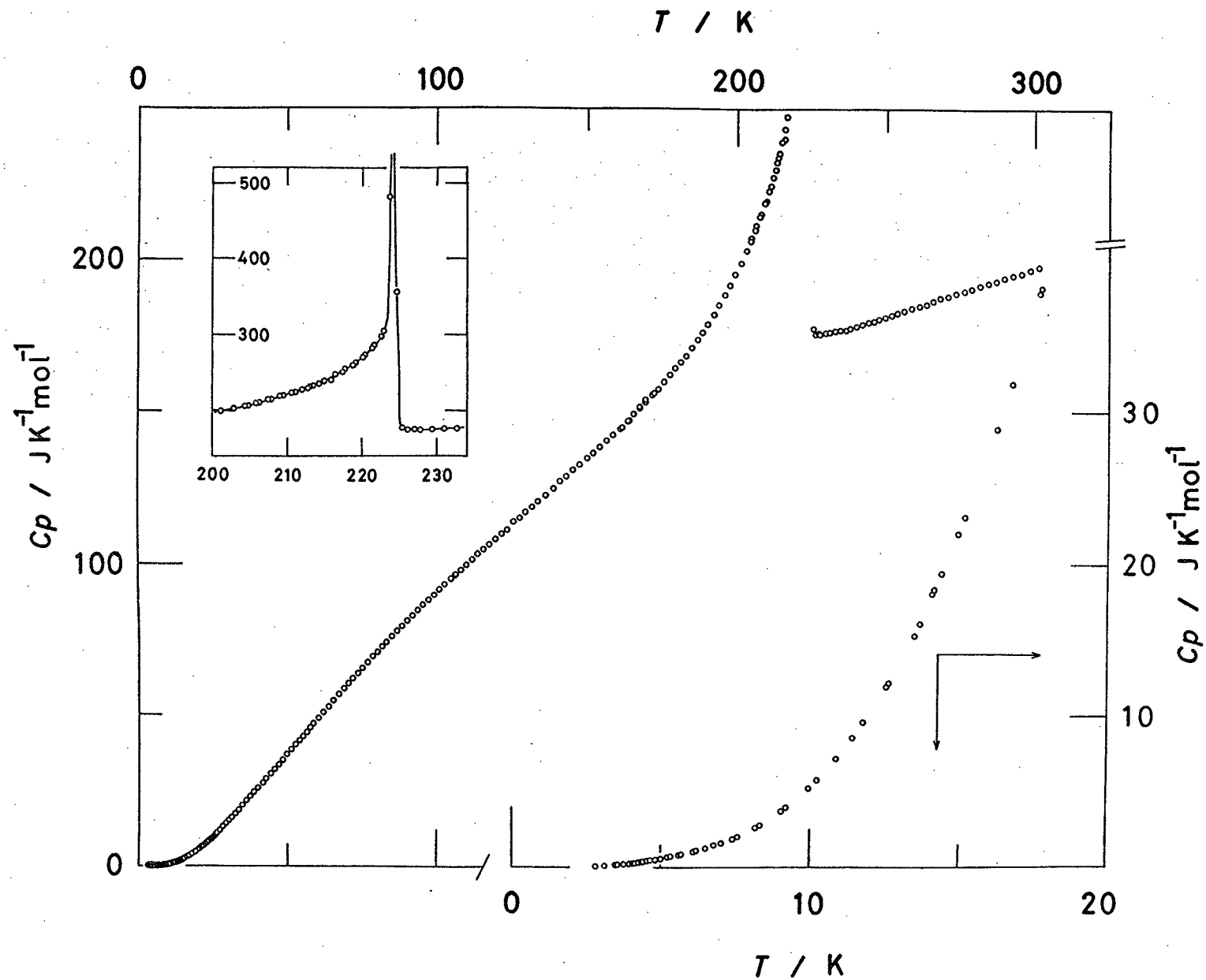
Fig. 3.2.8   Molar heat capacity of $(ND_4)_2SO_4$.
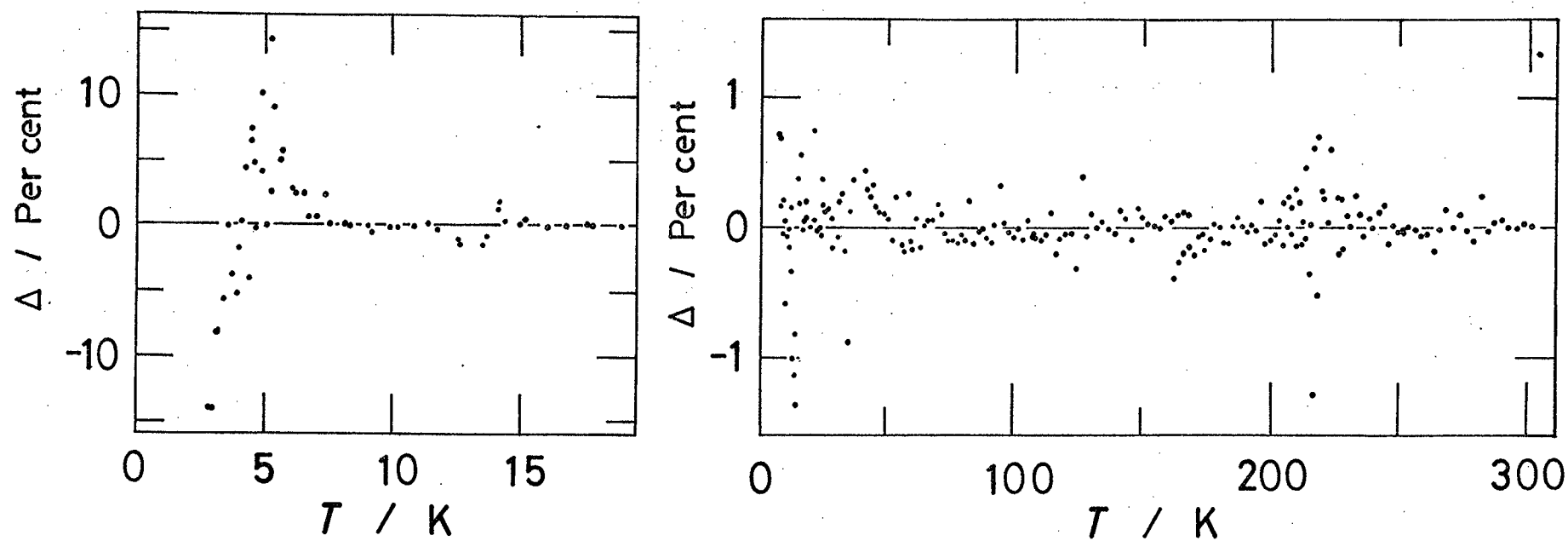
Fig. 3.2.9   Per cent deviations from the smoothed heat capacity of $(ND_4)_2SO_4$.
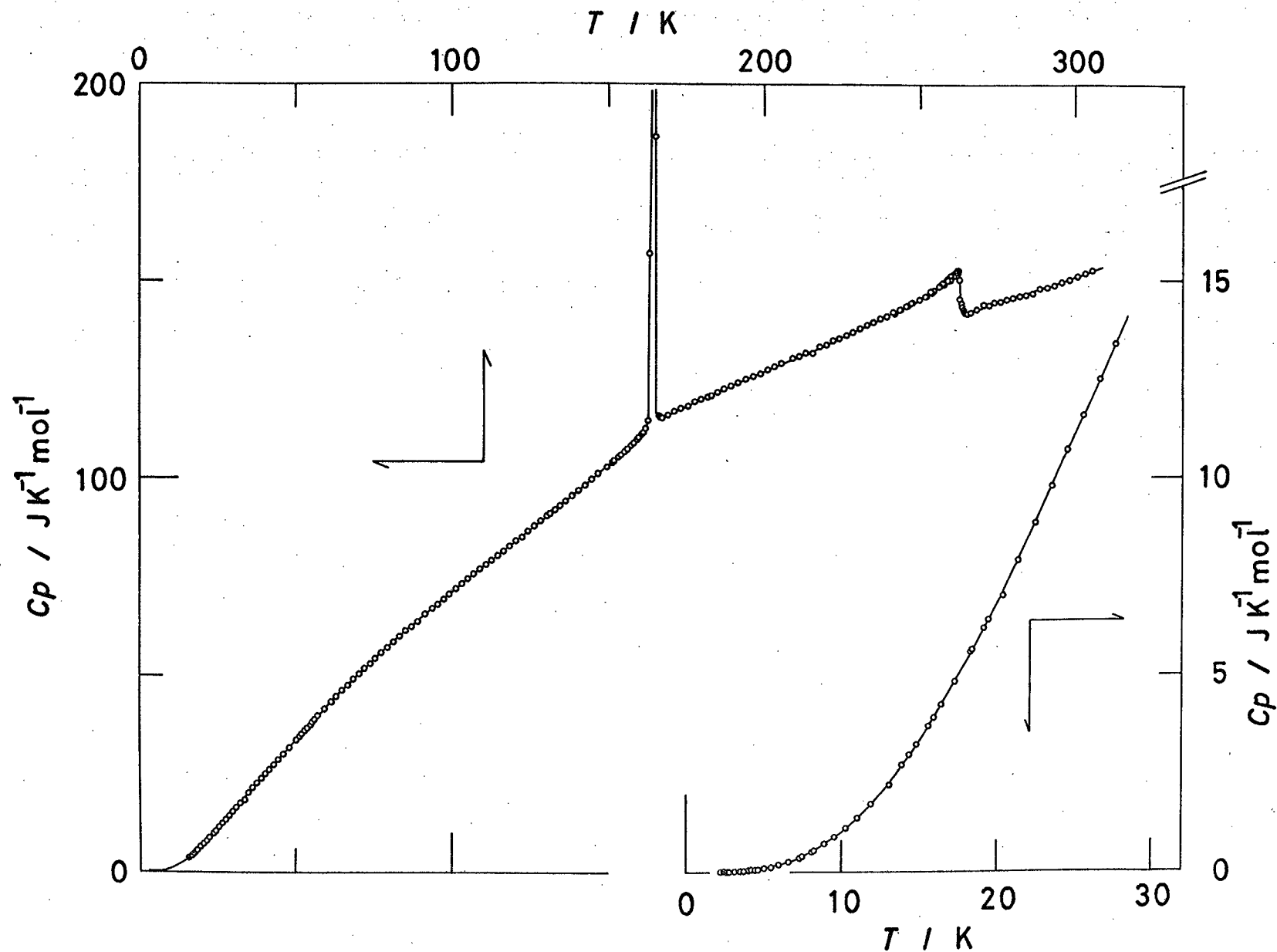
Fig. 3.2.10   Molar heat capacity of ND_4DSO_4.
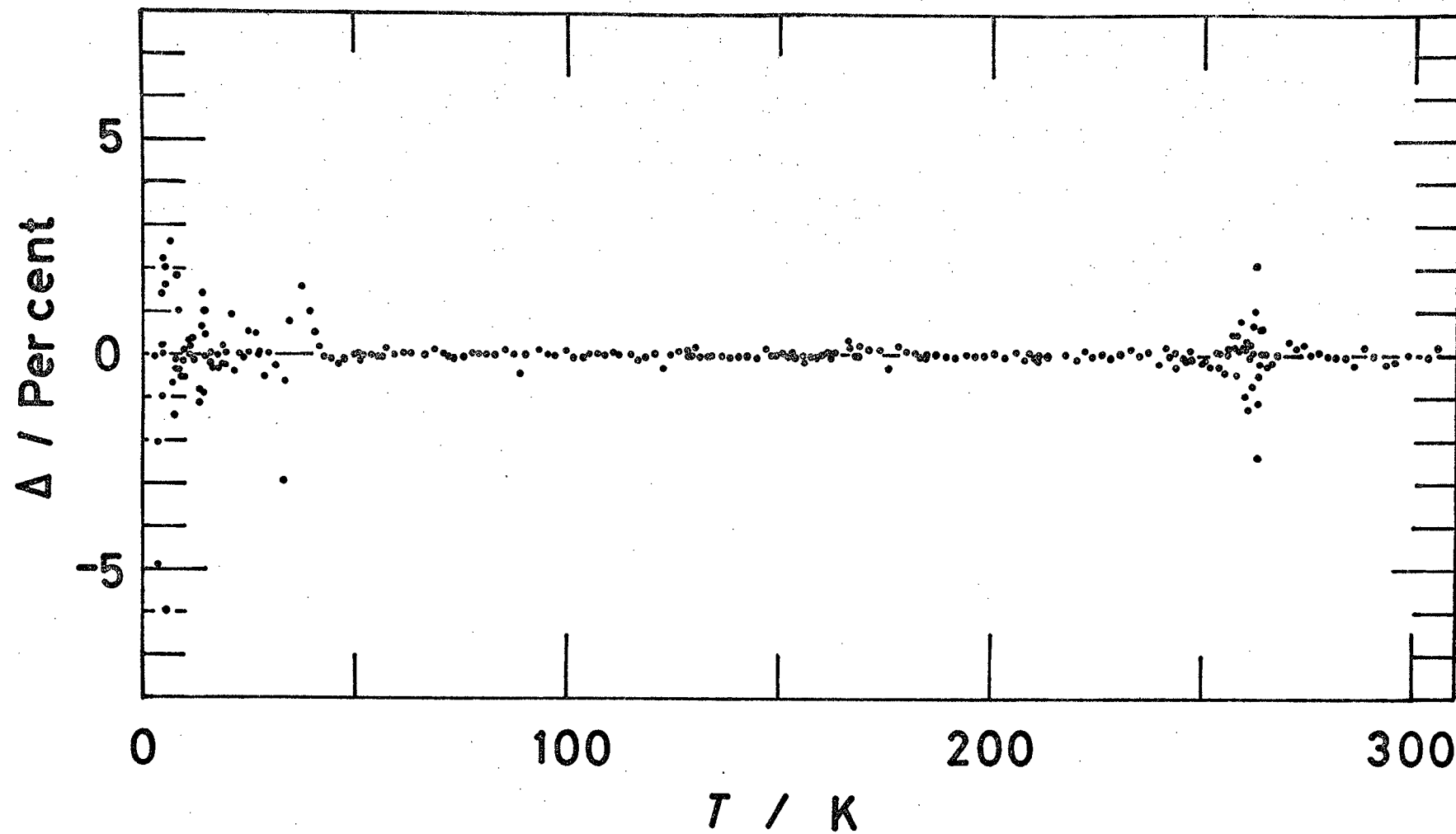
Fig. 3.2.11   Per cent deviations from the smoothed heat capacity of ND_4DSO_4.
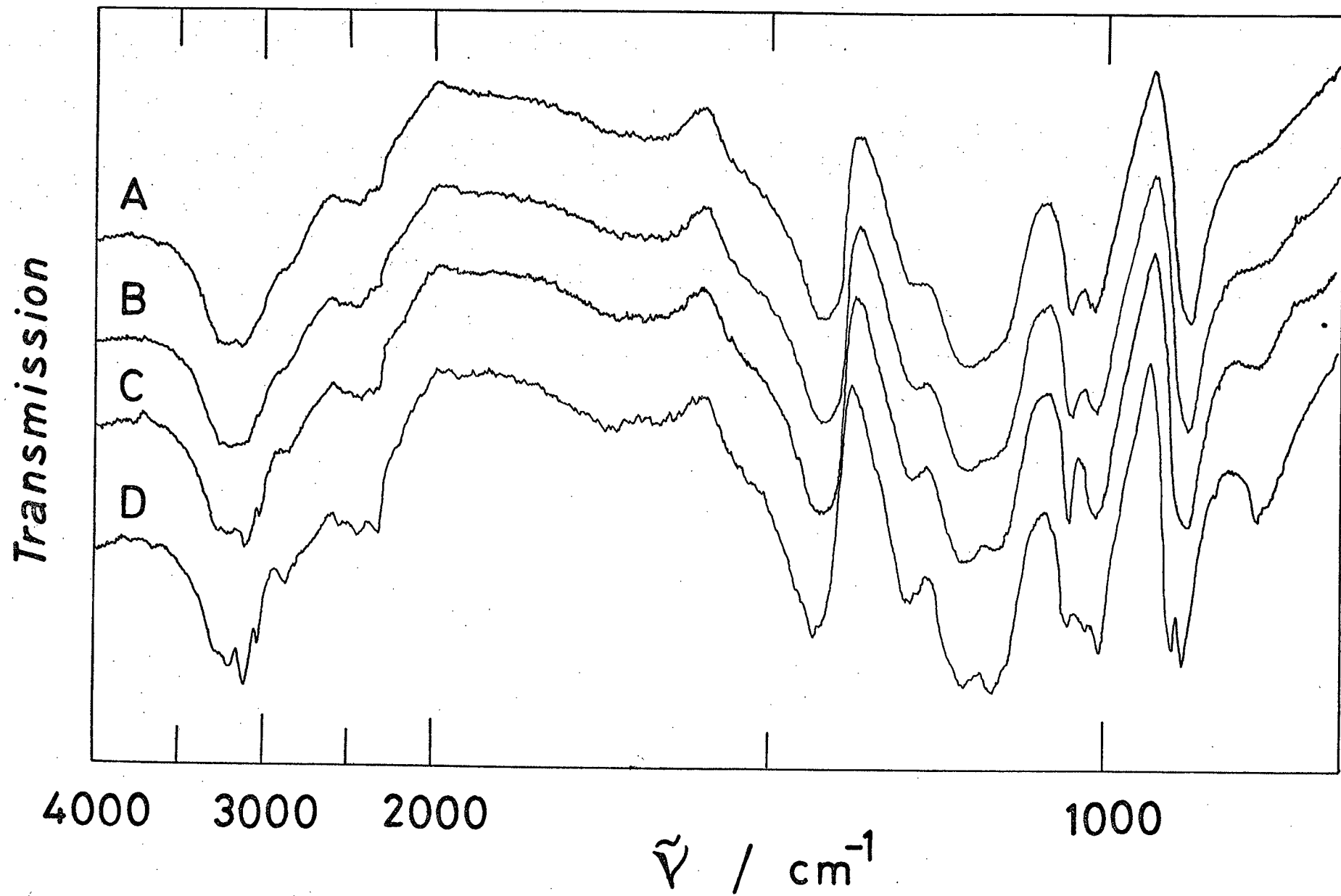
Fig. 3.3.1   Infrared spectra of NH_4HSO_4 (A at 298 K, B at 270 K, C at 203 K, D at 98 K)
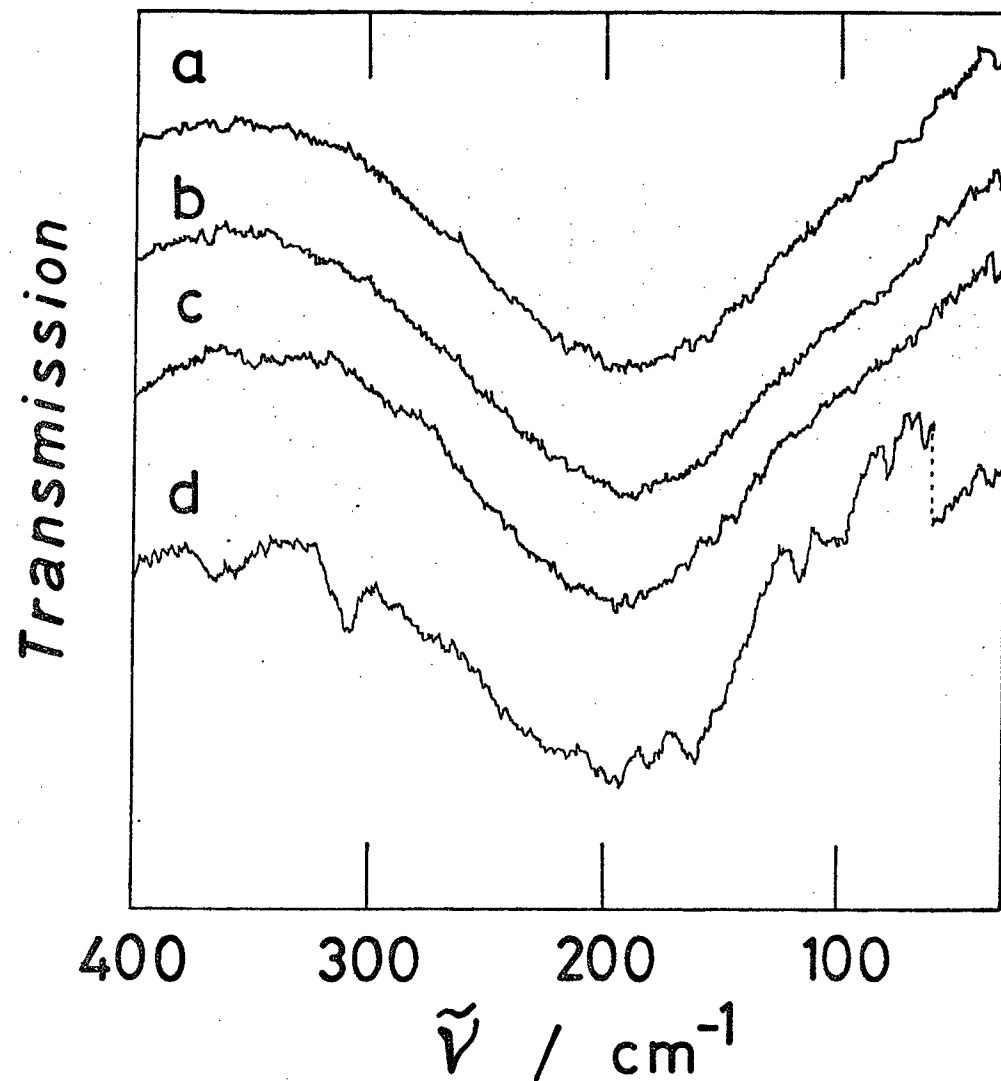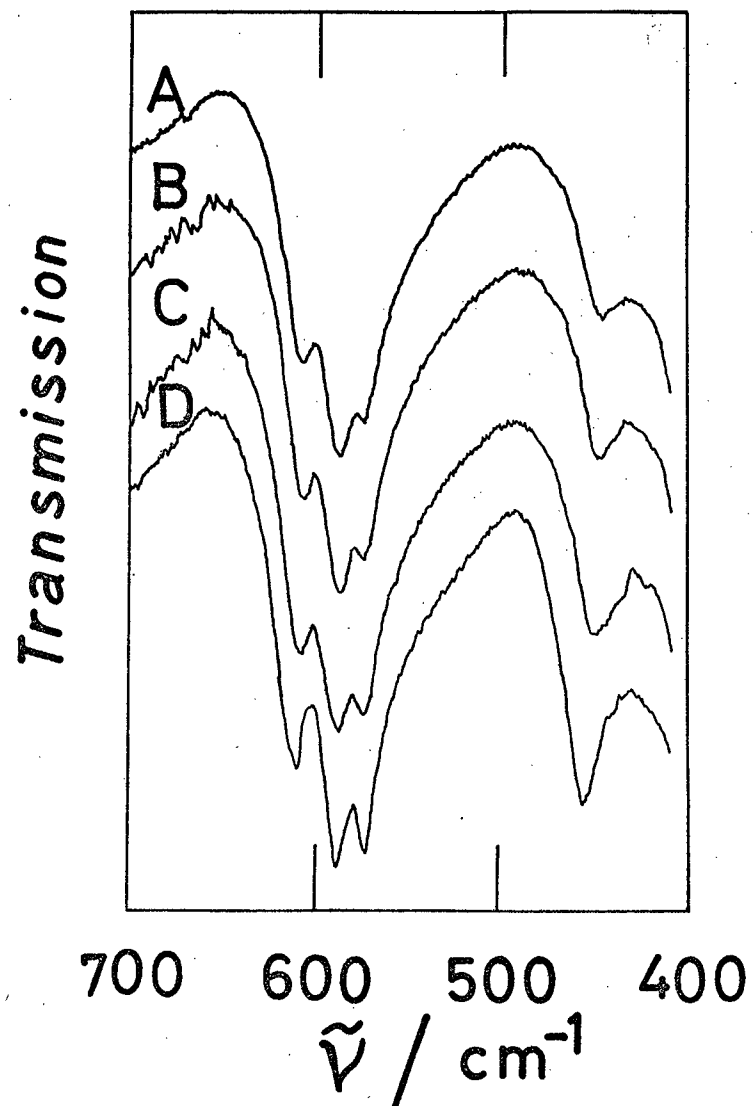
Fig. 3.3.2   Infrared and far-infrared spectra of NH$_4$HSO$_4$ (A at 298 K, B at 270 K
C at 203 K, D at 98 K, a at 298 K, b at 270 K, c at 203 K, d at 98 K; a at 273 K,
b at 263 K, c at 173 K, and d at 123 K)

94 K

200 K

290 K

Intensity

$\tilde{\nu}$ / cm^{-1}

4000 3000 2000 1000 0
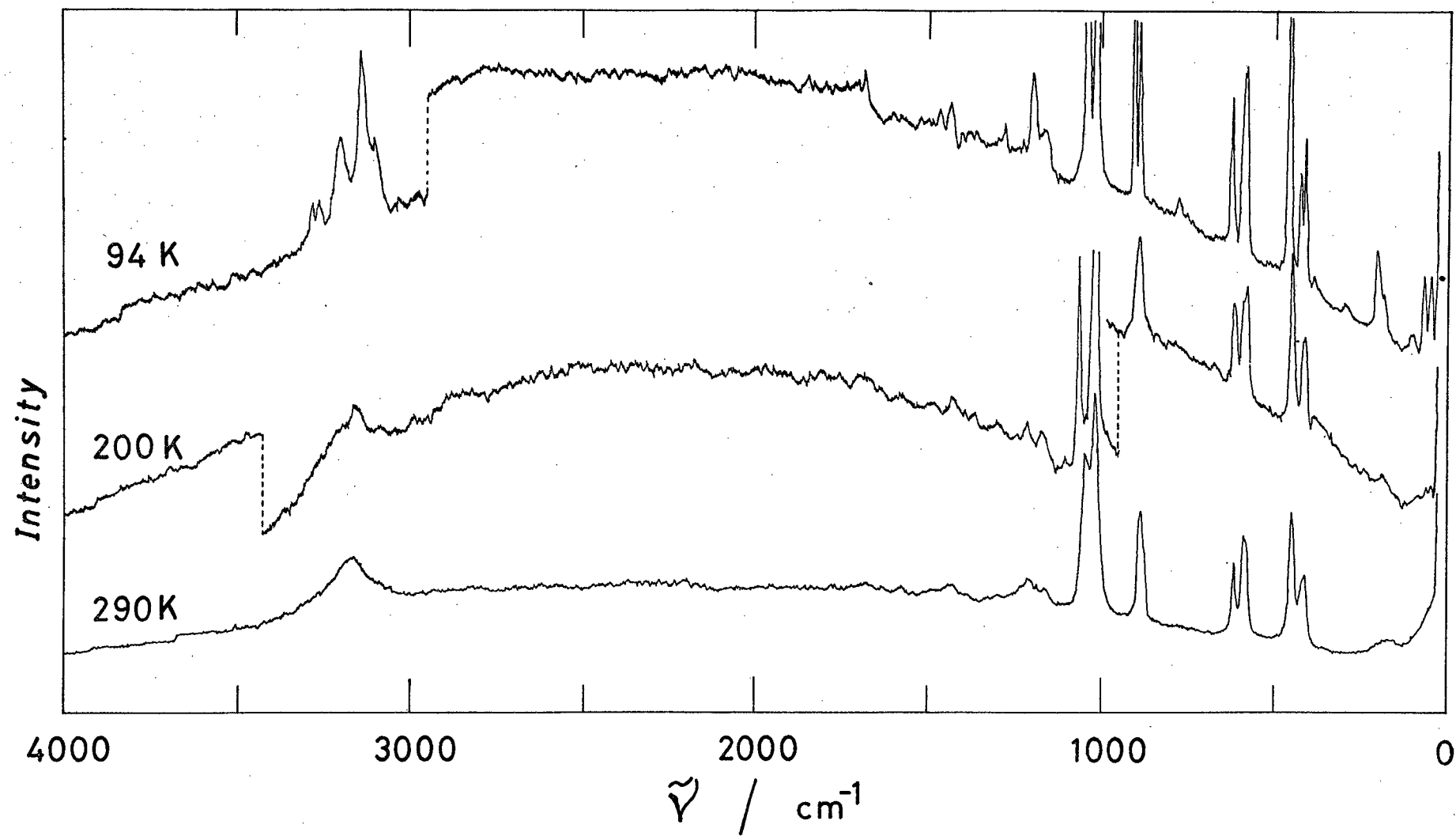
Fig. 3.3.3   Raman spectra of NH$_4$HSO$_4$
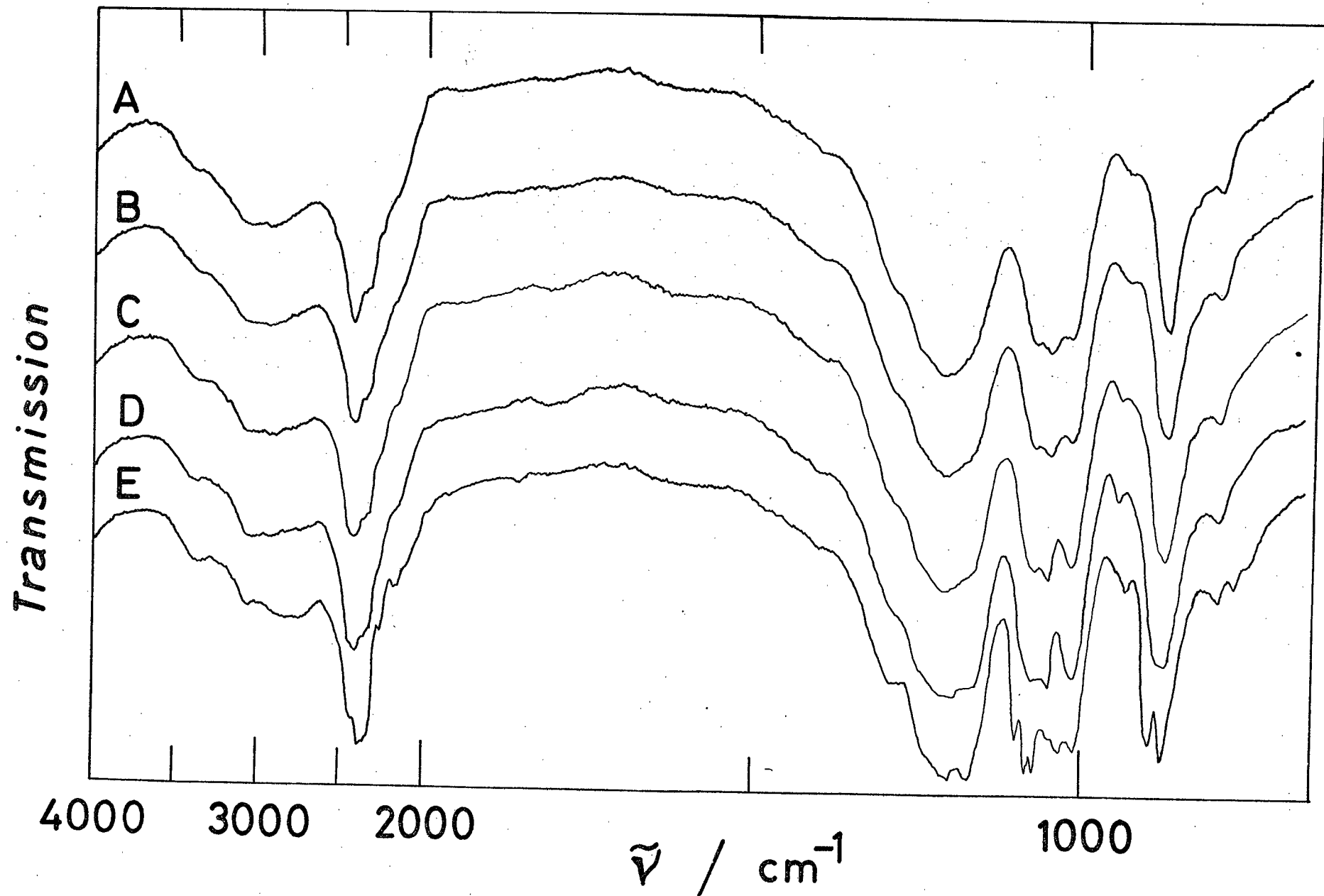
Fig. 3.3.4   Infrared spectra of ND_4DSO_4 (A at 304 K, B at 273 K, C at 223 K, D at 173 K, and E at 98 K)

120
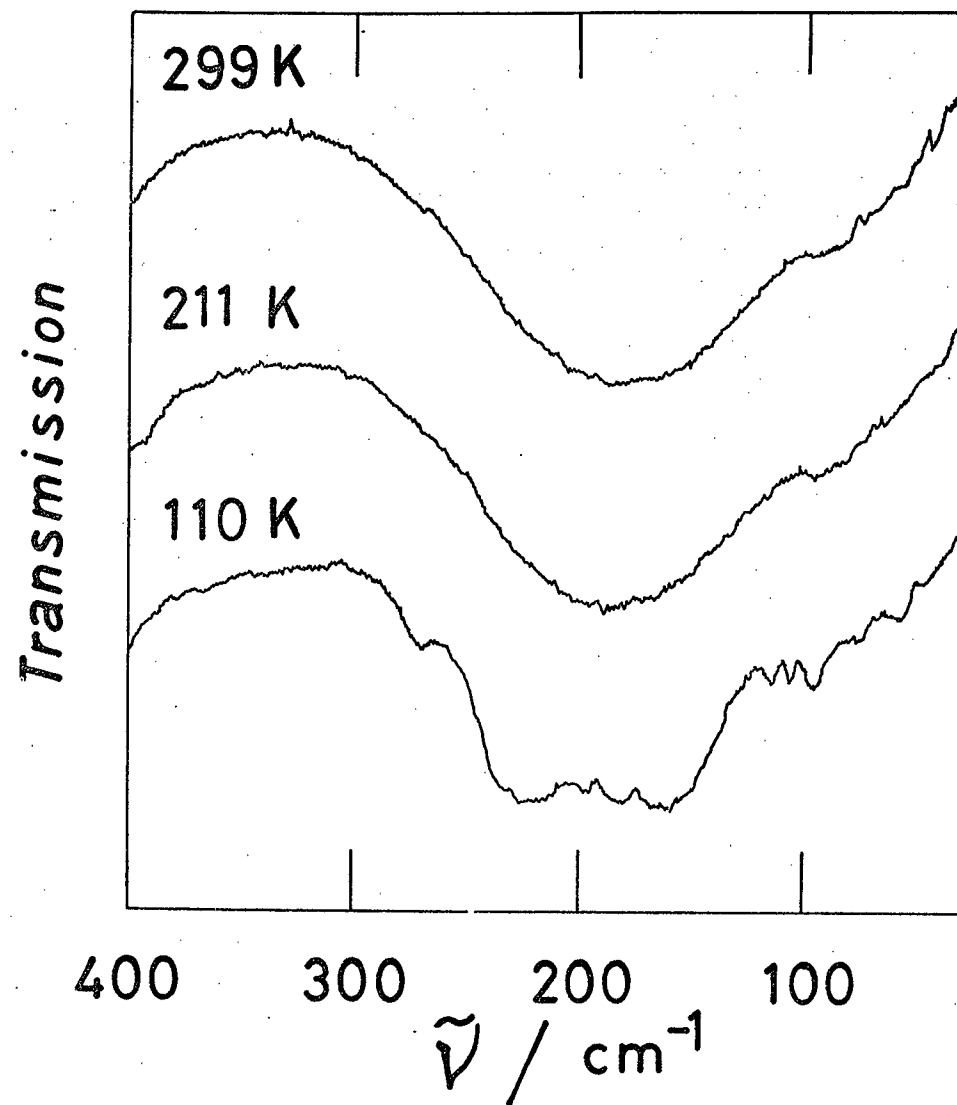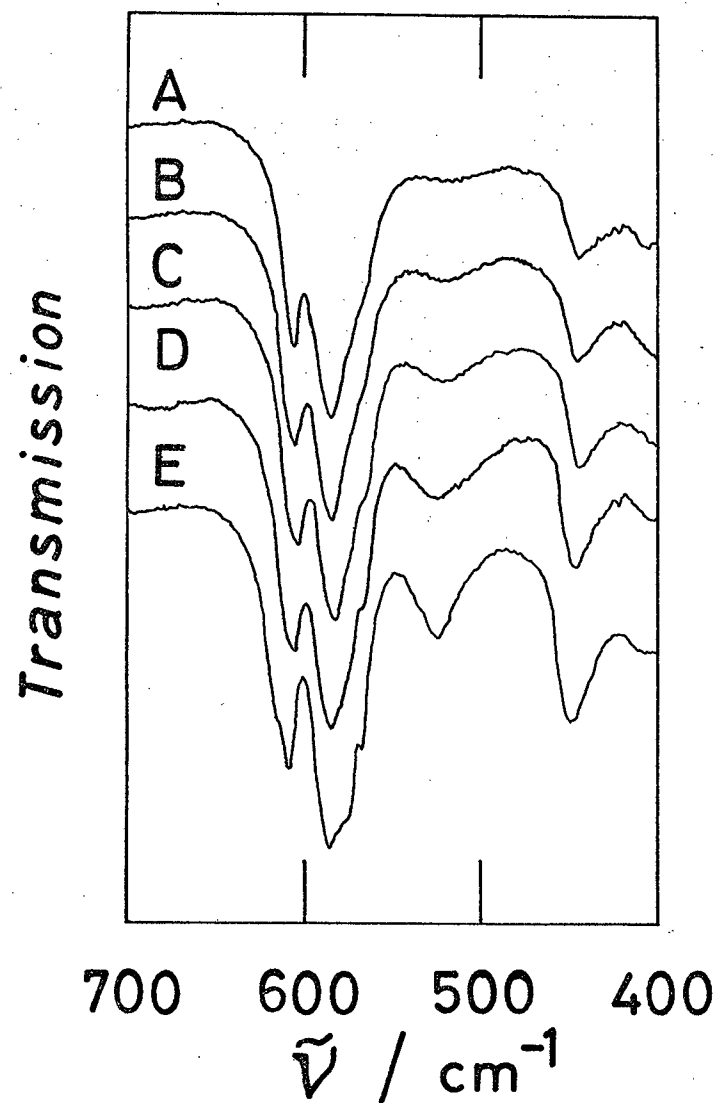
Fig. 3.3.5 Infrared and far-infrared spectra of ND_4DSO_4 (A at 304 K, B at 273 K, C at 223 K, D at 173 K, and E at 98 K)
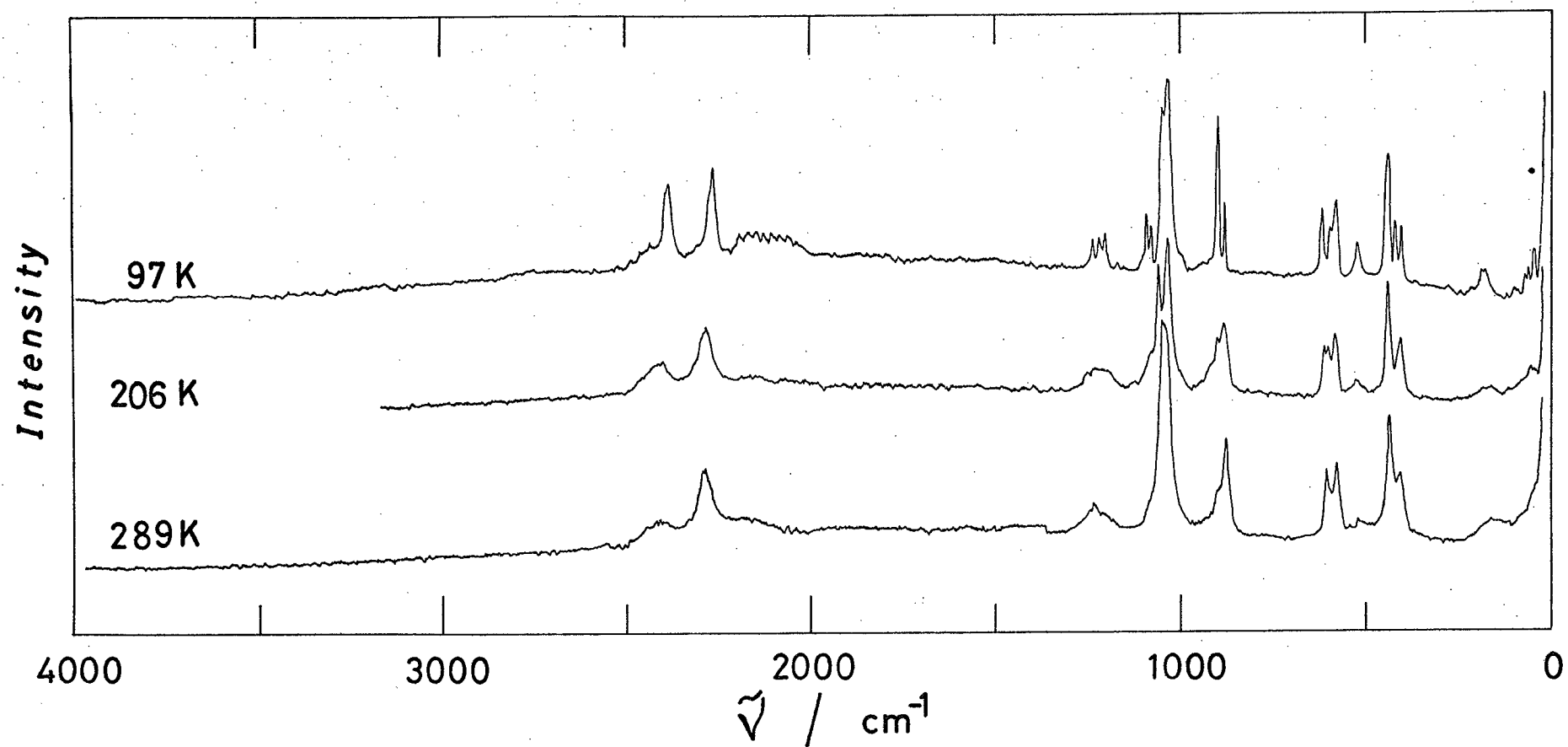
Fig. 3.3.6   Raman spectra of ND_4DSO_4
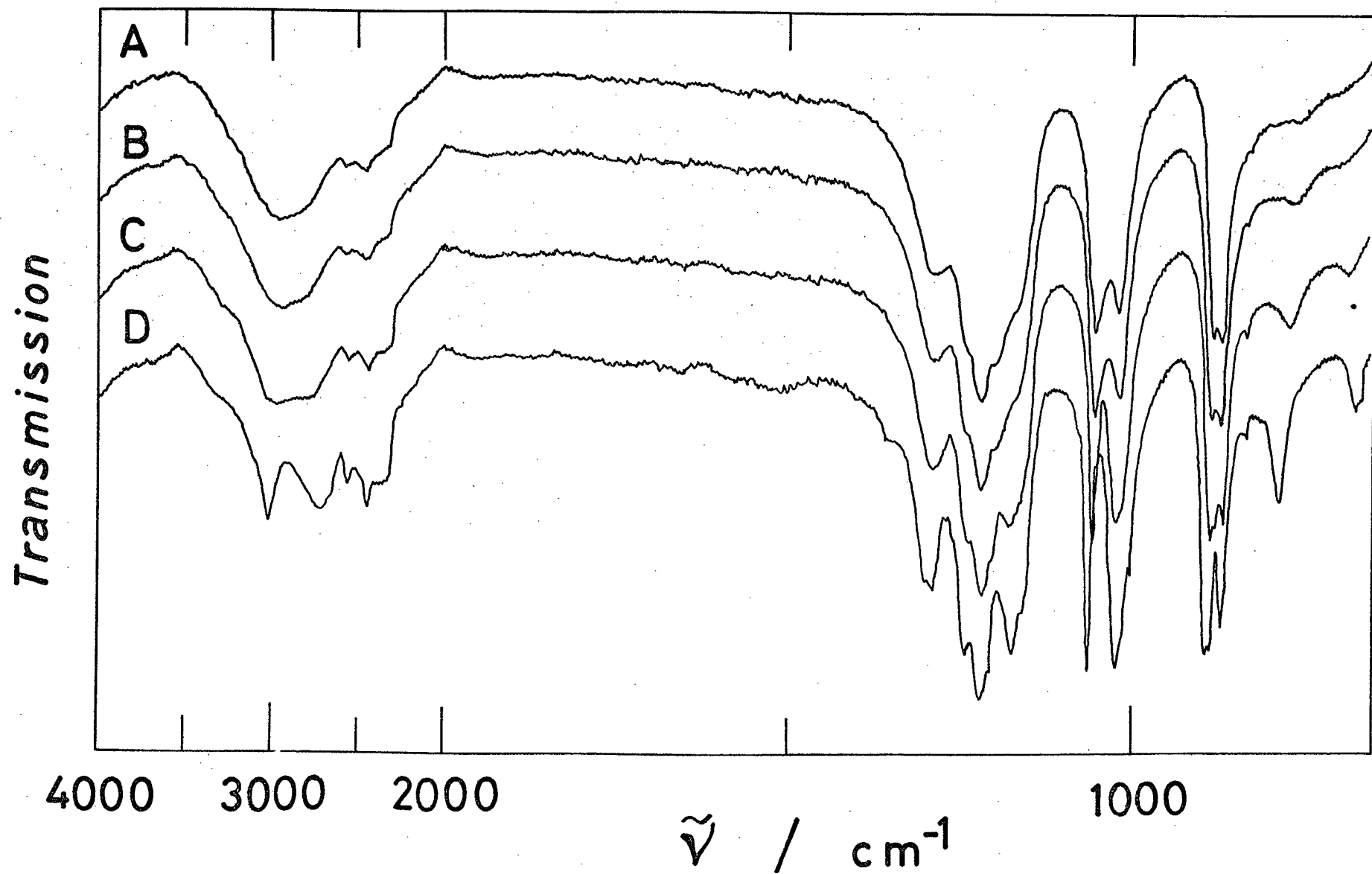
Fig. 3.3.7 Infrared spectra of RbHSO$_4$ (A at 300 K, B at 273 K, C at 223 K, D at 98 K)
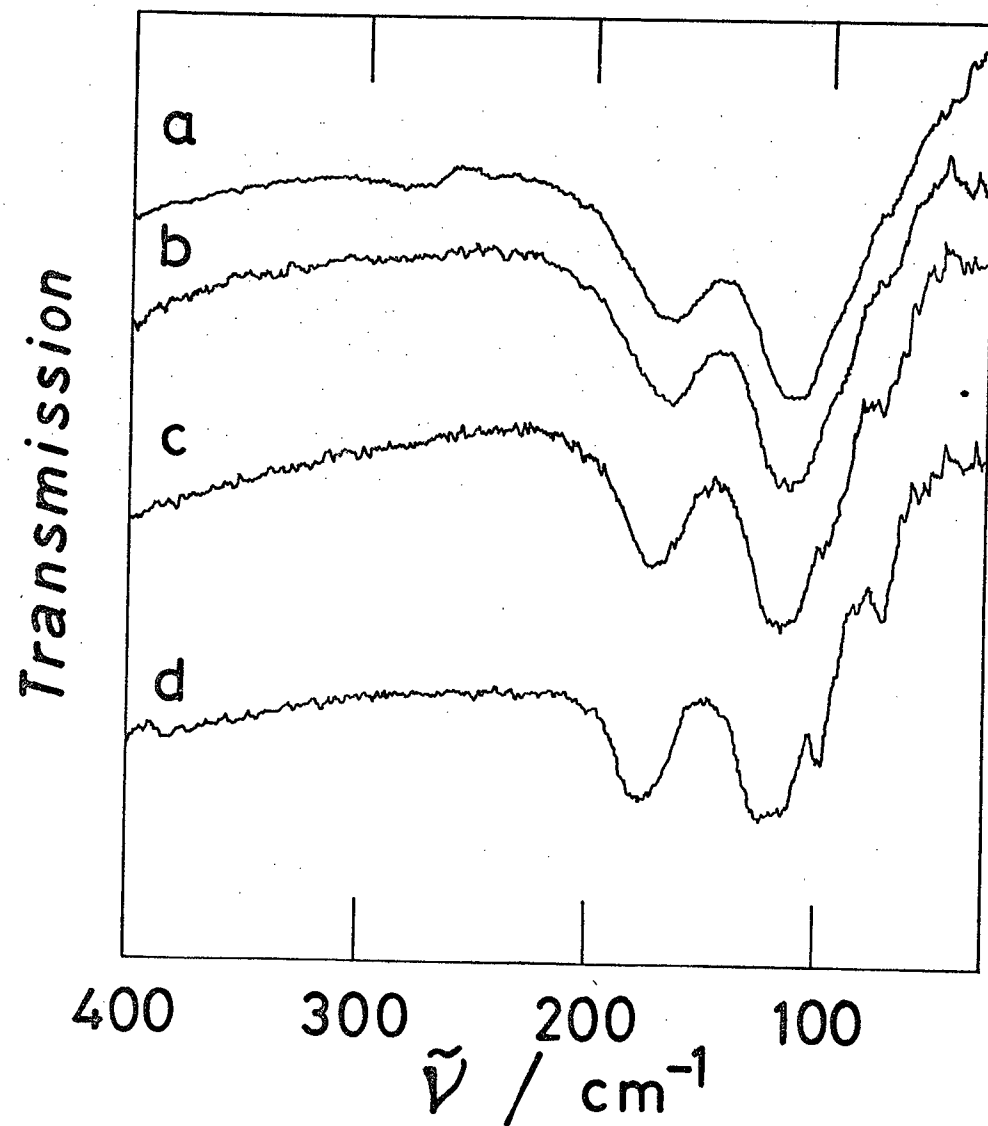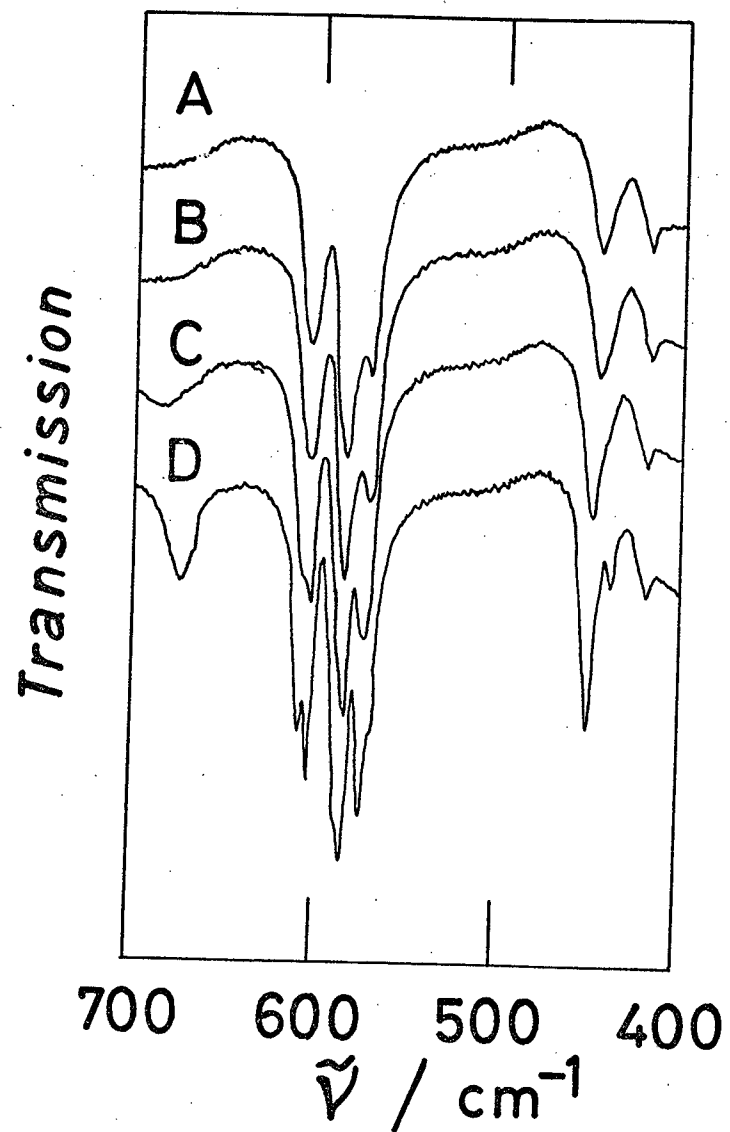
Fig. 3.3.8   Infrared and far-infrared spectra of RbHSO$_4$ (A at 300 K, B at 273 K, C at 223 K, D at 98 K, a at 300 K, b at 273 K, c at 223 K, d at 98 K)
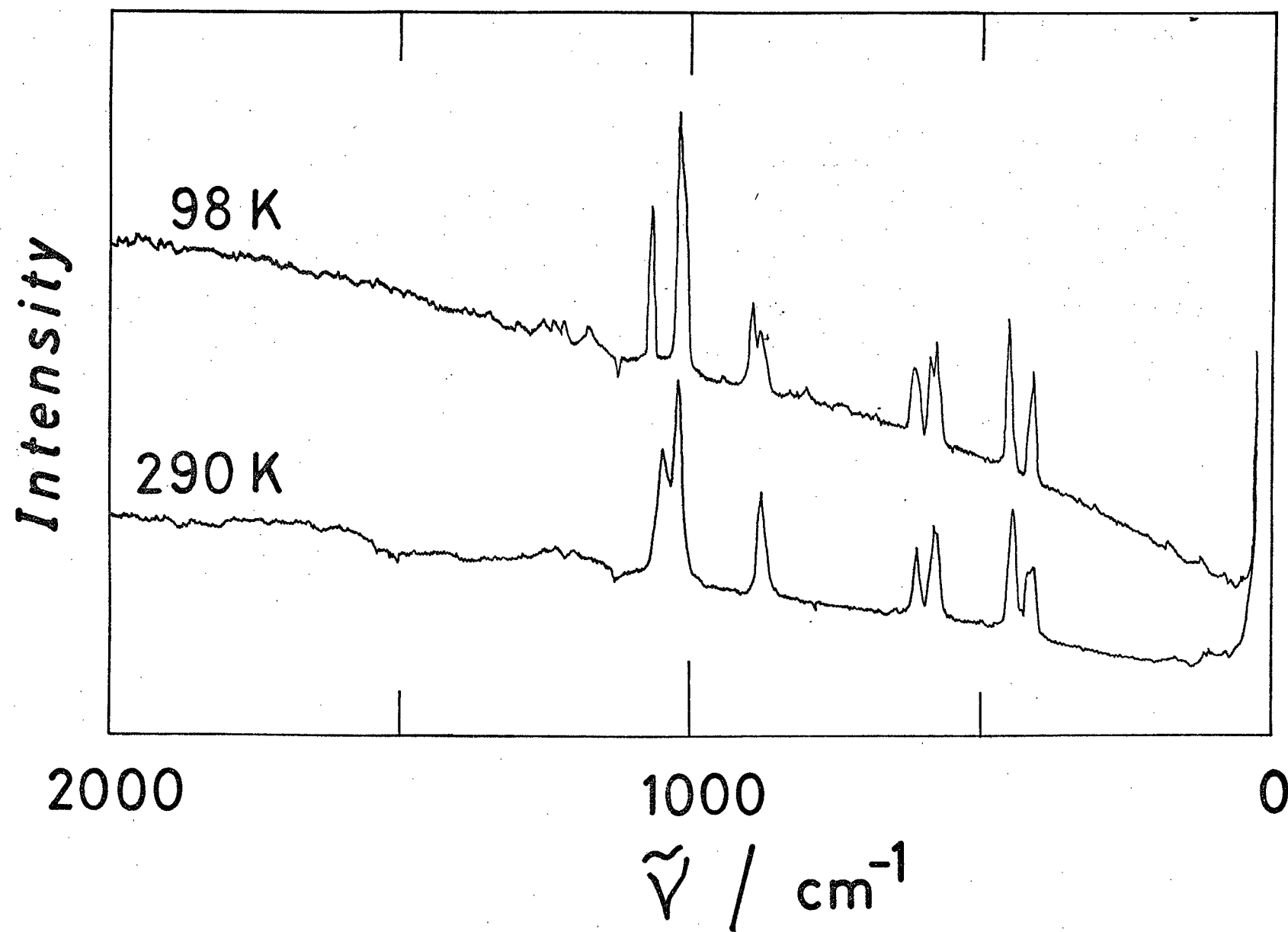
Fig. 3.3.9   Raman spectra of $RbHSO_4$
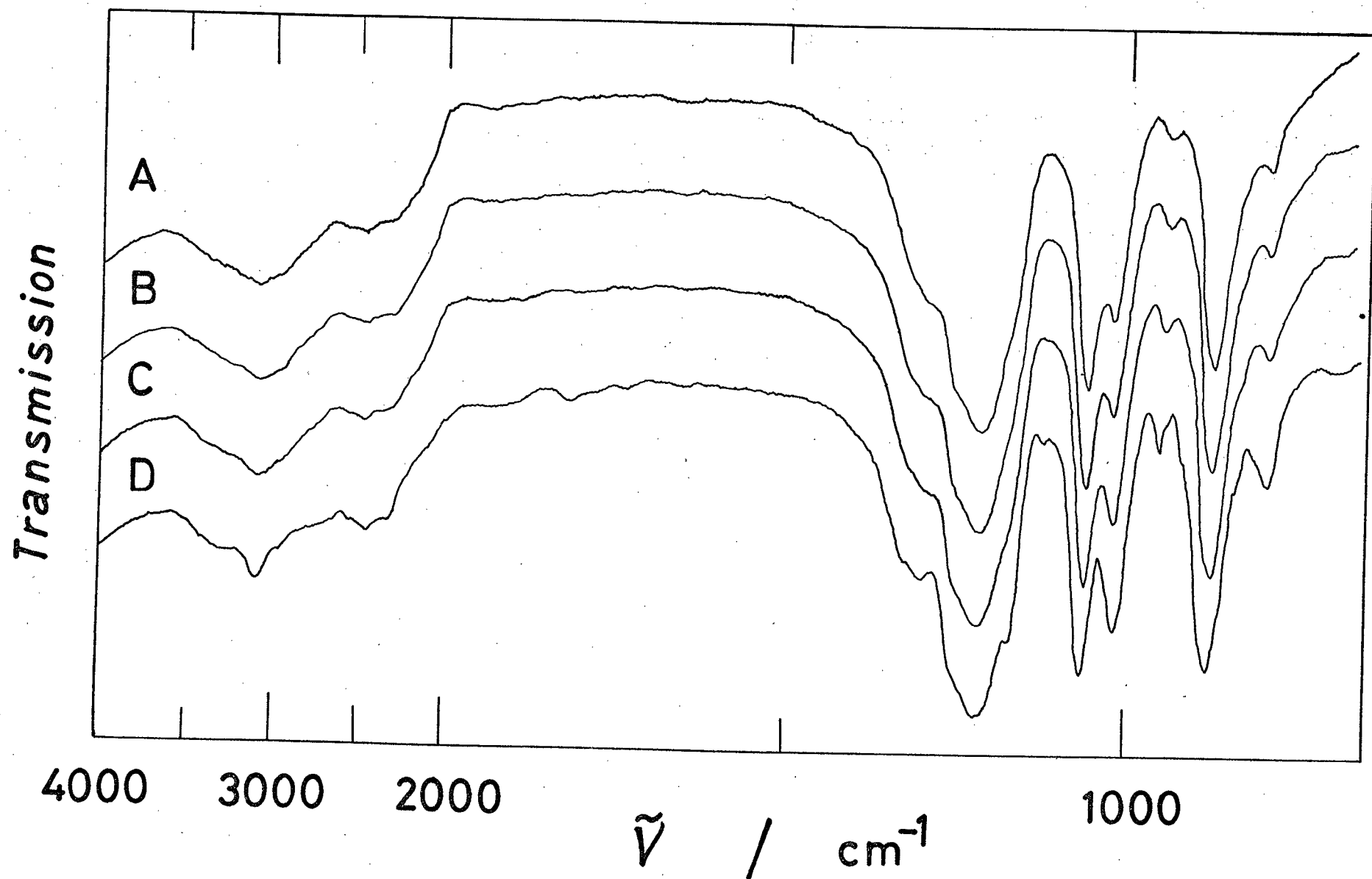
Fig. 3.3.10   Infrared spectra of RbDSO$_4$ (A at 300 K, B at 273 K, C at 223 K, D at 93 K)
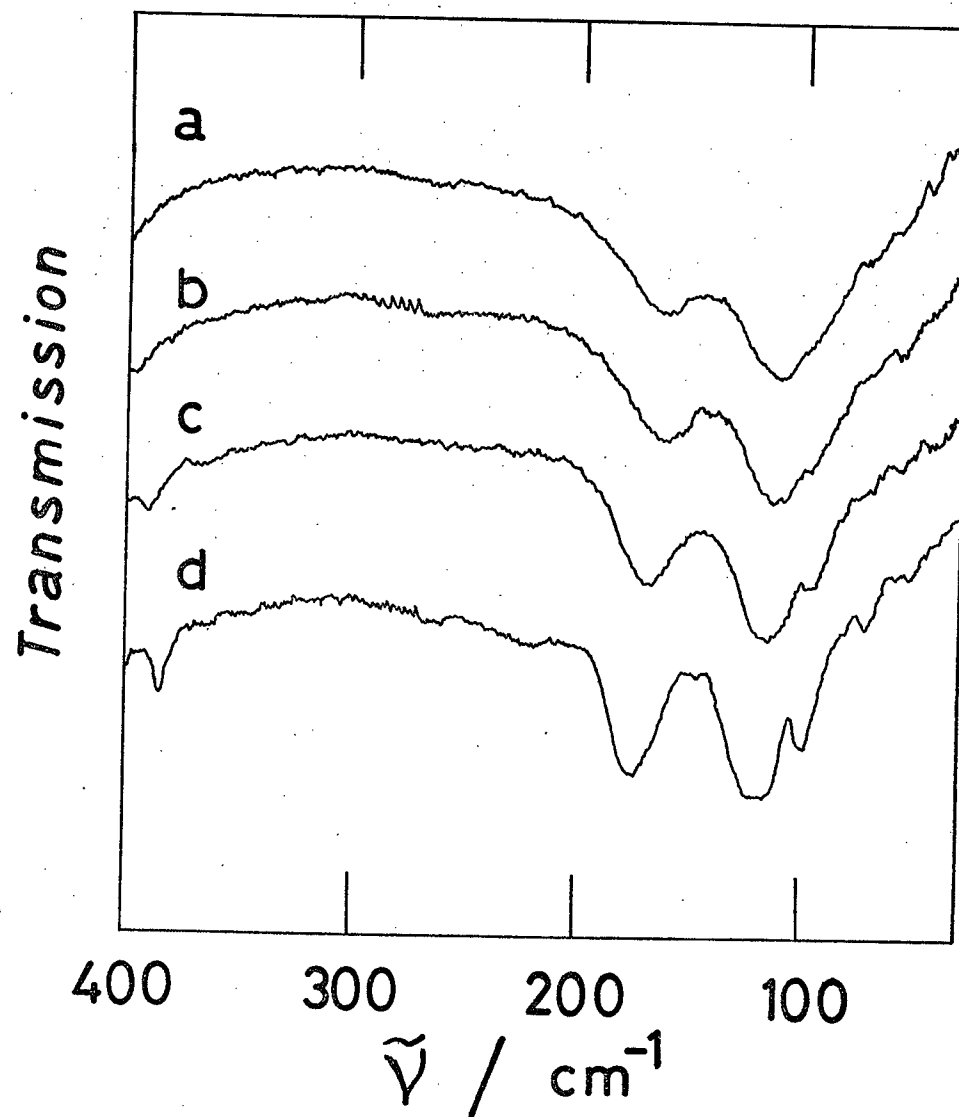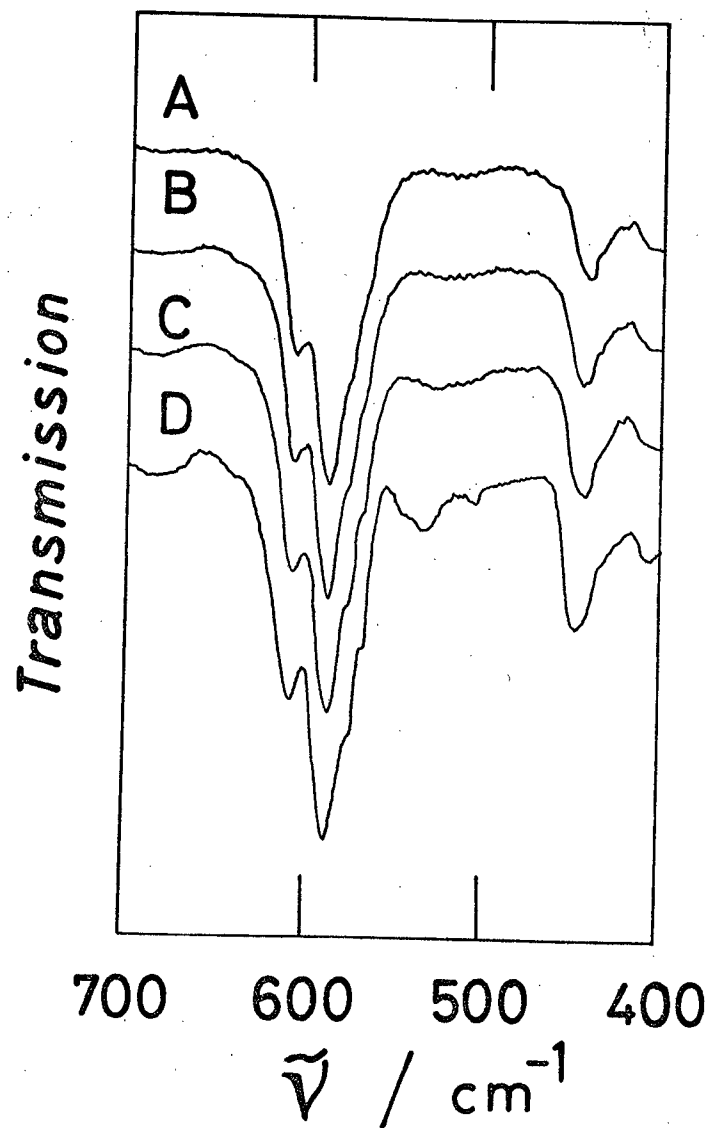
Fig. 3.3.11   Infrared and far-infrared spectra of RbDSO$_4$ (A at 304 K, B at 273 K, C at 223 K, D at 93 K, a at 299 K, b at 273 K, c at 203 K, d at 123 K)
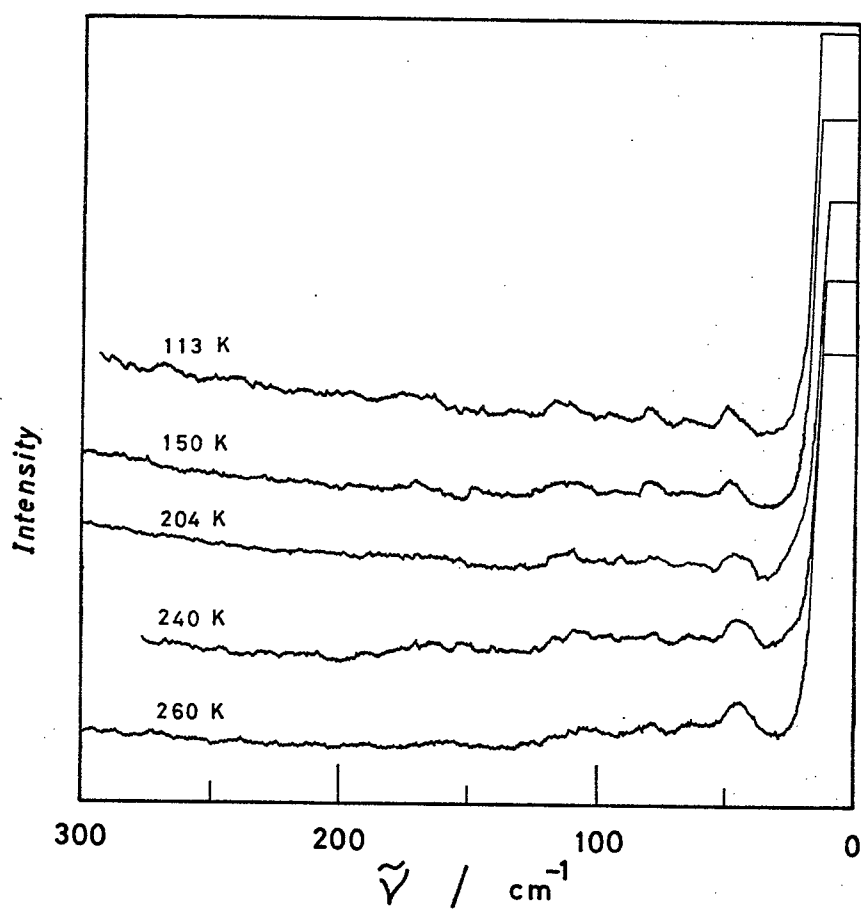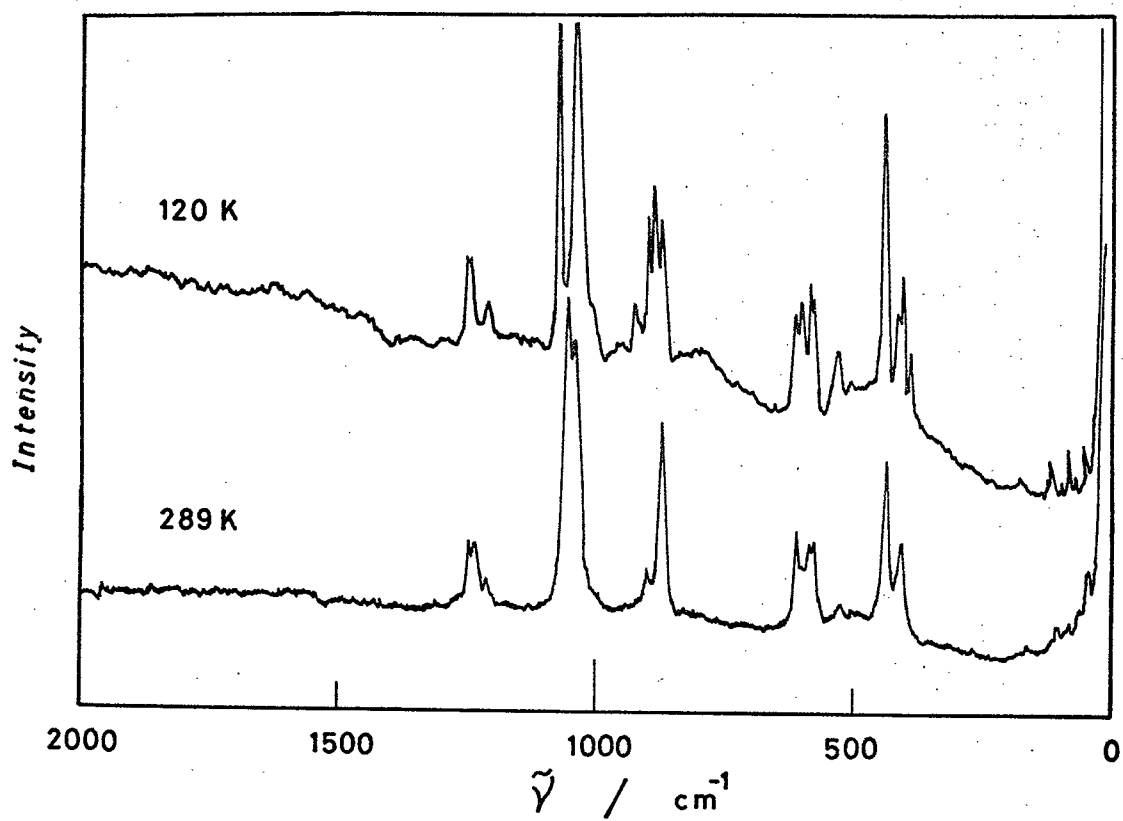
Fig. 3.3.12   Raman spectra of RbDSO$_4$
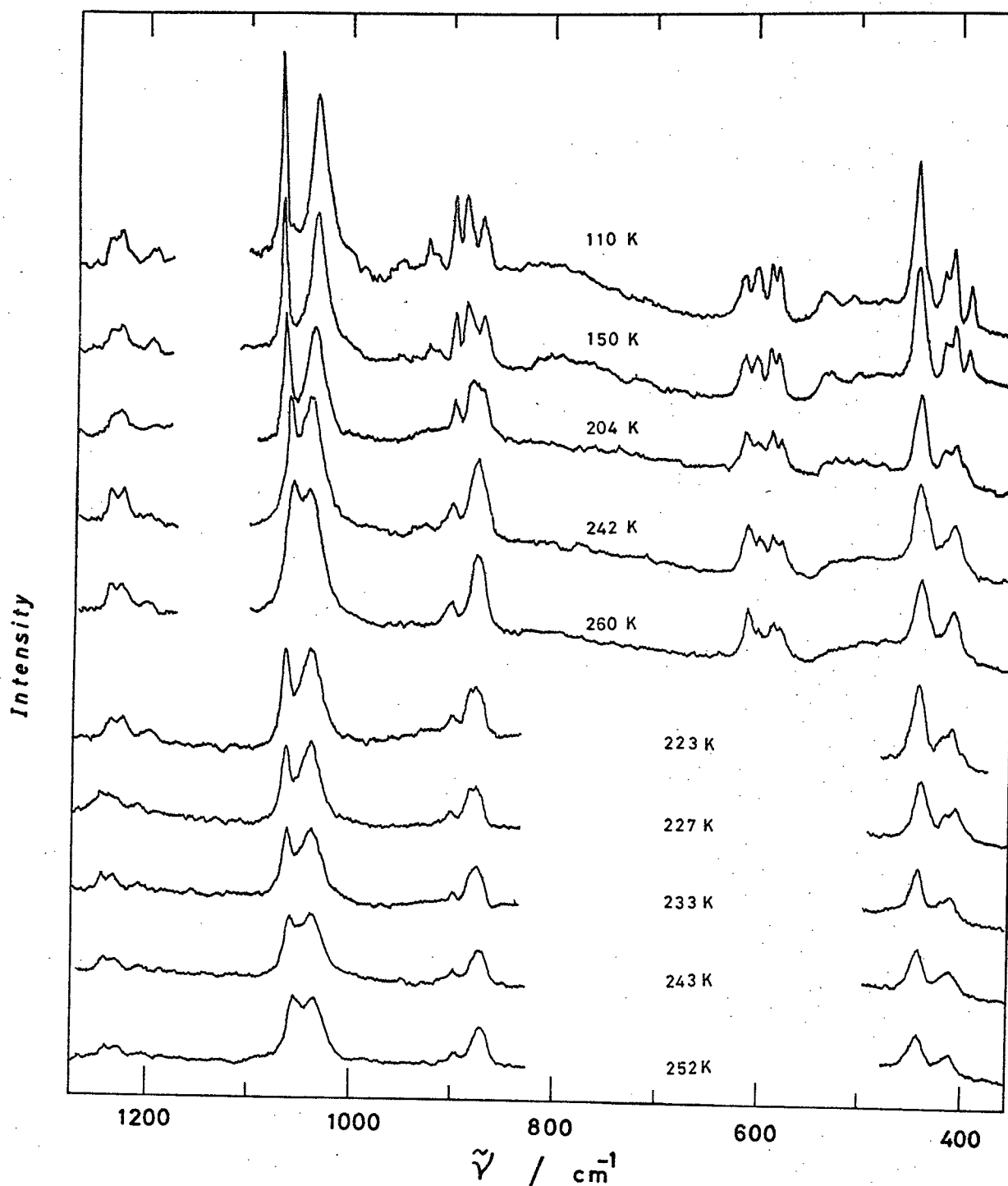
Fig. 3.3.13   Raman spectra of RbDSO$_4$
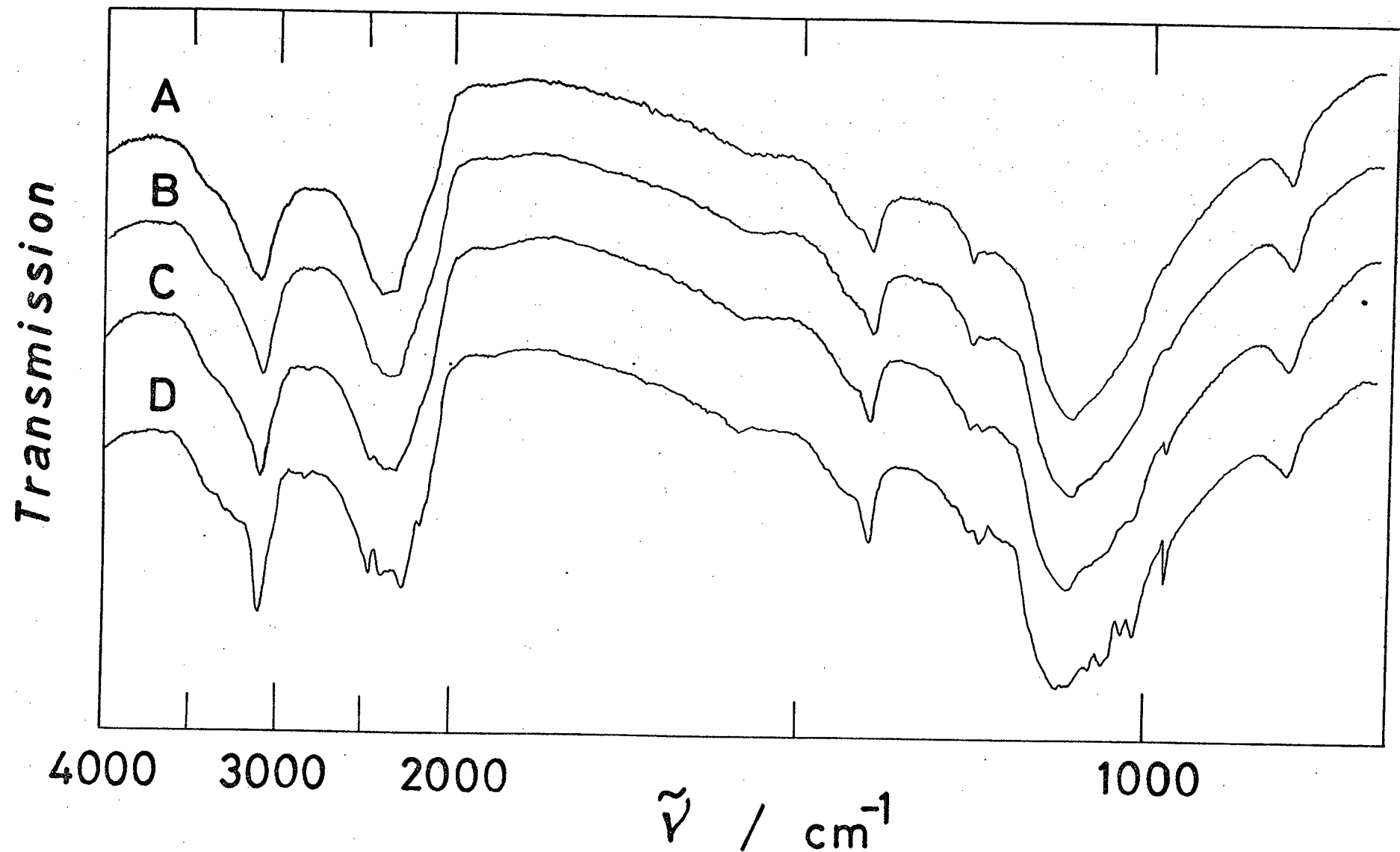
Fig. 3.3.14   Infrared spectra of $(ND_4)_2SO_4$ (A at 299 K, B at 233 K, C at 213 K, D at 99 K)
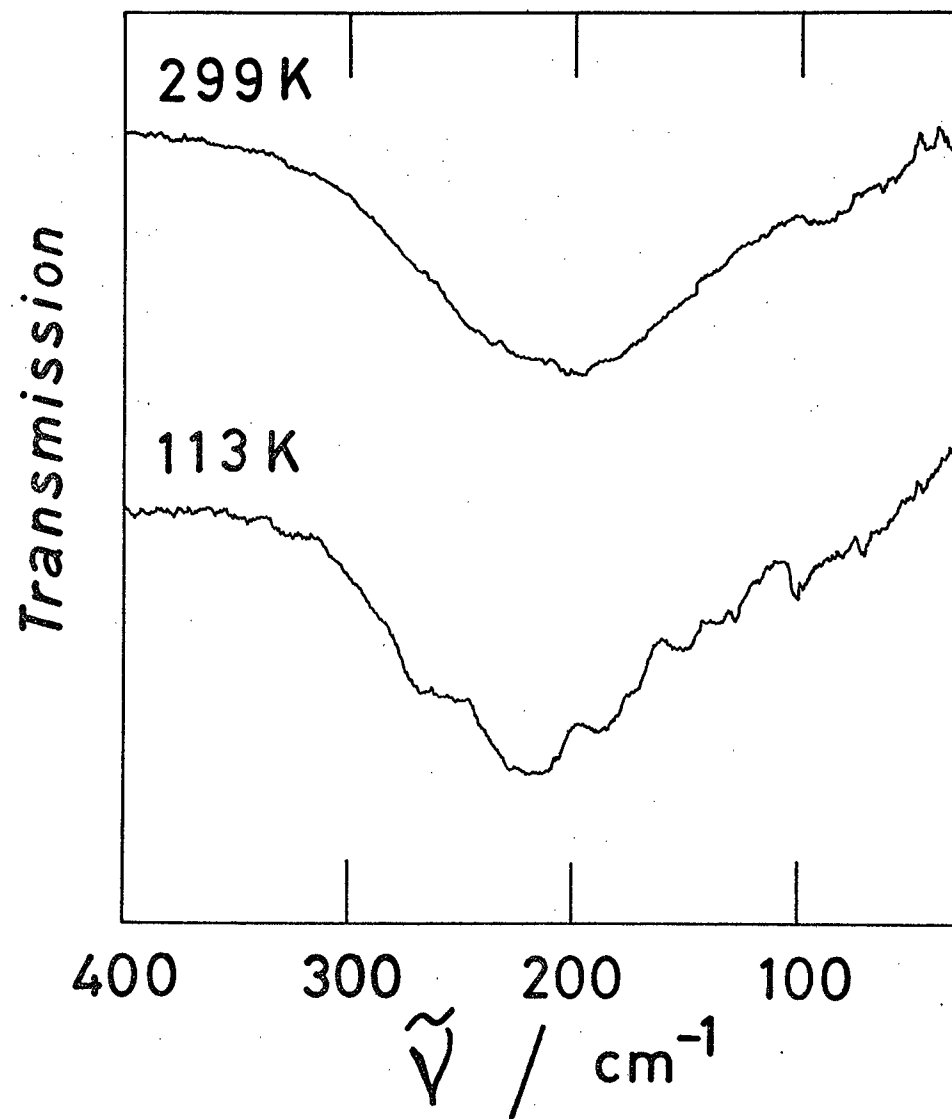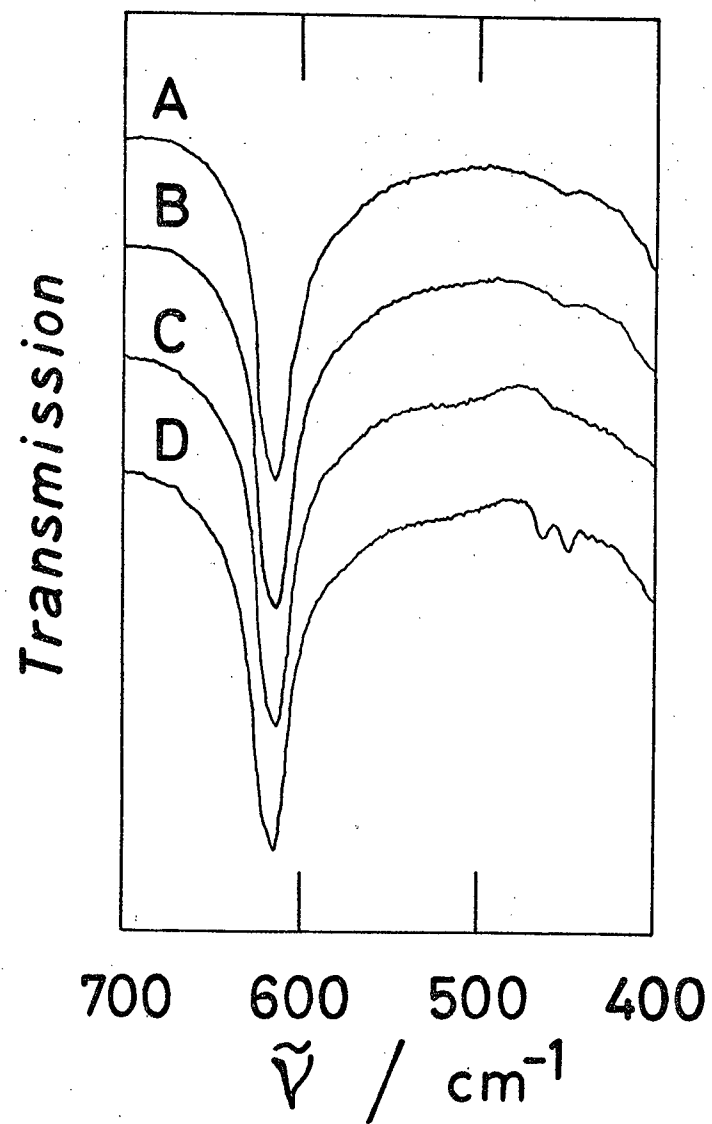
Fig. 3.3.15   Infrared and far-infrared spectra of $(ND_4)_2SO_4$

131
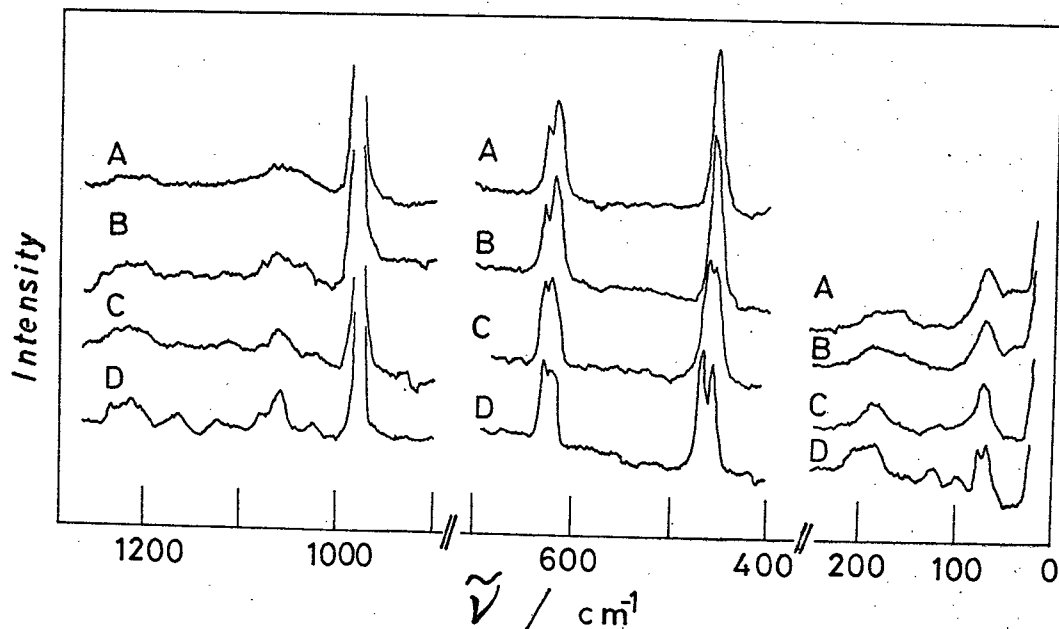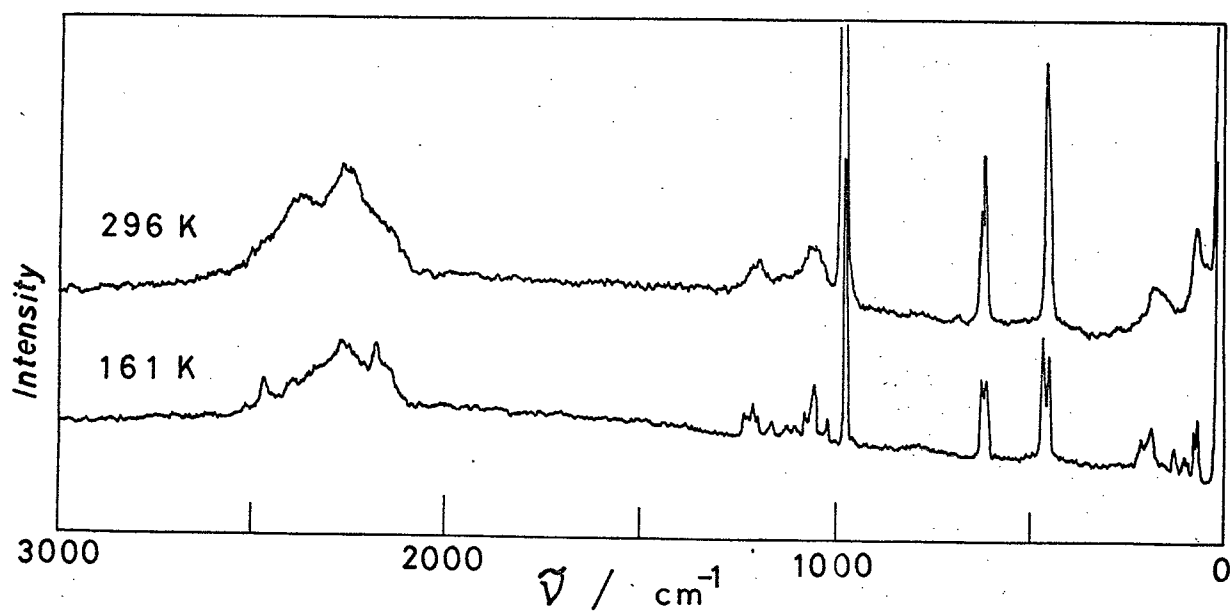
Fig. 3.3.16   Raman spectra of $(ND_4)_2SO_4$
(A at 298 K, B at 232 K, C at 219 K,
D at 174 K)

Chapter 4   Analysis and Discussion

4.1   Crystal structure

Symmetry aspects in ferroelectric are very important not only in revealing much of the behaviors of ferroelectric phase transitions but also in predicting many peculiarities in their behaviors. Shuvalov[1] was the first to develop the symmetry approach in the macroscopic theory of ferroelectricity.

Prior to the comparison of the results of the present thermodynamic study with those of the group-theoretical study by Takagi and his coworkers[2,3] as well as that of Aizu,[4] we tried to understand in detail the crystallographic characteristics of NH_4HSO_4, $RbHSO_4$ and $(NH_4)_2SO_4$, concentrating on the origin of ferroelectric polarization.

A ferroelectric state is an electrically polarized state which is reversible or reorientable. The polarization is defined as the number of dipole moment per unit volume. The electric dipole moment in crystal may be realized not only by the permanent dipole inherent in molecules and ionic groups but also by the vibration of ionic lattice itself.

A regular tetrahedral ion such as a free NH_4^+ or SO_4^{--} never has an electric dipole but has an octopole moment. If these tetrahedral ions can be distorted in the radial interatomic distance and in the bond angle by the effects of electrostatic crystal field and the hydrogen bonds, then the origin of ferroelectric polarization may be ascribed to the distortions of these ions. In fact the angular distortion of ND_4^+ in $(ND_4)_2SO_4$, for example, is reported by Chiba[5] in the DMR experiment and confirmed later by O'Reilly and Tang,[6] who regarded the highly distorted ND_4^+ as the origin of spontaneous polarization. So far the distortion in SO_4^{--} has been scarcely discussed in connection with the

ferroelectric transition in crystals having SO_4^{--}. The distortions of

SO_4^{--} in some crystals, revealed by X-ray and neutron diffraction

experiment, are compared in Table 4.1.1, where the radial and angular

distortions are distinguished each other. The radial distortion index

Δr is given in parentheses, which is calculated by the equation $4 \cdot (\Delta r)^2$

$= \sum_i (r_i - \bar{r})^2$, where r_i and $\bar{r}$ mean the observed and averaged bond

length. While the angular distortion index $\Delta \theta$ is given by $6 \cdot (\Delta \theta)^2 =$

$\sum_i (\theta_i - \theta(tetra))^2$, where $\theta(tetra)$ denotes the tetrahedral angle of

$109°28'$. The structures of NH_4^+(I) and NH_4^+(II) in $(NH_4)_2SO_4$ at 298 K

is characterized by the average N-H distances of 1.08 Å (0.02 Å) and

1.06 Å (0.01 Å) and the average H-N-H angles of 109.3° (4.3°) and 109.3°

(4.8°), while the structures at 180 K is characterized by the average

distances of 1.05 Å (0.02 Å) and 1.05 Å (0.01 Å) and the average angles

of 109.5° (2.0°) and 109.5° (3.2°), respectively. The radial and angular

distortion indexes are given in parentheses after the corresponding

average values. These values and Table 4.1.1 show the the S-O and N-H

bonds in $(NH_4)_2SO_4$ tend to contract in length within experimental error

on passing into the ferroelectric phase and two ammonium ions become

less distorted in angle. It seems impossible to regard the angular

deformation of NH_4^+ as the origin of polarization, taking into account

of the original T_d symmetry of NH_4^+.

Table 4.1.3 is intended to ask whether the ionic displacements of

NH_4^+ and SO_4^{--} produce the polarization or not. The shifts of constituent

atoms in the crystallographic X and Y directions are larger than that

in the Z direction but do not contribute to the P_s because of presence

of symmetry operations such as glide planes ($\sigma_v(xz)$, $\sigma_v(yz)$) in the

ferroelectric phase. When each oxygen in SO_4^{--} has a charge of -0.5 e

and each hydrogen in NH_4^+ has +0.25 e, then the dipole moment per one

formula unit, μ, amounts to 0.074 e$\overset{\circ}{A}$, the direction of which is along

the z axis. On the other hand, the spontaneous polarization P_s in

$(NH_4)_2SO_4$ parallel to the z axis may be related to the equation $P_s =$

$\mu z / V_c$, where z denotes the number of formula per unit cell volume V_c.

Using $z = 4$, $V_c = 496 \overset{\circ}{A}{}^3$ [13] and $P_s = 0.45 \ \mu C / cm^2$, [14] we obtain $\mu =$

0.035 e$\overset{\circ}{A}$ which is comparable with the predicted value. Thus, we may

propose that the occurrence of polarization should be due to the ionic

displacements in $(NH_4)_2SO_4$. In conjunction with these calculations,

an interesting thing is that the contribution of SO_4^{--}, NH_4^+(I) and

NH_4^+(II) to the resultant dipole moment is found to be 45 %, 120 % and

-65 % respectively.

NH_4HSO_4 and $RbHSO_4$ crystals in their paraelectric phase have two

inequivalent HSO_4^- ions, which are highly distorted in bond lengths

and angles, as shown in Table 4.1.1. It follows that the S-O(H) bond

is longer than the remaining three S-O bonds by about 0.10 $\overset{\circ}{A}$ and the

(H)O-S-O angles are all smaller than the tetrahedral angle and the other

O-S-O angles are all greater than the tetrahedral angle. Here we may

remark that these radial and angular distortions occur also in the non-

ferroelectric crystals such as $KHSO_4$ and $H_2SO_4 \cdot H_2O$ and so on. Therefore,

it seems that these distortions are not sufficient condition for the

occurrence of ferroelectric polarization in these crystals containing

HSO_4^-.

Nelmes[7,8] reported that only one distorted SO_4^{--}(I) in NH_4HSO_4 is

disordered between two sites denoted as Sl_D^+ and Sl_D^- in the paraelectric

phase at room temperature. From his results the magnitude of atomic

shifts in SO_4^{--}(I) ion between these two sites is calculated and presented

in Table 4.1.2, which shows that the largest displacement occurs in the

Z direction, almost parallel to the direction of spontaneous polarization

in NH_4HSO_4.

Though the ionic radius of K^+ is well known to be nearly comparable to that of Rb^+ and NH_4^+, K^+ itself seems to play a different role in appearance and disappearance of ferroelectricity. For example, after the discovery of ferroelectricity in Rochelle salt ($NaKC_4H_4O_6 \cdot 4H_2O$), the sodium rubidium tartrate tetrahydrate ($NaRbC_4H_4O_6 \cdot 4H_2O$), which is isomorphous with the Rochelle salt, has been examined by several authors[15] whether it becomes ferroelectric or not and found that it shows no ferroelectric behavior between 4.2 K and its dehydration point (333 K).

Table 4.1.4 compares the environment around certain cation in several ferroelectrics and non-ferroelectrics containing tetrahedral anions such as SO_4^{--} and PO_4^{---} in terms of the coordination number (CN). Shannon and Prewitt[16] reported that K^+, Rb^+, Cs^+ and Tl^+ have the CNs ranging 6 to 12 and their effective ionic radii increase with the CN. On the other hand, Khan and Bauer[17] emphasized the dual properties of NH_4^+ that when the CN is small (4-5) the hydrogen-bonding tendency of the NH_4^+ is prevalent, and when the CN is larger (7 to 9) its pseudo alkali character dominates. Considering the large number of coordination around the ammonium ion in ferroelectric NH_4HSO_4, then we may expect ferroelectric behavior in $RbHSO_4$, which had been actually confirmed after the discovery of ferroelectricity in NH_4HSO_4. If we confine our attention to the magnitude of the CN given in Table 4.1.4, then we may expect that $KHSO_4$ becomes ferroelectric since both NH_4HSO_4 and $RbHSO_4$ exhibited ferroelectricity. In practice, however, the high sensitive DTA thermograph[18] on $KHSO_4$ from 100 to 300 K revealed no such a heat anomaly as is accompanied by the ferroelectric transition in NH_4HSO_4 and $RbHSO_4$. Moreover, the crystal structure of $KHSO_4$ (Pbca) is not isomorphous with those of $RbHSO_4$ and NH_4HSO_4 ($B2_1/a$) and has not a

pseudo-orthorhombic symmetry found in $RbHSO_4$ and NH_4HSO_4 but complete orthorhombic symmetry.

In the case of $TlHSO_4$, we may expect that it should become ferroelectric, judging from the Fig. 2 in the reference.[16]

The change with temperature which is worthy of note is the decrease in the CN around ammonium ion in $(NH_4)_2SO_4$, which shows that the hydrogen-bonding tendency is more pronounced in the ferroelectric phase, while the pseudo alkali ion character is dominant in the paraelectric phase.

Next we examine two main aspects of the O-H$\cdots$O hydrogen bonds in crystals containing HSO_4^-. The first one is the static properties connected with the position of hydrogen atom and the O$\cdots$O bond length, which is revealed by diffraction experiments, and the second is the dynamical properties associated with the motion of hydrogen atom in these bonds, which is obtained by IR and Raman, and NMR and DMR experiments.

In 1955 Ubbelohde and Gallagher published a summary paper[24] in which various hydrogen bonded crystals were classified according to their geometrical arrangements as follows;

(a) Isolated simple acid salt (KH bisphenylacetate)

(b) Closed-circuit type (Cyclic dimer structure of mono- and dicarboxylic acids)

$$R(O-O) = 2.62 \text{ Å} \quad \text{for } KHSO_4 \text{ [10]}$$

(c) Bond chains (often arranged spirally, hydrate)

$$R(O-O) = 2.51 \text{ Å}$$
$$= 2.60 \text{ Å} \quad \text{for } NH_4HSO_4 \text{ [7,8]}$$

$$R(O-O) = 2.62 \text{ Å}$$
$$= 2.59 \text{ Å} \quad \text{for } RbHSO_4 \text{ [9]}$$

$$R(O\text{-}O) = 2.66 \text{ Å}$$
$$= 2.50 \text{ Å} \quad \text{for RbHSO}_4 \text{[25]}$$

$$R(O\text{-}O) = 2.72 \text{ Å}$$
$$= 2.61 \text{ Å} \quad \text{for RbDSO}_4 \text{[25]}$$

$$R(O\text{-}O) = 2.62 \text{ Å} \quad \text{for KHSO}_4 \text{[10]}$$

(d) Two-dimensional hydrogen bonded system ($HNO_3 \cdot H_2O$)

(e) Three-dimensional network (KH_2PO_4)

where the O-O distances for several hydrogen sulfate compounds are given for the sake of comparison. Figure 1.2.1 and 4.1.1 show that the directions of two infinite zigzag chains of hydrogen bonds in NH_4HSO_4 and $RbHSO_4$ are parallel to each other and also perpendicular to the P_s, as in the case of KH_2PO_4. $KHSO_4$ is constructed of two types of hydrogen bonding (chain and dimer structures). It is surprising to find the same role of HSO_4^-(I) in $KHSO_4$ as that of HCO_3^- in $KHCO_3$.[26]

Rogers and Ubbelohde[27] attributed the low melting points of hydrogen sulfates to the two effects;

(a) the large entropy of fusion (approx. 96 $JK^{-1}mol^{-1}$ for $KHSO_4$, compared with value of KNO_3 (18 $JK^{-1}mol^{-1}$))

(b) the comparatively low activation of a substitutional defects associated with the proton migration in the solid.

Ubbelohde and Gallagher futher suggested that all the classes except the (a) class should exhibit the cooperative proton transfer defect in the crystals if the energy of defect formation is not large compared with kT. In connection with this, the defect formation near the ferro-electric transition temperatures observed in NH_4HSO_4, $RbHSO_4$ and so on will be discussed in section 4.3.

The most striking effects on the O-O distances in the hydrogen

bonds arises when hydrogen is replaced by deuterium. Ubbelohde and

Gallagher reported that when a short hydrogen bond is present in the

crystal (less than 2.75 $\overset{o}{A}$ for the O-O distance), in all the examples

yet investigated there is a marked expansion of the O-O bond length on

replacing H by D. This effect in the case of $RbHSO_4$ was observed by

Yamada (See class (c)), showing agreement with the above statement.

Another effect to be expected on deuterium substitution may appear

on the static aspect such as the heat capacity value and on the dynamical

one given by IR and Raman spectra since the deuterium substitution

invariably cause the decrease of all the energy levels associated with

motion of the deuterium atom.

4.2   Analysis and Discussion of vibration spectra

In the studies of lattice dynamical theories,[27,28,29] ferroelectric

transitions are considered as the results of instability of the crystal

for certain types of transverse optical lattice vibrations, the charac-

teristic frequency of which tends to zero as the temperature approaches

the Curie temperature T_c from the non-ferroelectric phase. Such a mode

is known as a ferroelectric soft mode. For example, Raman scattering

measurements on KH_2PO_4,[30] for the first time, revealed a broad, low-

frequency ferroelectric mode, which could be described by a simple

over-damped harmonic oscillator. Another example may be the neutron

inelastic scattering experiments on $SrTiO_3$.[31] In recent years soft

modes[32,33] in ferroelectrics have been reviewed as one of various soft

modes occuring in the structural phase transitions.

Study of vibration spectra of NH_4HSO_4, ND_4DSO_4, $RbHSO_4$, $RbDSO_4$, and $(ND_4)_2SO_4$ will help not only in ascertaining the nature of ferroelectricity but also in estimating the normal behavior of heat capacities in these ferroelectrics.

The assignments of vibrations in $(ND_4)_2SO_4$ is first made because they have been established well by various authors.[34,35] Next, vibration spectra of $RbHSO_4$ and $RbDSO_4$ is assigned, taking into consideration that they have a smaller number of freedom of vibrations than that of NH_4HSO_4 and ND_4DSO_4.

4.2.1   Analysis of the spectroscopic results

[A]   Correlation diagrams

Free NH_4^+ and SO_4^{--} ions are both five atomic molecules with T_d symmetry. Therefore, each ion has nine internal vibrations, of which symmetry species of normal modes, associated frequencies in cm^{-1} and activities are summerized in Table 4.2.7 from the standard reference book[36] as well as the previously reported results of NH_4X and ND_4X (X = Cl, Br, I),[37] and $(NH_4)_2SO_4$ and $(ND_4)_2SO_4$.[34,35] When the molecule such as a NH_4^+ ion is located in a crystal then the static and correlation field produce changes in the free ion selection rules, and result in splitting of the certain bands.[38] These effects may be conveniently sumarized in the correlation diagrams in Fig. 4.2.1 for NH_4HSO_4 and ND_4DSO_4 and Fig. 4.2.2 for $(NH_4)_2SO_4$, respectively. In making these diagrams, factor group analysis and site group analysis are made, based on the crystal symmetries of NH_4HSO_4 and $(NH_4)_2SO_4$ described in the preceding section. Being isomorphous with the crystal structure of NH_4HSO_4 in the phase I and II, the correlation diagrams for $RbHSO_4$ and

RbDSO$_4$ resemble Fig. 4.2.1

If only the site group symmetry for SO$_4{}^{--}$ in (ND$_4$)$_2$SO$_4$ is taken into account, then the intrinsic degeneracies of the internal modes should be completely removed in both phases and the Raman and the infrared frequencies should be coincident. If only the factor group symmetry of the unit cell is taken, on the other hand, then the following peaks of the SO$_4{}^{--}$ ion should be observed as follows:

	In paraelectric phase	In ferroelectric phase
$\nu_1(A_1) \rightarrow$	$3A_g + 3B_{1g} + 3B_{2u} + 3B_{3u}$	$3A_1 + 3A_2 + 3B_1 + 3B_2$
$\nu_2(E) \rightarrow$	$3A_g + 3B_{1g} + 3B_{2g} + 3B_{3g} + 3A_u$ $3B_{1u} + 3B_{2u} + 3B_{3u}$	$6A_1 + 6A_2 + 6B_1 + 6B_2$
$\left.\begin{array}{c}\nu_3(F_2) \\ \nu_4(F_2)\end{array}\right\} \rightarrow$	$4A_g + 4B_{1g} + 2B_{2g} + 2B_{3g} +$ $2B_{1u} + 4B_{2u} + 4B_{3u}$	$9A_1 + 9A_2 + 9B_1 + 9B_2$

where A_1, B_1, and B_2 species are both Raman and infrared active, and A_2 is only Raman active.

For the NH$_4{}^{+}$ ion the number of peaks is twice that for the SO$_4{}^{--}$, since there are two inequivalent ammonium ions for each sulfate.

From the correlation diagrams the 69 lattice modes consist of 33 translational optical modes and 36 librational modes are predicted to be non-degenerate and Raman and infrared active:

	In the paraelectric phase	In the ferroelectric phase
$\Gamma(AT) \rightarrow$	$B_{1u} + B_{2u} + B_{3u}$	$A_1 + B_1 + B_2$
$\Gamma(OT) \rightarrow$	$6A_g + 6B_{1g} + 3B_{2g} + 3B_{3g} +$ $3A_u + 2B_{1u} + 5B_{2u} + 5B_{3u}$	$8A_1 + 9A_2 + 8B_1 + 8B_2$
$\Gamma(OL) \rightarrow$	$3A_g + 3B_{1g} + 6B_{2g} + 6B_{3g} +$ $6A_u + 6B_{1u} + 3B_{2u} + 3B_{3u}$	$9A_1 + 9A_2 + 9B_1 + 9B_2$

141

The above analysis applies to modes which have zero wave vector. However, this condition would not hold in the paraelectric phase, and vibration spectra would be more complicated than that expected based on the factor group analysis alone, because of disorder nature as supported by the calorimetric results in the subsequent section.

As $RbHSO_4$ has a monoclinic unit cell of space group $P2_1/c$ with eight formula units, the SO_4^{--} ion occupies a general position and hence its site symmetry is represented as C_1. The static field under the C_1 site group should cause a splitting of the "free ion" degenerate bending and stretching vibrations of SO_4^{--} in the paraelectric phase and also in the ferroelectric phase. The irreducible representations, predicted by the correlation field under the C_{2h} and C_s factor groups, for the internal, optical translatory (OT), optical libratory (OL), and acoustical translatory (AT) vibrational modes can be summerized as:

	in the paraelectric phase	in the ferroelectric phase
Γ(external)		
Γ(OT) $\longrightarrow$	$12A_g + 24B_g + 23A_u + 10B_u$	$46A' + 23A''$
$(\Gamma(Rb^+$ or $H^+))\rightarrow$	$(4A_g + 8B_g + 8A_u + 4B_u)$	$(16A' + 8A'')$
Γ(OL) $\longrightarrow$	$8A_g + 4B_g + 4A_u + 8B_u$	$8A' + 16A''$
Γ(AT) $\longrightarrow$	$A_u + 2B_u$	$2A' + A''$
Γ(internal)		
$\nu_1(A_1)$ $\longrightarrow$	$4A_g + 4B_u$	$8A'$
$\nu_2(E)$ $\longrightarrow$	$4A_g + 4B_g + 4A_u + 4B_u$	$8A' + 8A''$
$\nu_3, \nu_4(F_2)$ $\longrightarrow$	$4A_g + 8B_g + 8A_u + 4B_u$	$16A' + 8A''$

All vibrations of gerade symmetry may appear in the Raman effect, while in the infrared vibrations of ungerade symmetry are active. Both A' and A" symmetry modes are Raman and infrared active.

The correlation diagrams for the three phases of NH_4HSO_4 show that if only the site group is taken into account, then the intrinsic degeneracies of the internal modes of NH_4^+ and SO_4^{--} should be completely lifted, so that in all three phases we obtain

$$\nu_1 \longrightarrow 1 \text{ (R, IR) peak}$$
$$\nu_2 \longrightarrow 3 \text{ (R, IR) peaks}$$
$$\nu_3, \nu_4 \longrightarrow 3 \text{ (R, IR) peaks for each mode.}$$

If the full symmetry of the unit cell is considered, on the other hand, the following peaks for the SO_4^{--} ion and the NH_4^+ ion should be observed in the three phases:

	in Phase I	in Phase II	in Phase III
$\nu_1 \longrightarrow$	$8A_g + 8B_u$	$16A'$	$16A$
$\nu_2 \longrightarrow$	$8A_g + 8B_g + 8A_u + 8B_u$	$16A' + 16A''$	$32A$
$\nu_3, \nu_4 \longrightarrow$	$16A_g + 8B_g + 8A_u + 16B_u$	$16A' + 8A''$	$48A$

The external modes in the three phases can be classified, as in the case of $RbHSO_4$, as follows:

	in Phase I	in Phase II	in Phase III
$\Gamma(OT) \longrightarrow$	$24A_u + 12B_g + 11A_u + 22B_u$	$46A' + 23A''$	$69A$
$\Gamma(OL) \longrightarrow$	$8A_g + 16B_g + 16A_u + 8B_u$	$16A' + 32A''$	$48A$
$\Gamma(AT) \longrightarrow$	$A_u + 2B_u$	$2A' + A''$	$3A$

[B]   Assignment of the peaks

It is always necessary to use a single crystal in order to assign the observed bands in Raman and infrared spectra as precisely as possible. Present experiments are done for the powder samples and hence the assignments of the peaks are somewhat inconclusive. The assigned values of the fundamental frequencies of $(ND_4)_2SO_4$ are presented in Table 4.2.1, and $RbHSO_4$ and $RbDSO_4$ in Table 4.2.2 for their paraelectric phase and in Table 4.2.3 for their ferroelectric phase, and NH_4HSO_4 and ND_4DSO_4 in Table 4.2.4 for Phase I and in Table 4.2.5 for Phase II and in Table 4.2.6 for Phase III, respectively.

B-1   Lattice modes

A detailed assignment of the lower frequency peaks than 400 cm^{-1} is not possible but some general assignments can be made by using isotope effect as well as cation effect and comparing the previous results supported by other experiments such as neutron inelastic scattering.[39] On deuterium substitution librational modes of ammonium ion is expected to show a marked reduction in frequency by a factor of $1/\sqrt{2}$, whilst, for the translational modes, the factor is $\sqrt{18/22}$. Cation effect predicts $\nu(TO$ in $RbHSO_4) / \nu(TO$ in $NH_4HSO_4) = \sqrt{18/85}$, where TO means the translational optical mode in which cations participate.

B-2   Internal modes

The internal mode frequencies of NH_4^+, ND_4^+ and SO_4^{--} can be readily assigned by comparison with the frequencies presented in Table 4.2.7. Furthermore, the Teller-Redlich frequency product ratio for the two F_2 species gives in the harmonic approximation, $(\nu_3 \nu_4)_D / (\nu_3 \nu_4)_H = (My / My')\sqrt{(Mx + 4My')/(Mx + 4My)}$ for a tetrahedral XY_4 molecule where

144

the dash notation refers to the deuterated molecule and the M's stand

for the masses of the atoms.

4.2.2   Discussion

The observed spectra of five ferroelectrics (Fig. 3.2.1 - 16) and

Fig. 4.2.1 reveal that a smaller number of peaks in both Raman and IR

spectra than that predicted by the factor group analysis is observed.

This means that any intermolecular coupling is not strong enough to

cause splitting especially as far as internal modes are concerned.

Among the higher frequency bands than about 1500 cm^{-1} the most

interesting band is the O-H stretching bands. Special attention have

been devoted by several authors[40] to examine the shape of the potential

curve governing the motion of a hydrogen atom in the O-H···O bond and

to suggest the possibility of the tunnelling motion since the mechanism

of ferroelectricity is in many cases closely associated with the dis-

placement of hydrogen atoms. At present there are, however, contradicting

suggestions[41] on this problem.

A hydrogen in the O-H···O bonds in NH_4HSO_4 and a deuterium in the

O-D···O bond in $RbDSO_4$ are found to occupy an acentric site in these

bonds, so we expect no tunnel effect in these crystals.

Two broad bands at about 3100 and 2450 cm^{-1} appeared in common with

all the ferroelectrics investigated. Especially the band shape at about

2450 cm^{-1} in NH_4HSO_4 resembles the corresponding bands of $RbHSO_4$ and

$RbDSO_4$, which may be assigned as the bands associated with the H bond

and the D bond but showed no marked reduction in frequency on deuteration,

notwithstanding that the O-D···O bond length is generally longer than

the O-H···O bond and the mass of deuterium is twice that of hydrogen.

The corresponding band in ND_4DSO_4 is superimposed by the ν_3 and ν_1 bands

of ND_4^+ and appeared in a complicated fashion. Broadness of the bands at about 3100 cm^{-1} responsible for the N-H and N-D stretching may be attributed to the existence of moderately strong hydrogen bonds in NH_4HSO_4, ND_4DSO_4 and $(ND_4)_2SO_4$.

The change with temperature which is worthy of note is the splitting of the band at 2900 cm^{-1} in the infrared spectra of $RbHSO_4$ (Fig. 3.3.7). The magnitude of this splitting amounting to 320 cm^{-1} at 98 K is also observed in the KH_2PO_4 family[42] but it is not certain whether this splitting is introduced by the ferroelectric transition or whether it was present also in the paraelectric phase and became more pronounced on cooling.

Using the reported values[34] of ν_3 = 3150 and ν_4 = 1405 cm^{-1} in $(NH_4)_2SO_4$ and the present values of ν_3 = 2390 and ν_4 = 1032 cm^{-1} in $(ND_4)_2SO_4$, the Teller Redlich product ratio is calculated to be 0.557, which show a good agreement with the theoretical value of 0.553, considering that the ratio[37] for ammonium chloride and bromide in their lowest phase is observed as 0.561 and 0.560 respectively. In the case of ammonium hydrogen sulfate the product is found to be 0.543. This low value may be attributed to the anharmonic vibrations due to the hydrogen bonding.

Myasnikova and Yatsenko[43] reported the bands at 977 cm^{-1} in NH_4HSO_4 and at 969 cm^{-1} in $RbHSO_4$ and assigned them as the fundamental $\nu_1(A_1)$ of SO_4^{--} only from their IR spectra. However, we could not observe those bands. Instead, the strong Raman band at about 880 cm^{-1} in NH_4HSO_4 and $RbHSO_4$ was assigned as such. The most distinctive feature in the internal vibration region of SO_4^{--} ion appears in the frequency shift due to the hydrogen bond formation. The fundamental frequency of $\nu_1(A_1)$ mode of SO_4^{--} in $(ND_4)_2SO_4$ was higher by about 80 cm^{-1} than those so assigned in four other ferroelectrics having HSO_4^- or DSO_4^-, supporting the conclusion

that the O–H···O and O–D···O bands are stronger than the N–D···O bonds.

A number of bands below 400 cm^{-1} may be related to the external

modes such as the translational and librational modes of NH_4^+, ND_4^+ and

SO_4^{--}. The assignment of the peak at 300 cm^{-1} in NH_4HSO_4 as a librational

modes confirms the results of neutron inelastic scattering[39] where in

the paraelectric phase below the ferroelectric transition a strong peak

at 290 ± 25 cm^{-1} was observed at 125 K and so assigned. Another peak

at 190 ± 16 cm^{-1} was revealed by the neutron work and assigned probably

as a librational mode. However, the Raman and IR results suggest that

this peak is actually of translational origin. It is found that on

deuteration the corresponding librational frequency decreases to 227 cm^{-1}

by a factor of 0.76 instead of theoretical value of $1/\sqrt{2}$ (= 0.71).

On the other hand the present spectroscopic results suggest that another

peak at about 370 cm^{-1} in NH_4HSO_4 is also assigned as the librational

mode since the frequency of this mode shifts to lower frequency side

to 270 cm^{-1} with a reduction factor of 0.73 and since the fundamental

frequencies[37] ν_6 of ammonium chloride and bromide and their deuterium

analog was observed in the range from 225 to 389 cm^{-1} and revealed the

reduction factor of 0.72 on deuteration. In the case of $(ND_4)_2SO_4$ we

assigned the IR band at 260 cm^{-1} as the librational mode, which is in

good agreement with the value (255 cm^{-1}) reported by Torrie, et al.[35]

It is worthy to note here that the isotope effect on the fundamental

ν_6 mode gives rise to the reduction factor of 0.75 in ammonium sulfate,

the value of which is also observed in the case of ammonium hydrogen

sulfate. Difference in the frequency value itself of librational mode

and in the coordination number around ammonium ion does suggest that

the rotational freedom of the NH_4^+ and ND_4^+ ions is greater in NH_4HSO_4

and ND_4DSO_4 than in $(NH_4)_2SO_4$ and $(ND_4)_2SO_4$.

Though the assignments of librational modes of SO_4^{--} in the five ferroelectrics contain some ambiguity, we may be able to estimate them from the temperature dependence of the corresponding bands below about 200 cm^{-1} since they depend on the intermolecular forces. For example, the strong IR band at 120 and 175 cm^{-1} in $RbHSO_4$ and $RbDSO_4$ may be assigned as such. Appearance of the two bands may be explained by taking the symmetry of SO_4^{--} in $RbHSO_4$ as the C_{3v} symmetry. In this case we may predict that the triply degenerate librational modes (F_1) in the T_d symmetry should split into the A_2 mode and the doubly degenerate E mode. The evidence of C_{3v} symmetry is described in the preceding section 4.1 in connection with the distortion in a tetrahedral ion.

The phase transition in $(NH_4)_2SO_4$ from D_{2h} to C_{2v} is induced by the irreducible representation B_{1u}.[3] This B_{1u} soft mode is infrared active but Raman inactive. Detailed temperature dependence of the infrared spectra of $(ND_4)_2SO_4$ was not measured but there is an interesting point to be noted here about the Raman spectra. Fig. 3.3.16 show that the shoulder on the Rayleigh band tail exhibit a tendency to go into the Rayleigh band as the temperature approaches the Curie temperature T_c from room temperature and disappear completely below the T_c. In the case of NH_4HSO_4 and $RbHSO_4$ the soft mode to be associated with the phase transition from C_{2h} to C_s may be given by the A_u irreducible representation, which is also only infrared active. Low-frequency vibrations having decreasing frequency at the Curie point were not found in our infrared spectra.

4.3 Analysis and Discussion on Calorimetric Results

4.3.1 General remarks

Section 4.3 is devoted to the analysis and discussion on the calorimetric results of NH_4HSO_4, ND_4DSO_4, $RbHSO_4$, $RbDSO_4$ and $(ND_4)_2SO_4$ in order to shed light on their ferroelectric transition mechanism from the viewpoint of thermodynamics.

To begin with, we intend to analyze the thermal behavior at lowest temperature region measured to characterize the lattice vibrations of these solids with the help of lattice dynamical theory.[44] Next we try to explain the normal behavior of heat capacity curves, which are estimated from the temperature dependence of the apparent Debye characteristic temperature, in terms of lattice vibrations, librations of NH_4^+, ND_4^+ and SO_4^{--} and internal vibrations of these tetrahedral ions. Thermal motion of NH_4^+ is examined by comparing the estimated normal heat capacity values of NH_4HSO_4 and $RbHSO_4$. In section 4.3.4 anomalous behaviors associated with ferroelectric transitions will be characterized by the thermodynamic quantities such as transition temperature, transition enthalpy and transition entropy. Our calorimetric results will be compared with those derived from group theoretical methods proposed by several authors.[2,3,4] We pay our attention to the detailed behavior of estimated anomalous heat capacity curves to uncover the elementary process of phase transitions that appears associated with those ferroelectrics as well as some ammonium halides.

4.3.2 Heat capacity at low temperatures

It is necessary to convert C_p to C_v when we intend to compare the experimental results with the theoretical. To do this, the following

two relations are usually used;

The exact thermodynamic relation:

$$C_p - C_v = C_p \left\{ 1 + (\chi_s C_p / V\beta^2 T) \right\}^{-1}, \qquad 4 - 1$$

where the coefficient of cubical expansion $\beta = V^{-1}(\partial V / \partial T)_p$, the adiabatic compressibility $\chi_s = -V^{-1}(\partial V / \partial P)_s$ and the volume V and the thermodynamic temperature T and the approximate Nernst-Lindeman relation based on the Grüneisen's equation of state:

$$C_p - C_v = A C_p^{\,2} T, \qquad 4 - 2$$

where $A = V\beta^2 / \chi_T C_p^{\,2}$ is known to be nearly constant over a wide range of temperature.

It is well known that the difference between C_p and C_v is about 5 % in most solids at room temperatures and decreases rapidly as the temperature is lowered.[45] In the case of RbCl,[46] for example, the value of $C_p - C_v$ is estimated to be negligibly small below 50 K, 0.1 % of C_p at 100 K, 0.2 % at 200 K, and 0.4 % at 300 K, based on the exact thermodynamic relation. As to our five calorimetric samples investigated there was no complete set of data of β, χ_s, and V and therefore exact conversion of C_p to C_v was not possible. Thus in the absence of better alternatives, we proceed to analyze the observed heat capacity at constant pressure taking into considerations that $C_p = C_D + C_L + C_E + C_A + (C_p - C_v)$, where C_D is the Debye heat capacity, C_L the contribution of librational modes, C_E the contribution of internal modes, C_A the anomalous heat capacity associated with the ferroelectric phase transition.

The normal modes of lattice vibrations in many dielectric solids

are excited over the entire temperature range and so contribute observable heat capacity at all temperatures. At very low temperatures, the atoms in a crystal lattice execute harmonic vibrations with small amplitudes and low frequency modes with long wave lengths are excited at lower temperatures. Thus, the behavior of $g(\omega)$ in the Debye approximation and the behavior for discrete lattice models developed by Born and von-Kármán is the same for small ω. If the Debye model is valid for the five ferroelectrics investigated, the corresponding Debye characteristic temperature would be expected to be constant against the temperature. However, Fig. 4.3.1 shows that the value of Θ_D derived from experiment for 6N degrees of freedom per formulae unit appropriate to the four ferroelectrics containing HSO_4^- or DSO_4^- depends on the temperature. NH_4HSO_4 (ND_4DSO_4) and $RbHSO_4$ ($RbDSO_4$) have a shallow minimum value of 155 K and 135 K at 11 K and 10 K, respectively. In the case of $(ND_4)_2SO_4$ a minimum (203 K for 9N) occurs at 20 K. Decrease in $\Theta_D(T)$ of $RbHSO_4$ and $RbDSO_4$ above 30 K must be due to the contribution of librational modes of SO_4^{--}. If the Θ_D curve is corrected for this effect, it is found that $\Theta_D(T)$ of $RbHSO_4$ is practically constant (140 $\pm$ 5 K) between 4 and 80 K. Anyway the $\Theta_D(T)$ curve of the four ferroelectrics drops gradually. This temperature-dependence of the Debye Θ is a consequence of the inadequacy of the Debye spectrum as an approximation to the true spectrum of these crystals.

Attemps have been made from time to time to improve the Debye spectrum. One of the earliest of these consisted of defining cutoff frequencies for the longitudinal and transverse vibration modes by normalizing them separately to rN and 2rN, respectively. Another suggestion was to describe only the acoustic mode spectrum by the Debye

approximation while the optical mode contribution was described by $3r - 3$
suitably normalized delta-functions located at frequencies approximating
the optical mode frequencies by a certain average.

Among the methods expressing frequency spectra Houston's method[47]
seems more suitable for computational purposes. When we consider only
the three acoustic branches of the frequency spectrum, then we have the
expansion (for a three dimensions)

$$g(\omega) = a_2 \omega^2 + a_4 \omega^4 + \cdots \qquad 4 - 3$$

This spectrum gives the asymptotic heat capacity at low temperatures;

$$C_v(T) = 3rNk \ [(4\pi^4/15)(kT/\hbar)^3 a_2 + (16\pi^2/21)(kT/\hbar)^5 a_4 + \cdots] \quad 4 - 4$$

where the coefficient a_2 is evaluated from the angular average of
velocities of the three elastic waves but a_4 has not been so extensively
studied as a_2 since its evaluation requires the assumption of a special
model for the interatomic forces. The temperature dependence of Θ_D is
obtained from eqs. (1 - 10) and (4 - 4), and can be expressed as

$$\Theta_D(T) = \Theta_D(0) \ [1 - (20\pi^2/21)(a_4/a_2)(kT/\hbar)^2 + \cdots] \qquad 4 - 5$$

where $k^3 \Theta_D(0)^3 a_2 = 3\hbar^3$. This equation is depicted schematically in
Fig. 4.3.1 by a solid line (extrapolation) below about 5 K.

The Debye characteristic temperature at 0 K, $\Theta_D(0)$, was calculated
from the interaction at $T^2 = 0$ of the $C_p T^{-3}$ versus T^2 plot (Figs. 4.3.2 - 4)
and summarized in Table 4.3.1. Figs. 4.3.2 - 4 reveal that the heat
capacities (in units of $JK^{-1}mol^{-1}$) below 5 K are written as;

$$10^4 c_p T^{-3} = (6.75 \pm 0.15) + 0.08 \ T^2 \ \text{for NH}_4\text{HSO}_4$$

$$10^4 c_p T^{-3} = (4.23 \pm 0.60) + 0.13 \ T^2 \ \text{for ND}_4\text{DSO}_4$$

$$10^4 c_p T^{-3} = (12.25 \pm 0.20) + 0.06 \ T^2 \ \text{for RbHSO}_4$$

$$10^4 c_p T^{-3} = (11.85 \pm 0.20) + 0.01 \ T^2 \ \text{for RbDSO}_4$$

$$10^4 c_p T^{-3} = (4.28 \pm 0.04) + 0.003 \ T^2 \ \text{for (ND}_4)_2\text{SO}_4$$

where the coefficient of second terms have uncertainty of about 15 %.

Table 4.3.1   Comparison of the Debye characteristic temperature at 0 K.

	$\Theta_D(0)$	Freedom
NH_4HSO_4	179 ± 1	6N
	142 ± 1	3N
ND_4DSO_4	209 ± 10	6N
	166 ± 8	3N
RbHSO_4	147.0 ± 0.8	6N
	116.6 ± 0.6	3N
RbDSO_4	148.6 ± 0.8	6N
	117.9 ± 0.7	3N
$(\text{ND}_4)_2\text{SO}_4$	238.8 ± 0.7	9N
	165.6 ± 0.5	3N

The $\Theta_D(0)$ values of the rubidium salts are smaller than those of the ammonium salts, supporting the Blackman's conclusion[48] that the $\Theta_D(0)^2$ is inversely proportional to the molecular weight. However, beyond the estimated error the $\Theta_D(0)$ value of ND_4DSO_4 is higher than that of NH_4HSO_4,

corresponding to the fact that the heat capacity of ND_4DSO_4 is smaller than that of NH_4HSO_4 at very low temperature and that $a_2(D) < a_2(H)$ and $a_4(D) > a_4(H)$. From the analogy of vibrations of a diatomic chain,[44] we may conclude that the larger effective force constants in ND_4DSO_4 than those in NH_4HSO_4 lead to the higher velocities of anisotropic elastic waves in ND_4DSO_4. In connection with this deuteration effect on the frequency spectrum it is worthy to note that this kind of behavior in the heat capacity was also observed in the ferroelectric phase of ammonium hydrogen bis(chloroacetate).[49]

4.3.3   Normal behavior of heat capacity

Even if the details of crystal structure and the intra- and inter-molecular forces in our five ferroelectrics are given, at the present time it is impossible to divide theoretically the observed heat capacity C_p into two parts composed of the normal and anomalous heat capacities. However, by the use of the apparent Debye characteristic temperature which can be converted from the observed C_p with appropriate degrees of freedom we tried to separate the anomalous heat capacity from the observed C_p value in order to determine the thermodynamic quantities concerned with the ferroelectric transition.

In the case of NH_4HSO_4 we took 6N and 33N degrees of freedom per formula unit and plotted the corresponding Debye temperatures ($_6\theta_D^P$ and $_{33}\theta_D^P$) in Fig. 4.3.5, where $_6\theta_D^P$ means that each NH_4^+ and HSO_4^- is assumed as a rigid ion and each has 3N translational degrees of freedom while $_{33}\theta_D^P$ corresponds to the case of the largest degrees of freedom that NH_4HSO_4 can have as a whole. When 6N degrees of freedom is considered, the $_6\theta_D^P$ values goes to zero at about 75 K due to the thermal excitation of librational modes. Though this tendence may be ascribed

to the occurrence of the anharmonicity of lattice vibrations themselves or the lack of the correction of $C_p - C_v$, we believe these contribution to the Θ_D value to be small in the temperature region in question. Therefore, we took the maximum degrees of freedom to avoid this tendency of the Θ_D to zero and to estimate the most probable normal C_p values. This does not mean that all the degrees of freedom have been fully excited to give corresponding Debye spectrum, but the method is merely a convention to estimate the normal C_p curves on the notion that the Θ_D curve should be of a continuous, smooth shape if there were no phase transitions. The solid line shown in Fig. 4.3.5 was adopted as the base line II corresponding to the normal C_p curve. The other extreme of base line is possible and shown as the dotted line. However, the $_6\Theta_D{}^L$ curve, which is obtained from the observed C_p values subtracted by the librational and internal contributions due to $NH_4{}^+$ and $SO_4{}^{--}$, revealed that the base line II is more appropriate than the base line I as the base line on which to describe the upper transition behavior in the ferroelectric phase II. The validity of this base line II is also supported by the evidence that the spontaneous polarization of NH_4HSO_4 levels off from 200 K down to the lower transition point. The base line I is used as the normal C_p curve for the lowest phase III. The estimated normal C_p values of NH_4HSO_4 is presented in Table 4.3.2.

In a similar method we estimate the normal C_p values of $RbHSO_4$, $RbDSO_4$, ND_4DSO_4 and $(ND_4)_2SO_4$ from the temperature dependence of the Θ_D curve with the maximum degrees of freedom for each ferroelectric and without the $C_p - C_v$ corrections. The smooth Θ_D curve equivalent to the normal heat capacity are shown in Figs. 4.3.6 - 8 and the results thus obtained are presented in Table 4.3.3 - 6.

In this section we also summarize the estimated normal C_p of NH_4Br[79)] and ND_4Br,[80)] $(NH_4)_2SO_4$,[78)] and VCl_3 in Table 4.3.7-10, which will be used in next section.

Here we examine to what extent the values of the estimated normal heat capacity of $RbHSO_4$ and $RbDSO_4$ can be interpreted in terms of the external and internal modes. We first intend to determine the contributions of the translational lattice vibrations, which are usually approximated by the Debye model. At high temperatures the heat capacity of an insulator can be expressed as the power series of μ_{2n} / T^{2n} where μ_{2n} is the 2n-th moment of spectrum. Therefore, many moments are required to get the heat capacity in the Thirring's approach.[50)] On the other hand Domb and Salter[51)] derived the conclusion that the heat capacity at high temperatures $(T > \Theta_D)$ could be expressed with a single parameter Θ_∞ which corresponds to the Debye characteristic temperature at infinitely high temperature. In this quasiharmonic approximation the Debye temperature is expressed as a function of temperature,

$$\Theta_D^2(T) = \Theta_\infty^2 \left\{ 1 - A(\Theta_\infty / T)^2 + B(\Theta_\infty / T)^4 - \cdots \right\} . \qquad 4-6$$

The Θ_∞ values of $RbHSO_4$ and $RbDSO_4$ are determined to be 141.9 ± 0.3 and 140.5 ± 0.3 K for 6N degrees of freedom, respectively, assuming that the $C_p - C_v$ correction is negligibly small below 20 K. (See Fig. 4.3.9). The decrease of Θ_D^2 at temperatures higher than about 20 K may be attributed to the thermal axcitation of SO_4^{--} librational modes. Generally, these librational modes are not very dependent on the wave vectors as the acoustic modes. (See references for NH_4Cl[52)] and for hexamine[53)]). In other words, their behaviors are well described by the Einstein modes. Now their librational frequencies are estimated in Fig. 4.3.10 to be

145 cm^{-1} for both crystals, assuming that these modes are triply degen-
erate. It is worthy to be noted that this value is very close to the

mean value of the two spectroscopic bands (119 and 177 cm^{-1} for both

crystals) assigned as the librational modes of SO_4^{--} (Fig. 3.3.8 and 11).

Using the fundamental frequencies of the internal modes in SO_4^{--} given

in Table 4.2.3, we summarize the above analysis in Fig. 4.3.11 where

the internal contributions are of course evaluated by the Einstein

functions. The value of $(C_D + C_L + C_E)$ amounted to 95 % of C_p (normal)

of RbHSO$_4$ at 100 K, 92 % at 200 K and 88 % at 300 K. The remaining

part of the normal heat capacity will be interpreted with good certainty

by the $(C_p - C_v)$ correction and the anharmonicity of the external modes.

Next we analyze the estimated normal heat capacity of $(ND_4)_2SO_4$.
We may divide 27N degrees of freedom as a whole into the 9N lattice

vibrational modes, 3N librational modes of SO_4^{--}, 6N librational modes

of ND_4^+, 9N internal modes of SO_4^{--} and 18N internal modes of ND_4^+.
The lattice contributions to the normal heat capacity are derived from

the Debye function with the $\theta_D(0) = 238$ K and other contributions are

estimated from the assigned values listed in Table 4.2.1. In Fig. 4.3.12

the sum total of these modes are shown by the dotted line which accounts

for most of the normal heat capacity above 120 K but exceeds by about

10 JK^{-1}mol^{-1} at 80 K. Generally in the intermediate temperature region

the experimental value of heat capacity has good accuracy and precision

and the anharmonic effect is too small to be detected even if it is

present. Moreover the value of heat capacity itself is very sensitive

to the actual shape of the frequency spectrum. Thus, the overestimation

neat 80 K is possibly due to the inadequate estimation of lattice con-

tributions. The 9N degrees of freedom can furthermore be separated into

the 3N degrees of freedom for the acoustic modes and 6N optical modes.

Since the translational optical modes are nearly independent of their wave vectors, we tried to evaluate the averaged frequency of these modes by means of Einstein functions. This is shown in Fig. 4.3.13 where ΔC is obtained as the difference between the normal heat capacity and all the contributions except 6N optical translational modes. As to the acoustic modes the $\Theta_D(0) = 165.6$ K given in Table 4.3.1 is used. Best fitting was obtained when the average frequency $= 185$ cm^{-1}. This value is confirmed by the our broad IR band at about 180 cm^{-1} which is assigned to the translational mode of ND_4^+ in Table 4.2.1 (See also Fig. 3.3.15). This value also shows a good agreement with the broad peak (200 ± 16 cm^{-1}) in the inelastic neutron scattering experiment,[39] the assignment of which is the same as ours. Figure 4.3.14 shows the final analysis on the normal heat capacity of $(ND_4)_2SO_4$. About 10 % of the normal C_p at 200 K and 14 % at 300 K remain to be analyzed. Half of the remaining part may be interpreted as due to the correction of $C_p - C_v$ and the other half as due to anharmonicity of the librational and translational modes.

The motional state of ammonium ion in NH_4HSO_4 solid is examined by comparison of the normal heat capacities of the NH_4HSO_4 and $RbHSO_4$ which are isomorphous and have almost the same lattice dimension (Table 1.2.1 and 2). In Fig. 4.3.15 (upper) the difference in the observed heat capacities of the ammonium and rubidium salts in units of R (gas constant) is plotted against temperature. At high temperatures the difference appears quite complicate due to the phase transitions but at low temperatures it is noteworthy that $\Delta C_p = C_p(NH_4HSO_4) - C_p(RbHSO_4)$ has a broad minimum at about 50 K. This behavior can be derived from the facts that the $\Theta_D(0)$ value of NH_4HSO_4 is larger than that of $RbHSO_4$. The difference in the corresponding lattice heat capacities is shown by the dotted line, which explains roughly the observed behavior.

Figure 4.3.15 (lower) shows the difference in normal heat capacities which is depicted as the dotted line, and the solid line was derived by subtracting the internal vibrational contributions of NH_4^+ from the above difference. The contribution to the heat capacity due to thermal motions of NH_4^+ shows an abrupt jump at the transition temperature, which is consistent with the T_1 behavior revealed in the NMR.[54] The practically constant value of 3R in the ferroelectric phase and the upper paraelectric phase below 305 K strongly suggests that the NH_4^+ in NH_4HSO_4 undergoes the highly excited torsional oscillations in the two phases. Taking into account the fact that the ammonium ions in $(NH_4)_2SnCl_6$,[55] $(NH_4)_2SnBr_6$,[55] $(NH_4)_2SiF_6$[56] and NH_4ClO_4[57] at about 200 K are known to be restricted rotators with comparatively low energy barriers by the similar analysis of their heat capacities, this behavior of NH_4^+ in NH_4HSO_4 seems quite strange and probably it is attributable to the existence of ferroelectric phase. The above statement indirectly suggests that the NH_4^+ takes part in the succesive ferroelectric transitions in NH_4HSO_4. More direct evidence will be given in the next section.

4.3.4   Anomalous behavior of heat capacity

As are seen in Fig. 3.2.1 for NH_4HSO_4 and Fig. 3.2.10 for ND_4DSO_4, these specimen show two successive heat capacity anomalies composed of an abrupt peak at the lower transition (II - III) and a gradual rise in the heat capacity followed by a sharp fall at the upper phase transition (I - II). On the other hand Fig. 3.2.4 for $RbHSO_4$ and Fig. 3.2.6 for $RbDSO_4$ exhibit no trace of anomaly analogous to the lower transition observed in NH_4HSO_4 and ND_4DSO_4 down to the liquid helium temperature and show only a small anomlous peak with a long tail on the low temperature

side, which resembles well the upper anomaly in NH_4HSO_4 and ND_4DSO_4. Thus these facts give us a strong suggestion that the lower ferroelectric phase transition is directly related to the sudden change in motional state of the NH_4^+ and ND_4^+ and that the upper one is associated with the gradual change of state in HSO_4^- and DSO_4^-.

Considering that there was no isothermal absorption of heat within the limits of accuracy and no anomalous equilibration time, the upper transition in NH_4HSO_4 and ND_4DSO_4 and the corresponding transition in $RbHSO_4$ and $RbDSO_4$ are expected to be of second or higher order. The apparent shape of anomalous heat capacity (Figs. 4.3.16 and 17) bears resemblance to that due to the onset of superconductivity (for example, vanadium[58]) which is well known as a typical second order phase transition. Another direct evidence of second order transition is revealed by the temperature dependence of P_s for NH_4HSO_4[59] ($P_s^2 \propto (T_c - T)$; $-20°C < T - T_c < 0$). Thus we may conclude the corresponding ferroelectric phase transitions observed in these crystals to be of second order. The ferroelectric phase transition model proposed by Aizu predicts the first order transition for the upper transition in NH_4HSO_4.[4] This model may be ruled out from the view point of thermodynamic results mentioned above. On the other hand, the lower transition in NH_4HSO_4 and ND_4DSO_4 and the single transition in $(ND_4)_2SO_4$ may be characterized as the first order transition since the quasiisothermal absorption of heat in the heat capacity measurements was observed as inferred from the series XI, XIII and XIV in Table 3.2.1 for NH_4HSO_4, the series IV, V and VIII in Table 3.2.6 for $(ND_4)_2SO_4$ and the series V and VI in Table 3.2.9 for ND_4DSO_4, respectively. Another support comes from the very slow equilibration rate observed only in the vicinity of corresponding transition temperatures, for example, as shown in Fig. 4.3.18 for NH_4HSO_4. In this

connection it is noteworthy that the DTA thermograms of NH_4HSO_4 and

ND_4DSO_4 (Fig. 3.1.2) exhibited a supercooling and superheating phenomenon

which is characteristic of a first order transition.

The transition temperatures of the second order transitions appeared

in these ferroelectrics having HSO_4^- and DSO_4^- were estimated from the

intersection of heat capacity obtained by smooth extrapolation from the

high and low temperature sides. Using the estimated normal heat capacity

we determined the transition enthalpy and entropy as follows. By sub-

tracting the estimated base line (II) for NH_4HSO_4 from the observed

heat capacity, the anomalous heat capacity (ΔC_p) are drawn on a large-

scale plot (Fig. 4.3.18) and the associated enthalpy of transition was

estimated to be 357 $JK^{-1}mol^{-1}$ by graphical integration. The corres-

ponding entropy of transition is then determined graphically from the

large plot of $T^{-1}\Delta C_p$ versus T to be 1.56 $JK^{-1}mol^{-1}$. Another two inde-

pendent determinations of the entropy of transition were taken in order

to assess the influence of the different probable base lines. If a

different, possible base line on the plot of $T^{-1}C_p$ (observed) versus T

is drawn, we obtain ΔS_{tr} = 1.33 $JK^{-1}mol^{-1}$ while the still other possible

base line on the graph of C_p (observed) versus T gave ΔS_{tr} = 1.78 $JK^{-1}mol^{-1}$.

Thus we assigned the value of 0.23 $JK^{-1}mol^{-1}$ as the uncertainty of the

entropy of transition for NH_4HSO_4.

As to the first order phase transition as observed in $(ND_4)_2SO_4$

it seems difficult to estimate the normal heat capacity since to some

extent there exists a jump in the heat capacity at the transition

temperature. Though this jump may be expected lattice-dynamically

from the changes in frequency spectrum due to structural changes, its

estimation is not possible at the present time. In anyway we believe

it best to use the $\Theta_D(T)$ curve as the standard method to determine the

normal heat capacity, at least in the case of the diffuse first order

transition which happened to be observed in $(ND_4)_2SO_4$.

Table 4.3.12   Thermodynamic quantities associated with the
ferroelectric phase transitions.

Crystal	Transition	$\dfrac{T_{tr}}{K}$	$\dfrac{\Delta H_{tr}}{J\ mol^{-1}}$	$\dfrac{\Delta S_{tr}}{J\ K^{-1}mol^{-1}}$
NH_4HSO_4	I - II	269.9	357 ± 55	1.56 ± 0.23
	II - III	159.2	1202 ± 10	7.96 ± 0.05
ND_4DSO_4	I - II	261.7	424	1.85
	II - III	163.9	1470	9.04
$RbHSO_4$	I - II	263.8	204 ± 29	0.81 ± 0.12
$RbHSO_4$	I - II	249.8	203 ± 29	0.87 ± 0.13
$(ND_4)_2SO_4$	I - II	223.9	4270	20.35

$$(\frac{1}{2}\ R\ \ln\ 2 = 2.88\ J\ K^{-1}mol^{-1})$$

The first order transition temperature was estimated as the temperature

which gives the maximum point of the heat capacity observed. In facts

there occurred the rounding near the maximum due to the insufficient

temperature resolution of the thermometers used. From this rounding

the error of transition temperature was estimated. Thus we determined

the transition temperature to be 223.94 ± 0.03 K for $(ND_4)_2SO_4$, 159.2

± 0.1 K for NH_4HSO_4 and 163.9 ± 0.1 K for ND_4DSO_4, respectively. The

detailed procedures of determining the enthalpy and entropy of transition

associated with the lower ferroelectric transition in ND_4DSO_4 is

summarized in Table 4.3.11.

The thermodynamic results thus obtained are presented in 4.3.12.

A great number of ferroelectric transition have been interpreted

with success by one of the two representative mechanisms, one being

continuous displacive mechanism and the other order-disorder mechanism.

In the case of the ferroelectric transitions observed in NH_4HSO_4, $RbHSO_4$

and $(NH_4)_2SO_4$ some possible models have been proposed and they are

summarized in chapters 1 - 2. Now, these models will be compared with

the present thermodynamic results, first concentrating on the order-

disorder model.

Nelmes conjectured from his first structural analysis[7] that the

upper transition in NH_4HSO_4 would be associated with the 'freezing-in'

of a well-defined transverse optical mode rather than with a very over-

damped oscillator model as in KH_2PO_4, and he modified such conjecture

from his later experiment[8] and proposed the order-disorder model for

the corresponding transition, with respect to the orientations (S1$^+$ and

S1$^-$) of only S1 sulfate group. According to his conclusions, one may

expect the transition entropy to be $\frac{1}{2} R \ln 2$, or 2.88 $JK^{-1}mol^{-1}$,

whereas the observed entropy change amounts to only half of the expected

value, as seen from Table 4.3.12. In order to reduce the discrepancy

between the X-ray diffraction and calorimetric results it is necessary

to impose some kind of condition on the disordered paraelectric state.

One possible way to allow us to have the same diffraction pattern of

X-rays as Nelmes obtained is to take a virtual disordered state where

two S1 groups are so correlated to undergo a kind of gear motion, keeping

their center of inversion preserved. Here, gear motion of two S1 groups

means that when one Sl occupies the Sl$^+$ site the other Sl the Sl$^-$ site and vice versa. However, this conditional order-disorder model will be ruled out when we encounter the case of RbHSO$_4$, which is known to be isomorphous with the para- and ferroelectric phases of NH$_4$HSO$_4$. The structure of the paraelectric RbHSO$_4$ has parameters closely similar to NH$_4$HSO$_4$, including the appearance of large temperature factors in the Sl group. Thus we may expect the value of $\frac{1}{2}$ R ln 2 as the entropy of transition, similarly to the case of NH$_4$HSO$_4$. Actually, the observed transition entropy was found to be a quarter of the expected and amounted to half the value observed in NH$_4$HSO$_4$.

The other approach to reduce the discrepancy is to introduce some kind of disorder in the ferroelectric phase. According to the Boltzman's principle the entropy of transition is expressed as $\Delta S/R = \ln 2 - 0.5$ $[(1 + x) \ln (1 + x) + (1 - x) \ln (1 - x)]$, where the reduced moment $x = P_s(max)/N\mu$ and N denotes the number of the effective dipole moment (μ) per unit volume. In ordinary cases one can put $P_s(max) = N\mu$ at least at 0 K, leading to the entropy of transition of R ln 2. In our ferro-electrics such as NH$_4$HSO$_4$ and ND$_4$DSO$_4$ the lowest phase is paraelectric and hence we expect that $P_s(max) \neq N\mu$. The observed entropy of transi-tion gives x = 0.59 for NH$_4$HSO$_4$, x = 0.64 for ND$_4$DSO$_4$, x = 0.43 for RbHSO$_4$ and x = 0.45 for RbDSO$_4$, respectively. There may be three possible interpretations of these values.

1) The ferroelectric configuration of effective dipole moments is less disordered in the ammonium salts than in the rubidium salts. Thus in the case of the rubidium salts one may expect the zero point entropy amounting to 60 % of R ln 2.

2) Taking into account the isomorphism between the ammonium salt

and the rubidium and their similar dimensions of unit cell (Tables 1.2.1 and 2), the dipole moment in the ammonium salts is larger in magnitude than that in the rubidium salts. This may be supported by the fact that in the ferroelectric phase the ammonium ions can contribute more to the dipole moment than the rubidium ions since the rubidium ions have spherical symmetry.

3)   When we take μ as an averaged value over the whole unit cell, the fact that $P_{max} < N\mu$ may lead to the onset of ferrielectricity due to two nonequivalent molecules.

These interpretations, however, may result in something unreasonable and contradicting consequences. In the first place, the estimated values of x are close to 0.5, which characterizes the ferroelectric state as the half ordered and half disordered one. Such a state should have been observed in the X-ray diffraction pattern but Nelmes did not report that the ferroelectric phase was disordered. There is nothing peculiar in the observed temperature dependence of spontaneous polarizations of $RbHSO_4$[60] and NH_4HSO_4[14]. The ferrielectric behavior was not recorded in the D-E hysteresis loop, as was the case in $RbLiSO_4$.[61]

Next we pay our attention to the ferroelectrics which exhibited the so-called order-disorder transition. In terms of critical X-ray scattering in the vicinity of the ferroelectric transition Shibuya and Mitsui[62] revealed that the phase transition in triglycine sulfate was of the order-disorder type and proposed the entropy of transition of R ln 2. On the other hand three different authors have so far reported the entropy of transition of triglycine sulfate to be 2.0,[63] 4.60[64] and 4.48[65] $JK^{-1}mol^{-1}$, respectively, showing that all the values reported are less than R ln 2(5.76 $JK^{-1}mol^{-1}$). In the case of triglycine sulfate

the departure from the predicted value may be partly due to physical

and chemical impurity of the calorimetric specimen used and the accuracy

of the experimental method employed and partly to the inevitable uncer-

tainty in determining the base line of the gradual transition. In the

case of KH_2PO_4[66] (including the same type of ferroelectrics) the

experimental entropy value of 3.1 ± 0.3 $JK^{-1}mol^{-1}$ is in satisfactory

agreement with the theoretical entropy change, $R \ln 3/2 = 3.4$ $JK^{-1}mol^{-1}$,

calculated from the number of completely disordered configurations of

the hydrogen bonds as is the case in ice crystal.[67]

It is well known that the agreement of entropy of transition

between the experimental value and the theoretical one based on the

order-disorder model is not sufficient but necessary condition for the

order-disorder transition. Here we summarize that the ferroelectric

transitions in question do not belong to the so-called order-disorder type.

Until now we have concentrated ourselves on the order-disorder

model in which the transition was described by the discrete variables

such as the number of equilibrium sites of the reorientable dipoles,

with equal probabilities (or energy minima). Next we examine the

observed entropies of transition in terms of a displacive model in which

the transition is described by the continuous variables such as the

normal coordinates of soft ferroelectric modes. Direct evidence of a

displacive transition may be given by the spectroscopic experiments.

However, a displacive ferroelectric transition shows characteristic

thermodynamic behaviors. The oxide ferroelectrics known as the dis-

placive type generally show the successive transitions and their enthalpy

and entropy of transition are also generally smaller than the order-

disorder ferroelectrics such as $NaNO_2$, KH_2PO_4 and $(NH_2CH_2COOH)_3H_2SO_4$.

For example $BaTiO_3$[68] shows $\Delta H_{tr} = 200$ J mol^{-1} and $\Delta S_{tr} = 0.51$ JK^{-1}mol^{-1}

for the I - II transition at 120°C, $\Delta H_{tr} = 78$ J mol^{-1} and $\Delta S_{tr} = 0.27$

JK^{-1}mol^{-1} for the II - III transition at 5°C, $\Delta H_{tr} = 47$ J mol^{-1} and $\Delta S_{tr} = $

0.24 JK^{-1}mol^{-1} for the III - IV transition at -90°C. Comparing these data

with ours (Table 4.3.12), we do not think that the upper transition of

NH_4HSO_4 and the transition of $RbHSO_4$ are of displacive type. The

magnitude of the Curie-Weiss constant also supports this view as we

shall see later.

It is noteworthy that the value of $\Delta H_{tr}(I - II) / RT_{tr}$ is found to

be 0.16 for NH_4HSO_4, 0.19 for ND_4DSO_4, 0.09 for $RbHSO_4$ and 0.10 for

$RbDSO_4$, respectively, where $\Delta H_{tr}(I - II)$ is the enthalpy transition

associated with the I - II transition at the corresponding transition

temperature T_{tr}.

Such analyses and comparison lead to the conclusion that neither

the simple order-disordered model nor the typical displacive model can

be substantiated from thermodynamic point of view. It is possible that

the entropy gained by an order-disorder mechanism becomes partially

compensated by a loss in entropy due to displacive or other mechanism

to give an over-all intermediate magnitude of the entropy of transition

as observed.

Now we examine the first order transitions observed in NH_4HSO_4,

ND_4DSO_4 and $(ND_4)_2SO_4$. The most outstanding difference among them is

that below the first order transition temperature NH_4HSO_4 and ND_4DSO_4

exhibit no ferroelectricity while $(NH_4)_2SO_4$ and $(ND_4)_2SO_4$ show it.

This difference will be expected to be seen in the thermodynamic

behaviors. Accumulated transition enthalpy and entropy are shown as

a function of temperature in Fig. 4.3.19 for $(ND_4)_2SO_4$ and in Fig. 4.3.20

for ND_4DSO_4. These figures reveal that the transition enthalpy and

entropy of $(ND_4)_2SO_4$ is about twice as large as those of ND_4DSO_4 and

that the transition entropy due to the latent heat is 8.3 $JK^{-1}mol^{-1}$ for

ND_4DSO_4, the value being close to the corresponding one (8.1 $JK^{-1}mol^{-1}$)

for $(ND_4)_2SO_4$. As to the ferroelectric transition of $(ND_4)_2SO_4$, there

are two features to be mentioned. As shown in Fig. 4.3.25, anomalous

heat capacity of $(ND_4)_2SO_4$ as well as $(NH_4)_2SO_4$ appears more diffuse

with the long tail extending down to much lower temperature than NH_4HSO_4

and ND_4DSO_4. Another interesting feature is that, as depicted in the

insert of Fig. 3.2.8 and in Fig. 4.3.34, this anomaly apparently consists

of two regions; one is the broad region from about 120 to 223 K corres-

ponding to the gradual increase of the anomalous heat capacity and the

other is the narrow component between 223 and 226 K corresponding to

thermal singularity. In this connection it is worthwhile to note that

the short tail of the anomalous heat capacity of ND_4DSO_4 contributes

only 10 % of the total transition enthalpy and entropy, whereas the

long tail of $(ND_4)_2SO_4$ contributes about 60 % of the total enthalpy

and entropy changes.

The relatively large values of the transition enthalpy and entropy

suggest that the main process of these first order transitions is not

due to the continuous displacement of ion groups but possibly due to the

rearrangement of the reorientable ion groups. The observed transition

entropies of first order can be re-expressed as R ln 2.60 for NH_4HSO_4,

R ln 2.97 for ND_4DSO_4 and R ln 11.6 for $(ND_4)_2SO_4$, respectively.

Considering that the transition entropy increases beyond the combined

error on deuteration, the II - III transition proved to be associated with

a change in the motional state of the ammonium ion with respect to its

angular freedom, consistent with the previous interpretation made in

section 4.3.3. Of course, this transition cannot simply be described

as an order-disorder transition because of the deuteration effect of the transition entropy, though ND_4DSO_4 exhibits the close value of R ln 3.

As to the transition of $(ND_4)_2SO_4$, O'Reilly and Tsang[6] proposed that the order-disorder model, assuming that two ammonium cations and one sulfate anion take two possible sites with equal probability independently above the transition temperature. Their interpretation should lead to the transition entropy of R ln 8 (= 17.3 $JK^{-1}mol^{-1}$). When we employ the same uncertainty of the transition entropy as in the case of NH_4HSO_4 for the gradual tail of the anomalous heat capacity of $(ND_4)_2SO_4$, we obtain 1.8 $JK^{-1}mol^{-1}$ as the uncertainty in entropy due to the uncertainty of the base line. The observed entropy change is somewhat larger than the value of 17.3 $\pm$ 1.8 $JK^{-1}mol^{-1}$ but the mechanism of the transition seems to be of order-disorder type because the small disagreement (1.3 $JK^{-1}mol^{-1}$) may be attributed to the entropy change due to other degrees of freedom than the reorientational degrees of freedom.

Applying the group-theoretical phonomenology, Sawada, et al.[21] explained successfully the improper ferroelectric behaviors of $(NH_4)_2SO_4$, such as the low Curie-Weiss constant and the large electrostrictive constant. However, they calculated the transition entropy as 5.0 $JK^{-1}mol^{-1}$, the value of which is smaller than the observed value of 20.4 $JK^{-1}mol^{-1}$ and also smaller than the entropy value (8.1 $JK^{-1}mol^{-1}$) associated with the latent heat portion. Thus their model did not prove to be good as far as the thermodynamic aspects are concerned. In connection with the largeness of transition entropy it is noteworthy that the transition entropy of $(ND_4)_2SO_4$ as well as of $(NH_4)_2SO_4$ belongs to one of the largest values among the ferroelectrics which have ever been observed.

Schlemper and Hamilton[13] stressed the change of the hydrogen

bond in passing the transition and so the transition enthalpy may be

estimated from the N-H···O hydrogen bonding energy.[69] However the

presence of multifurcated hydrogen bonds around a ammonium ion makes

its evaluation complicated.

4.3.5 Possible transition mechanism

In the preceding section the mechanism governing the ferroelectric

transitions in NH_4HSO_4 and $RbHSO_4$ and their deuterium analogs proved

to be neither of order-disorder type nor of displacive one. Consequently,

possible mechanisms will be sought in this section, taking into account

the isotope and pressure effects on the transition temperature and the

shape of anomalous heat capacity.

A distinct deuteration effect on the ferroelectric transition

temperature was observed, as seen from Fig. 4.3.21. The ratio of the

transition temperatures of normal and deuterated crystals is listed in

Table 4.3.13 and compared with other ferroelectrics having the O-H···O

hydrogen bonds, together with NH_4Br[79,80] and $(NH_4)_2BeF_4$.[14] Except

the transition of $RbHSO_4$, the upper transition of NH_4HSO_4 and the lower

transition of Rochelle salt, all the ferroelectrics listed show that

their transition temperatures shift to the high temperature side on

deuteration. Thus, this peculiar deuteration effect in $RbHSO_4$ and

NH_4HSO_4 may be associated with two kinds of one dimensional chain of

the short O-H···O hydrogen bond since other ferroelectrics tabulated

here have two or three dimensional networks of the O-H···O hydrogen

bonds. In the case of KH_2PO_4[28] family its large isotope effect of the

transition temperature is explained on the basis of the coupling between

the proton tunneling mode and the optical mode vibration of the $[K-PO_4]$ complexes. However, the proton tunneling modes in NH_4HSO_4 and $RbHSO_4$ is not expected to be present, in accordance to X-ray results by Nelmes.[7] With regard to the very small upward shift of the transition temperature on deuteration the behavior of $(NH_4)_2SO_4$ is very similar to that of NH_4Cl,[82] which is well known to exhibit the typical order-disorder transition. From this kind of analogous behavior, we cannot always conclude that the transition in $(NH_4)_2SO_4$ is of order-disorder type because the order-disorder transition of NH_4Br at 235 K appears at the lower temperature of 215 K on deuteration. Thus there seems to be no distinct relation between the order-disorder transition and its transition temperature shift on deuteration. It is interesting to find out the same isotope effect in NH_4Br as in NH_4HSO_4, including the first and second order transitions. Thus in later section we will examine the transition behavior of NH_4HSO_4 by referring to that of NH_4Br. Table 4.3.13 suggests that the first order transition temperature do not always increase on deuteration as inferred from the melting transitions of hydrogen halides and the first order transitions of $(NH_4)_2SO_4$ and NH_4HSO_4.

It is worthwhile to remark the facts[58] that, at least for Sn, Tl, Hg, Pb the superconducting transition temperature was a function of the isotopic mass; $T_c \propto 1/\sqrt{M}$. The I - II transitions in NH_4HSO_4 and ND_4DSO_4 and the corresponding transitions in $RbHSO_4$ and $RbDSO_4$ did not show the constant value of $T_c \sqrt{M}$ even if M is taken as the molecular weight or the reduced mass of NH_4^+ or ND_4^+ or Rb^+ and HSO_4^- or DSO_4^-. However, if we take M as the formula weight of HSO_4^- or DSO_4^- then we obtain the value (in units of $K\ g^{-\frac{1}{2}}\ mol^{-\frac{1}{2}}$) of 2659 for NH_4HSO_4,

2592 for ND_4DSO_4, 2599 for $RbHSO_4$ and 2474 for $RbDSO_4$, respectively,

yielding the averaged value of 2581 ± 107 where the error means the

maximum deviation which amounts to only 4 % of the average. This

constancy of the product $T_c \sqrt{M}$ seems to suggest that the ferroelectric

transitions in question possess the similar nature in mechanism to the

superconductivity phase transition and also are primarily concerned

with the two hydrogen bonded chains in these crystals.

Next we pay our attention to the pressure effect on the ferroelectric

transition temperature. One may obtain the transition entropy change

at the transition temperature of $(NH_4)_2SO_4$ from the Clausius – Clapeyron

relation $dT_c / dp = \Delta V / \Delta S$ where the left hand side is the slope of the

transition line in the (T , p) plane and ΔV the volume change. By using

the value of dT_c / dp[83] (-4.0×10^{-3} K/Kg/cm^2) and the volume change[14]

$\Delta V = -2$ Å^3 at the transition temperature, we obtain $\Delta S = 5$ JK^{-1}mol^{-1},

which is close to the observed entropy change of $(ND_4)_2SO_4$ (8 JK^{-1}mol^{-1})

due to the latent heat. The negative sign of dT_c / dp is observed in

$BaTiO_3$[84] and also in KH_2PO_4.[85] In the case of KH_2PO_4 Novakovic[86]

have explained well the negative value, on the basis of the tunneling

mode of the proton in the O–H···O bond.

Geshi and Ozawa[87] observed the pressure coefficient of the Curie

temperature of 12.0 K kbar^{-1} for $RbHSO_4$ and 12.7 K kbar^{-1} for $RbDSO_4$,

respectively. According to the Ehrenfest relation together with the

above values and the discontinuous changes of heat capacity of $RbHSO_4$

(8.6 JK^{-1}mol^{-1}) and $RbDSO_4$ (8.0 JK^{-1}mol^{-1}) at the Curie temperature

one obtains the difference in the cubic thermal expansion coefficient

at T_c as $\Delta\alpha = -6.2 \times 10^{-5}$ K^{-1} for $RbHSO_4$ and $\Delta\alpha = -6.7$ K^{-1} for $RbDSO_4$,

respectively, assuming the same density of 2.9 g cm^{-3} for the normal

and deuterated crystals. Thus the changes[88] in the linear expansion

along the b- and c- axis of -1.25×10^{-4} K^{-1} and 2.5×10^{-5} K^{-1} yield

the change in the a sin β of 3.8×10^{-5} K^{-1}, suggesting that at the

Curie temperature there occurs the uniaxial change along the monoclinic

axis of b parallel to the infinite hydrogen bonded chains.[87] The

positive sign of dT_c / dp indicated that the positional order-disorder

of H or D in the their hydrogen bonds do not play so important role

for the onset of ferroelectricity in RbHSO$_4$ and RbDSO$_4$ as in the case

of KH$_2$PO$_4$, being consistent with the results of deuterium quadrupole

resonance by Kasahara and Tatsuzaki.[89]

Up to this point we have confined ourselves to discuss the

thermodynamic quantities associated with the difference between the

pre-transition state and the post-transition one. In what follows

we will be concentrating on the anomalous part of the observed heat

capacity and discuss the ferroelectric transition process in which some

different properties from the displacive or order-disordered ferro-

electrics will be expected to be seen. Figure 4.3.22 compares the

anomalous heat capacities of NH$_4$HSO$_4$ and ND$_4$DSO$_4$ corresponding to the

I - II transition on the temperature scale reduced with their Curie

temperatures. As seen from Fig. 4.3.22 the anomalous part of the heat

capacity of NH$_4$HSO$_4$ exhibits no trace of constant value below T_c,

contrary to the predictions from the ordinary phenomebological theory[90]

and also from the more sophisticated theory[3] combined with group

theory. From this figure the pre-transition effect proved to appear

just above the lower first order transition and amount to the maximum

value of 1.3R for NH$_4$HSO$_4$ and 1.5R for ND$_4$DSO$_4$ at their Curie tempera-

tures where R is the gas constant. In the case of RbHSO$_4$ and RbDSO$_4$

(Fig. 4.3.23) the pre-transition effect starts at about $0.7T_c$ and

ends just above T_c, which is practically the same as in the case of

NH_4HSO_4 and ND_4DSO_4. The maximum value of the anomalous heat capacity at T_c found to be roughly R for both the rubidium hydrogen and deuterium sulfates.

These anomalous behaviors may be compared with those predicted by the molecular field theory applied for the Ising spin system. Assuming the simple cubic lattice for this system, the thermodynamic functions are shown in Fig. 1.3.1 where $<S_z>$ is the long range order parameter corresponding to the spontaneous polarization, the temperature dependence of which can be obtained from the self-consistency equation equivalent to the condition that the polarization to be realized at equilibrium is the one with a minimum of free energy. At $T_c = zJ/K$ the polarization goes to zero as $\sqrt{T_c - T}$.[91] This decrease in polarization from the saturated value at 0 K gives rise to the anomalous heat capacity, the temperature dependence of which is analogous to the observed anomalous heat capacities in NH_4HSO_4 and $RbHSO_4$ and their deuterium analogs (Fig. 4.3.22 and 23). According to this molecular field theory the predicted anomaly will be observed experimentally at $T = 0.4\ T_c$ and the heat capacity anomaly will amount to 1.5R at T_c, as seen from Fig. 1.3.1, and will be associated with the transition entropy of $R \ln 2$. However, the experimental results do not support any quantitative aspects predicted by such a simple molecular field theory.

When NH_4^+ in NH_4HSO_4 is replaced by Rb^+, the anomalous heat capacity of $RbHSO_4$ proved to be smaller as a whole than that of NH_4HSO_4, suggesting indirect evidence that NH_4^+ is also responsible for the upper transition of NH_4HSO_4 though no noticeable change in NMR spectra was observed in the vicinity of transition temperature (See Fig. 4.3.24).

The anomalous parts in $(NH_4)_2SO_4$ and $(ND_4)_2SO_4$ (Fig. 4.3.25)

resemble those observed in the order-disorder transitions in NH_4Cl,[92] NH_4Br,[79] and ND_4Br.[80] It is worth noting that anomalous behaviors in $(ND_4)_2SO_4$ are different from the behaviors of magnetic heat capacities such as $CuK_2Cl_4 \cdot 2H_2O$ and $Cu(NH_4)_2Cl_4 \cdot 2H_2O$[93] showing the long tail above T_c. The Onsager's solution[94] to the problem of a two-dimensional cooperative transition explains such a long tail above T_c approximately although there is a difference in dimension. From these facts we can guess that the dipole-dipole interaction in our ferroelectrics cannot be approximated by the localized magnetic dipole such as the Ising spin.

Now we examine anomalous part of heat capacity below the transition temperature in terms of the process of defect formation. The process may be characterized by enthalpy of defect formation, the value of which is evaluated from the slope of linear part in the plot of $\ln (T^2 \Delta c_p)$ versus T^{-1} (called defect plot hereafter). Figures 4.3.26-32 show these defect plots for our ferroelectrics in question, together with other crystals such as NH_4Cl,[92] $(NH_4, Rb)Cl$,[95] NH_4Br,[79] ND_4Br,[80] $(NH_4)_2SO_4$,[78] VCl_3[96] and $C_{10}H_{16}$ (adamantane)[97], for the sake of comparison. The enthalpies thus obtained are presented in Table 4.3.14.

Figure 4.3.26 for $RbHSO_4$ and $RbDSO_4$, Fig. 4.3.27 for NH_4HSO_4 and ND_4DSO_4, Fig. 4.3.28 for VCl_3 and Fig. 4.3.32 for $C_{10}H_{16}$ reveal the outstanding feature that up to the immediate neighborhood of their transition temperatures their anomalous heat capacities give straight lines of the defect plot. Especially, as to NH_4HSO_4 and ND_4DSO_4 the enthalpies of defect formation responsible for appearance (III - II transitions) and disappearance (II - I transitions) of ferroelectricity proved to be the same value within experimental error.

On the other hand, other crystals show large deviation from a straight line predicted by the defect formation even at a temperature

about 15 K lower than their transition temperatures. These deviations seem to be strongly assocaited with the cooperative effect to be observed in the vicinity of phase transition.

The values for enthalpy of defect formation may be interpreted on various statistical models.

Model A   Thermally activated defects

The Schottky and Frenkel defects described in Chapter 1 are representative. Even if both defects are present at the same time in a crystal, Eq. 1 - 32 holds as far as h(Frenkel) and h(Schottky) >> kT.[98]

We examine the weakly coupled system which consists of N localized particles with two energy levels (ε_1 and ε_2). Assuming that these two states are associated with two possible orientations of an electric dipole moment, we call the state with energy ε_2 "defect" which is higher by $\varepsilon = \varepsilon_2 - \varepsilon_1$ than the ground state. Using the energy $U = \varepsilon_1 N_1 + \varepsilon_2 N_2$ and the mixing entropy $S = k \ln (N! / N_1! N_2!)$, the free energy can be written as $A = U - TS$. The self consistency equation with respect to the defect density gives $N_2 / N = (1 + e^x)^{-1}$ where $x = \varepsilon / kT$ and the + sign means that the defect under consideration is not of Frenkel type but of Schottky type. In connection with ferroelectric transitions we may suppose that the Schottky defects in question carry some kind of charge on the crystal surfaces and reduce the surface charge due to the ferroelectric spontaneous polarization.

Using the defect density N_2 / N, the thermodynamic functions of this system are summarized as follows;

$$F / kNT = (\varepsilon_1 / kT) - \ln (1 + e^{-x}), \qquad 4 - 7$$

$$U / kN = (\varepsilon_1 / k) + x(1 + e^x)^{-1}, \qquad 4 - 8$$

$$S / kN = x(1 + e^{-x})^{-1} + \ln (1 + e^{-x}), \qquad 4 - 9$$

$$C_v / kN = x^2 e^x (1 + e^x)^{-2}. \qquad\qquad 4 - 10$$

These results are the same as the exact solutions in one dimensional Ising spin system which, of course, exhibit no phase transition. As far as $x \gg 1$ the heat capacity can be re-expressed as $C_v / kN = x^2 e^{-x}$.

Using the observed entropy changes we estimated the values of x which satisfy Eq.4 - 9 and using the observed I - II transition temperatures we obtained the energy gap of 6.79 kJ mol^{-1} for NH_4HSO_4, 6.05 for ND_4DSO_4, 8.55 for $RbHSO_4$ and 7.91 for $RbDSO_4$, respectively. Agreement between the values thus obtained and the corresponding values in Table 4.3.14 is found to be good in the cases of NH_4HSO_4 and ND_4DSO_4 and to be poor in the cases of $RbHSO_4$ and $RbDSO_4$.

The ratio of energy gap h(Table 4.3.14) and $k T_{tr}$(I -II) (Table 4.3.11) is found to be 4.7 for NH_4HSO_4, 5.7 for ND_4DSO_4, 8.9 for $RbHSO_4$ and 8.8 for $RbDSO_4$, respectively, which are comparable with experimental values and the predicted value (3.52) by the BCS theory.[100]

Model B   Einstein mode

An Einstein heat capacity may be expanded as

$$C_E = 3R(T_E / T)^2 \exp(-T_E / T), \quad T_E \gg T, \qquad 4 - 11$$

where $T_E = \hbar \omega_E / k$ and ω_E is the Einstein frequency. Judging from the values of the I - II transition temperatures, the frequency value (ω_E) in wave numbers must be much larger than 208 cm^{-1} equivalent to 300 K in temperature. It is impossible to consider such a virtual Einstein mode because we used all the modes that the crystals such as $RbHSO_4$ can have in order to explain the normal heat capacity. Thus, this model may be rejected, on the basis of the limited number of degrees of freedom.

Model C   Schottky effect

It is well known that if the (fictitious) spins become noncoopera-
tively ordered, a smooth Schottky maximum appears. For the sake of
simplicity, consider a system with two levels; the ground state with
degeneracy g_o and the excited state with degeneracy g_1, separated from
the ground state by an energy $\varepsilon = k\delta$, then we obtain

$$C_{Sch} = R(g_1 / g_o)^2 (\delta / T)^2 \exp(-\delta / T), \quad T << \delta \qquad 4 - 12$$

$$= R g_o g_1 (g_o + g_1)^{-2} (\delta / T)^2 \quad , \quad T >> \delta \qquad 4 - 13$$

and $\Delta S = R \ln (g_o + g_1) / g_o.$

This Schottky effect should be observed in the high temperature side
of T_{tr} but we could not detect such a behavior $(4-13)$, as seen from
Figs. 4.3.23 - 25.

Model D   Low temperature expansion in molecular field theory

In this theory we may approximate the ferroelectric dipoles as
the Ising spins and take into account nearest neighbor interactions
alone, then we have

$$C_{HF} = 4 R (T_c / T)^2 \exp(-2T_c / T), \quad T << T_c, \qquad 4 - 14$$

where $T_c = z J / k.$ [91)]

Equation 4 - 14 allows us to regard the process of defect formation
as the elementary process of phase transition because this equation
contains a cooperative effect. According to this expansion, the value
of $h / k T_{tr}$ should be 2, which shows a disagreement with the observed
values.

Next we examine the critical behaviors of the anomalous heat capacity

of $RbHSO_4$ and $RbDSO_4$ since Kasahara and Tatsuzaki[89] reported the
critical index of the P_s and the separation of the resonance lines as
$\beta = 0.33$. However, Fig. 4.3.33 does not reveal that the anomalous heat
capacity of $RbHSO_4$ and $RbDSO_4$ have a definite critical index over a
wide range. This kind of situation is also observed in the case of
$(NH_4)_2SO_4$ and $(ND_4)_2SO_4$ as seen from Fig. 4.3.34. Thus, this property
having no definite index proved to be common to our ferroelectrics.

It is noteworthy that within $|T - T_c| / T_c \simeq 0.1$ anomalous behaviors
associated with the order-disorder transitions in NH_4Br and ND_4Br have
a definite critical index of 0.5, the value in the random phase approx-
imation,[91] as seen from the solid line in Fig. 4.3.35.

According to the classification of ferroelectrics by Nakamura
et al.[99] there seem three typical groups. Group I such as $BaTiO_3$ is
called a displacive type which is characterized by the large Curie-Weiss
constant of about 10^5 K. (See Table 4.3.17) The origin of the P_s is
often ascribed to the displacement of constituent ions from the equilibrium
positions in the high temperature phase. On the other hand, Group II
such as triglycine sulfate is classified as an order-disorder type which
shows the Curie-Weiss constant C of about 10^3 K. The P_s often appears
as a result of the ordering of rotatable permanent dipoles. The crystals
such as $(NH_4)_2SO_4$ with low value of C are classified as Group III.

Judging from the Curie-Weiss law, the small value of C correspond
to the fact the very rapid decrease of the dielectric constant just
above the extrapolated Curie temperature. It may be interpreted as
arising from the very rapid disappearance of local order with increase
of temperature. This interpretation has been confirmed by the very
small and short tail of anomalous heat capacities above T_c(I - II) for

NH_4HSO_4, ND_4DSO_4, $RbHSO_4$, $RbDSO_4$ and $(ND_4)_2SO_4$. (See Figs. 4.3.23 - 25). According to the Weiss type theory the value of C/T_c is inversely proportional to a molecular field coupling constant. Thus the small value of the ratio C/T_c for Group III indicates a strong coupling between dipoles which however seems to be more or less inconsistent with the quick disappearance of short range order. As to the thermodynamic behavior, we can suggest that the I - II ferroelectric transitions in NH_4HSO_4 and $RbHSO_4$ and their deuterium analogs are due to a weak cooperative effect.

Reference to Chapter 4

1) L. A. Shvalov, J. Phys. Soc. Japan, $\underline{28}$, 38 (1970)

2) A. Sawada, Y. Takagi and Y. Ishibashi, J. Phys. Soc. Japan, $\underline{34}$, 748 (1973)

3) T. Kondo, Y. Ishibashi and Y. Takagi, J. Phys. Soc. Japan, $\underline{39}$, 1326 (1975)

4) K. Aizu, J. Phys. Soc. Japan, $\underline{36}$, 937 (1974)

5) T. Chiba, J. Chem. Phys., $\underline{36}$, 1122 (1962)

6) D. E. O'Reilly and T. Tsang, J. Chem. Phys., $\underline{50}$, 2274 (1969)

7) R. J. Nelmes, Acta Cryst., $\underline{B27}$, 272 (1971)

8) R. J. Nelmes, Acta Cryst., $\underline{A28}$, 445 (1972)

  Presented at the 2nd European Meeting on Ferroelectricity,

  Dijan (France) Sept., 1971

  Ferroelectrics, $\underline{4}$, 133 (1972)

9) W. G. Mumme, Acta Cryst., $\underline{B29}$, 1072 (1972)

10) L. H. Loopstra and C. H. MacGillavry, Acta Cryst., $\underline{11}$, 349 (1958)

   D. W. J. Cruickshank, Acta Cryst., $\underline{17}$, 682 (1962)

11) I. Taesler and I. Olovsson, Acta Cryst., $\underline{B24}$, 299 (1968)

12) S. Grimvall, Acta Chem. Scand., $\underline{25}$, 3213 (1971)

13) E. O. Schlemper and W. C. Hamilton, J. Chem. Phys., $\underline{44}$, 4498 (1966)

14) S. Hoshino, K. Vedam, Y. Okaya and R. Pepinsky, Phys. Rev., $\underline{112}$, 405, (1958)

15) F. Jona and R. Pepinsky, Phys. Rev., $\underline{92}$, 1577 (1953)

   R. S. Krishnan, H. V. Tiwary and P. S. Narayanan, J. Phys. Soc. Japan, $\underline{28}$, 167 (1970)

16) R. D. Schannon and C. T. Prewitt, Acta Cryst., $\underline{B25}$, 925 (1969)

17) A. A. Khan and W. H. Baur, Acta Cryst., $\underline{B28}$, 683 (1972)

18) Y. Higashigaki, unpublished results

19) W. A. Dollase, Acta Cryst., B25, 2298 (1969)

20) G. e. Bacon and R. S. Pease, Proc. Roy. Soc., A220, 397 (1953)

21) L. A. Beevers and W. Hughes, Proc. roy. soc. A177, 251 (1941)

   B. C. Frazer, M. McKeown and R. Pepinsky, Phys. Rev., 94, 1435 (1954)

22) A. Kalman, J. S. Stephens and D. W. Cruickshank, Acta Cryst.,
   B26, 1451 (1970)

23) H. G. Smith and H. A. Levy, Acta Cryst., 15, 1201 (1962)

24) A. R. Ubbelohde and K. J. Gallagher, Acta Cryst., 8, 71 (1955)

25) RbDSO$_4$; M. Yamada, Presented at the 28th Annual Meeting of the
      Physical Society of Japan (5a-F-5) 1973

   RbHSO$_4$; J. P. Ashmore, Physical Abstracts, 78497

26) I. Nitta, Y. Tomiie and C. H. Koo, Acta Cryst., 7, 140 (1954)

   P. P. Herpin and P. Meriel, J. Phys. (Paris) 25, 484 (1964)

27) W. Cochran, Adv. in Phys., 9, 387 (1960) and 10, 401 (1961)

28) K. K. Kobayashi, J. Phys. Soc. Japan, 24, 497 (1968)

29) M. Tokunaga and T. Matsubara, Progr. Theo. Phys., 35, 581 (1966)

   M. Tokunaga, Progr. Theo. Phys., 36, 857 (1966)

31) Y. Yamada and G. Shirane, J. Phys. Soc. Japan, 26, 396 (1969)

32) "Structural Phase Transitions and Soft Modes" edited by E. J.
   Samuelson, E. Andersen and J. Feder, Universitetsforlaget, Oslo 1971

33) J. F. Scott, Rev. Mod. Phys., 46, 83 (1974)

   G. Shirane, Rev. Mod. Phys., 46, 437 (1974)

34) C. J. H. Schutte and A. M. Heyns, J. Chem. Phys., 52, 864 (1970)

35) B. H. Torrie, C. C. Lin, O. S. Binbrek and A. Anderson,
   J. Phys. Chem. Solids, 33, 697 (1972)

36) G. Herzberg, "Infrared and Raman Spectra", D. van Nostrand Co. Inc.,
   New York 1945

37) E. L. Wagner and D. F. Hornig, J. Chem. Phys., 18, 296 and 305 (1950)

N. E. Schumaker and C. W. Garland, J. Chem. Phys., $\underline{53}$, 392 (1971)

J. R. Durig and D. J. Anton, J. Chem. Phys., $\underline{51}$, 3639 (1967)

C. H. Perry and R. P. Lowndes, J. Chem. Phys., $\underline{51}$, 3648 (1969)

38) G. Turrell, "Infrared and Raman Spectra of Crystals", Chapter 4

Academic Press 1972

39) J. J. Rush and T. T. Taylor, IAEA symposium on Inelastic Scattering

of Neutrons in Solids and Liquids, $\underline{2}$, 333 (1965)

40) K. Nakamoto, M. Margoshes and R. E. Rundle, J. Amer. Chem. Soc.,

$\underline{77}$, 6480 (1955)

R. Blinc, D. Hadzi and A. Novak, Ber. Bunseng. Phys. Chem.,

$\underline{64}$, 567 (1960)

C. Reid, J. Chem. Phys., $\underline{30}$, 182 (1959)

41) A. N. Lazarev and A. S. Zaitseva, Soviet Physics- Solid State,

$\underline{2}$, 2688 (1961)

42) R. Blinc and D. Hadzi, Molec. Phys., $\underline{1}$, 391 (1958)

43) T. P. Myasnikova and A. F. Yatsenko, Soviet Physics-Solid State,

$\underline{4}$, 475 (1962)

44) A. A. Maradudin, E. W. Montroll, G. H. Weiss and I. P. Ipatova,

"Theroy of Lattice Dynamics in the Harmonic Approximation"

Solid State Physics, Vol. 3 Academic Press 1971

M. Born and K. Huang, "Dynamical Theory of Crystal Lattices"

Oxford Univ. Press, London and New York 1954

45) E. S. R. Gopal, " Specific Heats at Low Temperatures" Chapter 2

Plenum Press 1966

46) Y. Higashigaki and H. Chihara, Bull. Chem. Soc. Japan, $\underline{49}$, 2089 (1976)

47) W. V. Houston, Rev. Mod. Phys., $\underline{20}$, 161 (1948)

48) M. Blackman, Proc. Roy. Soc., $\underline{A181}$, 58 (1942)

49) H. Chihara and A. Inaba, J. Phys. Soc. Japan, $\underline{40}$, 1383 (1976)

50) H. Thirring, Phys. Z., $\underline{14}$, 867 (1913)

51) C. Domb and L. Salter, Phil. Mag., $\underline{43}$, 1083 (1952)

52) H. C. Teh and B. N. Brockhouse, Phys. Rev., $\underline{B3}$, 2733 (1971)

53) J. A. K. Duckworth, B. T. M. Willis and G. S. Pawley,

Acta Cryst., $\underline{A26}$, 263 (1970)

G. Dolling and B. M. Powel, Proc. Roy. Soc., $\underline{A319}$, 209 (1970)

54) T. Mozume, G. Soda and H. Chihara, Unpublished work

55) R. G. S. Morfree, L. A. K. Staveley, S. T. Walters and D. L. Wigley,

J. Phys. Chem. Solids, $\underline{13}$, (1960)

56) C. C. Stephenson, C. A. Wulff and O. R. Lundell,

J. Chem. Phys., $\underline{40}$, 967 (1964)

57) E. F. Westrum, Jr. and B. H. Justice, J. Chem. Phys., $\underline{50}$, 5083 (1969)

58) W. S. Corak, B. B. Goodman, C. B. Satterthwaite and A. Wexler,

Phys. Rev., $\underline{96}$, 1442 (1954) ; $\underline{102}$, 656 (1956)

W. S. Corak and C. B. Satterthwaite, Phys. Rev., $\underline{102}$, 662 (1956)

59) B. S. Strukov, V. A. Koptsik and V. D. Ligasova,

Soviet Physics- Solid State, $\underline{4}$, 977 (1962)

60) R. Pepinsky and K. Vedam, Phys. Rev., $\underline{117}$, 1502 (1960)

61) Y. Shiroishi, A. Nakata and S. Sawada, J. Phys. Soc. Japan, $\underline{40}$, 911 (1976)

62) I. Shibuya and T. Mitsui, J. Phys. Soc. Japan, $\underline{16}$, 479 (1961)

63) S. Hoshino, T. Mitsui, F. Jona and R. Pepinsky,

Phys. Rev., $\underline{107}$, 1255 (1957)

64) B. A. Strukov, Soviet Physics-Solid State, $\underline{6}$, 2278 (1965)

65) M. J. Tello and J. A. Gonzalo, J. Phys. Soc. Japan, $\underline{28}$, 199 (1970)

66) C. C. Stephenson and J. G. Hooley, J. Amer. Chem, Soc., $\underline{66}$, 1397 (1944)

67) L. Pauling, J. Amer. Chem. Soc., $\underline{57}$, 2680 (1935)

68) G. Shirane and A. Takeda, J. Phys. Soc. Japan, $\underline{7}$, 1 (1952)

S. S. Todd and R. E. Lorenson, J. Amer. Chem. Soc., $\underline{74}$, 2043 (1952)

69) C. A. Coulson, "Valence" Chapter XII Clarendon Press 1953

70) J. Hablutzel, Helv. Phys. Acta, $\underline{8}$, 498 (1935)

71) H. Kiriyama, Bull. Chem. Soc. Japan, $\underline{35}$, 1199 (1962)

72) K. Okada, Phys. Rev., $\underline{164}$, 683 (1967)

75) M. Oguni. T. Matsuo. H. Suga and S. Seki,

Bull. Chem. Soc. Japan, $\underline{48}$, 379 (1975)

76) V. G. Vaks, N. E. Zein and B. A. Strukov, phys, stat. sol. (a),

$\underline{30}$, 801 (1975)

77) E. A. Wood, W. J. Merz and B. T. Matthias, Phys. Rev., $\underline{87}$, 544 (1952)

78) C. H. Shomate, J. Amer. Chem. Soc., $\underline{67}$, 1096 (1945)

79) M. Sorai, H. Suga and S. Seki, Bull. Chem. Soc. Japan, $\underline{38}$, 1125 (1965)

80) C. C. Stephenson and A. M. Karo, J. Chem. Phys., $\underline{48}$, 104 (1968)

86) A. Inaba, Thesis Osaka University 1976

82) I. Nitta and K. Suenaga, Bull. Chem. Soc. Japan, $\underline{13}$, 36 (1938)

83) S. Tsunekawa, Y. Ishibashi and Y. Takagi,

J. Phys. Soc. Japan, $\underline{33}$, 862 (1972)

84) G. A. Samara, Ferroelectrics, $\underline{2}$, 277 (1971)

85) H. Umebayashi, B. C. Frazer and G. Shirane,

Solid State Commun., $\underline{5}$, 591 (1967)

86) L. Novakovic, J. Phys. Chem. Solids, $\underline{29}$, 963 (1968)

87) K. Gesi and K. Ozawa, J. Phys. Soc. Japan, $\underline{38}$, 459 (1975)

88) N. Yamada and H. Shimizu, Presented at the 26th Annual Meeting of

the Physical Society of Japan, (1971)

89) M. Kasahara and I. Tatsuzaki, J. Phys. Soc. Japan, $\underline{38}$, 1389 (1975)

90) B. A. Strukov and M. N. Danilycheva, Soviet Physics- Solid State,

$\underline{5}$, 1253 (1963)

91) R. Brout, "Phase Transitions" Chapter 2 W. A. Benjamin, Inc.,

New York Amsterdam 1965

92) H. Chihara and M. Nakamura, Bull. Chem. Soc. Japan, $\underline{45}$, 133 (1972)

93) C. Domb and A. R. Miedema, Progr. Low Temp. Phys., $\underline{4}$, 296 (1964)

94) L. Onsager, Phys. Rev., $\underline{65}$, 117 (1944)

95) H. Chihara, Private communication

96) C. H. Shomate, J. Amer. Chem. Soc., $\underline{69}$, 220 (1947)

97) Shu-Sing Chang and E. F. Westrum, Jr., J. Phys. Chem., $\underline{64}$, 1547 (1960)

98) R. H. Fowler and E. A. Guggenheim, "Statistical Thermodynamics"

Chapter XIII, Cambridge 1965

99) E. Nakamura, T. Mitsui and J. Furuichi,

J. Phys. Soc. Japan, $\underline{18}$, 1477 (1963)

100) J. Bardeen, L. N. Cooper and J. R. Schrieffer,

Phys. Rev., $\underline{106}$, 162 and $\underline{108}$, 1175 (1957)

J. Bardeen and J. R. Schrieffer, Progr. Low Temp. Phys., $\underline{3}$, 170 (1961)

D. H. Douglass Jr. and L. M. Falicov

Progr. Low Temp. Phys., $\underline{4}$, 97 (1962)

Table 4.1.1 Comparison of the distortions in SO_4^{--}
D. = Bond distance, A.D. = Averaged bond distance,
A.A. = Averaged bond angle. The radial and angular
distortion index is given in parentheses.

Crystals		D. S-O(H) Å	A.D. S-O Å	A.A HO-S-O degree	A.A. O-S-O degree	Reference
	SO_4^{--}(I)	1.546 (0.051)	1.459	105.5 (4.5)	113.1	(7)
	SO_4^{--}(II)	1.557 (0.049)	1.473	106.6 (3.6)	112.7	
NH_4HSO_4	$S1_D^+$	1.56 (0.07)	1.46			(8)
	$S1_D^-$	1.57 (0.06)	1.48			
	SO_4^{--}(II)	1.564 (0.053)	1.474			
$RbHSO_4$	SO_4^{--}(I)	1.59 (0.06)	1.50			(9)
	SO_4^{--}(II)	1.54 (0.04)	1.48			
$KHSO_4$	SO_4^{--}(I)	1.56 (0.05)	1.49	105.2 (4.4)	113.5	(10)
	SO_4^{--}(II)	1.55 (0.04)	1.49	107.0 (3.0)	111.8	
H_3OHSO_4	SO_4^{--}	1.560 (0.049)	1.476	106.5 (3.3)	112.2	(11)
$NaHSO_4 \cdot H_2O$	SO_4^{--}	1.599 (0.065)	1.488	106.5 (3.5)	112.3	(12)
$(NH_4)_2SO_4$						
Paraelectric	SO_4^{--}		1.49 (0.00)		106.5 (0.8)	(13)
Ferroelectric	SO_4^{--}		1.48 (0.01)		109.5 (1.0)	

Table 4.1.2 Atomic shifts of SO_4^{--}(I) group in the disordered phase of NH_4HSO_4.[8] Coordinates are given in Å reffered to orthogonal axes $\underline{X}$, $\underline{Y}$ and $\underline{Z}$ where $\underline{X}$ is parallel to $\underline{a}$, $\underline{Y}$ is parallel to $\underline{b}^*$ and $\underline{Z}$ is parallel to $\underline{a} \times \underline{b}$.

NH_4HSO_4	ΔX	ΔY	ΔZ
$\Delta S(1)$	−0.024	+0.020	−0.083
$\Delta O(1)$	+0.057	−0.205	−0.158
$\Delta O(2)$	−0.048	+0.372	−0.210
$\Delta O(3)$	−0.418	−0.131	−0.350
$\Delta O(4)$	+0.378	−0.089	+0.086
Sum of displacement of O	−0.031	−0.053	−0.635
Relative displacement of O to S	−0.007	−0.073	−0.552

Table 4.1.3 Atomic shifts of NH_4^+ and SO_4^{--} groups through the ferroelectric transition. Coordinates are given in Å reffered to orthorhombic axes $\underline{X}$, $\underline{Y}$, and $\underline{Z}$. $\Delta X = X(Ferro) - X(Para)$, ...

$(NH_4)_2SO_4$	ΔX	ΔY	ΔZ
ΔS	+0.005	+0.011	−0.006
$\Delta O(1)$	+0.002	+0.013	−0.233
$\Delta O(2)$	+0.124	−0.003	−0.173
$\Delta O(3)$	+0.136	−0.227	+0.203
$\Delta O(4)$	−0.217	+0.155	+0.142
Sum of oxygen displacement	+0.050	−0.051	−0.067
$\Delta N(1)$	−0.031	−0.082	−0.036
$\Delta H(1)$	−0.261	−0.392	−0.293
$\Delta H(2)$	−0.249	+0.172	+0.269
$\Delta H(3)$	+0.154	+0.231	+0.206
$\Delta H(4)$	+0.084	−0.490	+0.170
Sum of hydrogen displacement	−0.272	−0.479	+0.352
$\Delta N(2)$	+0.146	−0.072	+0.030
$\Delta H(5)$	+0.269	+0.078	−0.173
$\Delta H(6)$	+0.047	−0.010	+0.083
$\Delta H(7)$	+0.073	−0.145	+0.104
$\Delta H(8)$	+0.457	−0.124	−0.205
Sum of hydrogen displacement	+0.846	−0.201	−0.191

Table 4.1.4   Comparison of coordination numbers (CN) and M – O

distances where M is alkali ion or ammonium ion

Crystal	Space group	Cation	CN	Range of distance
NH_4LiSO_4 [a]	$P2_1Cn$	Li^+	4	1.89 – 1.98
		NH_4^+	4	2.85 – 3.14
		(NH_4^+)	(8)	(2.85 – 3.33)
KH_2PO_4 [b]	$I\bar{4}2d$	K^+	8	2.83 – 2.89
$NaNH_4SO_4 \cdot 2H_2O$ [c]	$P2_12_12_1$	Na^+	6	2.34 – 2.47
		NH_4^+	5	2.82 – 3.01
		(NH_4^+)	(7)	(2.82 – 3.32)
$(NH_4)_2SO_4$ [d]	$Pnam$	NH_4^+	7	2.90 – 3.11
		NH_4^+	8	2.84 – 3.17
	$Pna2_1$	NH_4^+	6	2.86 – 3.17
		NH_4^+	6	2.83 – 3.11
NH_4HSO_4 [e]	$B2_1/a$	NH_4^+(I)	10	2.92 – 3.22
		NH_4^+(II)	9	2.97 – 3.25
$RbHSO_4$ [f]	$P2_1/c$	Rb^+(I)	9	2.97 – 3.56
		Rb^+(II)	10	2.91 – 3.15
K_2SeO_4 [g]	$Pnam$	K^+(I)	11	2.64 – 3.76
		K^+(II)	9	2.73 – 3.32
$KHSO_4$ [h]	$Pbca$	K^+(I)	9	2.68 – 3.06
		K^+(II)	9	2.58 – 3.02
$NaHSO_4 \cdot H_2O$ [i]	Cc	Na^+	6	2.33 – 2.48
NH_4ClO_4 [j]	$Pnma$	NH_4^+	8	2.94 – 3.08
$NaNH_4CrO_4 \cdot 2H_2O$ [k]	$P2_12_12_1$	Na^+	6	2.35 – 2.46
		NH_4^+	5	2.81 – 3.03
$H_2SO_4 \cdot H_2O$ [l]	$P2_1/c$	H_3O^+	3	2.54 – 2.65

a) Reference 19   b) Reference 20   c) Reference 21   d) Reference 13

e) Reference 7   f) Reference 9   g) Reference 22   h) Reference 10

i) Reference 12   j) Reference 23   k) Reference 17   l) Reference 11

Table 4.2.1 Raman and i.r. frequencies (in cm^{-1}) of $(ND_4)_2SO_4$

Paraelectric Phase (T close to 300 K)		Modes and Species	Ferroelectric Phase (T close to 100 K)	
Raman	I.R.		Raman	I.R.
	35	?		
	45	?		45
69		Trans.$(F_2)SO_4^{--}$	68	72
			79	
	90	Libr.$(F_1)SO_4^{--}$	102	100
			130	128
			165	152
180	200	Trans.$(F_2)ND_4^{+}$	185	190
210			214	220
		Libr. $(F_1)ND_4^{+}$		260
456		$\nu_2(E)SO_4^{--}$	454	449
			466	463
616	614	$\nu_4(F_4)SO_4^{--}$	614	614
626			626	
690	695			695
977		$\nu_1(A_1)SO_4^{--}$	975	972
	1010	$\nu_4(F_2)ND_4^{+}$		1015
1030			1022	1032
1050		and	1057	1060
1065			1080	1079
	1110	$\nu_3(F_3)SO_4^{--}$	1109	1110
			1126	1125
			1165	
1198		$\nu_2(E)ND_4^{+}$	1202	1205
			1215	
			1225	
	1235		1237	1235
	1252			1252
	1400			1400
	1580			1590
		$\nu_1(A_1)ND_4^{+}$	2180	2195
2270			2270	2280
2390		$\nu_3(F_3)ND_4^{+}$	2390	2400
			2470	2480
				2840
3105				3100

Table 4.2.2   Raman and i.r. frequencies (in cm^{-1}) of $RbHSO_4$ and $RbDSO_4$ in the paraelectric phase (T close to 300 K)

RbHSO$_4$		Modes and Species	RbDSO$_4$	
Raman	I.R.		Raman	I.R.
	45	?	45	45
58		Trans.$(F_2)SO_4^{--}$	60	60
78			82	75
110	112	Libr.(F_1) SO_4^{--}	105	110
158	165		160	160
408		$\nu_2(E)$ SO_4^{--}	407	
448	446		438	440
		?	525	
	572	$\nu_4(F_2)$ SO_4^{--}	577	575
584	585		585	586
611	604		610	608
				795
	872	$\nu_1(A_1)SO_4^{--}$		871
879	885		874	
			901	
				945
1024	1021	$\nu_3(F_2)$ SO_4^{--}	1043	1021
1050	1055		1056	1060
	1220	$2\nu_4(F_2)$ SO_4^{--}	1211	1215
			1235	
			1245	
	1290			1300
	2440			2480
	2560			
	2900			3100

Table 4.2.3   Raman and i.r. frequencies (in cm^{-1}) of $RbHSO_4$ and $RbDSO_4$ in the ferroelectric phase (T close to 100 K)

RbHSO$_4$		Modes and Species	RbDSO$_4$	
Raman	I.R.		Raman	I.R.
45	40	?		
50		?	50	55
77	74		70	72
	100	Trans.$(F_1)SO_4^{--}$	80	
				98
119	120	Libr.$(F_1)SO_4^{--}$	120	118
175	178		178	175
		?	391	385
409			406	406
	438	$\nu_2(E)SO_4^{--}$	416	
452	451		443	443
		?		505
			535	535
575	574		578	567
585	585	$\nu_4(F_2)SO_4^{--}$	585	575
	603		600	586
612	610		614	608
	675	?		685
	786			
798	835	$2\nu_2(E)SO_4^{--}$	800	795
	870		872	879
880	887	$\nu_1(A_1)SO_4^{--}$	887	
892	894		899	
		?	925	
			950	950
1039	1025	$\nu_3(F_2)SO_4^{--}$	1037	1015
1067	1065		1084	1065
	1160			
	1175	$2\nu_4(F_2)SO_4^{--}$		1170
	1221		1208	1220
	1245		1240	
			1250	1250
	1290			1300
	1300			1325
	2360			2340
	2440			2415
	2550			2560
	2700			2960
	3020			3100

Table 4.2.4   Raman and i.r. frequencies (in cm^{-1}) of NH_4HSO_4 and ND_4DSO_4 in the paraelectric phase (T close to 300 K)

NH₄HSO₄		Modes and Species	ND₄DSO₄	
Raman	I.R.		Raman	I.R.
		?		45
		?		90
		Libr. $(F_1)SO_4^{--}$	115	
175			155	
	195	Trans. $(F_2)NH_4^{+},ND_4^{+}$		195
412		$\nu_2(E)\ SO_4^{--}$	407	
452	445		435	445
		$2\nu_6(F_1)\ ND_4^{+}$	520	520
	573		577	
588	587	$\nu_4(F_2)\ SO_4^{--}$		585
616	608		606	606
		?		795
	875	$\nu_1(A_1)\ SO_4^{--}$	876	871
886			900	
		$2\nu_4(F_2)SO_4^{--}$	930	
1019	1020			1022
1046	1051	$\nu_3(F_2)\ SO_4$	1040	1050
				1073
	1205	$\nu_4(F_2)\ ND_4^{+}$	1235	1210
	1290	$\nu_2(E)\ ND_4^{+}$		1290
	1425	$\nu_4(F_2)\ NH_4^{+}$		1400
	1670			
		$\nu_1(A_1)\ ND_4^{+}$	2290	
	2360	$\nu_3(F_2)\ ND_4^{+}$	2385	2375
	2450			2430
	2550			
3175		$\nu_1(A_1)\ NH_4^{+}$		

Table 4.2.5   Raman and i.r. frequencies (in cm^{-1}) of NH_4HSO_4 and ND_4DSO_4 in the ferroelectric phase (T close to 200 K)

| NH_4HSO_4 | | Modes and Species | ND_4DSO_4 | |
Raman	I.R.		Raman	I.R.
45		?		
55		?	55	
85				90
115		Libr.(F_1) SO_4^{--}	118	
			165	
190	195	Trans.$(F_2)NH_4^+,ND_4^+$		195
360		Libr.(F_1) NH_4^+		
410	422	$\nu_2(E)$ SO_4^{--}	402	
450	447		437	446
		$2\nu_6(F_1)$ ND_4^+	524	523
575	574		580	567
589	587	$\nu_4(F_2)SO_4^{--}$	600	585
612	608		610	606
	770	$2\nu_2(E)$ SO_4^{--}		795
			882	
890	886	$\nu_1(A_1)$ SO_4^{--}	892	875
		$2\nu_4(F_2)$ SO_4^{--}		943
1014	1015		1033	1019
1059	1055	$\nu_3(F_2)$ SO_4^{--}	1057	1054
				1073
1168	1165	$\nu_4(F_2)$ ND_4^+		
1210	1210		1215	1210
	1290	$\nu_2(E)$ ND_4^+		1290
	1425	$\nu_4(F_2)$ NH_4		1400
	2360			2180
		$\nu_1(A_1)$ ND_4^+	2281	2375
	2420	$\nu_3(F_2)$ ND_4^+	2400	2420
	2865			
	3040			3095
3115	3120	$\nu_1(A_1)$ NH_4^+		
	3260	$\nu_3(F_2)$ NH_4^+		3400

Table 4.2.6   Raman and i.r. frequencies (in cm^{-1}) of NH_4HSO_4 and ND_4DSO_4 in the paraelectric phase (T close to 100 K)

NH_4HSO_4		Modes and Species	ND_4DSO_4	
Raman	I.R.		Raman	I.R.
46	44	?	42	48
	56	?		
66	63		61	
	77	Trans.(F_2) SO_4^{--}	70	75
95			90	95
105	102	Libr.(F_1) SO_4^{--}	100	106
121	116		120	114
182	194	Trans.$(F_2)NH_4^+,ND_4^+$		196
200	220			227
295	308	Libr.$(F_1)NH_4^+,ND_4^+$		270
380	360			
412			403	
425		$\nu_2(E)$ SO_4^{--}	409	
456	453		438	450
		$2\nu_6(F_1)$ ND_4^+	520	525
				567
581	573		577	575
588	580	$\nu_4(F_2)SO_4^{--}$		587
623	610		606	608
775	772	?	771	
			795	
	836	$2\nu_2(E)$ SO_4^{--}		834
893	884	$\nu_1(A_1)$ SO_4^{--}	879	879
910	900		898	898
				935
1019	1007	$\nu_3(F_2)$ SO_4^{--} and		1012
	1028	$\nu_4(F_2)$ ND_4^+	1034	1035
1046	1054		1049	1050
			1079	1074
			1091	1086

| NH$_4$HSO$_4$ | | Modes and Species | ND$_4$DSO$_4$ | |
Raman	I.R.		Raman	I.R.
	1140			1100
1165	1166			1175
1202	1210		1215	1202
1283	1275	ν_2(E) ND$_4^+$		1280
	1290			1400
	1420	ν_4(F$_2$) NH$_4$		
1437	1434			
1685	1700			
	2200		2100	2195
	2310	ν_1(A$_1$) ND$_4^+$	2264	2375
	2440	ν_3(F$_2$) ND$_4^+$	2385	2414
	2560			
	2880			
	3040			3080
	3108	ν_1(A$_1$) NH$_4^+$		
	3200	ν_3(F$_2$) NH$_4^+$		3360
	3770			

Table 4.2.7 Normal modes and associated frequencies in cm^{-1} and activities of NH_4^+, ND_4^+, and SO_4^{--} ions.

(R) = Raman active   (IR) = Infrared active

Normal modes of vibrations		Frequencies in cm^{-1}			Activity
		NH_4^+	ND_4^+	SO_4^{--}	
$\nu_1(A_1)$	Totally symmetric stretching vibration	3042	2214	981	(R)
$\nu_2(E)$	Doubly degenerate bending vibration	1711	1215	451	(R)
$\nu_3(F_2)$	Triply degenerate stretching vibration	3135	2350	1104	(IR)
$\nu_4(F_2)$	Triply degenerate bending vibration	1403	1066	613	(IR)

Table 4.3.2

Estimated normal heat capacities of NH_4HSO_4

at rounded temperatures   (Base line I)

$\dfrac{T}{K}$	$\dfrac{C_p}{J\ K^{-1}mol^{-1}}$	$\dfrac{T}{K}$	$\dfrac{C_p}{J\ K^{-1}mol^{-1}}$
115	74.52	200	115.92
120	77.56	205	117.72
125	80.40	210	119.52
130	83.20	215	121.20
135	86.00	220	122.84
140	88.68	225	124.48
145	91.32	230	126.04
150	93.92	235	127.56
155	96.44	240	129.08
160	98.88	245	130.52
165	101.24	250	131.92
170	103.56	255	133.24
175	105.76	260	134.60
180	107.92	265	135.84
185	110.00	270	137.08
190	112.00	275	138.32
195	114.00	280	139.52

Table 4.3.2

Estimated normal heat capccities of NH_4HSO_4
at rounded temperatures   (Base line Ⅱ)

T	C_p	T	C_p
K	$J\ K^{-1}mol^{-1}$	K	$J\ K^{-1}mol^{-1}$
160	106.04	225	125.40
165	107.64	230	126.80
170	109.20	235	128.16
175	110.76	240	129.52
180	112.28	245	130.84
185	113.80	250	132.12
190	115.32	255	133.40
195	116.80	260	134.64
200	118.28	265	135.88
205	119.72	270	137.12
210	121.20	275	138.32
215	122.60	280	139.56
220	124.00		

Table 4.3.3

Estimated normal heat capacities of ND_4DSO_4
at rounded temperatures (Base line I)

T	c_p	T	c_p
K	$J\ K^{-1}mol^{-1}$	K	$J\ K^{-1}mol^{-1}$
110	77.69	205	121.93
115	80.71	210	123.76
120	83.63	215	125.53
125	86.44	220	127.27
130	89.14	225	128.98
135	91.75	230	130.65
140	94.30	235	132.29
145	96.78	240	133.89
150	99.17	245	135.45
155	101.50	250	136.97
160	103.77	255	138.45
165	105.98	260	139.90
170	108.14	265	141.33
175	110.24	270	142.74
180	112.30	275	144.14
185	114.32	280	145.53
190	116.30	285	146.91
195	118.23	290	148.28
200	120.12	295	149.66

Table 4.3.3

Estimated normal heat capacities of ND_4DSO_4

at rounded temperatures   (Base line II)

T	c_p	T	c_p
K	$J\ K^{-k}mol^{-1}$	K	$J\ K^{-1}mol^{-1}$
150	110.87	230	132.03
155	112.08	235	133.38
160	113.33	240	134.74
165	114.61	245	136.10
170	115.91	250	137.46
175	117.23	255	138.83
180	118.56	260	140.20
185	119.90	265	141.57
190	121.24	270	142.93
195	122.59	275	144.29
200	123.93	280	145.64
205	125.28	285	146.97
210	126.63	290	148.27
215	127.97	295	149.54
220	129.32	300	150.77
225	130.67	305	151.95

Table 4.3.4

Estimated normal heat capacities of $RbHSO_4$
at rounded temperatures

T	C_p	T	C_p
K	$JK^{-1}mol^{-1}$	K	$JK^{-1}mol^{-1}$
150	80.39	220	98.83
155	81.82	225	100.03
160	83.22	230	101.21
165	84.61	235	102.37
170	85.97	240	103.51
175	87.32	245	104.62
180	88.66	250	105.70
185	89.99	255	106.76
190	91.30	260	107.81
195	92.60	265	108.86
200	93.89	270	109.91
205	95.15	275	110.94
210	96.38	280	111.95
215	97.61	285	112.95
		290	113.95

Table 4.3.5

Estimated normal heat capacities of $RbDSO_4$ at rounded temperatures

T	C_p	T	C_p
K	$JK^{-1}mol^{-1}$	K	$JK^{-1}mol^{-1}$
140	79.08	220	101.17
145	80.56	225	102.45
150	82.03	230	103.71
155	83.50	235	104.99
160	84.95	240	106.26
165	86.39	245	107.53
170	87.81	250	108.79
175	89.31	255	110.04
180	90.69	260	111.28
185	92.06	265	112.54
190	93.41	270	113.77
195	94.74	275	114.96
200	96.03	280	116.18
205	97.33	285	117.38
210	99.62	290	118.56
215	99.90		

Table 4.3.6

Estimated normal heat capacities of $(ND_4)_2SO_4$ at rounded temperatures

T	C_p	T	C_p	T	C_p	T	C_p
K	$JK^{-1}mol^{-1}$	K	$JK^{-1}mol^{-1}$	K	$JK^{-1}mol^{-1}$	K	$JK^{-1}mol^{-1}$
95	85.9	150	130.4	205	161.4	260	184.0
100	90.7	155	133.7	210	163.7	265	185.8
105	95.4	160	136.9	215	165.9	270	187.5
110	99.9	165	140.0	220	168.1	275	189.2
115	104.3	170	143.0	225	170.2	280	190.9
120	108.5	175	145.9	230	172.3	285	192.5
125	112.4	180	148.7	235	174.3	290	194.0
130	116.2	185	151.4	240	176.3	295	195.5
135	119.9	190	154.0	245	178.3	300	197.0
140	123.5	195	156.5	250	180.2	305	198.3
145	127.0	200	159.0	255	182.1	310	199.7

Table 4.3.7

Estimated normal heat capacities of $(NH_4)_2SO_4$ at rounded temperatures

T	C_p	T	C_p	T	C_p	T	C_p
K	$JK^{-1}mol^{-1}$	K	$JK^{-1}mol^{-1}$	K	$JK^{-1}mol^{-1}$	K	$JK^{-1}mol^{-1}$
100	80.07	150	117.9	200	148.0	250	171.1
105	84.31	155	121.2	205	150.6	255	173.0
110	88.46	160	124.5	210	153.2	260	174.9
115	92.46	165	127.6	215	155.6	265	176.7
120	96.28	170	130.7	220	158.0	270	178.4
125	100.0	175	133.8	225	160.4	275	180.3
130	103.8	180	136.8	230	162.6	280	182.0
135	107.4	185	139.7	235	164.9	285	183.7
140	111.0	190	142.5	240	167.0	290	185.2
145	114.5	195	145.3	245	169.1	295	186.8

Table 4.3.8

Estimated normal heat capacities of NH_4Br
at rounded temperatures

T	Cp	T	Cp
K	cal $K^{-1}mol^{-1}$	K	cal $K^{-1}mol^{-1}$
80	8.71	200	17.48
85	9.19	205	17.73
90	9.66	210	17.97
95	10.12	215	18.20
100	10.57	220	18.42
105	11.01	225	18.64
110	11.44	230	18.85
115	11.86	235	19.05
120	12.26	240	19.25
125	12.64	245	19.44
130	13.02	250	19.62
135	13.39	255	19.80
140	13.78	260	19.98
145	14.14	265	20.16
150	14.49	270	20.33
155	14.83	275	20.49
160	15.16	280	20.65
165	15.48	285	20.81
170	15.79	290	20.96
175	16.09	295	21.11
180	16.39	300	21.25
185	16.68	305	21.39
190	16.95	310	21.53
195	17.22	315	21.67

Table 4.3.9

Estimated normal heat capacities of ND_4Br

at rounded temperatures

$\dfrac{T}{K}$	$\dfrac{Cp}{\text{cal } K^{-1} mol^{-1}}$	$\dfrac{T}{K}$	$\dfrac{Cp}{\text{cal } K^{-1} mol^{-1}}$
100	11.98	200	18.60
105	12.42	205	18.84
110	12.84	210	19.08
115	13.24	215	19.33
120	13.65	220	19.57
125	14.04	225	19.80
130	14.42	230	20.02
135	14.78	235	20.23
140	15.13	240	20.44
145	15.47	245	20.66
150	15.80	250	20.88
155	16.12	255	21.09
160	16.43	260	21.30
165	16.73	265	21.50
170	17.02	270	21.70
175	17.30	275	21.91
180	17.57	280	22.12
185	17.83	285	22.32
190	18.09	290	22.52
195	18.35	295	22.72
		300	22.91

Table 4.3.10

Estimated normal heat capacities of VCl_3

at rounded temperatures

T	Cp	T	Cp
K	cal $K^{-1}mol^{-1}$	K	cal $K^{-1}mol^{-1}$
45	5.324	105	13.90
50	6.230	110	14.40
55	7.100	115	14.88
60	7.937	120	15.34
65	8.737	125	15.77
70	9.502	130	16.18
75	10.229	135.	16.57
80	10.92	140	16.93
85	11.58	145	17.27
90	12.21	150	17.59
95	12.81	155	17.90
100	13.37	160	18.18

Table 4.3.11　Enthalpy and entropy of the lower ferroelectric transition of ND_4DSO_4.

T_{tr} = 163.9 K	Series V	Series VI	Series VII
T_i	158.240	159.116	160.716
T_f	165.713	165.629	165.472
$\Delta H(T_f - T_i)$	2177.7	2078.7	1869.0
$\Delta H(T_i - 160)$	-192.7	-97.1	79.2
$\Delta H(170 - T_f)$	495.0	504.7	522.9

$\Delta H(170 - 160)$	2480.0	2486.3	2471.1

average　$\Delta H(170 - 160) = 2479.1 \pm 7.2$ J mol^{-1}

$\Delta H(T_f - T_i) = \Delta H(162.5 - T_i) + \Delta H(165.5 - 162.5) + \Delta H(T_f - 165.5)$

$\Delta H(162.5 - T_i)$	472.2	376.6	200.4
$\Delta H(T_f - 165.5)$	24.7	14.9	-3.3

$\Delta H(165.5 - 162.5)$	1680.8	1687.2	1671.9

$\Delta S(165.5 - 162.5) = \Delta H(165.5 - 162.5) / T_{tr}$

$\Delta S(165.5 - 162.5)$	10.25	10.29	10.20

average　$\Delta S(165.5 - 162.5) = 10.25 \pm 0.05$

$\Delta S(162.5 - 160) = 1.73$

$\Delta S(170 - 165.5) = 3.10$

$\Delta S(170 - 160) = 15.08 \pm 0.05$ J K^{-1}mol^{-1}

ΔH(Sample) $- \Delta H$(Base line I) $= 1521.1$　　(T = 100 $\sim$ 170 K)

ΔS(Sample) $- \Delta S$(Base line I) $= 9.35$

ΔH(Base line II) $- \Delta H$(Base line I) $= 50.5$　(T = $T_{tr} \sim$ 170 K)

ΔS(Base line II) $- \Delta S$(Base line I) $= 0.30$

$$\Delta H_{tr} = 1470.6 \pm 7.2 \quad \text{J mol}^{-1}$$

$$\Delta S_{tr} = 9.05 \pm 0.05 \quad \text{JK}^{-1}\text{mol}^{-1}$$

Table 4.3.13   Comparison of the deuteration effect on the ferroelectric transition temperature

Crystal	Transition Temperature		Ratio	Reference
	$T_{tr}(H)/K$	$T_{tr}(D)/K$	$T_{tr}(H)/T_{tr}(D)$	
$NaKC_4H_4O_6 4H_2O$ (lower)	255	251	0.984	(70)
(upper)	297	308	1.04	(70)
$Cu(HCOO)_2 4H_2O$	235.5	245.7	1.04	(71,72)
$(NH_2CH_2COOH)_2 H_2SO_4$	322.6	333.2	1.03	(73,74)
$K_4Fe(CN)_6 3H_2O$	247.8	252.5	1.019	(75)
KH_2PO_4	123	213	1.73	(76)
RbH_2PO_4	147	218	1.48	(76)
KH_2AsO_4	97	161	1.66	(76)
RbH_2AsO_4	110	173	1.57	(76)
CsH_2AsO_4	143	212	1.48	(76)
$NH_4H_2PO_4$	148	242	1.63	(77)
$(NH_4)_2SO_4$	223.4	223.9	1.002	(78)
$(NH_4)_2BeF_4$	176	179	1.02	(14)
NH_4HSO_4 (III-II)	159.2	163.9	1.295	This
(II-I)	269.9	261.7	0.9696	This
$RbHSO_4$	263.8	249.8	0.9469	This
NH_4Br (IV-III)	107.5	166.7	1.551	(79,80)
(III-II)	235.0	215.1	0.9151	(79,80)
HCl (III-I)	98.67	104.63	1.0604	(81)
(T_m)	159.05	158.41	0.9960	(81)
HBr (III-II)	89.53	93.67	1.046	(81)
(T_m)	186.50	185.64	0.9954	(81)
HI (III-II)	70.23	77.47	1.103	(81)
(II-I)	125.60	128.24	1.0210	(81)
(T_m)	223.50	221.51	0.9955	(81)

Table 4.3.14   Comparison of enthalpy (h) and entropy (s) of defect formation in some crystals   n/N is the defect density at the transition temperature and T_r is the temperature range corresponding to the linear part in the defect plot.

Crystals (Phase)		h $\overline{kJmol^{-1}}$	s $\overline{JK^{-1}mol^{-1}}$	$\dfrac{n}{N} \times 100$	T_r $\overline{K}$
NH_4HSO_4	(II)	10.5	12.1	4.1	180 ∿ 250
	(III)	11.7	32.8	0.8	125 ∿ 150
ND_4DSO_4	(II)	12.3	19.6	3.7	180 ∿ 255
	(III)	12.4	38.1	1.1	125 ∿ 160
$RbHSO_4$	(II)	19.6	35.8	0.9	180 ∿ 260
$RbDSO_4$	(II)	18.2	34.7	1.0	175 ∿ 245
NH_4Cl	(III)	23.7	65.4	0.5	180 ∿ 215
$(NH_4)_{1-x}Rb_xCl$					
x = 0.0158	(III)	25.5	73.6	0.6	190 ∿ 220
x = 0.0251	(III)	25.3	73.9	0.7	170 ∿ 220
NH_4Br	(III)	17.4	38.9	0.7	150 ∿ 215
ND_4Br	(III)	14.6	38.4	1.2	170 ∿ 195
VCl_3	(II)	7.3	40.7	3.1	70 ∿ 105
$C_{10}H_{12}$	(II)	42.1	157	0.5	180 ∿ 205

Table 4.3.15 The Curie-Weiss constant C and the ferroelectric transition temperature T_c

Crystal	$\dfrac{C}{K}$	$\dfrac{T_c}{K}$	C/T_c
$BaTiO_3$[a]	170000	381	446
$PbTiO_3$[a]	110000	763	144
$(NH_2CH_2COOH)_3H_2SO_4$[a]	3290	320	10.3
$NaNO_2$[a]	5130	437	11.7
KH_2PO_4[b]	3200	123	26.0
KD_2PO_4[b]	4700	220	21.4
RbH_2PO_4[b]	3500	147	23.8
RbD_2PO_4[b]	4200	250	16.8
KH_2AsO_4[b]	2500	96	26.0
KD_2AsO_4[b]	4940	163	30.3
$NaKC_4H_6O_6 \cdot 4H_2O$ (Upper)[a]	1700	297	5.72
NH_4HSO_4[a]	226	270	0.837
ND_4DSO_4[c]	250	262	0.954
$RbHSO_4$[a]	116	264	0.439
$(NH_4)_2SO_4$[a]	9.4	224	0.042

a) E. Nakamura, et.al., J. Phys. Soc. Japan, 18, 1477 (1963).

b) V. G. Vaks, et.al., Phys. Stat. Sol. (a) 30, 801 (1975).

c) M. Kasahara and I. Tatsuzaki, J. Phys. Soc. Japan, 29, 1392 (1970)
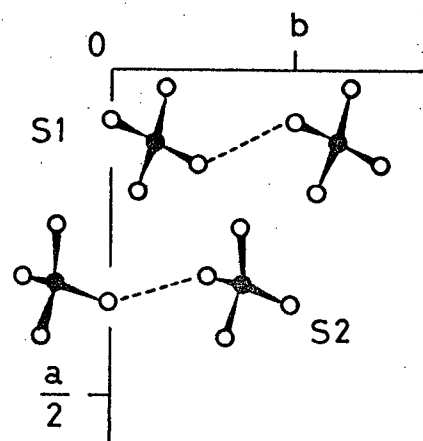
$S1 : (x, y, z)$
$S1' : (\bar{x}, \bar{y}, \bar{z})$

$S2 : (x, y, z)$
$S2' : (x+\frac{1}{2}, y, \frac{1}{2}-z)$

RbHSO$_4$

KHSO$_4$

212
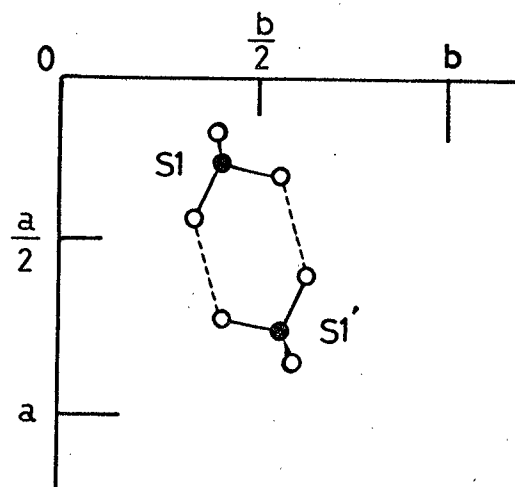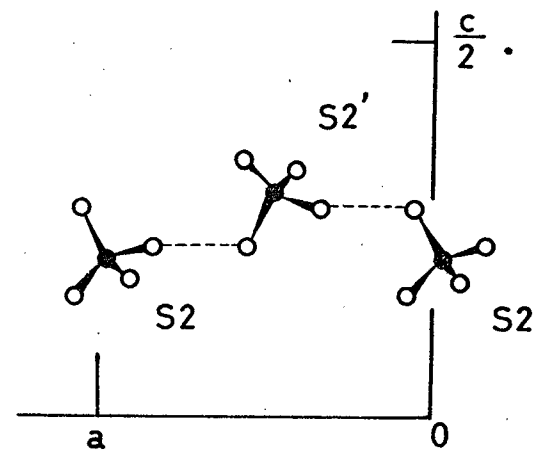
Fig. 4.1.1   Comparison of hydrogen bonds in RbHSO$_4$ and KHSO$_4$.

Modes (T>Tc)	Site Symmetry Cs	Free Ion Symmetry Td	Factor Symmetry D$_{2h}$

	Site Symmetry	Free Ion Symmetry	Factor Symmetry
Γtranslational	$2A'+A''$	F_2	$B_{1u}+B_{2u}+B_{3u}$
Γlibrational	$A'+2A''$	F_1	$B_{1g}+B_{2g}+B_{3g}$
Γvibrational	$6A'+3A''$	A_1+E+2F_2	$9A_g+8B_{1g}+5B_{2g}+$ $5B_{3g}+6A_u+5B_{1u}+$ $8B_{2u}+8B_{3u}$

Modes (T<Tc)	Site Symmetry C$_1$	Free Ion Symmetry Td	Factor Symmetry C$_{2v}$

	Site Symmetry	Free Ion Symmetry	Factor Symmetry
Γtranslational	$3A$	F_2	$A_1+B_1+B_2$
Γlibrational	$3A$	F_1	$A_2+B_1+B_2$
Γvibrational	$9A$	A_1+E+2F_2	$44A_1+44A_2+$ $43B_1+43B_2$

Fig. 4.2.1 Correlation diagram for $(NH_4)_2SO_4$ in the paraelectric and ferroelectric phases. L = Librational mode, T = Translational mode, (R) = Raman active, (IR) = Infrared active, (-) = Inactive.

213

Modes in Phase I	Site Symmetry C_1	Free Ion Symmetry T_d	Factor Symmetry C_{2h}

Diagram Phase I:

A (RIR) — correlates to:
- $\nu_1 (A_1)$ (R)
- $\nu_2 (E)$ (R)
- $L(F_1)$ (–)
- T, ν_3, ν_4 (F_2) (RIR)

→ A_g (R), B_g (R), A_u (IR), B_u (IR)

Γtranslational	3A	F_2	$A_u + 2B_u$
Γlibrational	3A	F_1	$A_g + 2B_g$
Γvibrational	9A	$A_1 + E + 2F_2$	$43A_g + 42B_g +$ $43A_u + 42A_u$

Modes in Phase II	Site Symmetry C_1	Free Ion Symmetry T_d	Factor Symmetry C_s

Diagram Phase II:

A (RIR) — correlates to:
- $\nu_1 (A_1)$ (R)
- $\nu_2 (E)$ (R)
- $L(F_1)$ (–)
- T, ν_3, ν_4 (F_2) (RIR)

→ A' (RIR), A'' (RIR)

Γtranslational	3A	F_2	$2A' + A''$
Γlibrational	3A	F_1	$A' + 2A''$
Γvibrational	9A	$A_1 + E + 2F_2$	$85A' + 85A''$

Modes in Phase III	Site Symmetry C_1	Free Ion Symmetry T_d	Factor Symmetry C_1

Diagram Phase III:

A (RIR) — correlates to:
- $\nu_1 (A_1)$ (R)
- $\nu_2 (E)$ (R)
- $L(F_1)$ (–)
- T, ν_3, ν_4 (F_2) (RIR)

→ A (RIR)

Γtranslational	3A	F_2	3A
Γlibrational	3A	F_1	3A
Γvibrational	9A	$A_1 + E + 2F_2$	170A

Fig. 4.2.2 Correlation diagram for NH_4HSO_4 in the paraelectric and ferroelectric phase. L = Librational mode T = Translational mode, (R) = Raman active, (IR) = Infrared active, (–) = Inactive.
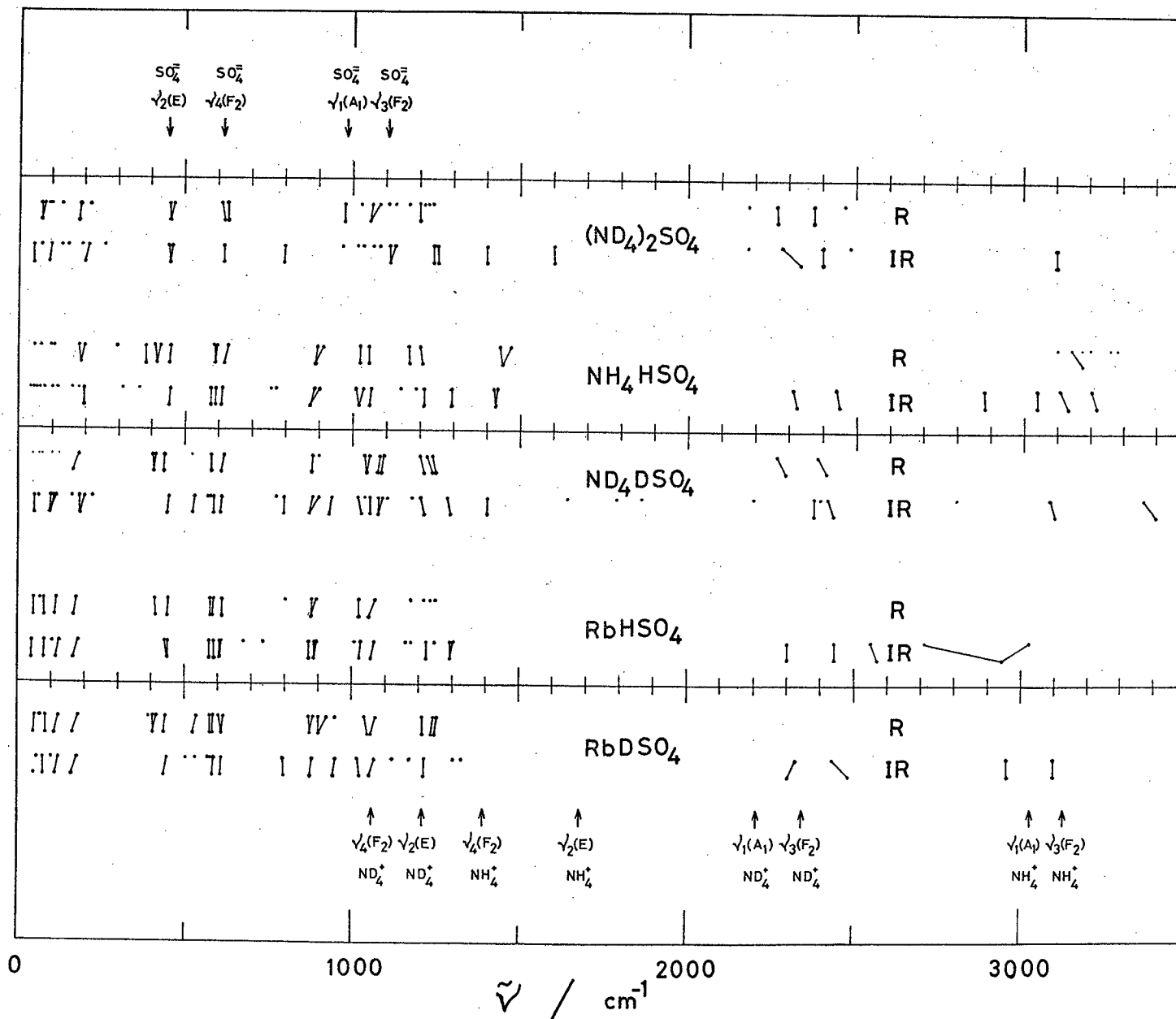
Fig. 4.2.3   Comparison of spectroscopic data (upper dots: 100K; lower dots: 300 K).
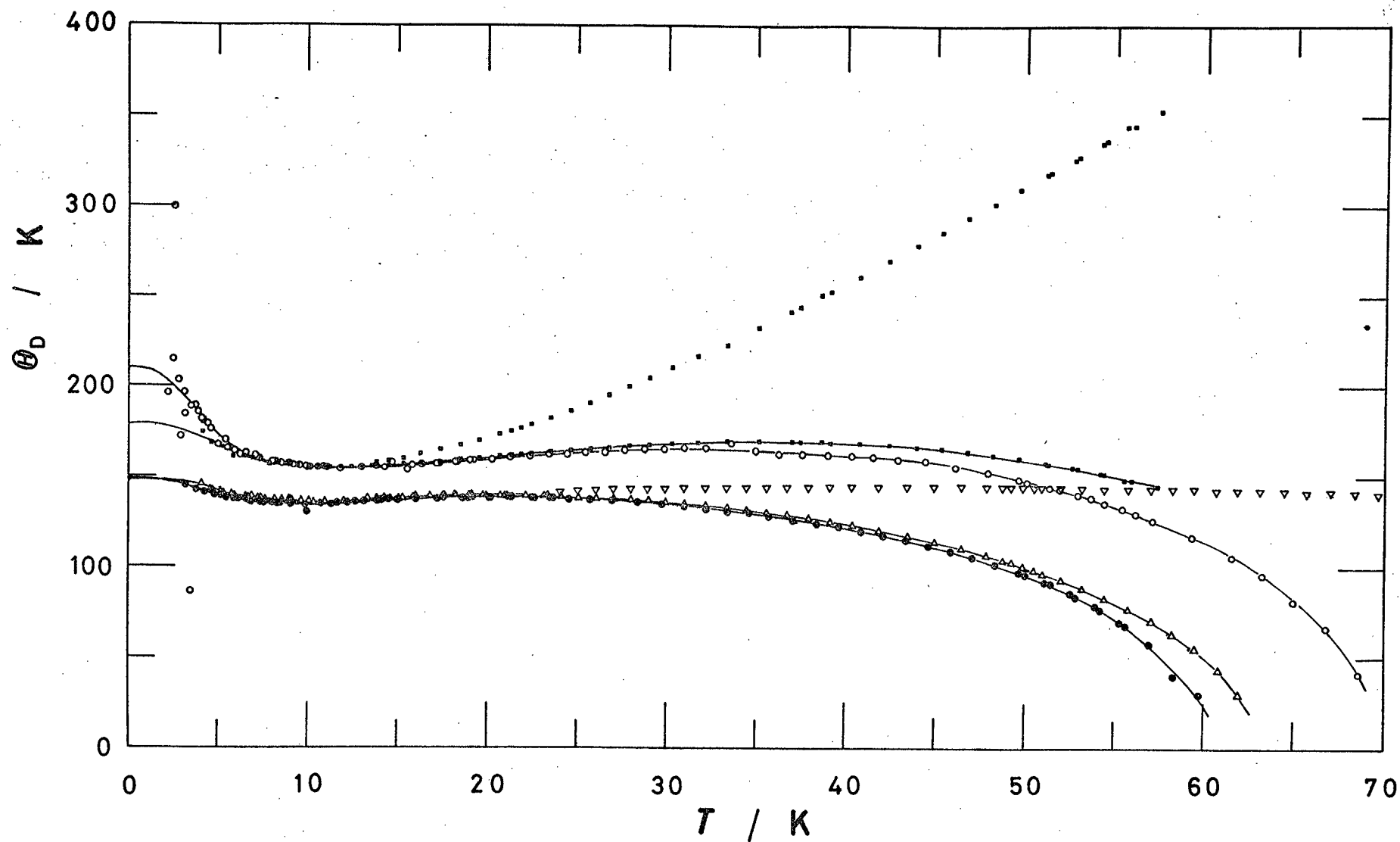
Fig. 4.3.1   Comparison of $\Theta_D(T)$ curves, assuming 6N degrees of freedom (-□- ; NH_4HSO_4, -○- ; ND_4DSO_4, -△- ; $RbHSO_4$, ● ; $RbDSO_4$, -□- ; NH_4HSO_4 (corrected for librational modes), -▽- ; $RbHSO_4$ (corrected for librational modes).
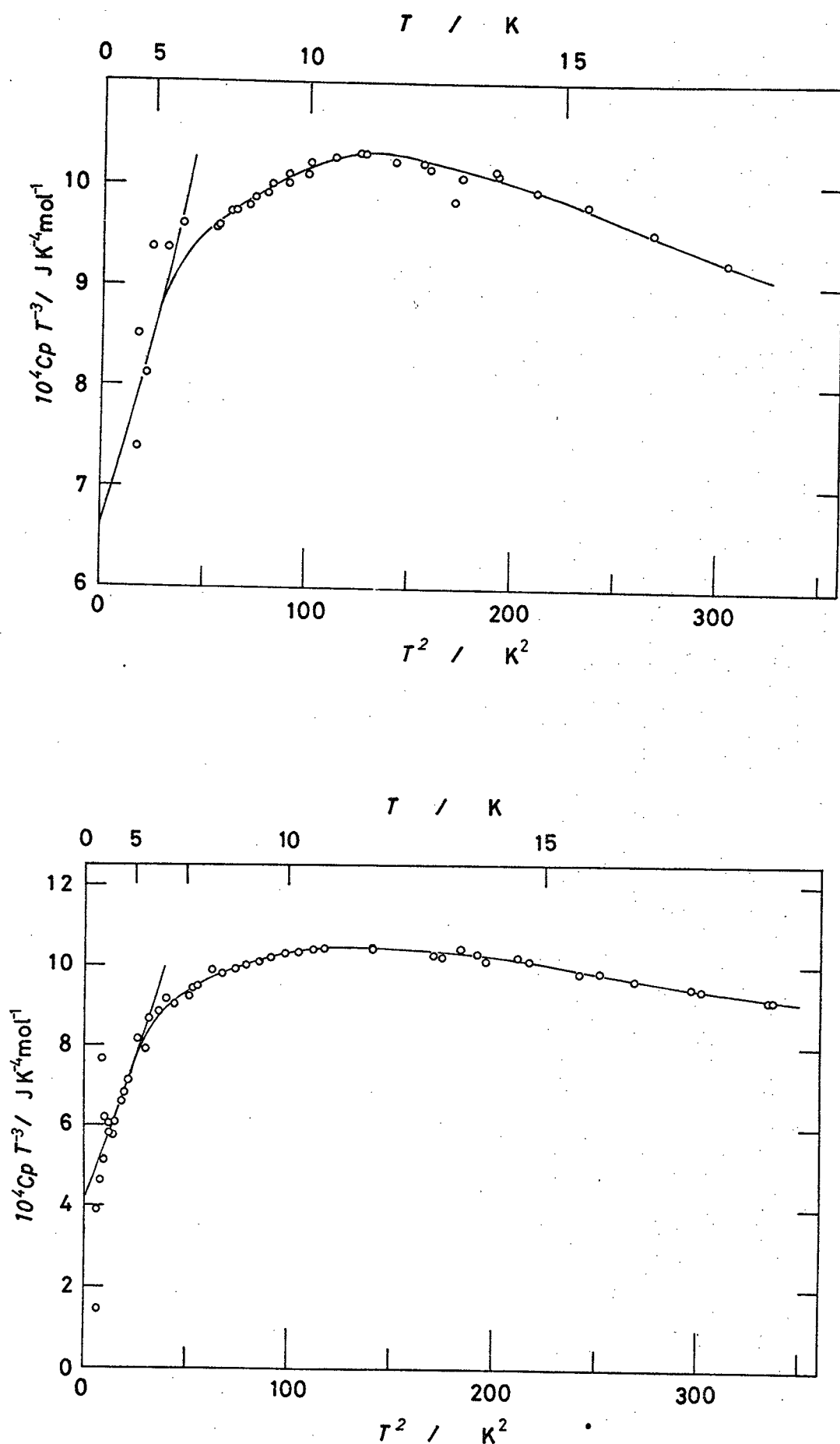
Fig. 4.3.2 Evaluation of the Debye characteristic temperature at 0 K of NH_4HSO_4 (above) and ND_4DSO_4 (below).

217
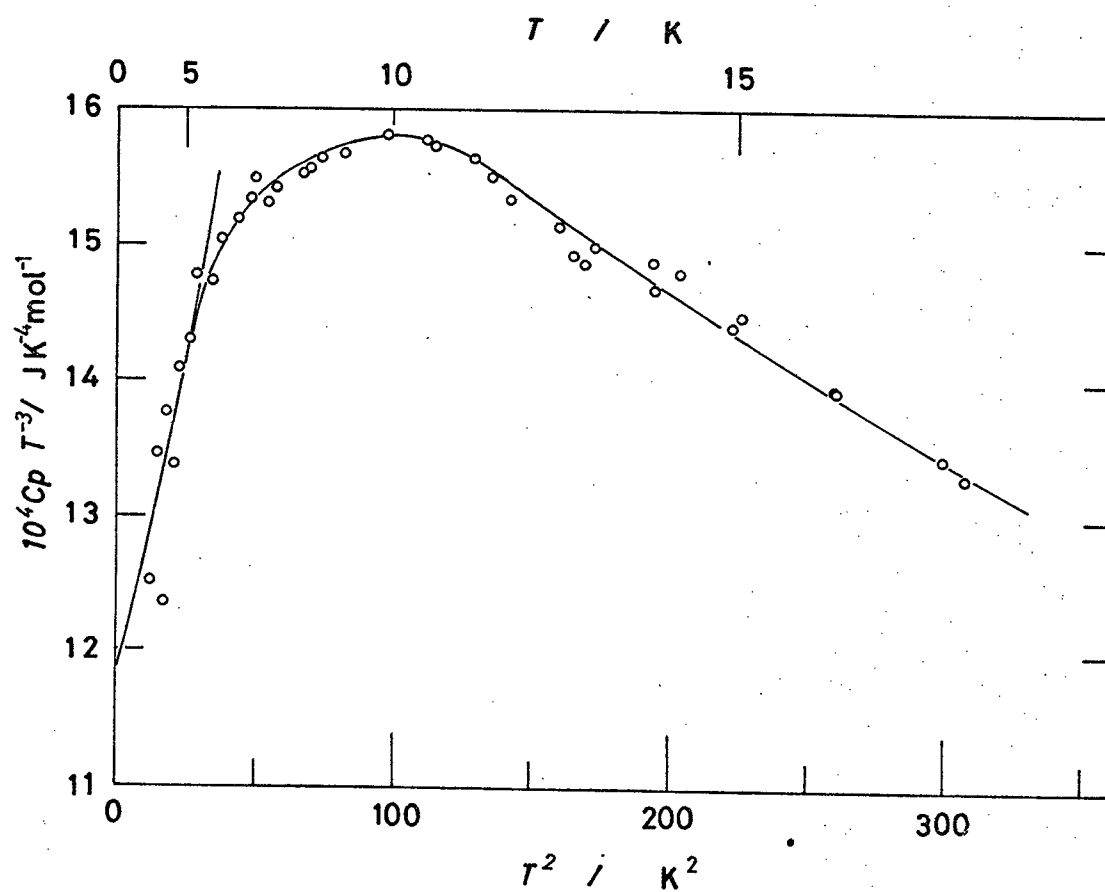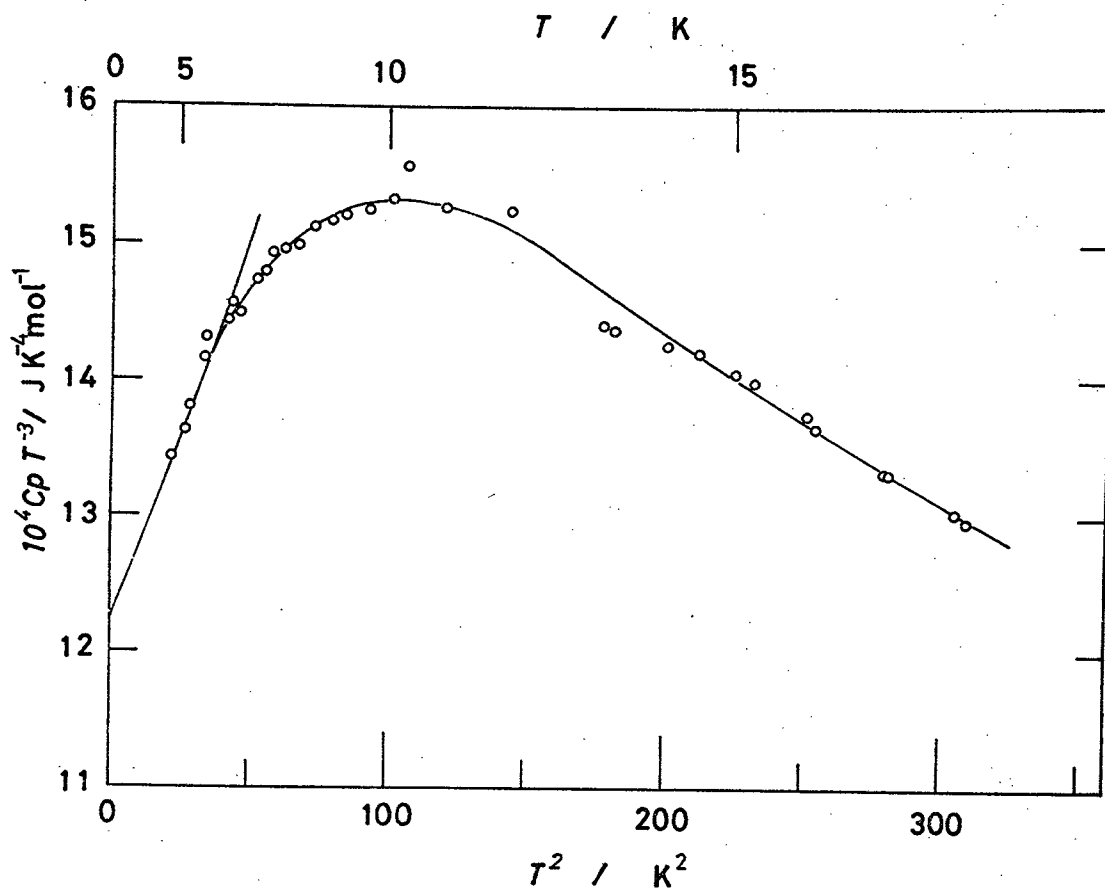
Fig. 4.3.3   Evaluation of the Debye characteristic tem-
perature at 0 K of RbHSO$_4$ (above) and RbDSO$_4$ (below).
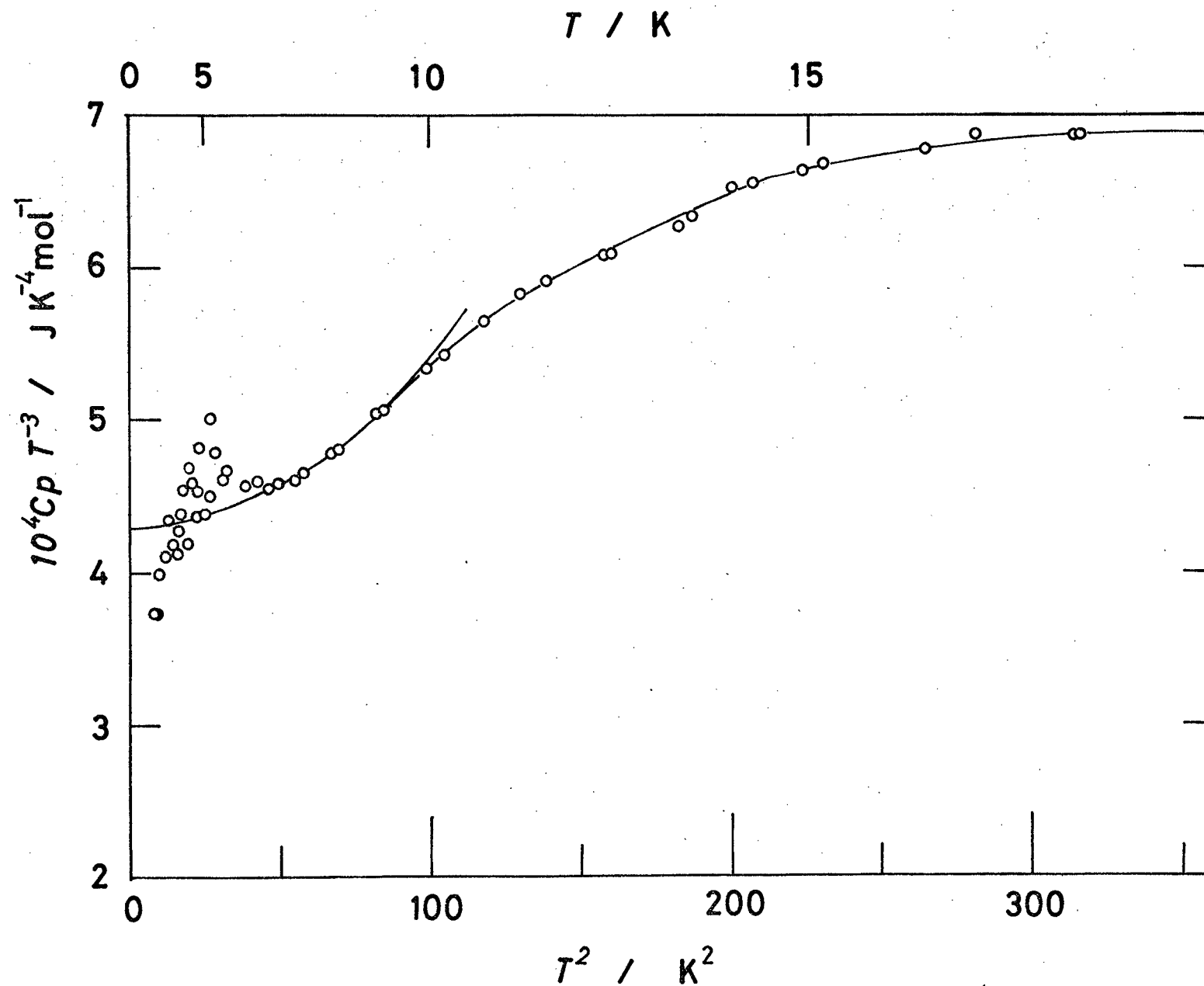
Fig. 4.3.4 Evaluation of the Debye characteristic temperature at 0 K of $(ND_4)_2SO$.
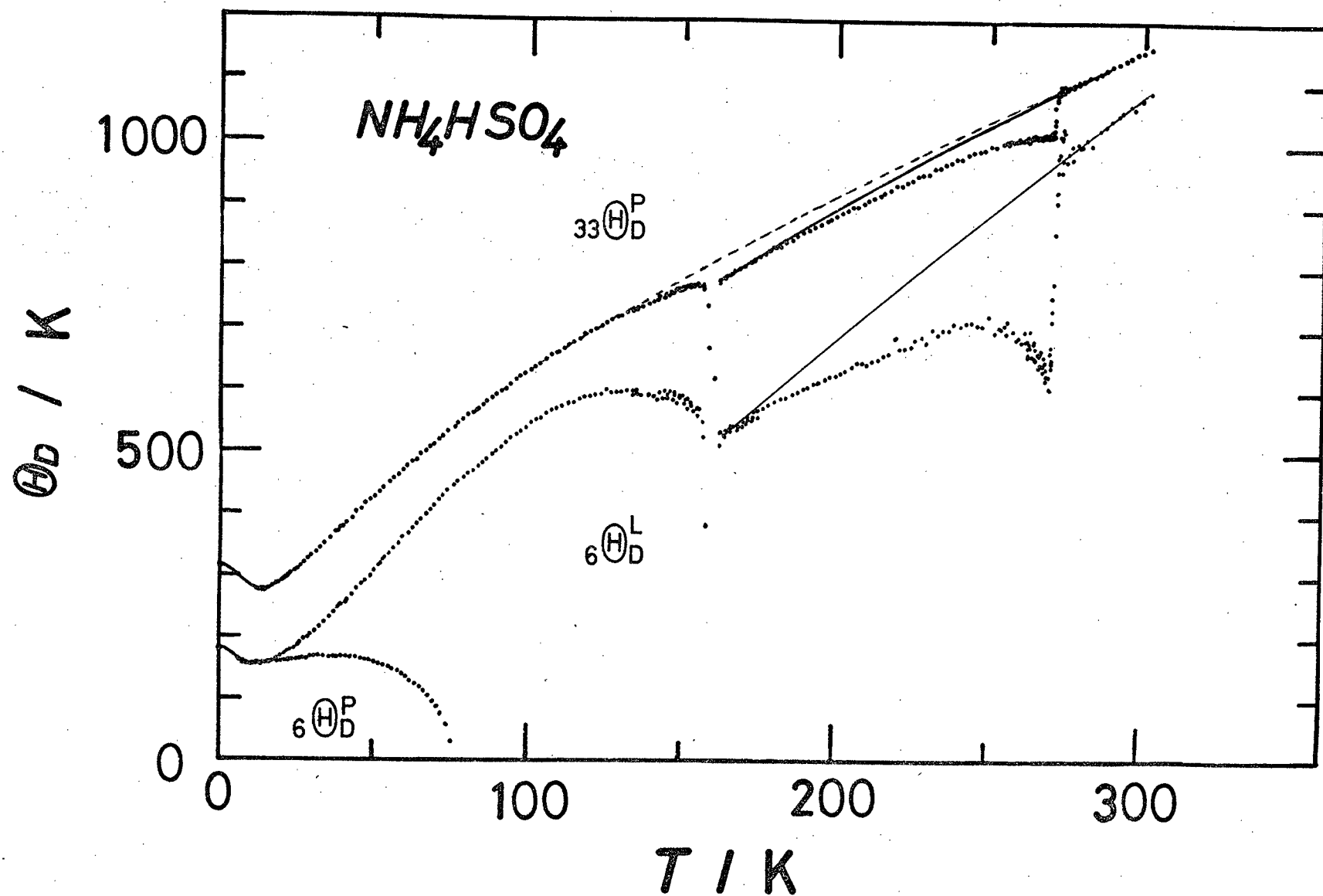
Fig. 4.3.5 Temperature dependence of the Debye characteristic temperature of NH_4HSO_4, calculated without the correction ($C_p - C_v$).
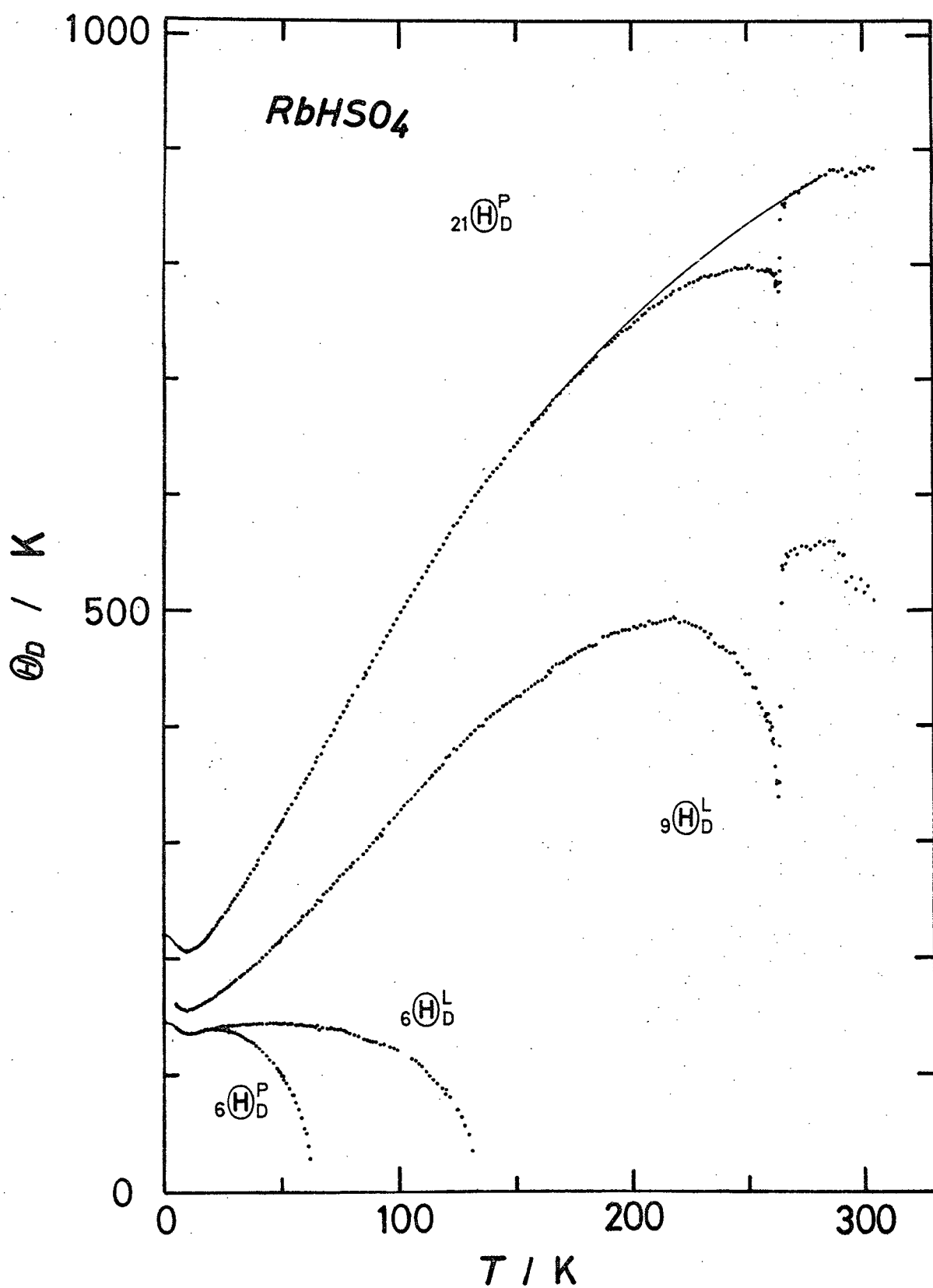
Fig. 4.3.6 Temperature dependence of the Debye characteristic temperature of $RbHSO_4$, calculated without the correction $(C_p - C_v)$.
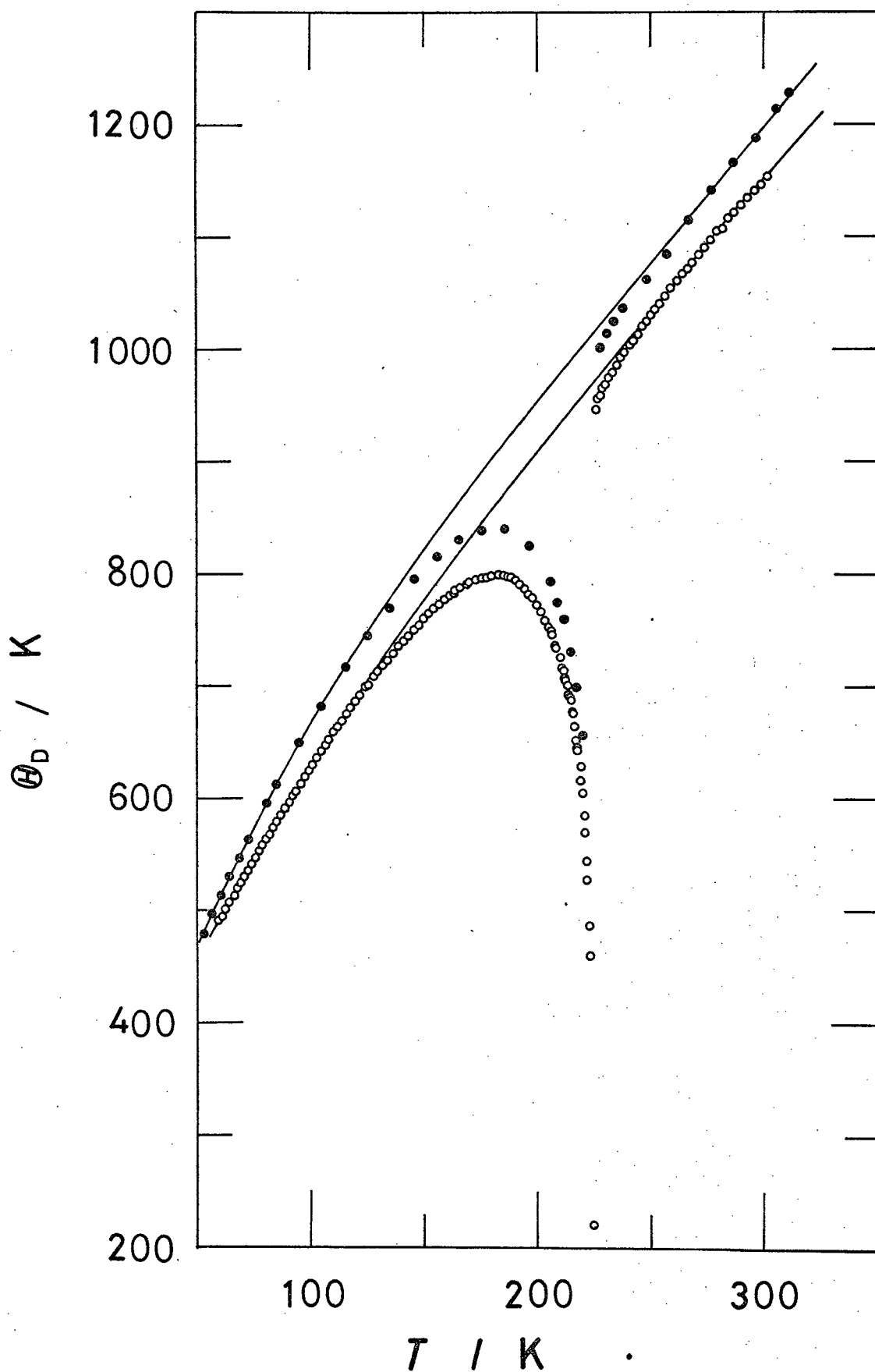
Fig. 4.3.7 Temperature dependence of the Debye characteristic temperature of $(NH_4)_2SO_4$ (●) and $(ND_4)_2SO_4$ (○) assuming 45N degrees of freedom.
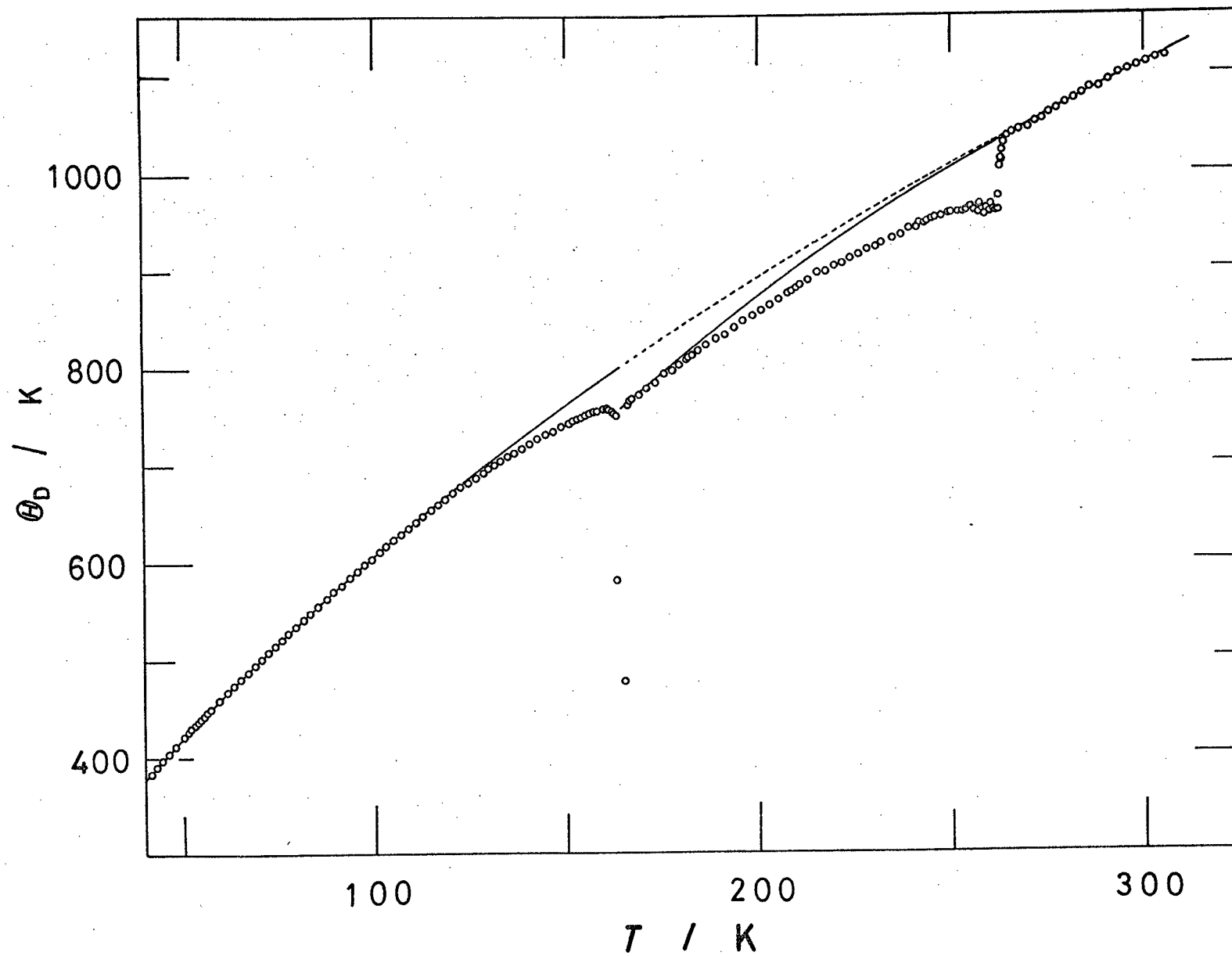
Fig. 4.3.8   Temperature dependence of the Debye characteristic temperature of ND_4DSO_4, assuming 33 N degrees of freedom.

223
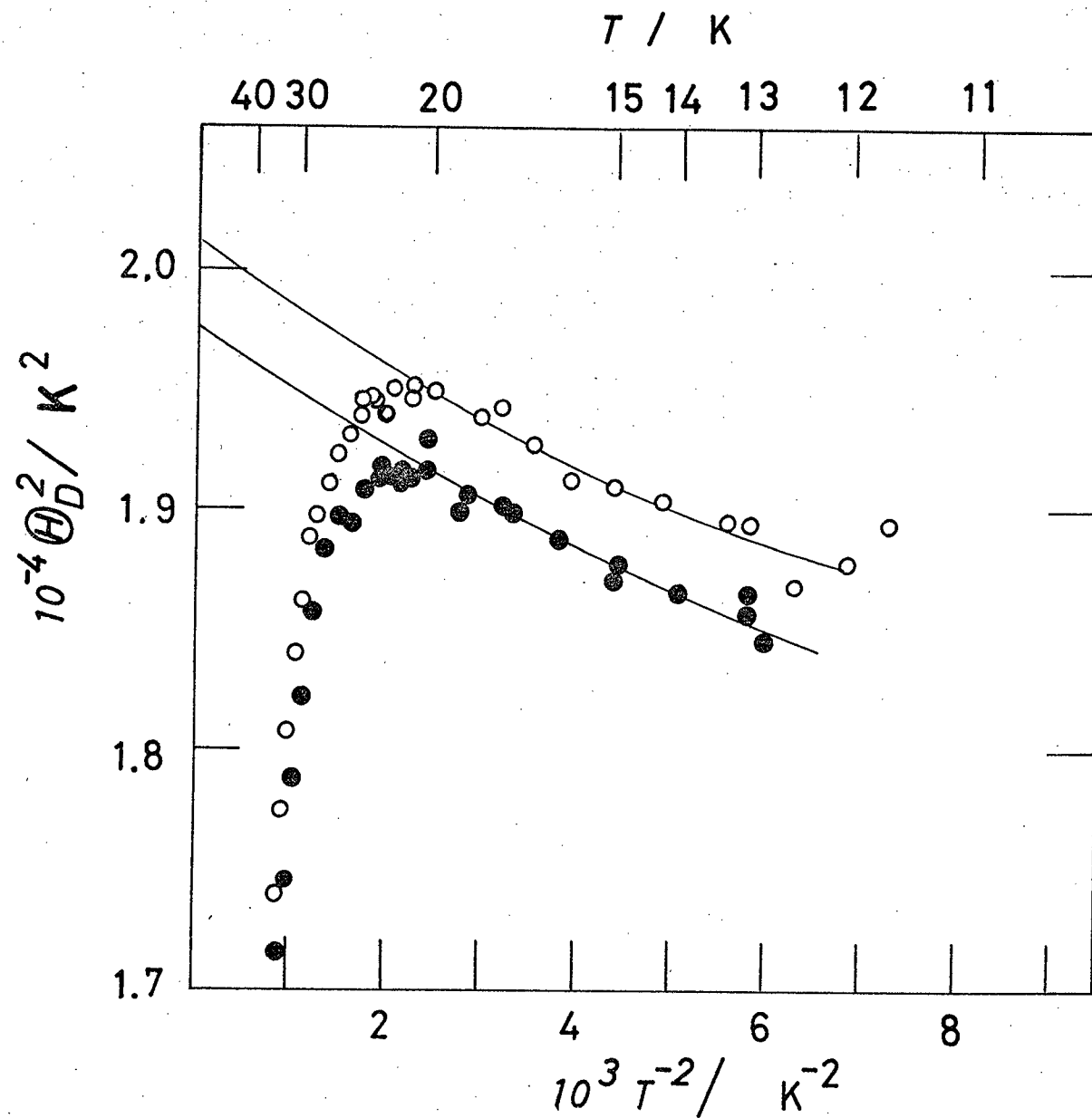
Fig. 4.3.9 Determination of θ_∞ of RbHSO$_4$ (◯) and RbDSO$_4$ (⬤).

229
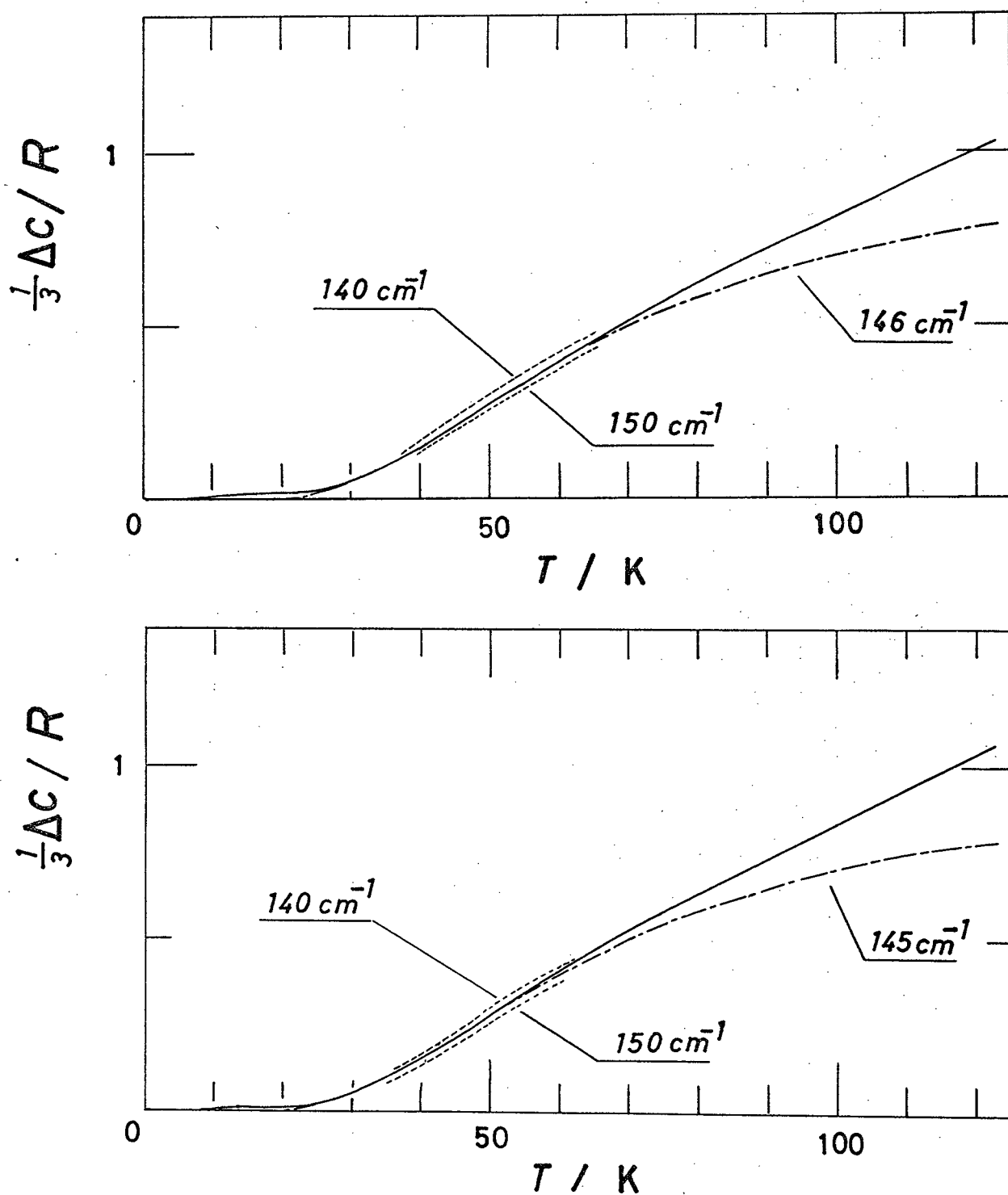
Fig. 4.3.10   Determination of librational frequencies of RbHSO$_4$ (above) and RbDSO$_4$ (below). $\Delta C = C_p$(Normal) $- C_D(\Theta_\infty/T)$.
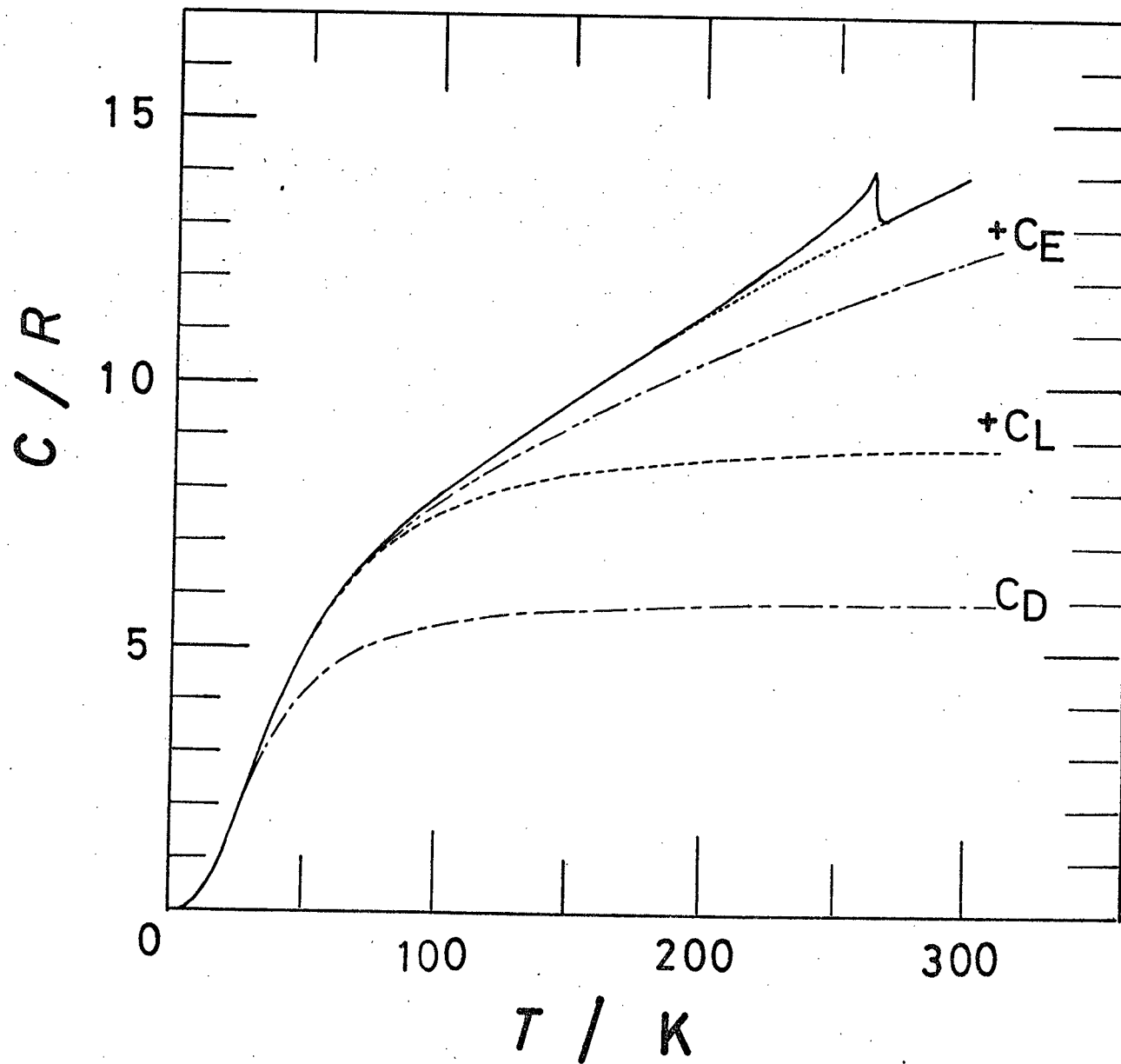
Fig. 4.3.11 Heat capacity contributions of translational lattice modes (C_D), librational modes (C_L) and internal modes (C_E).
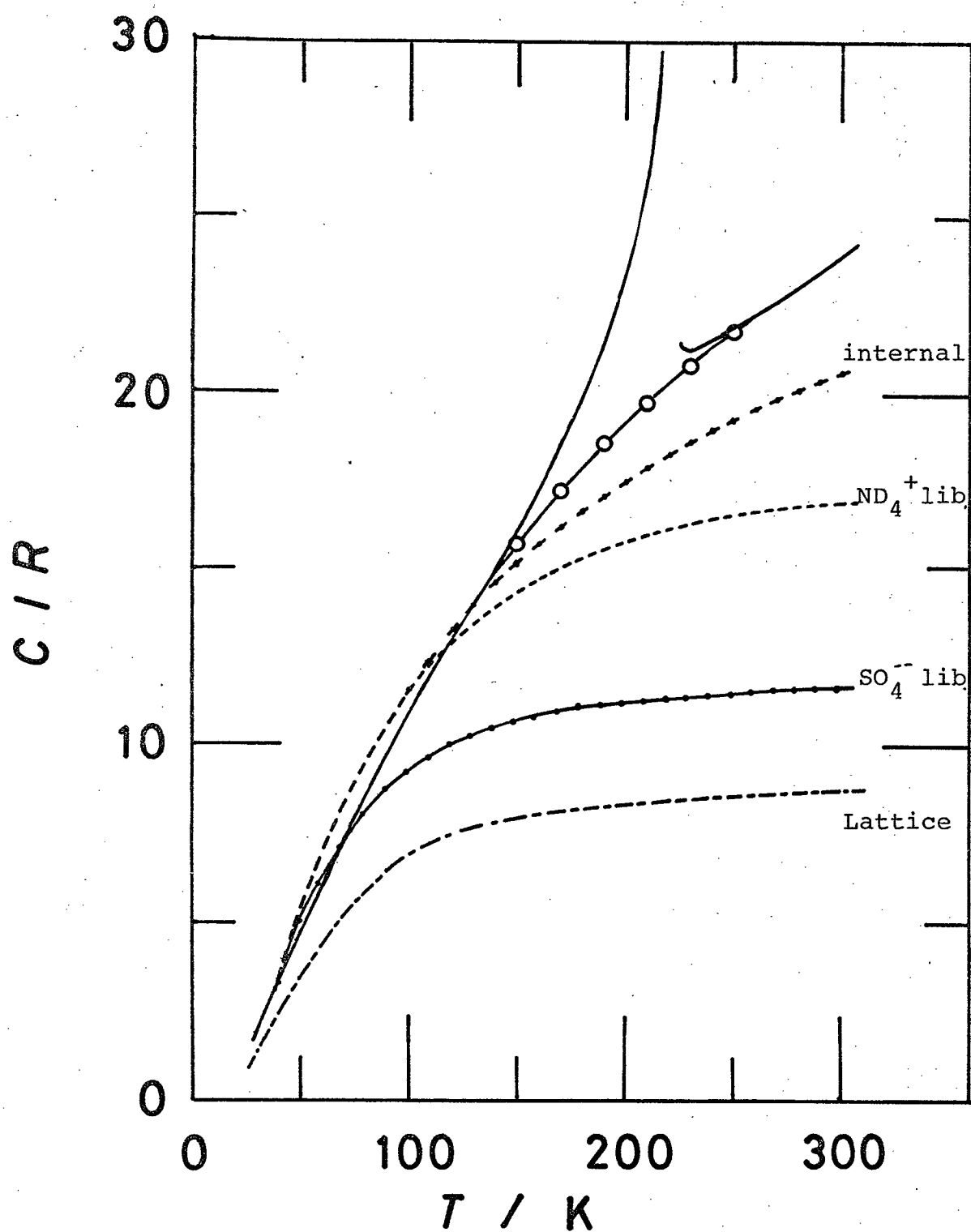
Fig. 4.3.12   Analysis of normal heat capacity of $(ND_4)_2SO_4$.
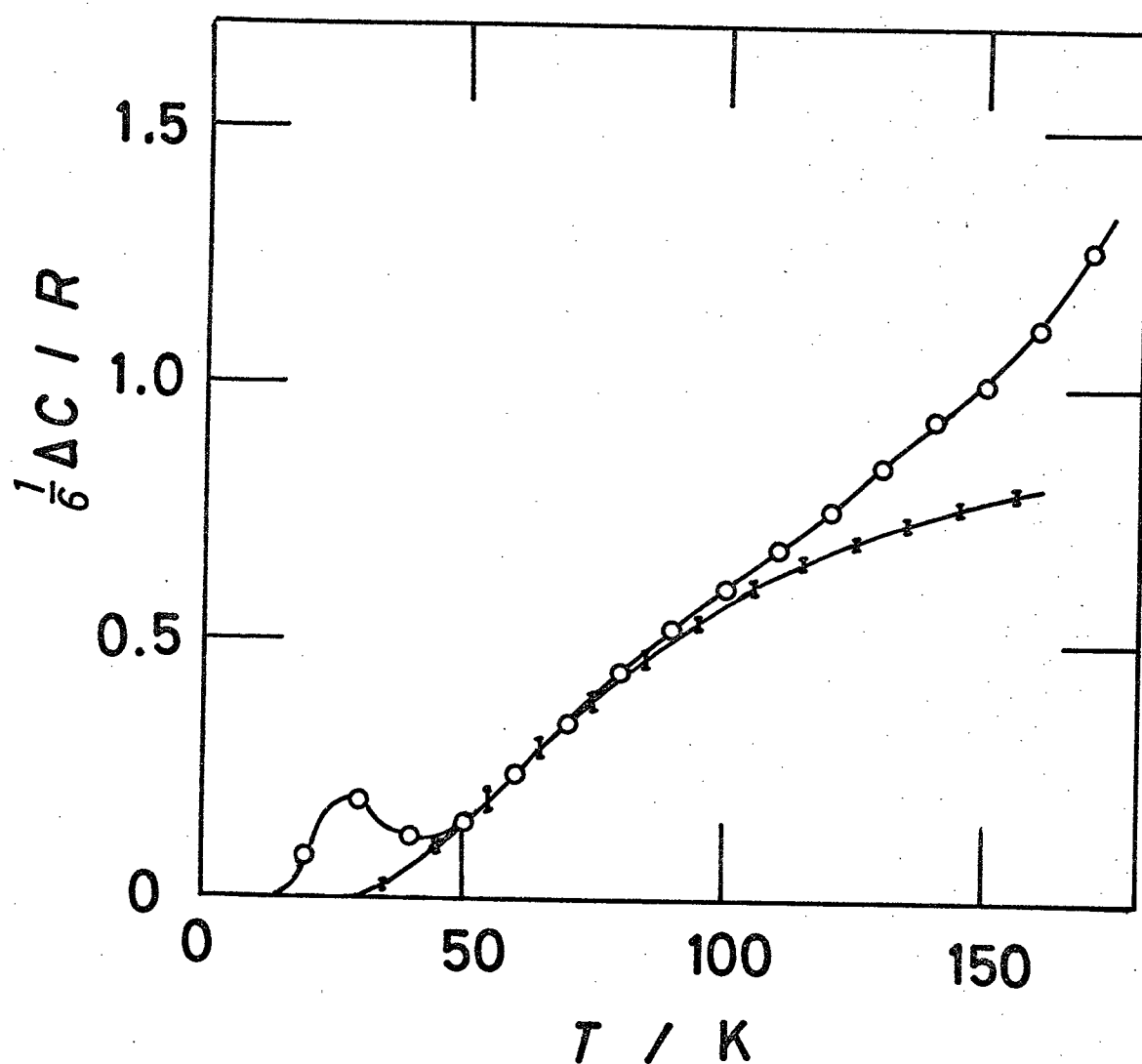
Fig. 4.3.13   Evaluation of averaged frequency of optical modes.
　┼; the Einstein heat capacity with the frequency of $185 \pm 5 \, \mathrm{cm}^{-1}$.
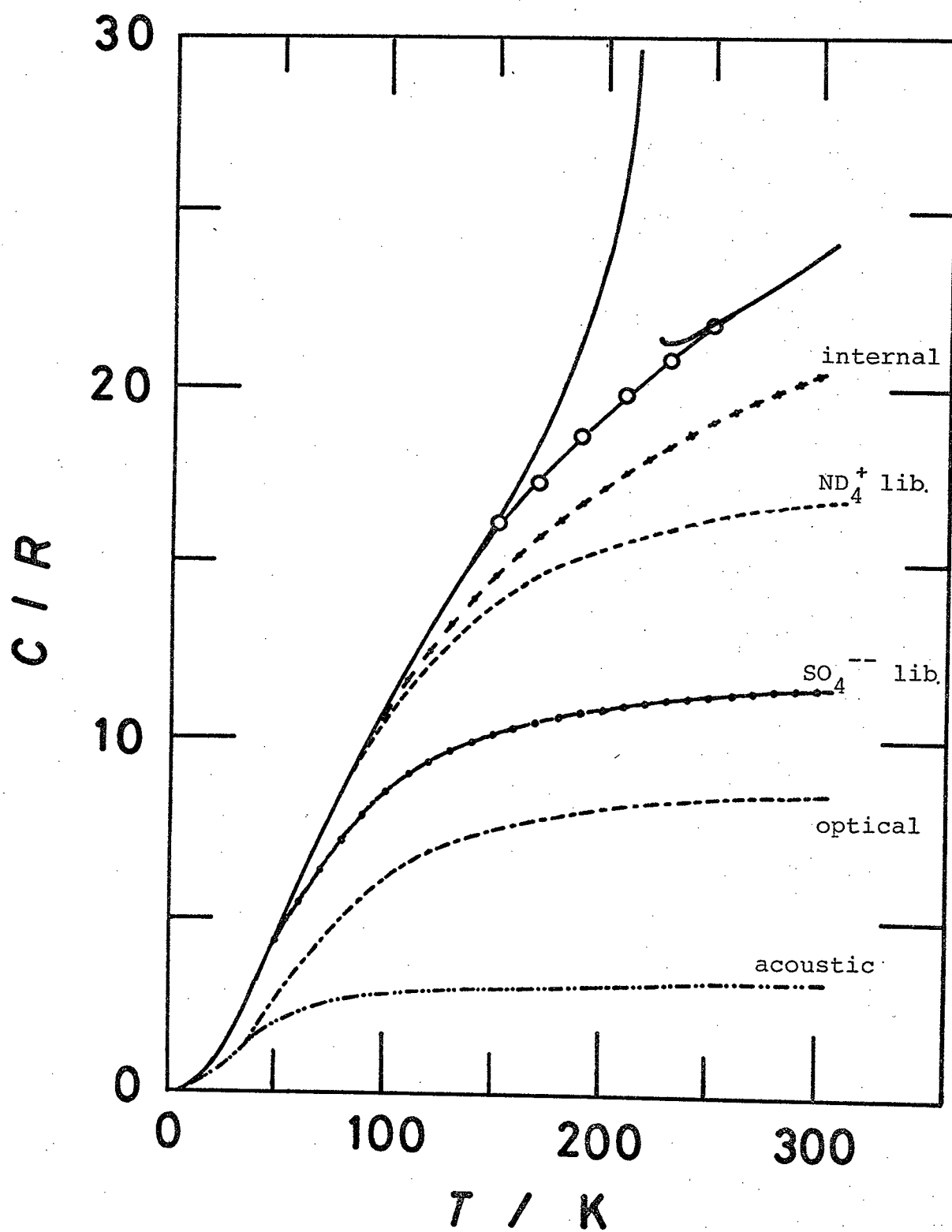
Fig. 4.3.14   Analysis of normal heat capacity of $(ND_4)_2SO_4$.
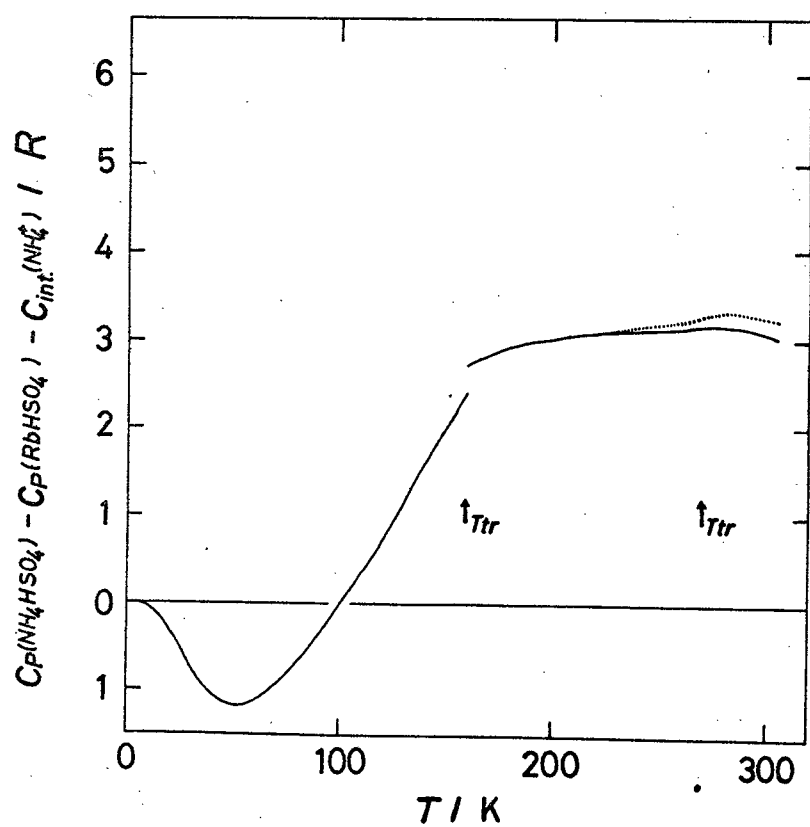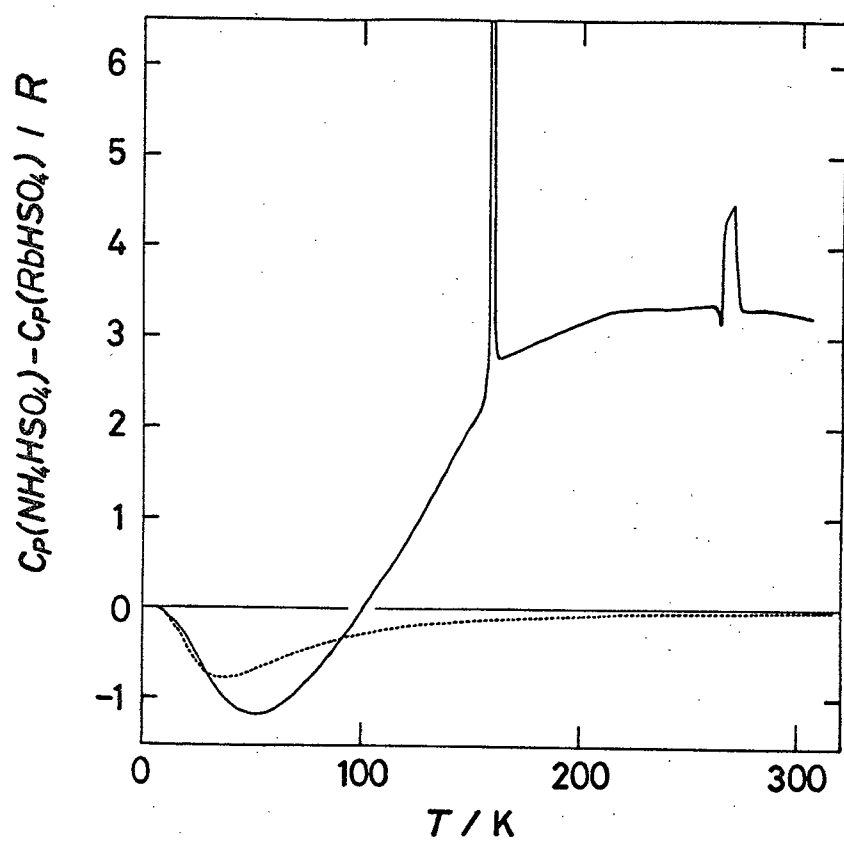
Fig. 4.3.15   Difference plot in the observed C_p values (upper)
in the normal C_p values (lower).
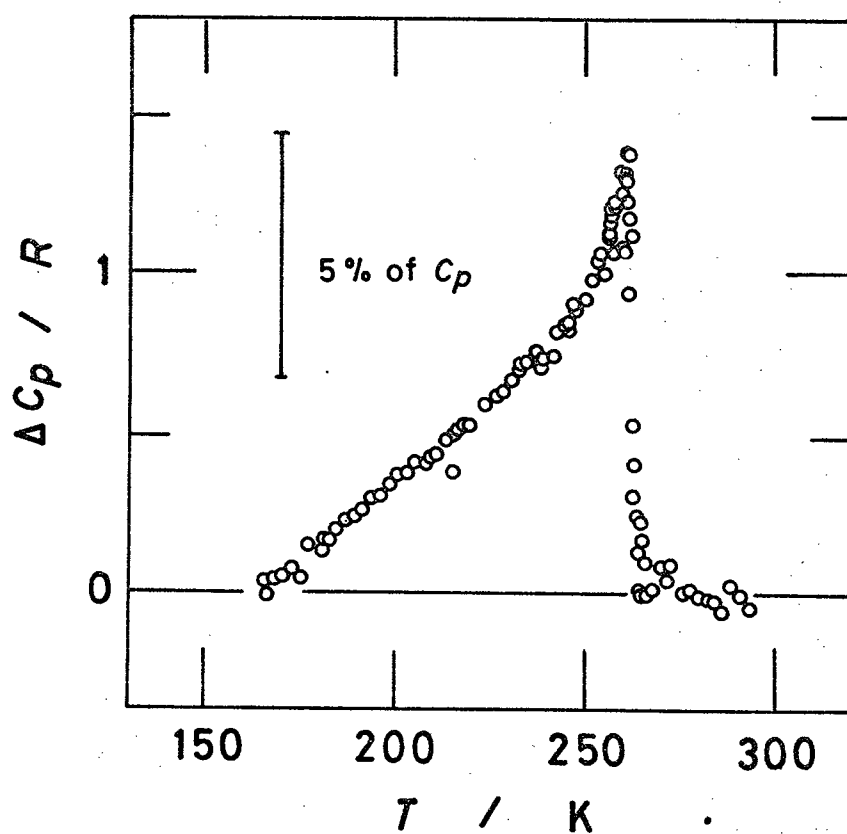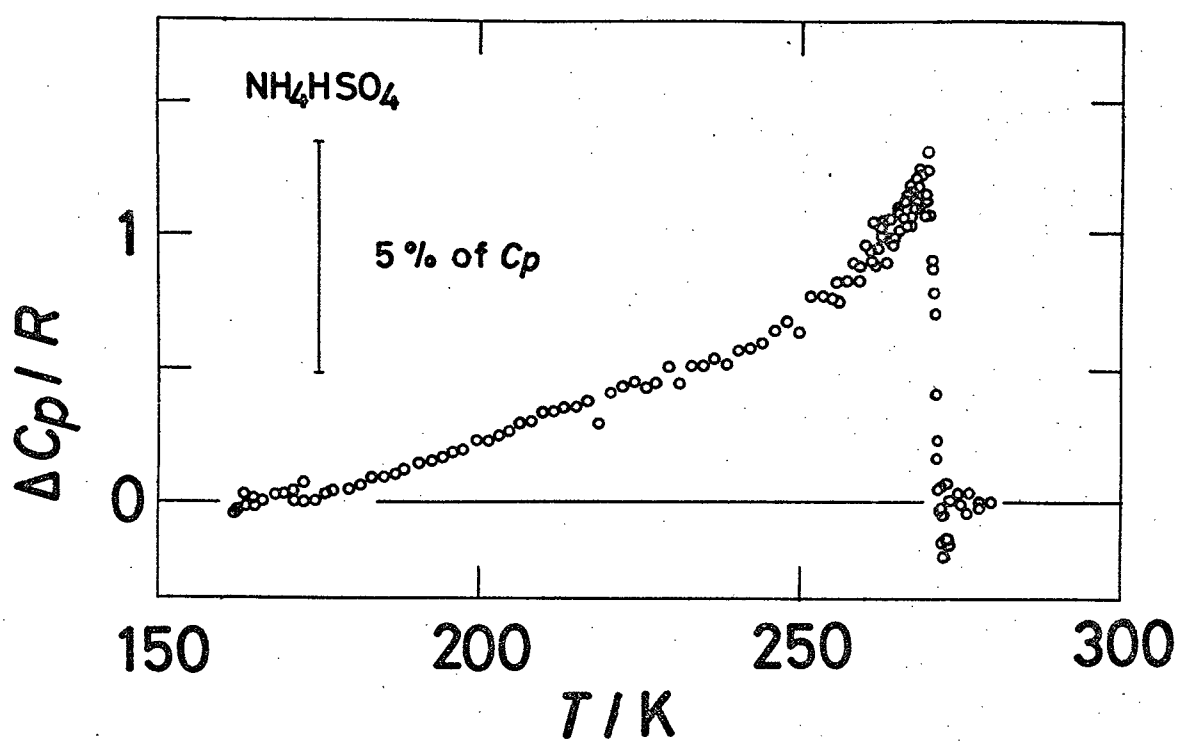
Fig. 4.3.16   Anomalous heat capacities of NH_4HSO_4 (upper)
and ND_4DSO_4 (lower).
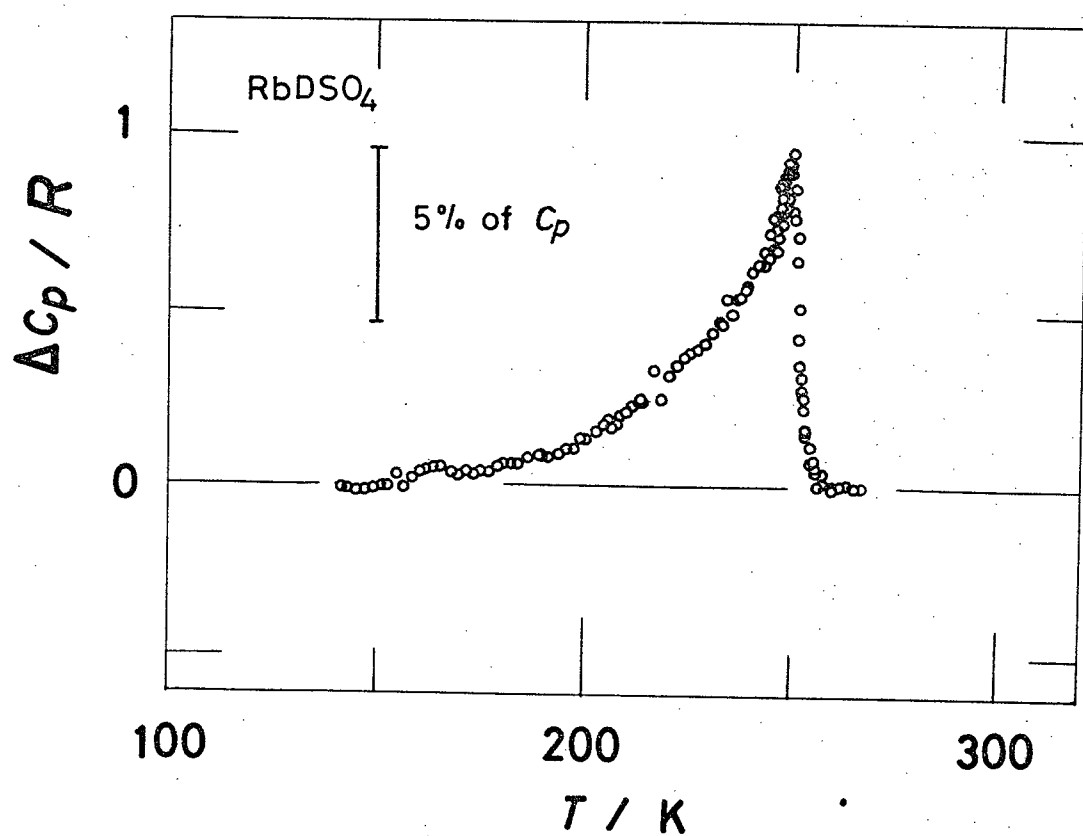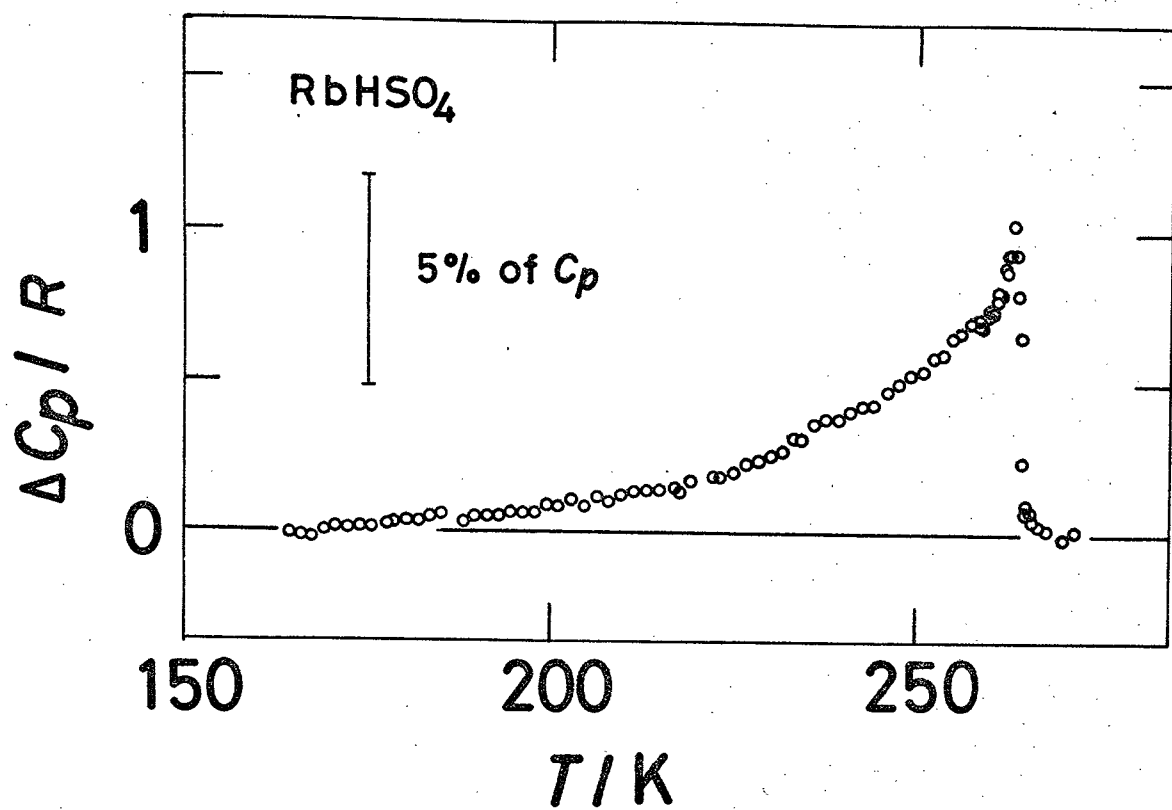
Fig. 4.3.17 Anomalous heat capacities of RbHSO₄ (upper) and
RbDSO₄ (lower).
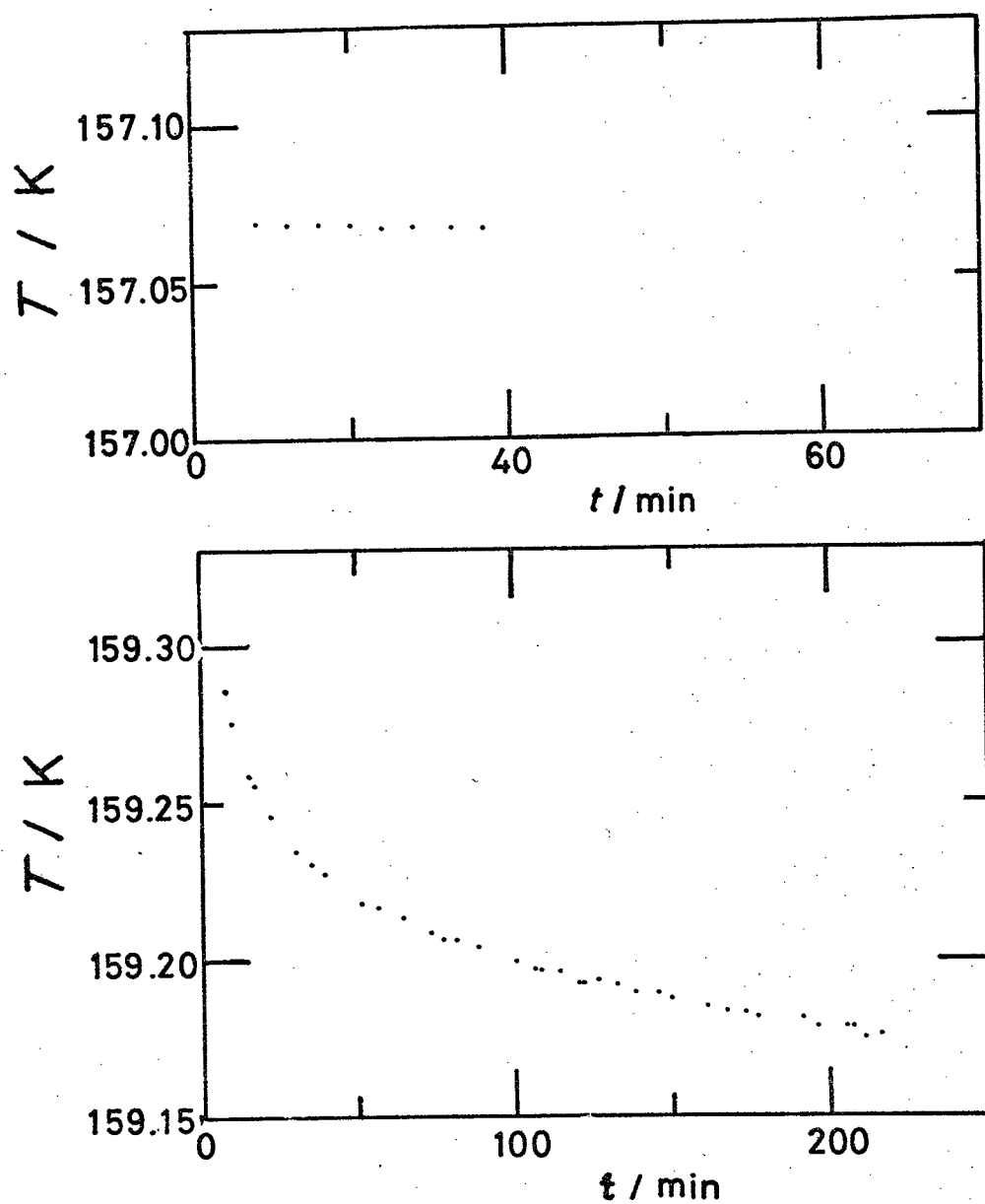
Fig. 4.3.18 Temperature drift near the lower ferroelectric transition in NH_4HSO_4.
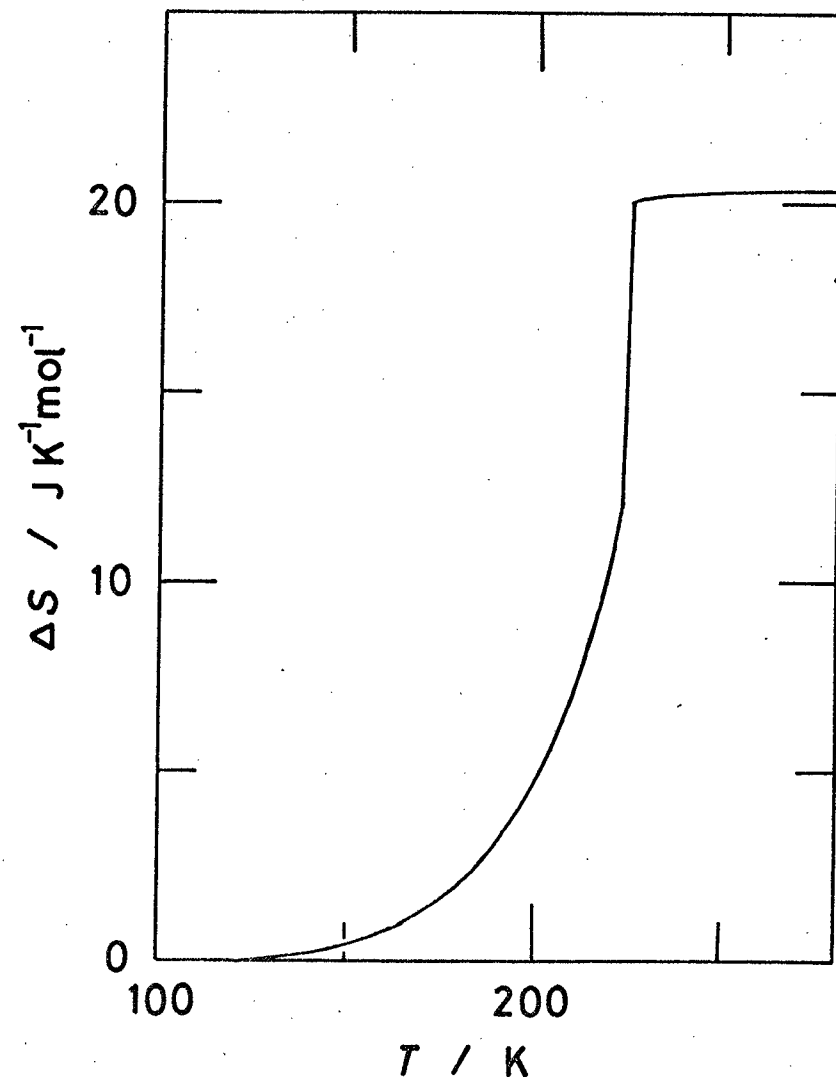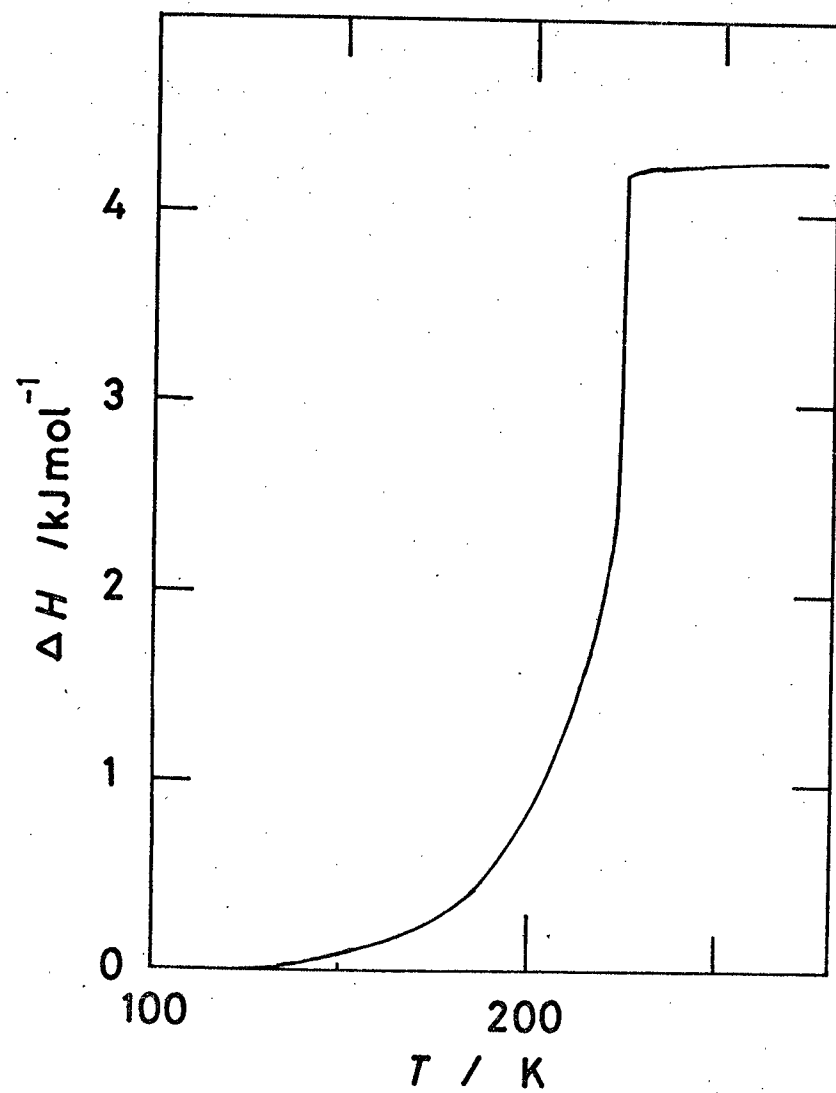
Fig. 4.3.19   Transition enthalpy and entropy of $(ND_4)_2SO_4$.

234
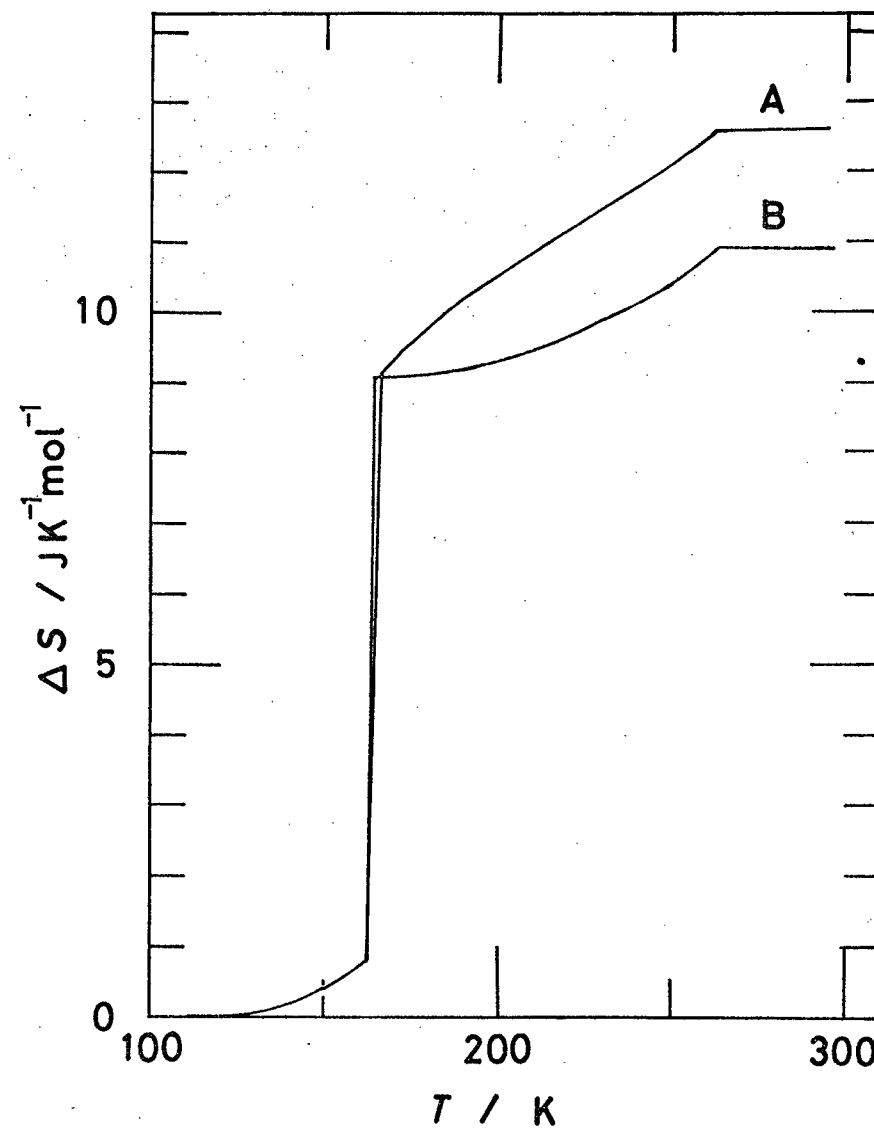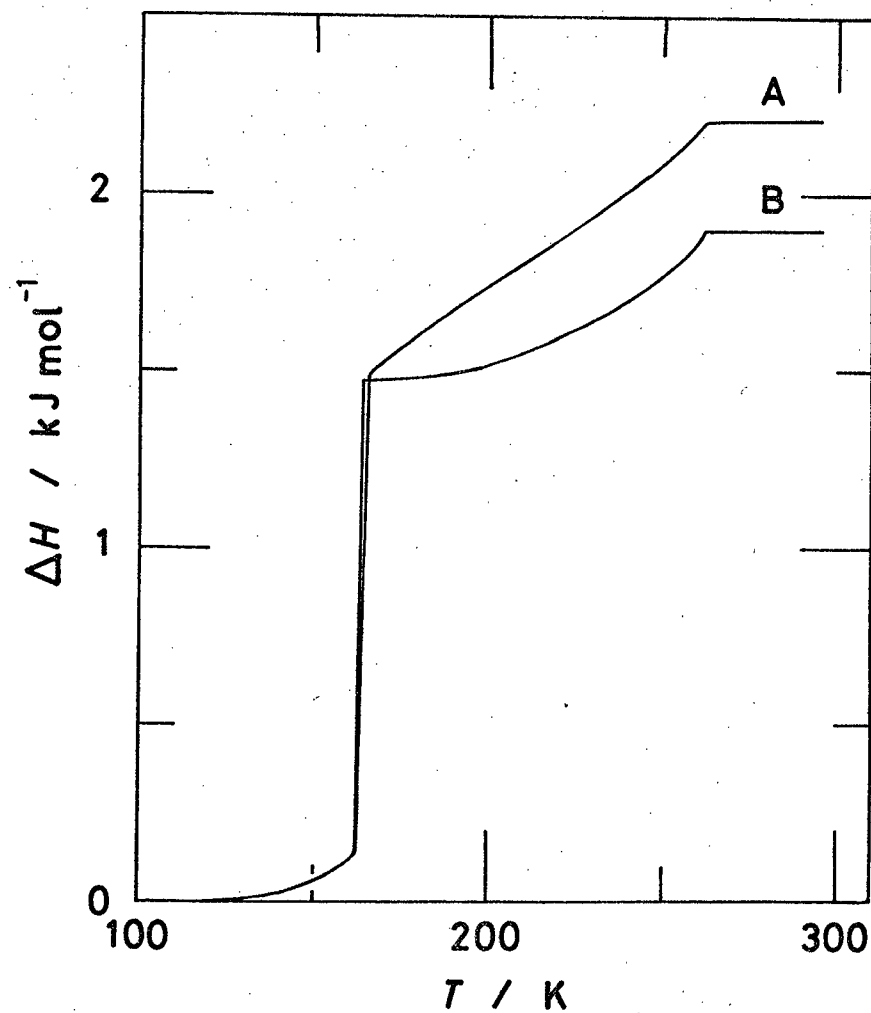
Fig. 4.3.20 Transition enthalpy and entropy of ND_4DSO_4 (A: Base line I. B: Base line II).

235
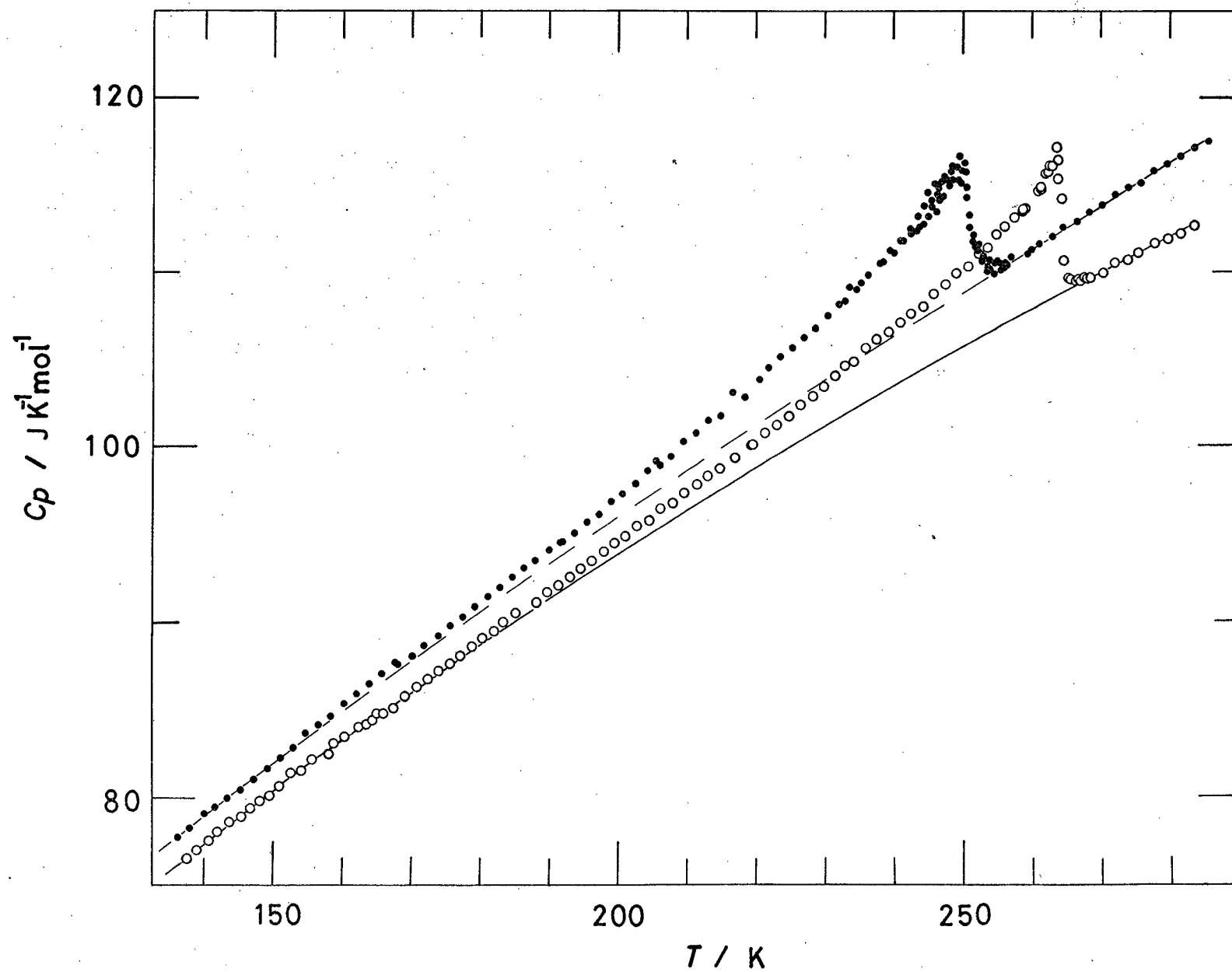
Fig. 4.3.21   Large plot of anomalous heat capacities of RbHSO$_4$ (O) and RbDSO$_4$ (●).
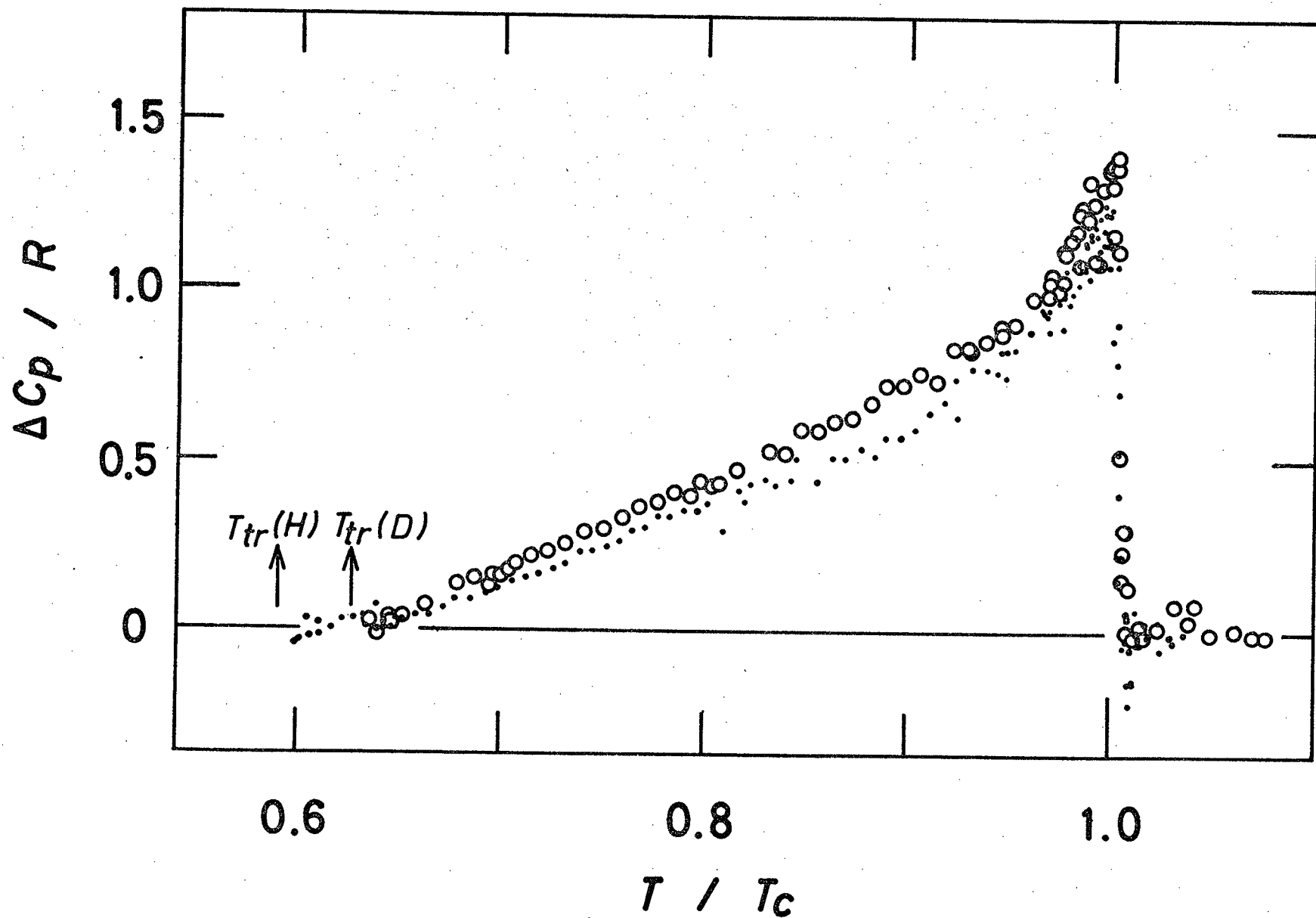
Fig. 4.3.22 Comparison of anomalous heat capacities of NH_4HSO_4 ($\bullet$) and ND_4DSO_4 ($\circ$).

237
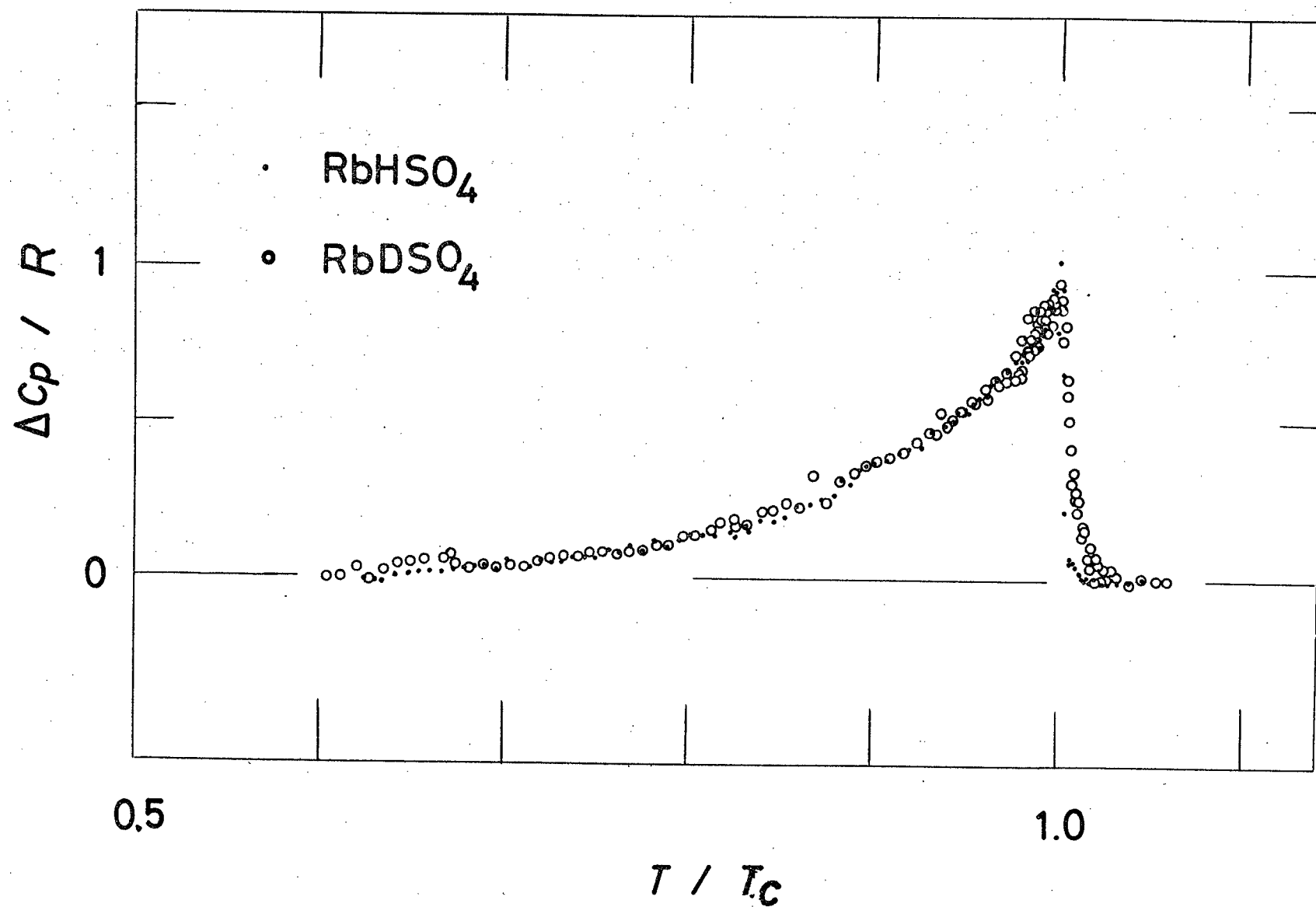
Fig. 4.3.23 Comparison of anomalous heat capacities of RbHSO$_4$ (●) and RbDSO$_4$ (o).
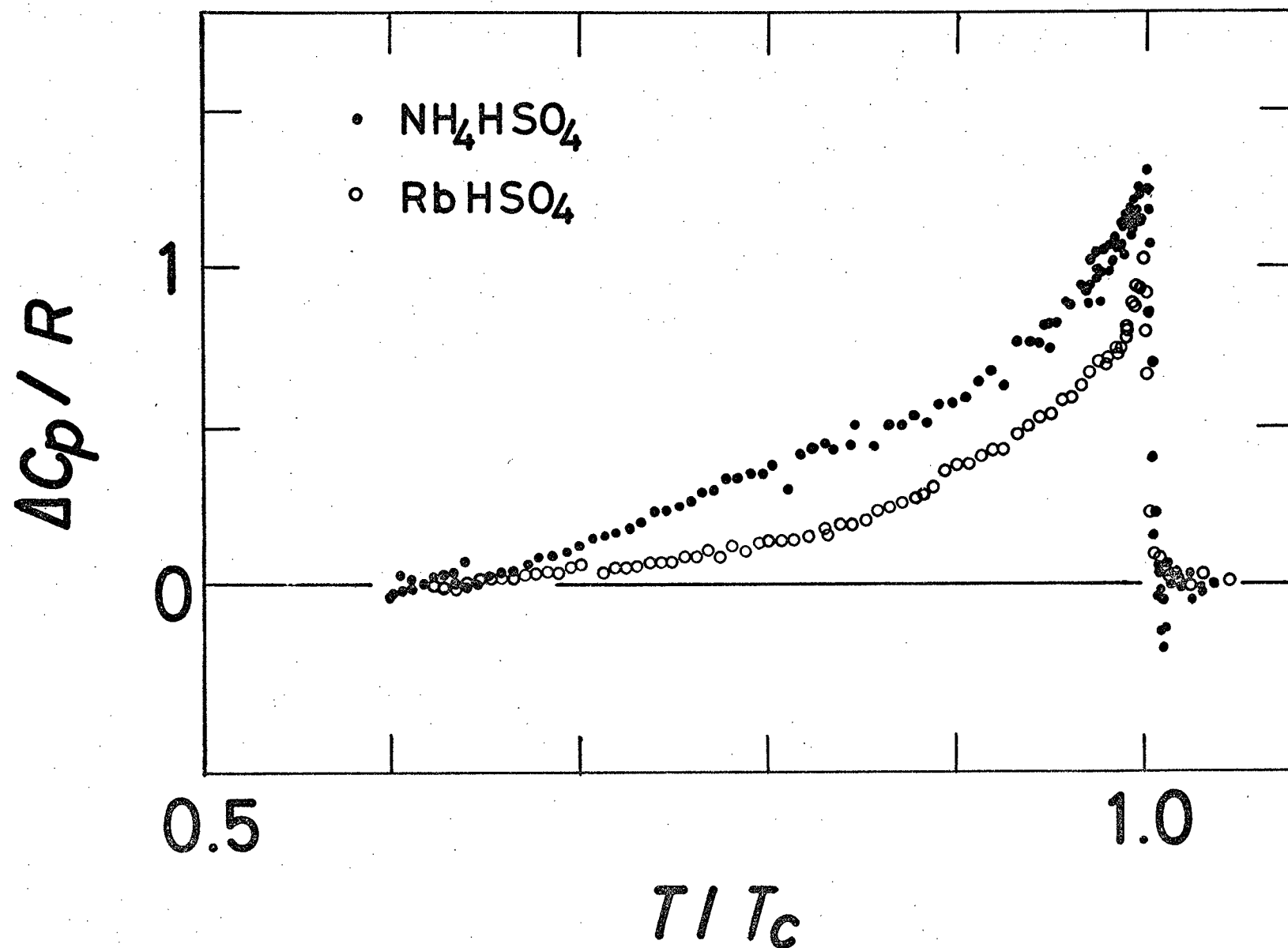
Fig. 4.3.24 Comparison of anomalous heat capacities of NH_4HSO_4 (●) and $RbHSO_4$ (O).
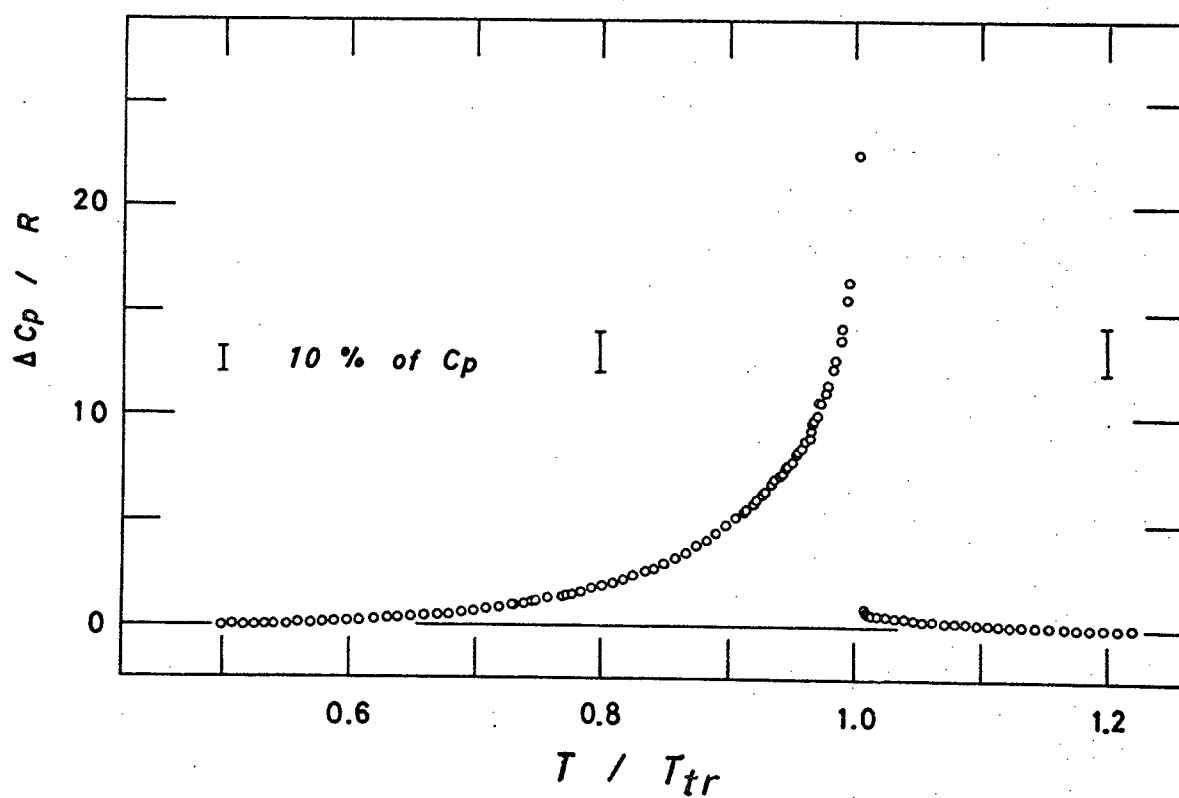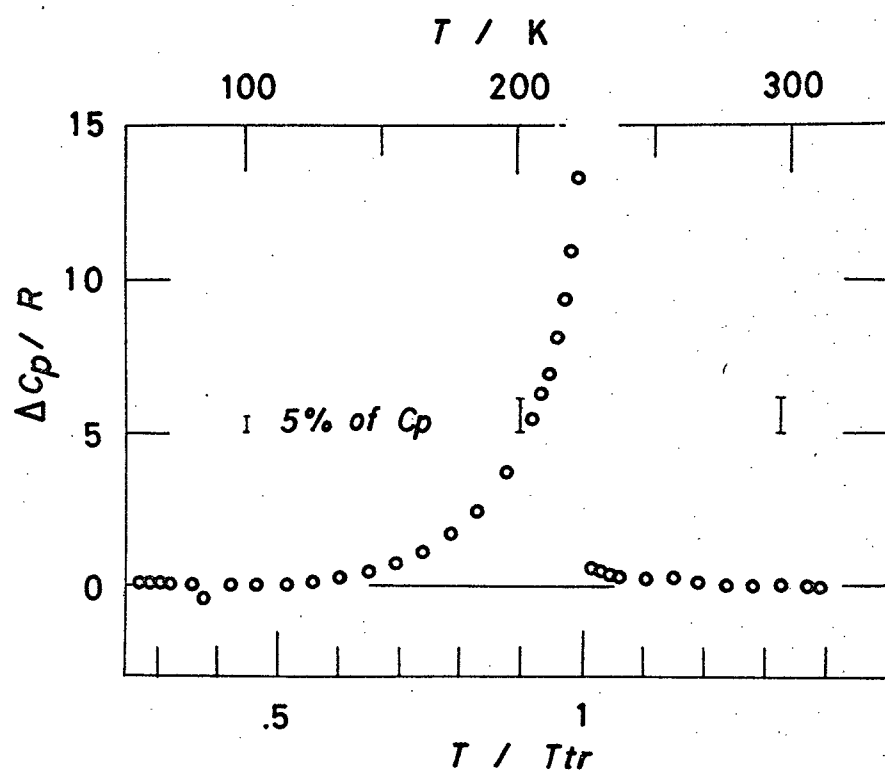
Fig. 4.3.25   Anomalous heat capacities of $(NH_4)_2SO_4$ (upper) and $(ND_4)_2SO_2$ (lower).
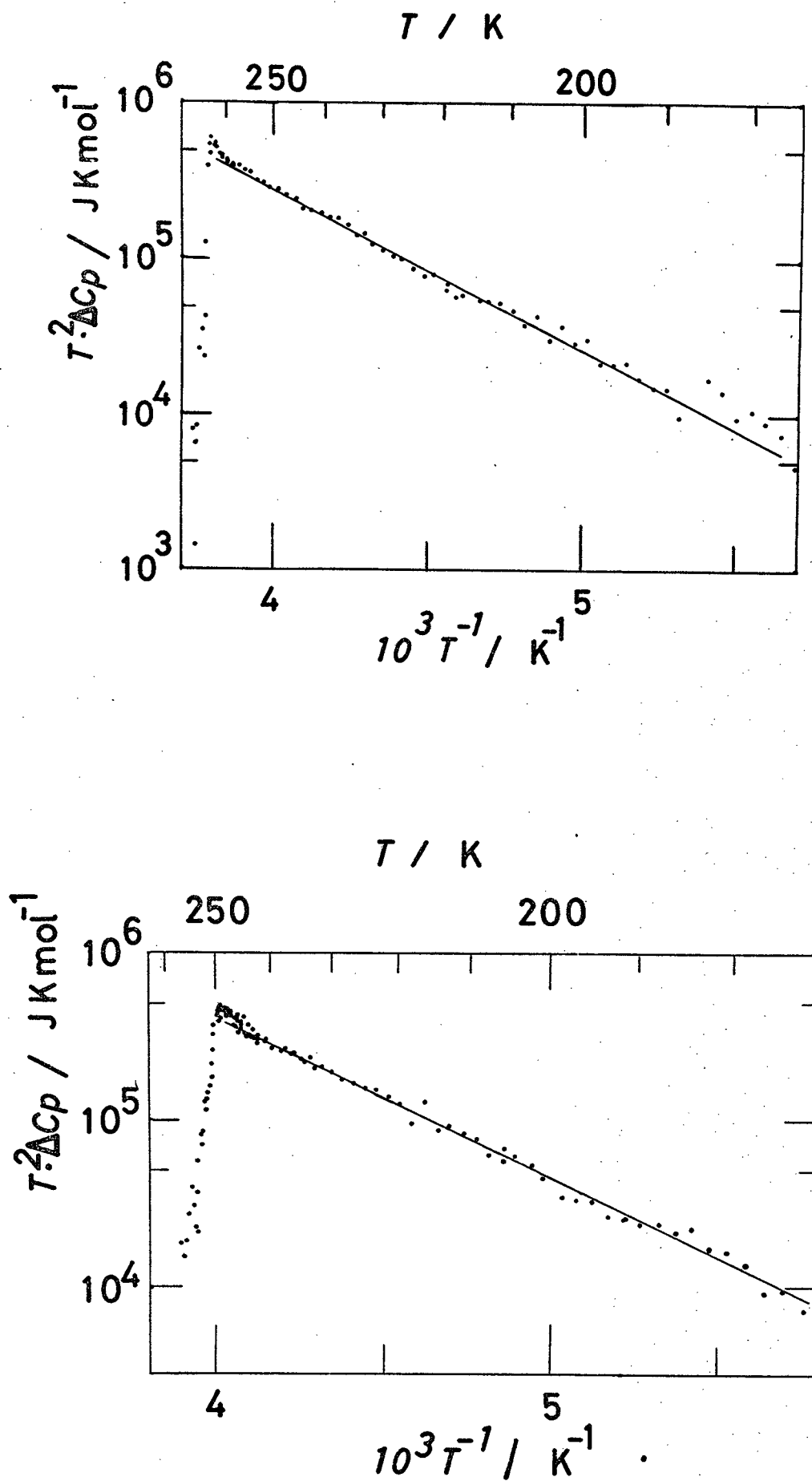
Fig. 4.3.26 Plot of $\ln(T^2 \Delta C)$ against T^{-1} for $RbHSO_4$ (upper)
$RbDSO_4$ (lower).

241
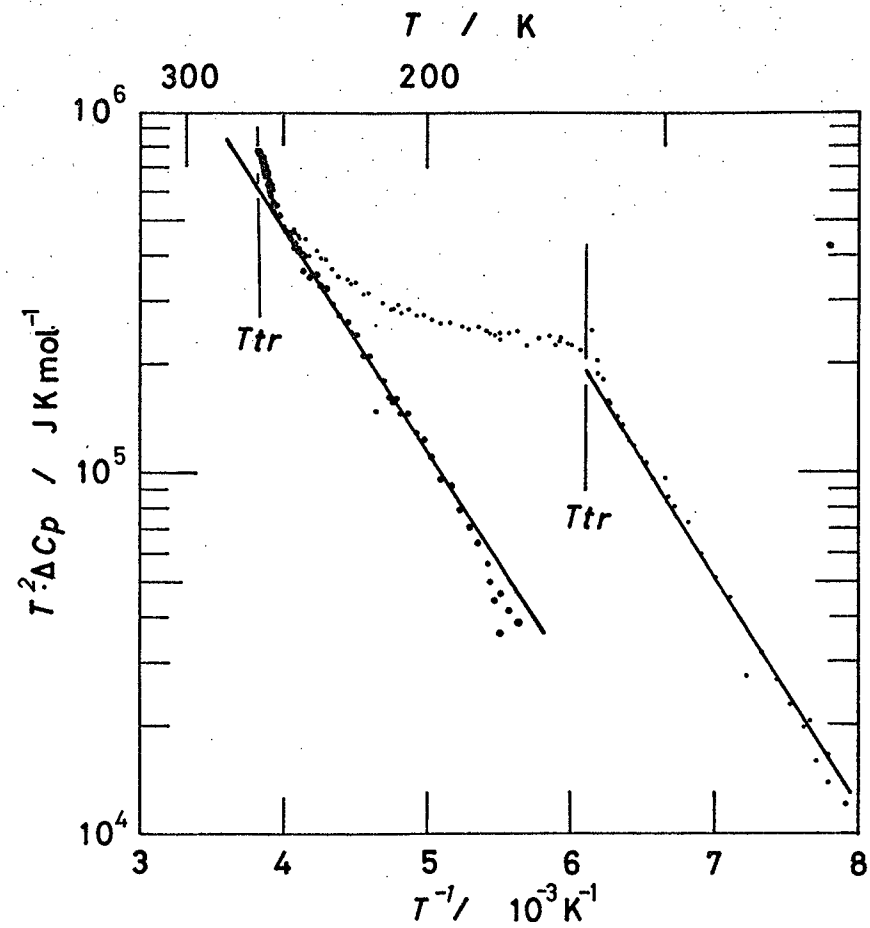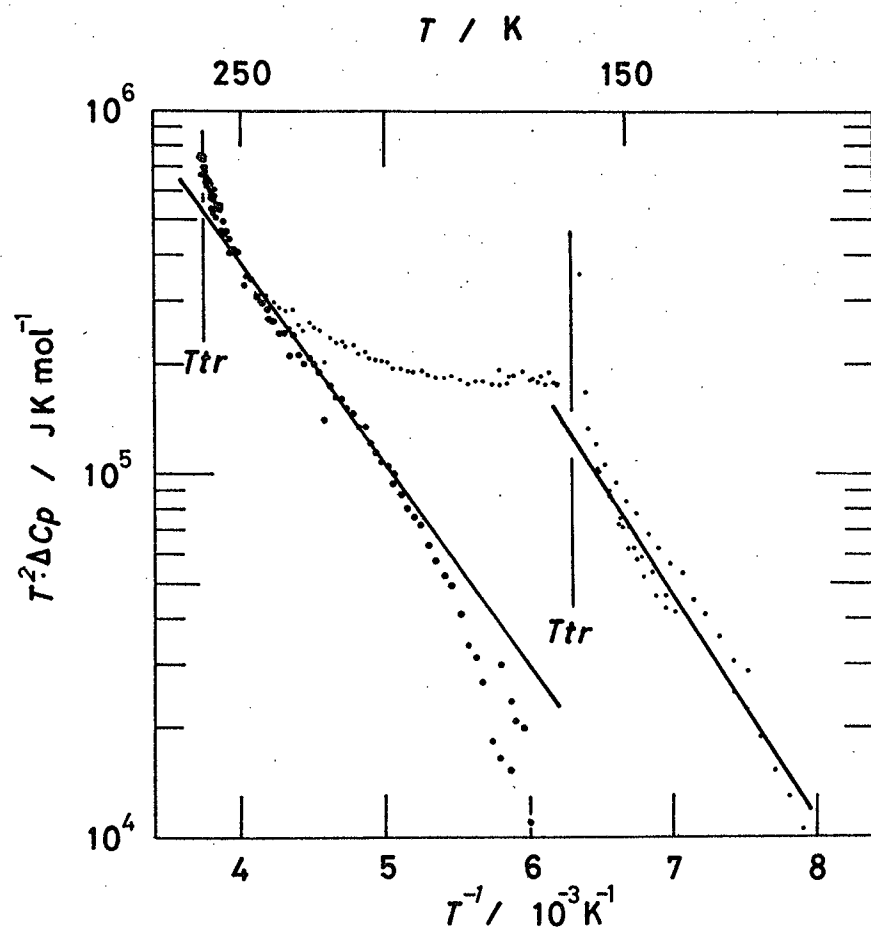
Fig. 4.3.27 Plot of ln ($T^2 \Delta C_p$) against T^{-1} of NH_4HSO_4 (left) and ND_4DSO_4 (right).

Fig. 4.3..28 Plot of ln $(T^2\Delta C)$ against T^{-1} for VCl_3.

Fig. 4.3.29 Plot of ln (T²ΔC) against T⁻¹ for $(NH_4)_2SO_4$ (left) and for $(ND_4)_2SO_4$ (right).

Fig. 4.3.30 Plot of ln $(T^2 \Delta C)$ against T^{-1} for NH_4Cl (left), $(NH_4)_{1-x}Rb_xCl$ (center, x = 0.0158 right, x = 0.0251).

245

Fig. 4.3.31 Plot of ln $(T^2\Delta C)$ against T^{-1} for NH_4Br (left) and for ND_4Br (right).

Fig. 4.3.32 Plot of ln (T^{2}ΔC) against T^{-1} for adamantane.
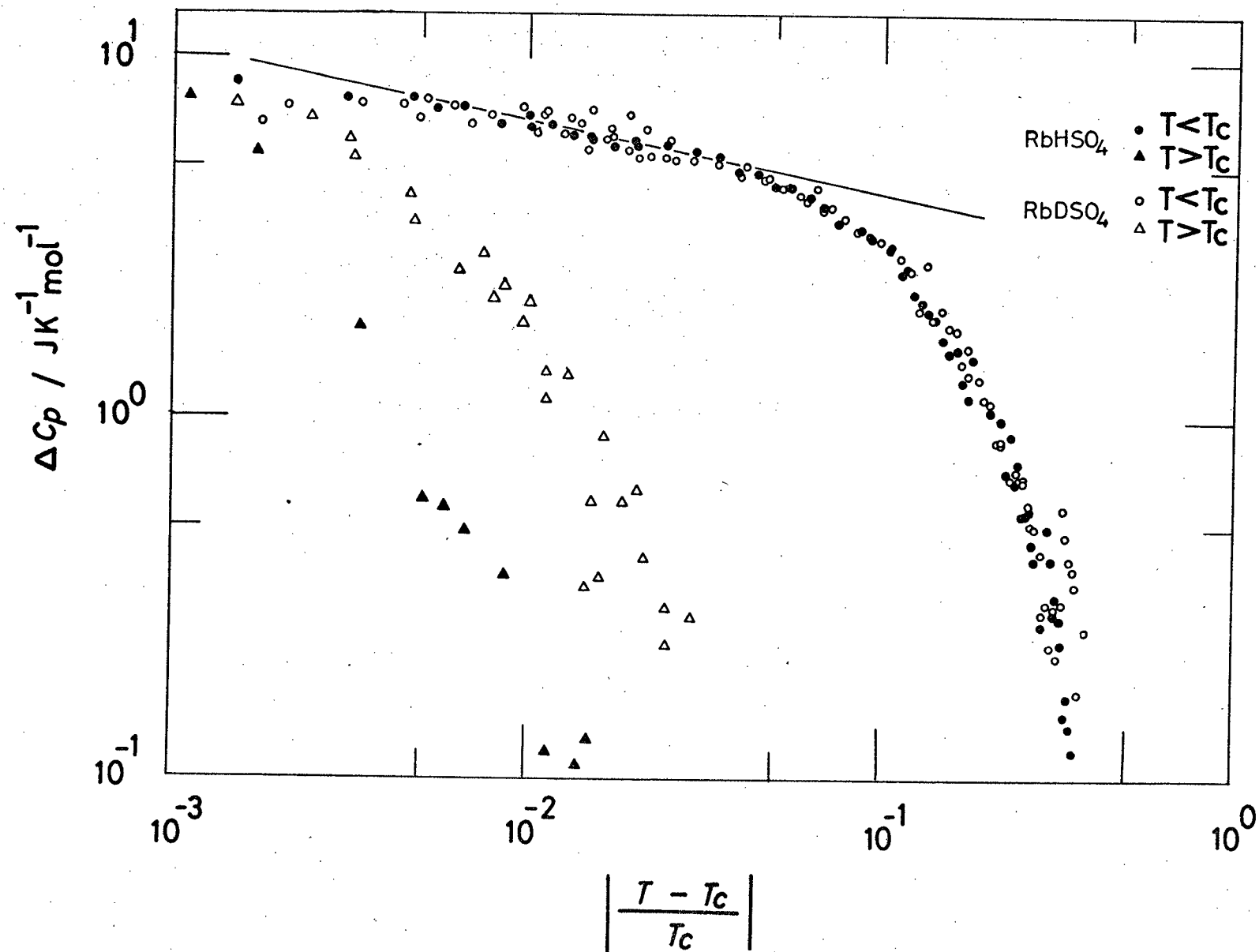
Fig. 4.3.33 Plot of ln ΔC against ln$|(T - Tc) / Tc|$ of RbHSO$_4$ (• , T < Tc; ▲ , T > Tc) and RbDSO$_4$ (o , T < Tc; △ , T > Tc).
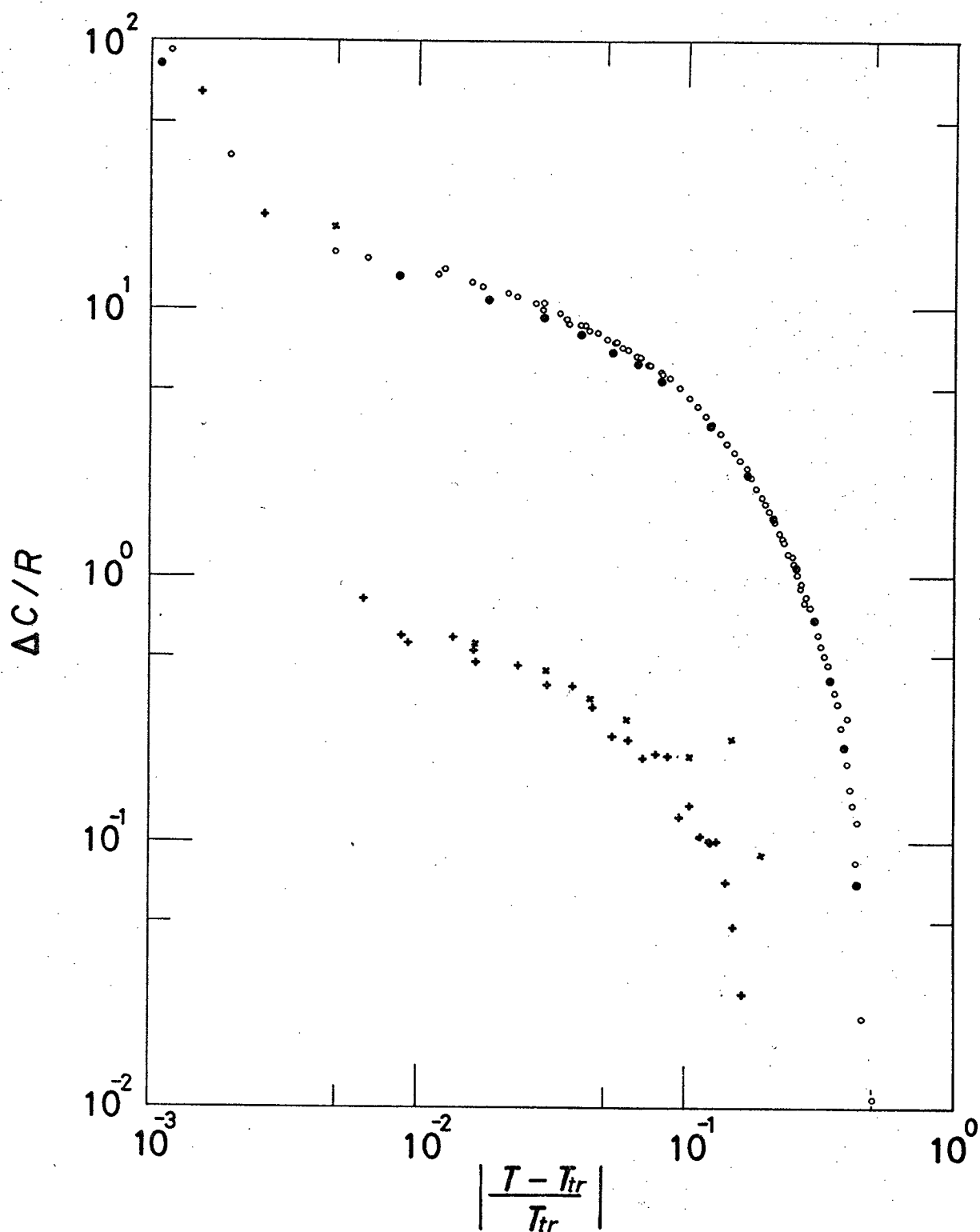
Fig. 4.3.34 =Plot of ln ΔC against ln $\left| (T - T_{tr}) / T_{tr} \right|$ of $(NH_4)_2SO_4$ ($\bullet$, $T < T_{tr}$; $\times$, $T > T_{tr}$) and $(ND_4)_2SO_4$ ($\circ$, $T < T_{tr}$; $+$ $T > T_{tr}$).
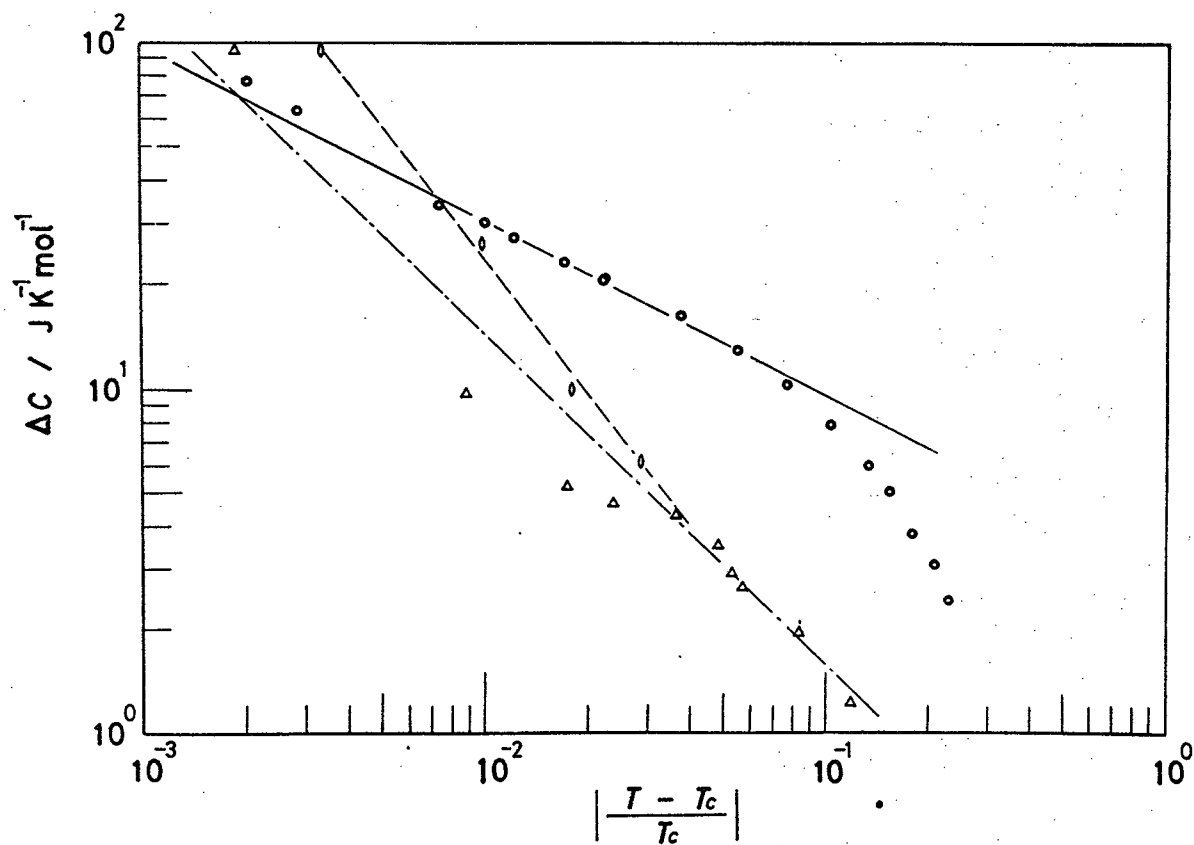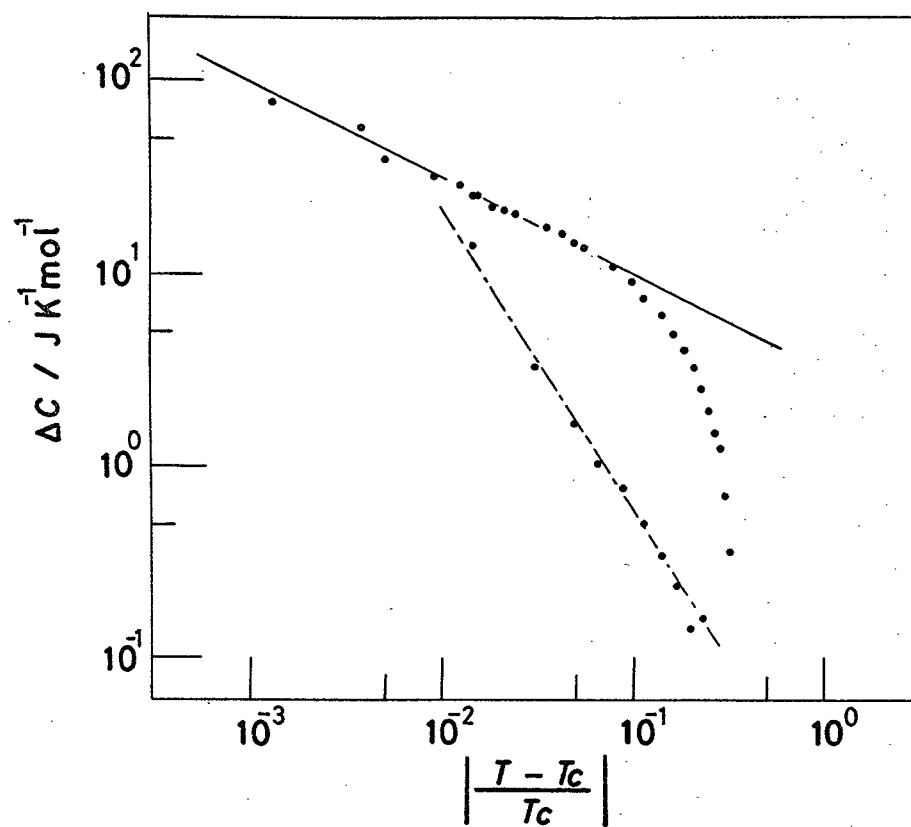
Fig. 4.3.35 Plot of ln ΔC against ln |(T - Tc) / Tc| for NH_4Br (upper)
ND_4Br (lower).

Appendix A

A simple phenomenological theory for the ferroelectric transitions in Rochelle salt.

Taking into account the smallness of spontaneous polarization P_s in Rochelle salt[1] and $G(P_s) = G(-P_s)$ in the ferroelectric phase, we may expand the thermodynamic potential in the powers of polarization P and trancate it above sixth order.

$$G = G_o + \frac{1}{2}\chi P^2 + \frac{1}{4}\xi P^4 \ , \quad \xi(p, T) > 0 \qquad \cdots\cdots 1$$

where G_o means potential at $P = 0$ and χ and ξ are the phenomenological constants depending on temperature T and pressure p. For simplicity, ξ is assumed to be a positive constant and then the polarization P to be realized is determined from the condition of potential minimum. This condition gives $P = 0$ or $P^2 = -\chi/\xi$, the former leads to $\Delta G = G - G_o = 0$ but the latter $\Delta G = -(\chi^2/4\xi) < 0$. Therefore, it follows that the polarized state is lower in thermodynamic potential than the non-polarized. Here another assumption is made that $\chi < 0$ when $T_\ell < T < T_u$ and $\chi > 0$ when $T < T_\ell$ or $T > T_u$. This assumption is satisfied by putting χ as;

$$\chi = \chi_o (T - T_\ell)(T - T_u) \ , \quad \chi_o > 0 \qquad \cdots\cdots 2$$

Using the equation 2, we can easily derive the temperature dependence of P_s, ΔG, ΔS, ΔC as follows;

$$P_s^2 = -\chi/\xi$$

$$= P_{max}^2 - \frac{\chi_o}{\xi}\left(T - \frac{T_u + T_\ell}{2}\right)^2 \ .$$

where
$$P_{max} = \frac{T_u - T_\ell}{2} (\chi_o / \xi)^{1/2}.$$

$$\Delta G = -\chi^2 / 4\xi = -\chi_o^2 (T - T_\ell)^2 (T - T_u)^2 / 4\xi$$

$$\Delta S = -(\partial \Delta G / \partial T)_p$$

$$= \chi_o^2 (T - T_u) \cdot (T - T_\ell) \cdot (T - \frac{T_u + T_\ell}{2}) / \xi$$

$$\Delta C = T(\partial \Delta S / \partial T)_p$$

$$= \chi_o^2 \cdot T \left\{ 3T^2 - 3(T_u + T_\ell)T + 1/2(T_u^2 + 4T_u T_\ell + T_\ell^2) \right\} / \xi$$

The static dielectric constant is related to the reciprocal dielectric susceptibility $\chi' = (\partial E / \partial P)_{E=0}$ by the relation

$$\varepsilon = 4\pi \chi'^{-1} + 1$$

and its temperature dependence is written down as follows.

at $T > T_u$
$$\varepsilon = \frac{4\pi}{\chi_o} \cdot \frac{1}{(T - T_\ell)(T - T_u)} + 1$$

at $T_\ell < T < T_u$
$$\varepsilon = \frac{2\pi}{\chi_o} \cdot \frac{1}{(T - T_\ell)(T - T_u)} + 1$$

at $T < T_\ell$
$$\varepsilon = \frac{4\pi}{\chi_o} \cdot \frac{1}{(T - T_\ell)(T - T_u)} + 1$$

The results thus obtained are illustrated in Fig. 1 schematically and summerized as follows

1. The sum of transition entropies at T_u and T_ℓ is zero.

2. The ratio of excess heat capacity $\Delta C(T_u) / \Delta C(T_\ell)$ is T_u / T_ℓ.

3. The law of 2 holds.

Some points of these results have been pointed out qualitatively by Takahashi.[2] Analogous results[3] have also been obtained by converting Mitsui's theory[4] to semiphenomenological one. The result to be pointed here is that our model can consistently explain all the thermal and dielectric behavior of Rochelle salt with only three parameters χ_o, T_u, T_ℓ.

Now equation 2 may be justified follows. An ordinary second order phase transition would be expected to occur only if $\chi > 0$ when $T > T_u$, and $\chi < 0$ when $T < T_u$. The phenomenological constant $\chi(T)$ may be expanded in power series of $(T - T_u)$;

$$\chi(T) = \chi(T_u) + \chi'(T_u)(T - T_u) + \chi''(T_u)(T - T_u)^2/2 + \cdots$$

Terms higher than the second order are neglected in an ordinary Landau theory which leads to

$$\chi(T) = \chi'(T_u)(T - T_u)$$

assuming implicitly that $\chi'(T_u) > 0$ and $|\chi'(T_u)| \gg |\chi'(T_u)(T - T_u)|$. In the Taylor expansion we may take into account the second order term and neglect higher terms, then the assumption to be proved is derived,

$$\chi = \frac{1}{2} \chi''(T_u)(T - T_u)(T - T_\ell)$$

where $\chi''(T_u) > 0$ and $\chi'(T_u) > 0$ are assumed, and $T_\ell = T_u - 2\chi'(T_u)/\chi''(T_u)$, at which temperature another second transition appears as second order transition.
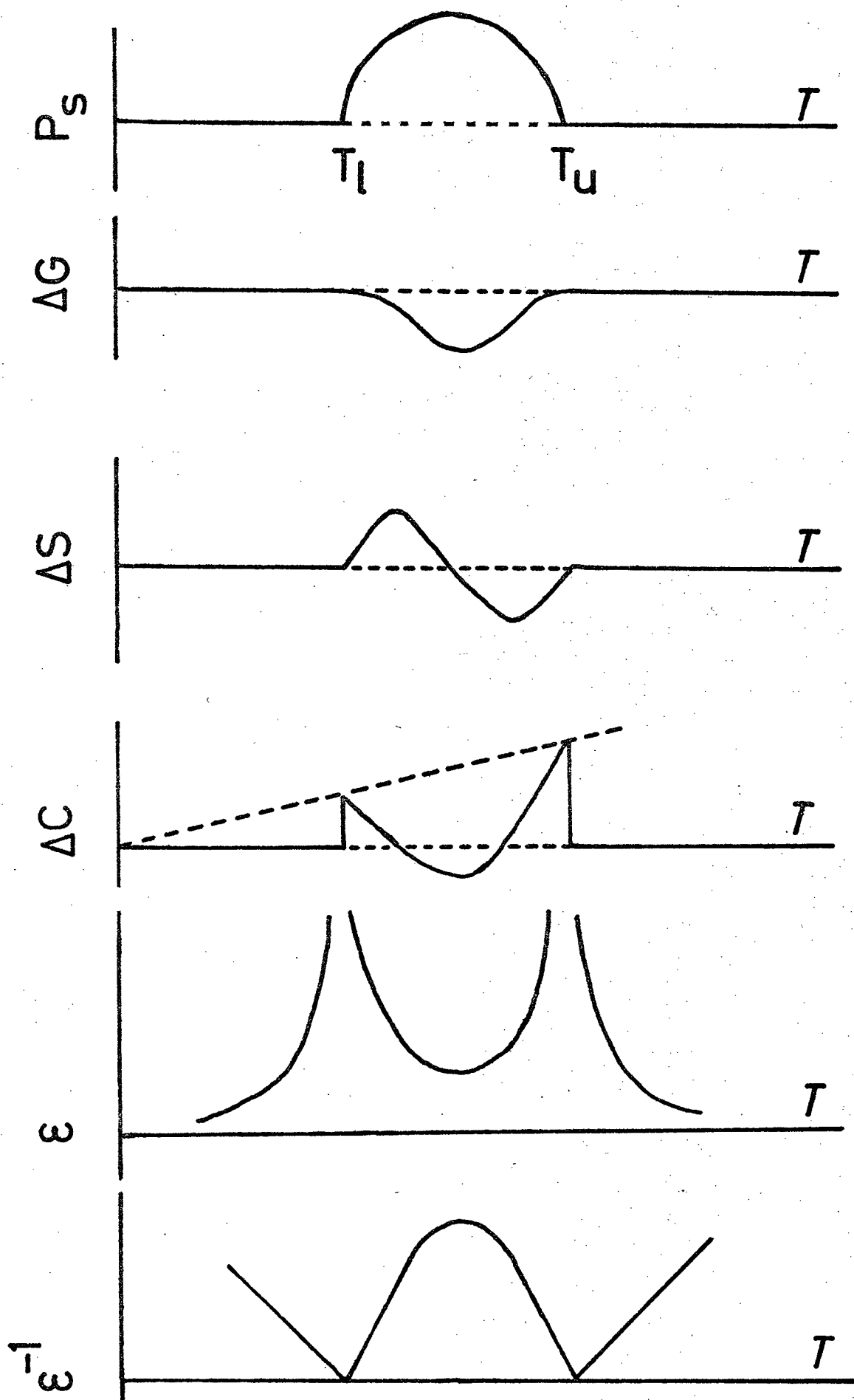
Fig. 1   Temperature dependence of P_s, ΔG, ΔS, ΔC, ε and ε^{-1}.

References

1) J. Hablützel, Helv. Phys. Acta, 12, 489 (1939).

2) H. Takahashi, Busseiron kenkyu, 22, 3 (1950).

3) R. Blinc and B. Žekš, Phys. Letters, 39A, 167 (1972).

4) T. Mitsui, Phys. Rev. 111, 1259 (1958).